MICROCOPY RESOLUTION TEST CHART
NATIONAL BUREAU OF STANDARDS-1963-A

MR 82-7 (I)

Surf Zone Currents

VOLUME I

State of Knowledge

by
David R. Basco

MISCELLANEOUS REPORT NO. 82-7 (I)

SEPTEMBER 1982

AD A122066

Prepared for

U.S. ARMY, CORPS OF ENGINEERS
COASTAL ENGINEERING
RESEARCH CENTER
Kingman Building
Fort Belvoir, Va. 22060

82 12 06 045

REPORT DOCUMENTATION PAGE		READ INSTRUCTIONS BEFORE COMPLETING FORM
1. REPORT NUMBER MR 82-7 (I)	2. GOVT ACCESSION NO.	3. RECIPIENT'S CATALOG NUMBER
4. TITLE *(and Subtitle)* SURF ZONE CURRENTS Volume I. State of Knowledge		5. TYPE OF REPORT & PERIOD COVERED Miscellaneous Report
		6. PERFORMING ORG. REPORT NUMBER
7. AUTHOR(s) David R. Basco		8. CONTRACT OR GRANT NUMBER(s) DACW72-80-C-0003
9. PERFORMING ORGANIZATION NAME AND ADDRESS Department of Civil Engineering Texas A&M University College Station, Texas 77843		10. PROGRAM ELEMENT, PROJECT, TASK AREA & WORK UNIT NUMBERS B31672
11. CONTROLLING OFFICE NAME AND ADDRESS Department of the Army Coastal Engineering Research Center (CERRE-CO) Kingman Building, Fort Belvoir, Virginia 22060		12. REPORT DATE September 1982
		13. NUMBER OF PAGES 243
14. MONITORING AGENCY NAME & ADDRESS(If different from Controlling Office)		15. SECURITY CLASS. *(of this report)* UNCLASSIFIED
		15a. DECLASSIFICATION/DOWNGRADING SCHEDULE

16. DISTRIBUTION STATEMENT *(of this Report)*

Approved for public release; distribution inlimited.

17. DISTRIBUTION STATEMENT *(of the abstract entered in Block 20, if different from Report)*

18. SUPPLEMENTARY NOTES

19. KEY WORDS *(Continue on reverse side if necessary and identify by block number)*

Coastal hydrodynamics	Rip currents
Longshore current	State-of-the-art
Nearshore circulations	Surf zone currents
Numerical models	

20. ABSTRACT *(Continue on reverse side if necessary and identify by block number)*

Investigations of surf zone currents have been conducted world wide for more than 60 years. The primary motivation has been to improve methods of understanding sediment and coastal pollution processes. This report (Vol. I) and a companion report entitled, "Annotated Bibliography of Surf Zone Currents" (Vol. II) are part of a major new study of coastal currents initiated by the Coastal Engineering Research Center in 1979. The two reports provide a

(continued)

DD FORM 1473   EDITION OF 1 NOV 68 IS OBSOLETE

state-of-the-art summary of theories and experiments investigated since 1967. The theories before 1967 have been included in previous summaries (e.g., Galvin, 1967).

Currents generated by short-period surface gravity waves both within and just beyond the breakers are of particular concern. The major types are longshore currents, nearshore circulations, rip currents, and wind-driven currents. Tidal currents are excluded. The study included the review of physical processes, theories, field and laboratory experiments, numerical models, and the measurement technology and instruments used to conduct the experiments. Related topics included are wave thrust (radiation stress) principles, wave setdown and setup, boundary and lateral mixing stress models, edge waves, wave breaking, and surf zone energy dissipation.

There are currently two major theoretical approaches to coastal hydro-dynamics, each in a different stage of development. Both approaches assume uniform currents with depth, require numerical computer methods for general solutions, and both suffer from a limited data base for verification. The older, time-averaged radiation stress theory is in the final refinement stage and is now generally accepted. The new Boussinesq theory, which is just being implemented, follows the instantaneous water surface and current variations to essentially go beyond the time-averaged mean to observe the physics occurring within each wave period.

The drawbacks and limitations of both approaches are different. The radiation stress approach requires a priori specification of wave height fields by separate means and closure coefficients obtained from time-averaged field data. The proper averaging time is unknown. A major limitation of the Boussinesq theory is the size and speed of computers needed to handle the vast grids and large number of time steps required for a meaningful simulation. Both methods rely on wave breaking and surf zone empiricism that needs considerable improvement.

Detailed state-of-the-art summaries are presented for both methods. For practical applications in coastal engineering, it is concluded that the knowledge gained from future research with the Boussinesq method will best serve to improve the time-averaged radiation stress approach and its eventual coupling to coastal sediment and pollutant transport simulations.

Accession For

NTIS GRA&I
DTIC TAB
Unannounced
Justification

PREFACE

This report (Vol. I) and the accompanying "Annotated Bibliography of Surf Zone Currents" (Vol. II) are published to provide a state-of-the-art summary of research on coastal hydrodynamics and its three main components: longshore currents, nearshore circulations, and rip currents. The two volumes concentrate on all theoretical aspects since 1967 but include physical descriptions and experimental data made much earlier. The work was carried out under the U.S. Army Coastal Engineering Research Center's (CERC) Nearshore Waves and Currents work unit, Harbor Entrances and Coastal Channels Program, Coastal Engineering Area of Civil Works Research and Development.

The report was prepared by Dr. David R. Basco, Associate Professor, Department of Civil Engineering, Texas A&M University, College Station, Texas, under CERC Contract No. DACW72-80-C-0003.

The author gratefully acknowledges the help of many individuals who contributed original copies of their journal articles and reports, and the assistance of R.A. Coleman, J. Hyden, and J. Wilkerson in completing this report.

Dr. C.L. Vincent, Chief, Coastal Oceanography Branch, was the CERC contract monitor, assisted by M. Mattie, under the general supervision of Mr. R.P. Savage, Chief, Research Division. The author wishes to acknowledge their assistance in providing useful references, technical review, and preparing the final manuscript.

Technical Director of CERC was Dr. Robert W. Whalin, P.E., upon publication of this report.

Comments on this report are invited.

Approved for publication in accordance with Public Law 166, 79th Congress, approved 31 July 1945, as supplemented by Public Law 172, 88th Congress, approved 7 November 1963.

TED E. BISHOP
Colonel, Corps of Engineers
Commander and Director

3

CONTENTS

CONTENTS

CHAPTER 3—Continued

CONTENTS--Continued

TABLES

FIGURES

6

CONTENTS

FIGURES—Continued

7

CONTENTS

FIGURES—Continued

CONTENTS

FIGURES--Continued

CONTENTS

FIGURES--Continued

CONTENTS

FIGURES--Continued

CONVERSION FACTORS, U.S. CUSTOMARY TO METRIC (SI) UNITS OF MEASUREMENT

U.S. customary units of measurement used in this report can be converted to metric (SI) units as follows:

Multiply	by	To obtain
inches	25.4	millimeters
	2.54	centimeters
square inches	6.452	square centimeters
cubic inches	16.39	cubic centimeters
feet	30.48	centimeters
	0.3048	meters
square feet	0.0929	square meters
cubic feet	0.0283	cubic meters
yards	0.9144	meters
square yards	0.836	square meters
cubic yards	0.7646	cubic meters
miles	1.6093	kilometers
square miles	259.0	hectares
knots	1.852	kilometers per hour
acres	0.4047	hectares
foot-pounds	1.3558	newton meters
millibars	1.0197×10^{-3}	kilograms per square centimeter
ounces	28.35	grams
pounds	453.6	grams
	0.4536	kilograms
ton, long	1.0160	metric tons
ton, short	0.9072	metric tons
degrees (angle)	0.01745	radians
Fahrenheit degrees	5/9	Celsius degrees or Kelvins[1]

[1]To obtain Celsius (C) temperature readings from Fahrenheit (F) readings, use formula: $C = (5/9) (F - 32)$.
  To obtain Kelvin (K) readings, use formula: $K = (5/9) (F - 32) + 273.15$.

SYMBOLS AND DEFINITIONS

A	coefficient in Longuet-Higgins' (1970) original theory
A_D	$(= \frac{\tan \beta \gamma}{8f})$, Dalrymple and Lozano (1978)[68]
a	wave amplitude; $a = H/2$
a	characterizes the vertical accelerations due to wave steepness $(= \frac{d^2h}{dt^2})$
a_o	deepwater wave amplitude
a_m	maximum horizontal excursion amplitude of wave orbital motion $(\doteq \frac{T}{2\pi} U_m)$ in shallow water
B_1, B_2	coefficients in Longuet-Higgins' (1970) original theory
b	characterizes the vertical accelerations due to bed-slope variations $(= \frac{d^2z}{dt^2})$
C	wave celerity
C_b	wave celerity at breaking
C_c	the Chezy friction coefficient
C_f	a boundary resistance coefficient due to both waves and longshore current, $\bar{v}$
C_g	wave group celerity
C_o	deepwater wave celerity
C_f^*	bed shear-stress coefficient, Huntley (1976)
c	cnoidal theory celerity
D	local rate of energy dissipation per unit area
d	water depth (bed to stillwater level, SWL)
d_b	depth of water at breaking wave
E	total energy density of the waves
$\bar{E}$	mean wave energy per unit area
E_f	fictitious wave energy per unit area

13

$E(m)$	complete elliptic integral of the second kind
erf	error function
F_x	general flux of energy toward the shore
f	Darcy-Weisbach type friction coefficient $(= 8C_f)$
$\bar{f}$	the mean frequency of the wave energy spectrum
f_c	current friction factor
f_{cw}	friction factor for waves and currents relative to total velocity
f_s	time-averaged friction coefficient
f_w	wave friction factor
g	acceleration due to gravity
H	wave height
$\underline{H}$	the stochastic wave height
H_b	breaking wave height
$H_{b,s}$	significant wave height at the breakers
$\overline{H_f^2}$	mean square value of the fictitious wave height
H_{frms}	the fictitious root-mean-square (rms) wave height
H_m	maximum possible wave height in the surf zone
H_o	deepwater wave height
H_o/L_o	wave steepness
H_{os}	deepwater significant wave height
H_{rms}	root-mean-square (rms) wave height
h	water depth to mean water level (MWL)
h_b	mean depth at breaking
I	incident wave front
I_r	Iribarren No.
$\bar{i}$	unit vector in the x-direction

$\bar{j}$	unit vector in the y-direction
K	ratio of setup slope to beach slope
k	wave number $(\frac{2\pi}{L})$
k_o	deepwater wave number $(\frac{2\pi}{L_o})$
L	wavelength
L_o	deepwater wavelength
L_r	rip current spacing
l	mixing length (Prandtl's hypothesis)
M	Mach stem
m	the corrected beach slope including wave setup
N	a dimensionless, turbulent closure coefficient for lateral wave mixing proposed by Longuet-Higgins (1970) to be of the order N < 0.016
N_L	lateral viscosity coefficient
n	wave celerity ratio, C_g/C
P	Longuet-Higgins (1970) parameter showing relative importance of mixing and bed shear
P	a parameter (= $T/\sqrt{gd_b}$) in which the magnitude of the longshore current depends, James (1974a)
P*	dimensionless mixing parameter
p	pressure at any distance below fluid surface; gage pressure
p	(=$N\rho g^{\frac{1}{2}}(\tan \beta)^{\frac{3}{2}}$) from Longuet-Higgins (1970)
p	a dimensionless parameter found from wave orbital velocity experiments relating to wave velocity at the bottom to that at the reference elevation
p	discharge per unit width at any d, y, and t
p	(uh) volumetric flow rates per unit width
Q_b	the probability that at a given point a wave height is associated with a breaking or broken wave
q	constant from Longuet-Higgins (1970) (=$(1/\pi)\rho C_f g^{\frac{1}{2}}\gamma(\tan \beta)^{\frac{1}{2}}$)
q	discharge per unit width at any x, y, and t
q	(=vh), volumetric flow rate per unit width

15

R	reflective wave front
R_e	Reynolds number ($=UL/\bar{\nu}_L$)
$\bar{R}_L$	time-averaged, lateral Reynolds number
r	constant from Longuet-Higgins (1970) $(=\frac{5}{16}\rho q^{3/2}\gamma^2(\tan\beta)^{5/2}(\frac{\sin\alpha}{c}))$
r	bottom roughness
S_{ij}	components of the radiation stress tensor
S_{ijf}	components of the fictitious radiation stress tensor without breaking
S_{xx}	time-averaged value of the total flux of horizontal momentum across a vertical plane minus the stillwater hydrostatic pressure force
S_{XX}	principal wave thrust (radiation stress) perpendicular to the wave crest
S_{xy}	the shear-stress component due to the excess momentum flux. The shear stress is exerted in the y-direction on a fluid surface constant in x
S_{yy}	component wave thrust parallel to shoreline
S_{YY}	principal wave thrust (radiation stress) parallel to wave crest
S_{yx}	the shear-stress component due to the excess momentum flux. The shear stress is exerted in the x-direction on a fluid surface constant in y
$S_{11}=S_{xx}$	transformed wave thrust component in x-direction
$S_{22}=S_{yy}$	transformed wave thrust component in y-direction
$S_{12}=S_{21}=S_{xy}$	transformed shear-stress component
T	wave period
T_o	deepwater wave period
T_L	lateral shear force
tan β*	slope of MWL due to wave setup
U	Ursell number

16

$\vec{U}$ vector sum of longshore current velocity $\vec{v}$ and bottom wave orbital velocity $\vec{U}_B$

u wave orbital velocity component on horizontal plane

u_B wave orbital velocity at the bottom

$\bar{u}_B$ mean wave orbital velocity near the bottom

$|u_{Bm}|$ the absolute value, maximum, wave orbital velocity near the bottom for sinusoidal motion

V dimensionless longshore current velocity $(\bar{v}/\bar{v}_0)$

V, v the wave orbital velocity in the YY-direction parallel to the wave crests

V a dimensionless longshore current velocity using V_B as velocity scale

$\bar{v}$ local longshore current velocity

$\bar{v}$ mean velocity across the surf zone

$\vec{v}$ longshore current velocity

V_b the breaker velocity, dimensionless

$V_{\frac{1}{2}}$ the midsurf velocity, dimensionless

V_{max} maximum V at X_{max}, dimensionless

v horizontal (y) component of local fluid velocity (water particle velocity)

$\bar{v}_b$ time-averaged velocity at breaker line, dimensional

$\bar{v}_m$ time-averaged maximum current velocity, dimensional

$\bar{v}_{\frac{1}{2}}$ time-average midsurf velocity, dimensional

$\tilde{v}$ velocity fluctuation in the y-direction

$\bar{v}^*$ longshore current velocity neglecting lateral turbulent mixing stresses

$\bar{v}_b^*$ reference longshore current velocity at the breaker line neglecting lateral turbulent mixing

$\bar{v}_{LH}^*$ modified $\bar{v}^*$ from theory of Longuet-Higgins (1970)

w	vertical (z) component of local fluid velocity or current velocity
X	$(=\bar{x}/\tilde{x}_b)$
X	a x-direction coordinate perpendicular to the wave crest
X	a dimensionless x-direction coordinate using x_B as the length scale
x	coordinate direction system where the origin is taken at the maximum setup line and a positive $\bar{x}$ is facing seaward
$\bar{x}$	a direction coordinate system where the origin is taken at the maximum setup line and a positive x is facing seaward
$|\bar{x}|$	distance from shore
$\bar{x}_b$	breaker position in $\bar{x}$ coordinates
$\bar{x}_{\frac{1}{2}}$	midsurf position
x_p	plunge point distance between the breakpoint and plunge point of a curling breaker
Y	a y-direction coordinate along the wave crest
Y	a dimensionless y-direction coordinate using y_B as the length scale
y	coordinate direction alongshore, positive to right when facing seaward
z_b	the vertical distance of the bed above an arbitrary datum and always positive
z	the bed elevation above an arbitrary datum
α	angle between wave crest and bottom contour
α	angle between wave crest and the shoreline
α_b	angle between breaking wave crest and shoreline
α_o	deepwater wave angle
$\bar{\alpha}_o$	mean deepwater approach angle
β	angle of beach slope with horizontal
Γ	horizontal (wave) mixing coefficient in surf zone, as introduced by Longuet-Higgins (1970, 1972a)

Γ	closure coefficient for the kinematic eddy viscosity
γ	ratio of breaking wave height to mean depth at breaking
γ_b	breaker index at breaker
σ	$(= \dfrac{\bar{v}(\text{measured}) - \bar{v}(\text{predicted})}{\bar{v}(\text{predicted})})$, Madsen, Ostendorf, and Reynolds (1978)
σ	scaling parameter $(= \dfrac{\eta_{max}}{d})$
ε	scaling parameter $(= \dfrac{d}{L})$
κ	von Karman Constant ≈ 0.4
$\bar{\zeta}$	mean vertical particle displacement caused by wave passage
η	displacement of water surface with respect to SWL by passage of wave
η	wave surface variation based on second-order cnoidal theory
$\bar{\eta}$	MWL change above or below the SWL
$\bar{\eta}_b$	magnitude of the wave setdown at the breakpoint
$\bar{\eta}_m$	maximum wave setup at the shoreline
λ	eigenvalues
μ	angle between $\vec{u}$ and $\vec{u}_B$
$\bar{\mu}_L$	the lateral turbulent eddy viscosity due to waves, time averaged
$\bar{v}_L$	kinematic eddy viscosity $(= \bar{\mu}_L/\rho)$
$\bar{v}_y$	kinematic eddy viscosity in the alongshore direction
ξ	amplitude of wave orbital particle displacement
ξ	surf similarity parameter, Battjes (1974b)
ξ_b	modified surf similarity parameter, Ostendorf and Madsen (1979)
ρ	mass density $(\rho = w/g)$
τ_b	bottom shear stress
τ_e	a true turbulent Reynolds stress due to random turbulent velocity interactions at scales far less than the wave orbital velocity scale

$\vec{\tau}_B$	instantaneous bottom shear stress
$\bar{\tau}_L$	the lateral turbulent eddy stress due to waves
$\bar{\tau}_{Bx}$	time-averaged bottom shear stress perpendicular to the shoreline
$\bar{\tau}_{By}$	time-averaged bottom shear stress parallel to the shoreline
$\bar{\tau}_{sx}$	time-averaged surface wind shear stress perpendicular to the shoreline
$\bar{\tau}_{sy}$	time-averaged surface wind shear stress parallel to the shoreline
$\bar{\tau}_{Lxx}$, etc.	the effective lateral stress components
Ψ	mass transport stream function
ω	wave angular frequency

SURF ZONE CURRENTS

Volume I. State of Knowledge

by
David R. Basco

CHAPTER 1

INTRODUCTION

For more than 60 years, investigations of coastal currents have been
conducted worldwide with the primary motivation of understanding sediment
transport, shoreline migration (erosion and accretion) processes, and the
transport and dispersion of pollutants. This report (Vol. I) and its com-
panion report entitled "Bibliography of Longshore and Nearshore Currents"
(Vol. II) are part of a major new study of nearshore currents in tiated by
the Coastal Engineering Research Center (CERC) in 1979.

Those currents generated by short-period surface gravity waves in water
depths generally less than 10 meters are particularly important. These cur-
rents are longshore currents, nearshore circulation cells, rip currents, on-
shore-offshore flows caused by winds, and wind-driven alongshore currents.
Articles and reports on the physical processes, theories, field and laboratory
experiments, and numerical models of these coastal flows were reviewed for
this study, along with the measurement technology and instruments used to
conduct the experiments. In addition, the following related topics were re-
viewed: wave thrust (radiation stress) principles, wave setdown and setup,
bed shear in oscillatory flow, edge waves, wave breaking, and surf zone hydro-
dynamics. Coastal currents induced by tides were excluded. Also, the vast
body of literature on fundamental, oscillatory, water wave theory, wave-current
interaction, and analytical theories for waves propagating over variable depth
bathymetry has been purposely left out. Sediment transport literature is
omitted except where coastal hydrodynamic investigations were a major part of
the effort.

Previous state-of-the-art studies and reviews were important contribu-
tions to this report. Galvin's (1967) analysis and conclusions were, no doubt,
in some way responsible for the emergence of the wave thrust theory of the
of the 1970's. Many explicit summaries of theoretical interest in longshore,
nearshore, and rip currents have ensued, including Longuet-Higgins (1972a,b),
Meyer and Taylor (1972), Jonsson, Skovgaard, and Jacobsen (1974), Miller and
Barcilon (1978), Dalrymple (1978), Komar (1976 a,b), Fisher and Dolan (1977),
and Horikawa (1978). Other valuable reviews of the literature can be found in
the doctoral dissertations of Bowen (1969a,b), Thornton (1969), Battjes (1974a,
b), Sasaki (1974-1975), Meadows (1977), and Gourlay (1978). Researchers con-
tinue to investigate various weak links in the field (e.g., Dean, 1976; Collins
1977). The ongoing Nearshore Sediment Transport Study (NSTS), sponsored by the
National Oceanic and Atmospheric Administration, will undoubtedly result in
future reassessments of current knowledge. In Europe, a recent mechanics con-
ference, Euromech 102 (1978), concentrated on new research efforts in coastal
hydrodynamics. And finally, many researchers who have developed numerical

21

simulation models of nearshore currents include extensive summaries of previous efforts (Lui and Mei, 1975; Ostendorf and Madsen, 1979; Ebersole and Dalrymple, 1979; Vreugdenhil, 1980).

The objectives of the work reported herein were to review and analyze pertinent literature for the preparation of a state-of-the-art report including major gaps in knowledge, data, and recommendations for future research. Chapter 2 gives a physical description of coastal flows, including magnitudes of currents measured in the field and the laboratory. The variability of these currents in both space and time is of primary interest. Forcing functions and mechanisms responsible for these currents are discussed. Instruments and systems devised to measure the currents are also reviewed. In Chapter 3 the fundamental equations, theory of longshore currents, and nearshore circulation are summarized. Details of all theories before 1967 are omitted. Both the time-averaged radiation stress theory and the new "Boussinesq-type" theory are presented in considerable detail; however, full derivations are not presented due to space limitations. Emphasis is on assumptions and limitations of each theory. In many cases, assumptions are made to permit analytical solutions of the appropriate equations. Numerical solution methods allow relaxation of these assumptions but at the expense of possible inaccuracies due to the researchers' discretion of the continuum. All theories and solution methods rely heavily on many empirical and relatively crude approximations in the surf zone. The chapter also includes the latest research efforts to improve on fundamental knowledge in this regard. The experimental verification (or otherwise) of the theories is the subject of Chapter 4. Unfortunately, the number of and complexities of the theories have far outstripped the number and extent of good data sets to confirm (or reject) them, so the state-of-the-art is then presented in this chapter. A brief summary, conclusions, and recommendations are given in Chapter 5.

CHAPTER 2

PHYSICAL DESCRIPTION OF NEARSHORE CURRENTS

I. FIELD OBSERVATIONS

One of the earliest known scientific descriptions of coastal currents was made by Johnson (1919). The longshore current was induced by an oblique angle of wave incidence. Undertows or rip currents were said to occur when waves struck the shore at right angles. The hydraulic currents were thought to be created by translation and asymmetric, shallow wave motion piling water up against the shore. This volume increase concept persisted for more than 50 years and even became the basis for some theories before 1967.

1. Measurements of Mean Values.

a. Longshore Currents. The wave-induced current that flows alongshore and is generally confined between the first breaker and the shoreline is termed the *longshore current*. It was first measured by Putnam, Munk, and Traylor (1949), using traveltimes and distances of floats and dye in the surf on the California coast. Currents up to 1.7 meters per second were recorded. Although, on the average, these currents are usually much smaller, these researchers reported 18 measurements that gave a mean of 0.9 meter per second. Shepard (1950) reported the results of more than 2,000 measurements of longshore currents over the entire southern California coast. Using floats, the maximum value given was only 0.5 meter per second. More detailed measurements taken at Torrey Pines Beach, California, were reported in Inman and Quinn (1955). Measurements by floats positioned near midsurf gave a maximum value of 0.4 meter per second with a mean of about 0.1 meter per second. Moore and Scholl (1961) also reported a maximum value of 0.4 meter per second using dye on an Alaskan beach. Galvin and Savage (1966) reported five measurements using floats at Nags Head, North Carolina. They obtained a maximum current of 1.3 meters per second.

Except for Shepard (1950), all these experiments included enough field information to be useful to Galvin's (1967) assessment, and they are still being used today. Since Galvin's study, more data sets have been reported but some failed to record the important independent variables. Many are extremely detailed with the introduction of an array of fixed current meters of the propeller or electromagnetic (EM) type to give continuous velocity readings. Appendix A provides a chronological tabulation of 38 experiments reported in the literature review. Also given are the range of wave data present, beach slope, observation method, and location of experiments as reported, if available in the reference. Measurements have been reported from all over the world (South Africa, Mexico, Japan, Australia, the North Sea, England, Egypt, India, Canada, and Poland). Surprisingly, no measurements could be found for the Gulf of Mexico coast of the United States. All other U.S. coasts have reported experiments, including some Lake Michigan measurements. The California coast is the most frequently observed.

23

Field experiments in the past 10 years have generally recognized the variability of longshore currents across the surf zone and down the coast. Mean values distort the true physical process. To date, the maximum longshore current value reported (see App. A) is less than 2 meters per second. Hom-ma, Horikawa, and Sonu (1962)[1] reported measurements (methods not stated) of surf zone swash reaching 3 meters per second during a typhoon in Japan (from Gourlay, 1978).

b. <u>Nearshore Circulation and Rip Currents</u>. Rip currents are narrow, strong return flows directed through the surf to sea. Together with longshore currents they can create a two-dimensional coastal current system within and beyond the surf zone termed *nearshore circulation*. The first detailed and well-documented measurements of such a system of currents were reported in Shepard and Inman (1950) for La Jolla, California (Fig. 1). Surf floats, drogues, and dye were used to measure the magnitude and directions. Mean values reported ranged from less than 0.1 meter per second outside the surf areas, 0.5 to 1.0 meter per second alongshore in the surf zone, and 0.25 to 1.0 meter per second entering into the rip currents. Detailed current speeds along the rips were not reported.

As early as 1936, Shepard reported on the qualitative aspects of rip currents (Shepard, 1936). Shepard, Emergy, and LaFond (1941) cited maximum rip speeds greater than 1 meter per second and occasionally extending more than 500 meters from the shoreline. These observations in California were confirmed by McKenzie (1958) in Australia and by Dobson and Draper (1965) on the Atlantic coast of England. The latter researchers used a theodolite to observe the speed of floats on the foam line. A maximum rip current speed of 2.5 meters per second in the surf zone was reported with a mean value of about 1.4 meters per second in the surf and 0.7 meter per second beyond the breakers. Rips were observed more than 300 meters from shore. Horikawa (1978) summarized Japanese field observations and concluded that speeds near the root are about 1 meter per second and can reach 2 meters per second under rough sea conditions. Surprisingly, there have been few actual rip current velocity measurements reported. Dalrymple (1976) presents a bibliography on rip currents that includes only 14 references to field observations. Many of these concentrated on nearshore circulation patterns as discussed below.

A series of rip currents is usually found along the coast with longshore currents feeding the rips and forming independent circulation cells. Spacings on the California coast have been reported as 30 to 100 meters (Inman and Bagnold, 1963)[2] and 400 meters on the average (Shepard and Inman, 1951). Horikawa (1978) observed some Japanese coasts with 200 to 300 meters in rip spacings and others with only 80- to 150-meter intervals. Little is known about the actual width of rip currents. Widths of 10 meters or less near their root and 30 meters at the head (beyond the breakers) are crude estimates.

---

[1]HOM-MA, M., HORIKAWA, K., and SONU, C., "Field Investigation at Tokai, Japan Conducted by Combined Procedure of Macroscopic and Microscopic Approaches," *Coastal Engineering in Japan*, Vol. 5, 1962, pp. 93-110 (not in bibliography).

[2]INMAN, D.L., and BAGNOLD, R.A., "Littoral Processes," *The Sea*, M.N. Hill, ed., Interscience, Vol. 3, New York, 1963, pp. 529-553 (not in bibliography).
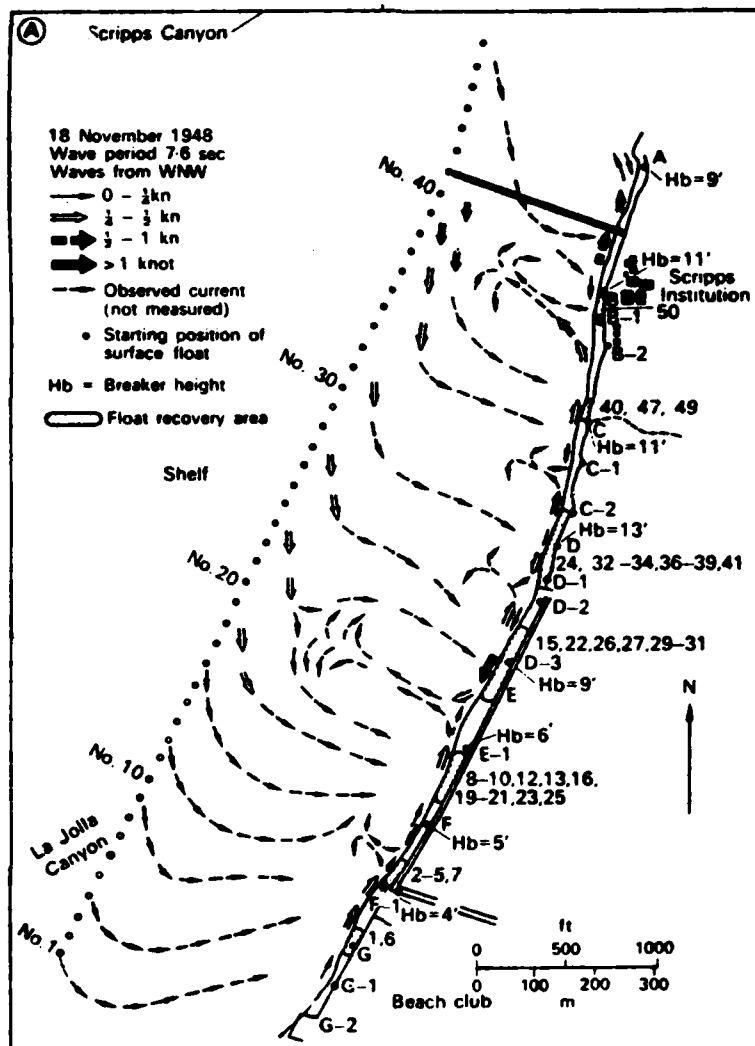
Figure 1. Nearshore current system at La Jolla Beach, California, December 1948 (from Shepard and Inman, 1951).

Shepard and Inman's (1950) early observations of nearshore circulation patterns and magnitudes in California were later confirmed and extended by Harris (1964, 1967, 1969) in South Africa and Sonu (1969a) on the northwest Florida coast. Sonu (1972), in a further analysis of these measurements, reported shoreward currents of 20 to 30 centimeters per second and rip velocities as high as 2 meters per second. Between these extremes, speeds gradually changed. When circulation velocities were low, the rip current was broad with no apparent root or stem visible. Sonu used weighted floats, dye, and a bi-directional, propeller-type current meter to obtain time-series records of

25

velocities. He also used photos taken from a tethered balloon to record dye
trajectories. These innovative techniques produced the first measurements
showing velocity variations with depth in the rip currents, and with time at
any position in the surf zone. Figure 2 shows the strengths of the circula-
tions and rip currents reported as transport velocity (i.e., flow rate per
unit width) at Seagrove Beach, Florida (Sonu, 1972).

These early field efforts concentrated on measuring mean values of the
currents in the nearshore zone and the wave heights, angles, etc. that
created them; however, it became evident that space and time variations of
the currents must also be measured. Mechanisms, cause-effect relations, and
theories stated by these researchers are discussed later in this report.

2. Space Variations of Longshore Currents.

a. Across Surf Zone. Ingle (1966) reported current measurements at
three to six points across the surf zone and beyond. A fluorescein dye patch
was timed and its travel distance noted. Although considerable scatter oc-
curred, it was noted that the largest longshore current developed midway be-
tween the swash zone and the breaker zone. Currents outside the breaker line
were small but in the same downcoast direction and never exceeded 0.3 meter
per second. The maximum velocity was 1.3 meters per second at the midsurf
position with values dropping rapidly on either side.

Galvin (1967) briefly mentions this variation across the surf, but does
not mention it as a possible reason for differences between field data and the
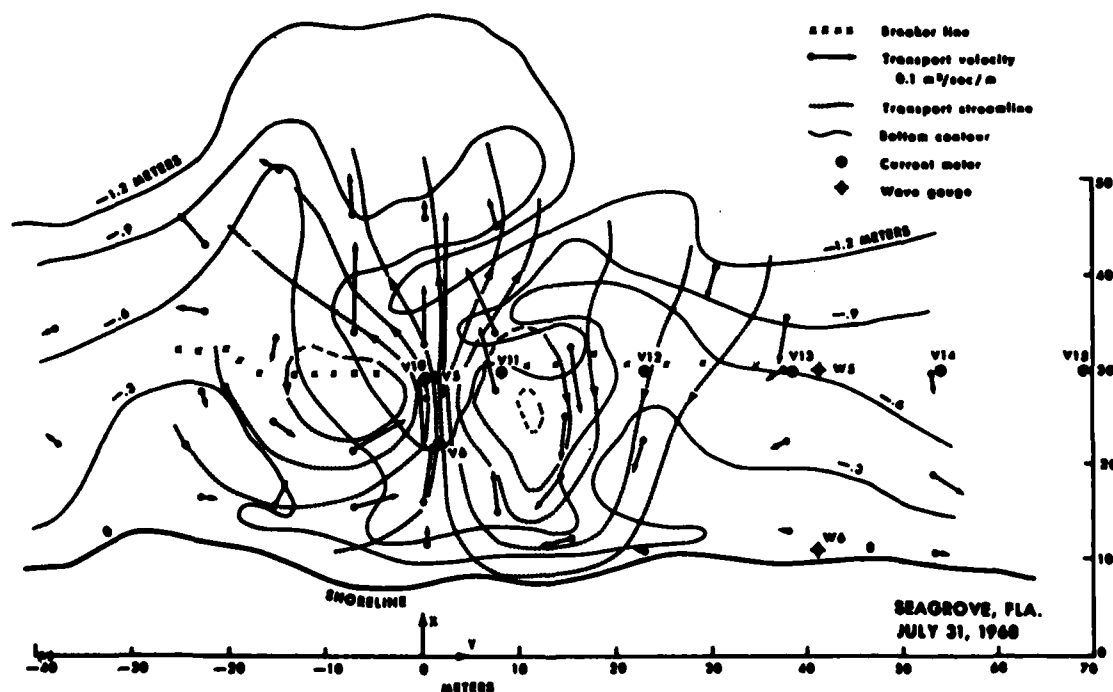
Figure 2. Rip current and nearshore currents at Seagrove, Florida, July 1968
(from Sonu, 1972).

theories of that time. Thornton (1969) discusses these early efforts and
that of Zenkovitch (1960) as examples of the distribution of longshore cur-
rent across the surf zone. Although Thornton measured currents through the
surf zone, he did not include enough detail to verify his own theories in
this regard.

About 1970, the radiation stress theory clearly demonstrated how the
time-averaged longshore current velocity must vary across the surf and beyond
the breakers. As indicated in Appendix A, some subsequent field measurement
programs have concentrated on obtaining data to validate the theory (Sasaki,
1975; Huntley and Bowen, 1974; Manohar, Mobarek, and Morcos, 1974; Wood, 1976;
Meadows, 1977; Allender, et al., 1978; Guza and Thornton, 1978, 1980a, 1980b;
Kraus and Sasaki, 1979). The magnitudes of the currents were in the same
range as those previously discussed. Unfortunately, many of these early data
sets were obtained from visual observations. Wave angle observations at the
breaker lacked the needed precision. The general trend has been to record
even stronger longshore currents in recent experiments than the maximum value
of 2 meters per second previously cited (Guza, personal communication, 1980).
This is probably due to the use of contiuous recording current meters on
solid supports that were operational during storm events. In this regard, no
evidence was found of a continuous velocity reading in the surf zone over ex-
tended time periods (months or years).

b. **Along the Coast.** It was apparent from even the earliest observa-
tions in the late 1940's that the mean current varied along the coast. This
is especially true on a scale of the circulation cell with rip currents pre-
sent or near coastal obstructions. Even on relatively straight beaches with
approximately parallel bottom contours, Inman and Quinn (1951) measured vari-
ability along the coast (measured by its standard deviation) that was equal
to or greater than the mean longshore current. Keeley and Bowen (1977)
measured mean currents over a 1-kilometer length of a Canadian beach and
found large-scale variation. Mechanisms and theories to account for the
variations will be discussed later.

c. **With Depth.** The most difficult space variable to observe is over
the water depth. Dye released in the surf will rapidly mix over the depth
and give a depth-integrated and time-averaged current value. To be visible,
surface floats must move with surface currents. Drogues help to obtain the
depth-averaged current. A vertical array of fixed current meters is the only
practical way to measure the current distribution over the depth.

Shepard and Inman (1950, 1951) made more than 1,600 observations of
surface and bottom current tendencies in the surf zone of southern
California beaches. Inside the breaker zone, their observations indicated
a net seaward drift along the bottom and a net shoreward movement at the
surface. These top-to-bottom, onshore-to-offshore tendencies were not obser-
ved beyond the breakers. Galvin (1967) stated that the nonuniformity of
currents had not been studied quantitatively at that time except as described
above, and it is assumed he meant variations over the vertical. The vertical
uniformity of the horizontal currents is implied by many field researchers
(e.g., Thornton, 1969; Komar and Inman, 1970[3]; Horikawa and Sasaki, 1972) who
never mention it.

---

[3]KOMAR, P.D., and INMAN, D.L., "Longshore Sand Transport on Beaches," *Journal
of Geophysical Research*, Vol. 75, No. 30, 1970, pp. 5914-5927 (not in bibli-
ography).

Sonu (1972) was the first to publish vertical velocity profiles from field measurements. Figure 3 shows values based on 2-minute averages in a rip current. Other similar profiles generally showed larger currents near the bed at the root (nearshore) with the maximum velocity moving upward farther seaward. Variations in current at three depths and three surf zone positions on the eastern Lake Michigan shoreline were measured by Wood and Meadows (1975). A summary of their work (Meadows, 1976) discusses time-dependent currents and says little about the vertical variations measured. A time history is shown in Figure 4. The average current is in the same direction but lower near the bottom. Brenninkmeyer, James, and Wood (1977) used two bidirectional EM current meters in the Massachusetts surf. The onshore-offshore direction was measured at two elevations. Four possible bore-backwash interaction patterns were observed along with the interactions of the bores themselves. Extremely complex three-dimensional flows result that also pulsate in time (Brenninkmeyer, 1978). In one figure in Brenninkmeyer, James, and Wood (1977), the upper current meter showed 6.6 meters per second onshore at the same instant a meter 15 centimeters below read 1.3 meters per second onshore. At other times the directions were reversed.

Zenkovich (1967) summarizes Russian thinking through 1960 and argues for a three-dimensional velocity structure in the nearshore zone. Most coasts were thought to have a bottom return flow which resulted in unstable, complicated circulation patterns with a horizontal axis. Less stable circulations with a vertical axis produced rip and gradient currents. No general picture of coastal hydrodynamics was felt possible at that time, due to complex and diverse boundary conditions and the instabilities involved.
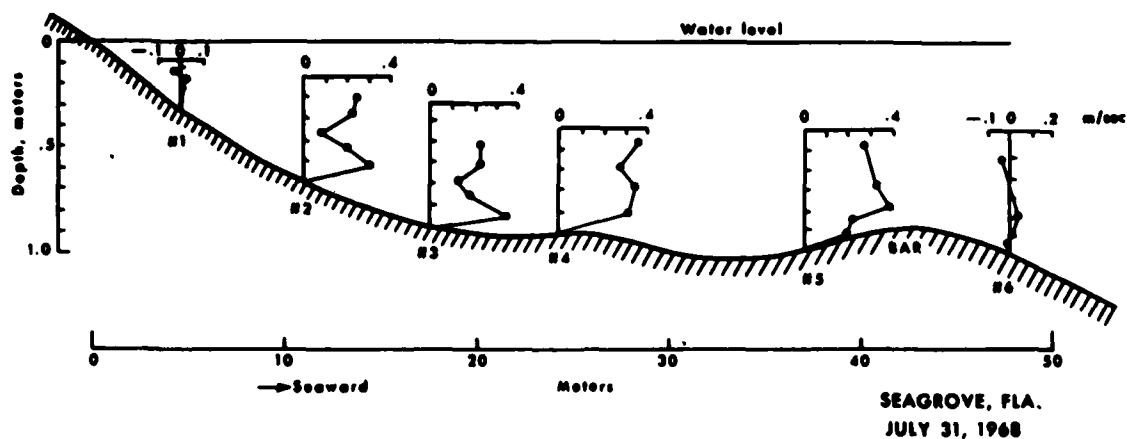
Figure 3. Velocity profile in a rip current at Seagrove, Florida, July 1968 (from Sonu, 1972).

28

UPPER CURRENT METER

MIDDLE CURRENT METER

BOTTOM CURRENT METER
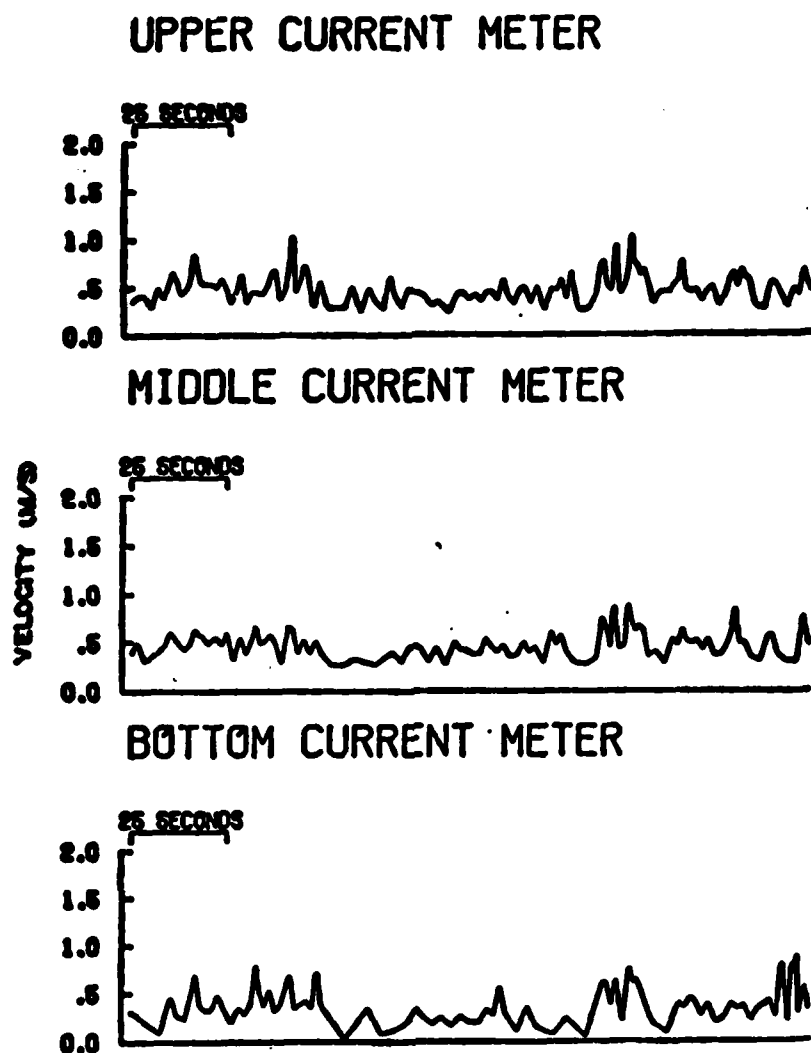
Figure 4. Longshore component current time histories at three elevations in the surf zone of eastern Lake Michigan (from Meadows, 1976).

The ongoing NSTS project assumes a uniform vertical velocity structure in the surf zone, in that no vertical current meter arrays are employed. However, the rip currents are being observed by a portable device that permits vertical velocity profiles to be taken (Gable, 1979). No results of vertical distributions are available at this writing.

3. Time Variations

By definition, the longshore current is a time-averaged current. Early field measurements with floats, dyes, drogues, etc., measured distance traveled over finite-time increments to obtain a mean value over the time interval employed. These are Lagrangian views of the velocity field. The use of continuous recording velocity meter arrays during the 1970's has permitted local Eulerican velocity fields and their time histories to be constructed. As shown previously (Fig. 4) and in Figure 5 (Dette and Fuhrboter, 1974), the longshore velocity components vary considerably with time and within a wave period. Early researchers gave little thought to the time interval for use in calculating the longshore current, but it has now become the central issue. The velocity recorded is due to the wave orbital motions, local return flows, mass transport by waves, tidal gradients, surface wind shears, effects of rip current shears, turbulent eddies, and other factors as discussed in more detail in a later section. Figure 5 also shows a mean longshore current value of $\bar{V}_L$ = 0.97 meter per second which is apparently the average over the 28-second record shown. Why was this time interval employed? Use of a shorter time interval such as the time for wave height repetitions (i.e., the wave period) would clearly give longshore current values that change in time (Fig. 5). Thus, Dette and Fuhrboter (1974) were perhaps the first to claim that longshore currents could not be regarded as steady or quasi-steady flows. They showed fluctuations in the range of ± 100 percent that occurred with periods from 1/4 to 1/9 of the wave period. A mean longshore current of 1.0 meter per second commonly fluctuated from 0 to ± 2 meters per second within shorter time intervals.

Somewhat similar results were reported by Wood and Meadows (1975) and Meadows (1976, 1977). Using demeaned (averaging time about 15 minutes) and band pass filtering techniques on the time series (see Fig. 4), Meadows concluded that the mean longshore current velocity varied in time at any point due to the horizontal wave particle velocity and a longer period component due to nearshore zone-induced wave interactions. An analysis was also made of the phase lag between the water surface time series and the surface longshore current time series. The long-period component was generally in-phase and the wave orbital component (short-period) was out-of-phase. Meadows (1976, 1977) stated that these fluctuations were at times more than 150 percent of the mean longshore current. Variations occurred over time periods of 3 to 80 seconds, i.e., at periods about equal to or greater than the wave height periods present (4.2 seconds).

Although primarily interested in the three-dimensional structure of the velocity field in the surf zone, Brenninkmeyer, James, and Wood (1977) also commented on the time histories of their velocity measurements. They found many strong oscillations within any one breaker period, the components of which appeared to move together. Maximum velocities (different values) were recorded in three component directions at the same time, indicating a dominant velocity vector. Superimposed were smaller, higher frequency oscillations with opposite phases. These were thought to show the secondary water motions (vertices and helices) found within a bore.

30
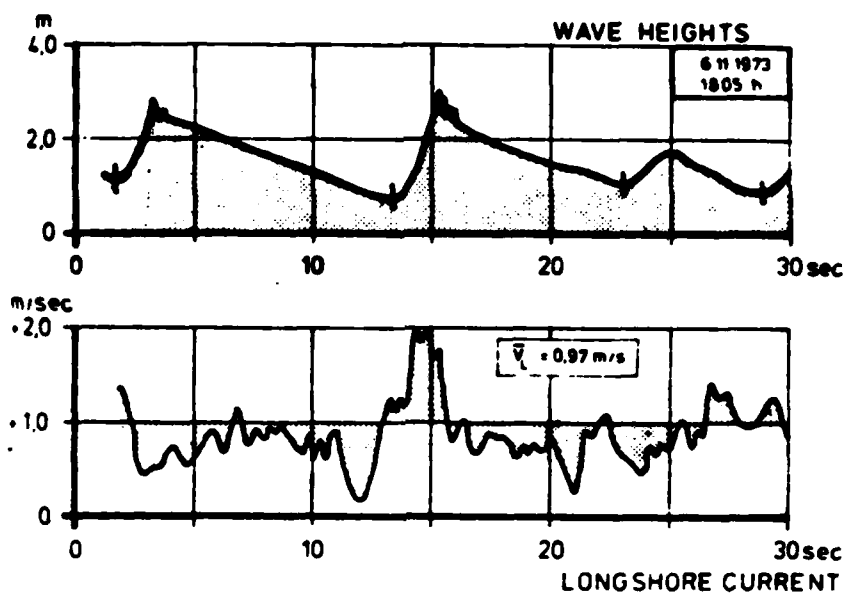
Figure 5. Time history of longshore velocity and wave height in surf zone
of North Sea, Isle of Sylt, Germany, November 1973 (from
Dette and Fuhrboter, 1974).

Six biaxial EM current meters were used to study variability of long-
shore currents in the inner surf zone at Torrey Pines Beach, California, in
March 1977 (Guza and Thornton, 1978). The ultimate goal was to test
theories relating mean longshore current and offshore values of radiation
stress (see Ch. 4). Figure 6 shows the meter array locations and some
longshore current values based on a 1,024-second (17.07 minutes) means of
the continuous records. They concluded that even on a relatively straight
beach such as Torrey Pines, with no obvious rip structures or visible
variations of the incident wave field, considerable time variations of
mean longshore currents can occur; considerable longshore spatial varia-
bility of the longshore current is also present. Spectral analysis of
more than 100 records over a month period (60 hours of observations) showed
the presence of large, low-frequency (long-period) components in the long-
shore current similar to those described by Woods and Meadows (1975) and
Meadows (1976, 1977). The temporal fluctuations are not site- or wave
regime-related since they have been observed in southern California, on the
Great Lakes (Woods and Meadows 1975), and also in the Atlantic, Nova Scotia
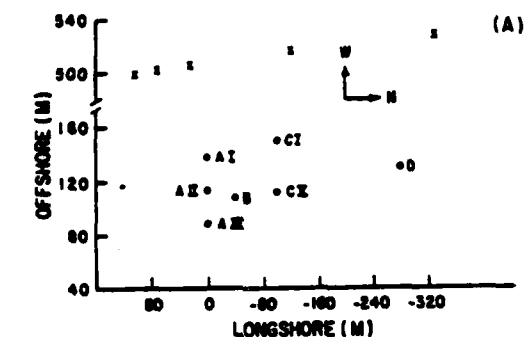
31
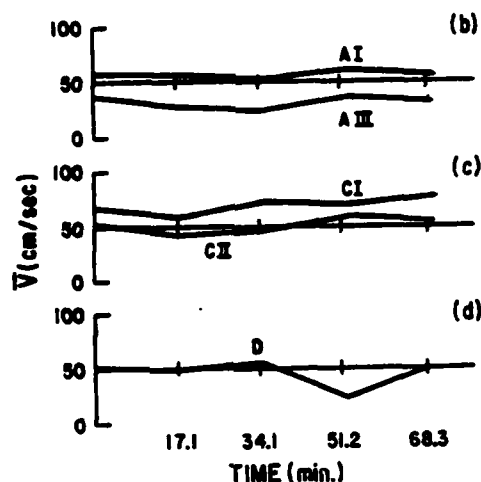
Figure 6.   Temporal variation of averaged (1,024 seconds) longshore currents
            at five locations in surf zone, Torrey Pines Beach, California,
            March 1977 (from Guza and Thornton, 1978).

(Holman, Huntley, and Bowen 1978)[4]. To study further the question of averag-
ing time, Guza and Thornton (1978) made additional 256-second (4.3 minutes)
averages from five closely spaced current meters (14-meter maximum separation)
at Scripps Institute Beach, La Jolla, California. Figure 7 shows how the
variations occur together indicating all meters were operating. Since a varia-
tion as much as 20 centimeters per second occurs at essentially the same loca-
tion, the 4.3-minute averaging time is not representative of the mean for long
time scales. It is concluded that:

        "An appropriate temporal averaging time for mean long-
        shore currents is not known." (p. 768)

[4]HOLMAN, R.A., HUNTLEY, D.A., and BOWEN, A.J., "Infragravity Waves in Storm
   Conditions," *Proceedings, 16th Coastal Engineering Conference,* Vol. I,
   Hamburg, 1978, pp. 268-284 (not in bibliography).
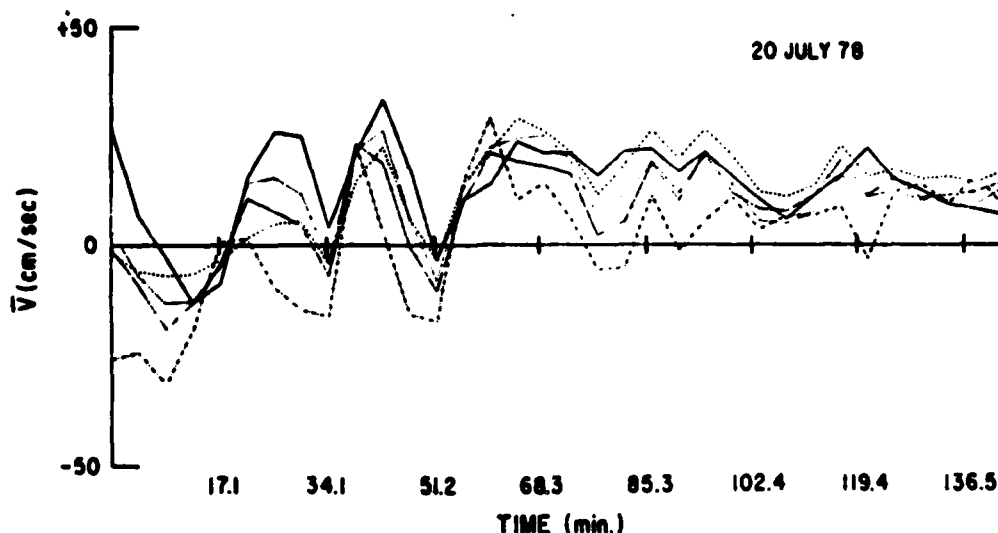
Figure 7. Time history of averaged (256 seconds) longshore current from five
closely spaced current meters, Scripps Beach, La Jolla, California,
July 1978 (from Guza and Thornton, 1978).

The latest results of the NSTS longshore current measurements are also
being analyzed by Guza and Thornton. Some early results of their November
1978 measurements at Torrey Pines, California, were reported in Guza and
Thornton (1980a). Again, 17.1-minute averages were used to obtain mean
values. The spatial and temporal averaging scales necessary to obtain mean
longshore currents will be discussed in a future paper by Guza and Thornton.

As indicated in the above discussion, longshore current space variations
can extend for considerable distance along the coast (nearshore circulation
cells), normal to the coast (surf zone widths), and vertically (water depths),
as might be expected. Time scales for velocity variation extend from frac-
tions of incident wave periods in seconds to minutes and beyond, depending
upon the coastal phenomenon of interest. The very definition of longshore
current as a time-averaged velocity is now subject to review since a univer-
sally accepted averaging interval is not known. This result may not have
been expected, and it follows a general trend in science and especially in
physical oceanography. As new instruments are used with better resolution,
new phenomena are discovered. Also, the shear volume of the numbers collec-
ted (millions for the NSTS project) make analysis time consuming. The
variability of field observations in time and space has made the use of
controlled laboratory experiments attractive to researchers, as discussed in
the next section.

33

II.   LABORATORY OBSERVATIONS

1.   Summary of Data.

There have been few general laboratory studies of longshore currents and nearshore circulations.   The 12 reviewed during this study are tabulated in Appendix B.   Monochromatic waves were used in all cases.   A maximum long-shore current of 0.7 meter per second was observed, and wave heights ranged up to 14 centimeters, with periods generally between 0.7 and 3 seconds. For space reasons, beach slopes were larger than in nature and about 0.1 for most tests.   A wide range of wave approach angles was tested.

The major studies before 1967 (Putnam, Munk, and Traylor, 1949; Saville, 1950[5]; Brebner and Kamphuis, 1963; Galvin and Eagleson, 1965) were thoroughly reviewed and discussed by Galvin (1967).   They continue to be used today to validate analytical theories and numerical models (e.g., Ostendorf and Madsen, 1979). ·

Krumbein's (1944) study on a movable bed used a 30° beach slope and was mainly concerned with sediment transport.   Data from it are not useful for relating to natural beach conditions.   Saville's (1950)[5] data, although for a 1 on 10 slope, are also of limited value.   Circulations in the vicinity of a coastal jetty were determined by Shimano, Hom-ma, and Horikawa (1958), but details were lacking as to how the velocities were measured.

Three studies (Putnam, Munk, and Traylor, 1949; Brebner and Kamphuis, 1963; Galvin and Eagleson, 1965) measured longshore currents induced by essentially two-dimensional, horizontally propagating, monochromatic water waves breaking on plane stationary, impermeable fixed-bed laboratory beaches set in basins with constant approach depths.   Velocities in the surf zone were measured by the traveltime on dye patches, immiscible fluids, or wooden floats.   Surface floats were found to move 1 to 10 percent faster than dye patches (midpoint), as measured by Galvin and Eagleson (1965).   These researchers also used a miniature current meter (5/8-inch diameter) to measure velocity profiles across the surf zone and along the beach. Unfortunately, in some cases, the instantaneous water depth was less than the diameter of the meter propeller.   The wave tank conditions were steady in time, so that it was tacitly assumed in all these studies that longshore currents were independent of averaging times (traveltimes).   As Galvin (1967) pointed out, velocities were measured at approximately the same (midpoint) position on the beach, thus reducing the influence of nonuniformity along the beach due to the end-wall effects; however, a spatial mean longshore current was never defined.   Brebner and Kamphuis (1963) measured dye travel just inside the breaker line and called this the maximum longshore current.

For some unknown reason, it was more than 10 years before the next mean-ingful laboratory investigation took place.   Perhaps Galvin's concern with the nonuniformity in profiles along the beach for closed basins and the subse-quent theory of longshore currents profile for infinite beaches made

---

[5]SAVILLE, T., "Model Study of Sand Transport Along on Infinitely Long Straight Beach," *Transactions American Geophysical Union*, Vol. 31, 1950, pp. 555-565 (not in bibliography).

researchers leery of laboratory basins for verifying the new theory. Gourlay (1976, 1978) avoided this problem by concentrating on the non-uniform system generated on a beach behind an offshore breakwater. The study employed an idealized geometry, in that the beach planform permitted simultaneous wave breaking crests parallel to the beach at all times. The alongshore gradient of breaking wave height resulted from diffraction in the lee of the offshore breakwater. The wave-generated longshore current and nearshore circulation system studied by Gourlay (1978) is shown in Figure 8. Spherical floats made of sealing wax (19 and 13 millimeters) were photographed with a movie camera to determine surface velocity distributions and circulation patterns (see Fig. 8). Current velocity profiles normal to the beach varied in shape at various positions along the beach, as anticipated. Figure 8 shows maximum surface current at about 0.4 meter per second along section I and well inside the surf zone. The scale of this model and variables were similar to those previously discussed (wave heights up to 12 centimeters, periods from 0.7 to 1.5 seconds, and a beach slope of 0.1).
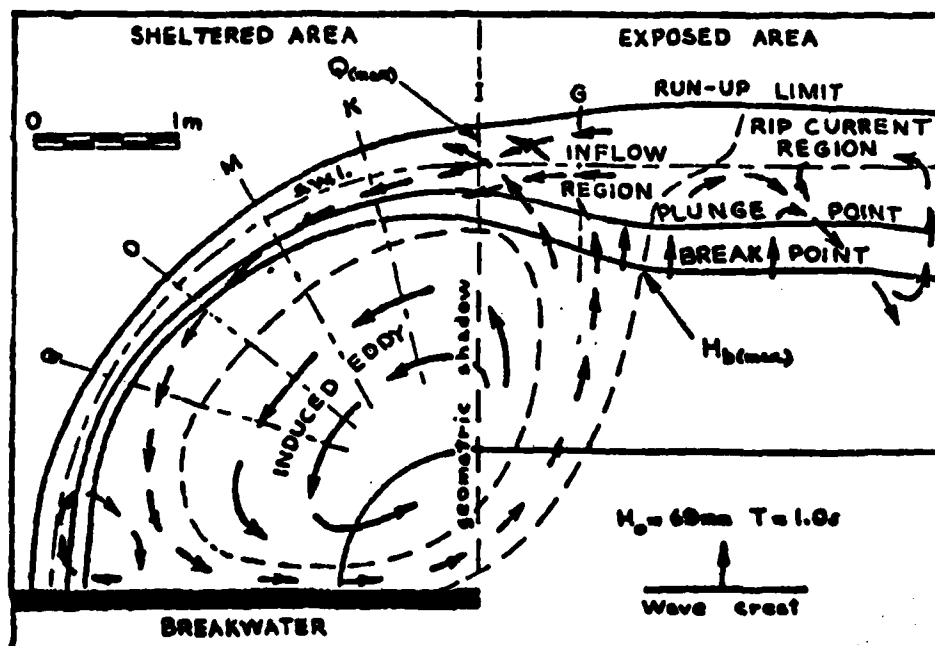
Figure 8. Wave-generated current system behind offshore breakwater (from) Gourlay, 1978).

Gourlay (1978) also measured the longshore and onshore-offshore vertical velocity distributions at section I in Figure 8. A specially constructed Pitot tube (pitometer) with forward and rear facing total head tubes was developed and calibrated to give results said to be qualitatively

35

satisfactory. No dynamic calibration was attempted. Nevertheless, information concerning vertical velocity distributions could be obtained as shown in Figure 9. At the inflow region, a helicoidal component was observed with a clockwise circulation with contours shown in Figure 9(a) for the longshore currents. The pitometer only measured velocities below the wave troughs (solid line) and these are connected (dotted line) to surface float values (MWL) to complete the isovelocity patterns. The maximum longshore current velocity occurred below low water levels near the midsurf area and was somewhat larger than the surface float values. All longshore vertical velocities were in the same direction at each location in the section. This was also true for the onshore-offshore vertical distribution (Fig. 9, b), except for a narrow zone near wave breaking. These velocities were offshore dominated by backwash in the upper layers and had onshore components near the bottom. It is obvious that the total velocity pattern is extremely complex at this location (section I) and for the circulation patterns induced by the breakwater. Gourlay's research was performed between 1971 and 1972 in Australia.

The results of some recent longshore current profile studies in Japan (Mizuguchi, Oshima, and Horikawa, 1978, in Japanese)[6] have been summarized by Kraus and Sasaki (1979). A 9-meter-long beach of plain concrete with a 1 to 10.4 slope was utilized. A propeller-type current meter measured the current at 15 to 20 points across the surf zone and averages were taken in the vertical direction. Wave period was held constant at 0.8 second, breaker heights were only 3 to 4.5 centimeters, and approach angles ranged from 4° to 15°. Maximum velocity recorded was 22 centimeters per second when the largest breaker angle was present. Kraus and Sasaki (1979) mentioned that the current velocity profile variation in the alongshore direction was monitored and ". . . no systematic acceleration or other significant anomaly in the alongshore direction was recorded." These researchers were obviously concerned about basin end-wall effects. It is not stated how nor over what alongshore distance this uniformity was obtained. A nonuniform profile created by basin end walls is not the only difficulty faced by laboratory researchers.

2. Laboratory Boundary and Scale Effects.

Dalrymple, Eubanks, and Birkemeier (1977) studied the mean wave-induced circulations in enclosed basins. They organized the previous studies and basins employed into three categories:

(a) Surf zone openings in both waveguide walls to permit recirculation outside the waveguide walls. The recirculation occurs behind and beneath the wave generator or through a pipe beneath the beach (used by Brebner and Kamphuis, 1963). The updrift current is enhanced by pumping to increase the length of the usable test section with uniform current profile (Kamphuis, 1977).

---

[6]MIZUGUCHI, M., OSHIMA, Y., and HORIKAWA, K., "Labora ry Experiments of Longshore Currents," *Proceedings, 25th Coastal Engineering Conference of Japan*, 1978, in Japanese (not in bibliography).
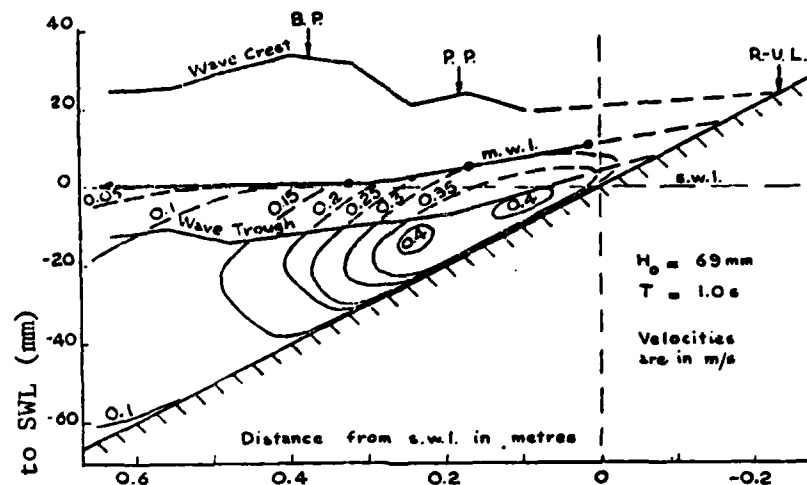
a) Alongshore vertical velocity distribution at profile
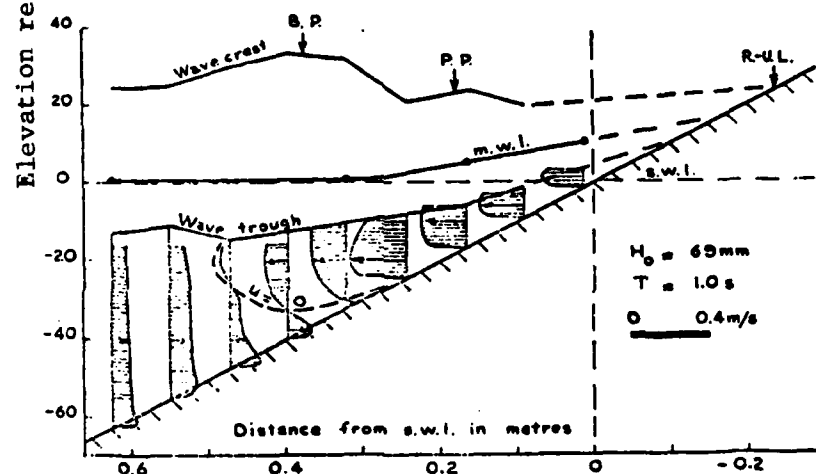
b) Onshore-offshore vertical velocity distribution at profile

igure 9. Vertical velocity distribution at profile section I for (a) long-
shore current and (b) onshore-offshore current (from Gourlay, 1978)

(b) A completely enclosed wave basin (used by Putnam, Munk, and
Traylor, 1949, and Saville, 1950).

(c) One surf zone opening in the downstream waveguide wall and
clearance beneath the wave generator board to permit recir-
culation (used by Galvin and Eagleson, 1965).

They conducted a theoretical analysis using radiation stress theory (Ch. 3) and the various types of boundary conditions for these categories. Although their theory neglected some of the terms in the equations of motion, their results did show that the mean circulation in the basin is strongly affected by the basin geometry. However, in the surf zone near the center of the basin, all three basin types gave similar theoretical results. Dalrymple, Eubanks, and Birkemeier (1977) therefore concluded that if a working recirculation procedure was devised, the type (a) basin would reduce the amount of return flow in the offshore region. The longshore current would be closer to that found on an infinite beach, since wave basin recirculating currents would not be included.

The aim of recent research efforts at the Delft Technical University (Fluid Mechanics Laboratory), The Netherlands, is to develop such a test basin (Visser, 1980). The criteria for proper longshore current flows in a laboratory basin are (a) a uniform current profile along the beach and (b) a zero slope of the MWL in the longshore direction. The width of the longshore current openings in both upstream and downstream waveguides and the recirculation flow rate must be adjusted empirically to determine an optimum combination. However, in a laboratory basin, MWL variation along-shore is difficult to measure. Consequently, the recirculation flow rate offshore and between the waveguides, Q_c, is used as an alternate criterion. In this method, the wave basin geometry (waveguide openings) and the pumped, recirculating flow rate, Q_r, are varied and a minimum Q_c found. It is then hypothesized that this Q_r gives the correct longshore current flow rate, Q, for a uniform current profile. Lower Q_r value will cause the excess Q to return offshore and raise Q_c. Conversely, higher Q_r values will generate a surplus wave circulation flow and also increase Q_c.

The method was verified by a series of well-planned meticulous experiments in a 16.6- by 34-meter wave basin with 20.9 meters between the waveguides. Regular waves are generated on a smooth concrete floor and 10:1 plain beach in 0.4-meter still water. The recirculation is through an 0.8-meter-diameter pipe beneath the beach to a pump on the updrift side. All tests were conducted with waves of 2-second period, 10.5 centimeters in height, and an incidence angle of about 21° at breaking. The depth-averaged mean velocity at a measuring point was calculated as the mean of the surface, bottom, plus twice the middepth velocity. The traveltime of a dye cloud over 0.8 meter was used to calculate velocity in the surf zone. To increase accuracy, two people made independent observations and a minimum of 20 independent readings were averaged to give one surf zone measurement at each depth. Also, the dye was injected at different wave phases during these readings to eliminate the influence of the orbital velocity on the measurement. These stringent procedures were relaxed in regions with slower currents and less turbulence. Flush-mounted piezo-meters on the beach and resistance wave probes measured MLW. The

38

volumetric flow rate was computed between adjacent points from the mean ve-
locity and MWL measured at these points. A maximum, depth-averaged longshore
current of 0.67 meter per second was measured abou.t midway in the surf zone.

This optimization based on minimizing Q_c proved successful. In addi-
tion, use of a flow distribution system in the upstream waveguide wall
that extended beyond the breaker line increased the region for uniform
current profile upstream to section 3, as shown in Figure 10. For con-
trast, results for essentially a type (a) basin are shown in Figure 11 as
found by Visser (1980). Major differences in profile shape are evident
at the midtank position (section 2). For the wave field-basin combination
employed, the author concluded that a rational procedure to establish a
uniform longshore current profile had been achieved. Thus it is now poss-
ible to use other wave fields and basin geometries and the methods devel-
oped to obtain uniform current profiles in the laboratory without lengthy
trial-and-error efforts. Additional tests are presently underway. These
studies also proved that considerable deviation in a uniform profile can
occur in nonoptimized basin geometries with improper recirculation flows.

Other effects due to scale are also present in laboratory models.
These result from improper representations of viscous effects (Reynolds
similarity) and surface tension (Weber number) influence on the air
entrainment during wave breaking in the surf zone. Viscous effects are
for both internal, turbulence decay, and at the boundaries from bed shear
(friction) and wind surface shear stresses. For these reasons, Dette and
Fuhrboter (1974) indicated surf zone research should be conducted only in
the field. However, all the laboratory experiments described were general
studies in which no prototype scale existed. These efforts tested the
theories available at the time and at the scale of the laboratory inves-
tigation conducted, and for this purpose they are entirely valid. The
ability to create a steady-state environment in which longshore current
measurements at a point in the surf are not dependent upon averaging time
is a major advantage of physical model studies. Surprisingly, the use of
such models to study longshore currents is not mentioned in a recent state-
of-the-art report by Hudson, et al. (1979).

Site specific model tests of longshore currents have been made (e.g.,
Gourlay, 1965[7]; Curren and Chatham, 1980) but will not be reviewed in this
report. Laboratory studies of rip currents, which are strongly associated
with forcing functions and mechanisms are discussed in the next section.

---

[7]GOURLAY, M.R., "Wave Generated Currents - Some Observations Made in Fixed
Bed Hydraulic Models," *Proceedings, Second Australian Conference Hydraulics
and Fluid Mechanics*, Auckland, December 1965 (not in bibliography).

Figure 10. Uniform, depth-averaged longshore current profiles and circulation velocities under optimum conditions of minimum circulations (Q_c = 19.2 liters per second), adjusted return flows (Q_r = 35 liters per second) and upstream distribution system (from Visser, 1980).

Figure 11. Measurements in wave basin with only surf zone openings in both waveguides and free recirculation (no pump) (from Visser, 1980).

III. FORCING FUNCTIONS AND MECHANISMS

A number of natural forces, geometric features, fluid properties, and sediment characteristics interact to create longshore currents, nearshore circulations, and rip currents. The fundamental cause-effect principles were first stated by Johnson (1919). Waves attacking the coast at oblique angles produced longshore currents while those arriving normal to the coast created rip currents. Thirty years later Shepard and Inman (1950) demonstrated how wave ray convergence and divergence patterns resulting from offshore bathymetry created regions of high and low breakers along the coast and explained nearshore circulation cells that result. Offshore return flows and rip currents occur where low breakers are found. The direction and period of approaching waves were also a factor in whether a longshore current system, a nearshore circulation system, or a mixed system was observed. These conclusions on forcing functions (wave characteristics, hydraulic water surface gradients) and mechanisms (offshore and local bathymetry) are still valid in explaining many coastal flows. A general classification of nearshore current systems by Harris (1969) is shown in Figure 12. Oblique wave attack produces longshore currents on plain, straight beaches. Normal wave attack is accompanied by some mechanism that triggers rip currents and also causes water surface gradients, producing currents normal and alongshore, i.e., circulation cells separated by the rips. The asymmetric case corresponds to the mixed system where the offshore flows (rips) are found to meander or move along the coast with a net longshore current translating down the coast.

Other forcing functions (tides, surface wind stress, atmospheric pressure) and mechanisms (wave interactions, boundary interactions) have been postulated to help explain the space and time variations observed in the field or laboratory. Continuous recording current meters at a fixed-point location in the surf indicate velocity variations due to many causes. The instantaneous velocity is due to wave orbital velocities, the rollers and eddies from wave breaking, bottom and rip current return flows, mass transport, tidal currents, wind-generated currents, currents due to mean water surface gradients (however induced), density-driven currents, bed shear-generated turbulence, and currents resulting from the excess momentum along the coast produced by wind waves breaking at an angle. All these currents can have components directed alongshore or onshore-offshore during some time interval. Some are random or periodic so that no net current results over a standard averaging period. The forces that create these currents are discussed in further detail below.

1. Forces Causing Currents in Alongshore Direction.

a. _Wind-Generated Waves_. Averaging water wave orbital motion over the wave period will result in a net longshore current under certain conditions.

(1) _Momentum Thrust_. Longuet-Higgins and Stewart (1962) set the principles by which gravity water waves, when integrated over the water column and averaged over the wave period, produce a net horizontal thrust (force) above the local hydrostatic force. A physical description can be found in Longuet-Higgins and Stewart (1964). The term "radiation
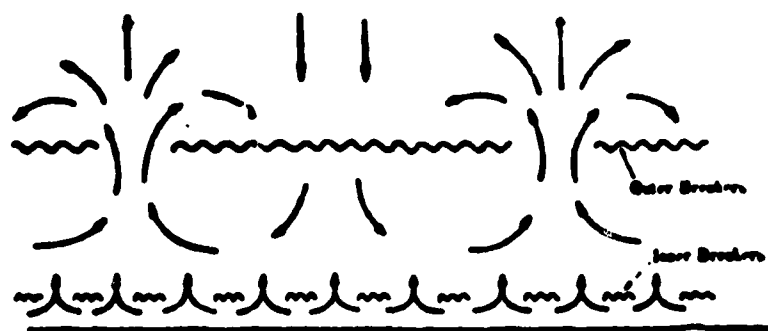
SYMMETRICAL CELLULAR

ASYMMETRICAL CELLULAR (MEANDER)

ALONGSHORE SYSTEM

Figure 12. Nearshore current classification system (after Harris, 1969).

42

stress" was employed to describe this wave-induced thrust even though the units were force per unit length and not a true stress. About the same time, Lundgren (1962, 1963) discussed these same principles as a wave-induced thrust and derived similar expressions which were later corrected (Danish Technical University, 1969)[8]. The term radiation stress is now generally accepted for this forcing function. It has significantly helped to unravel the mystery of how oblique wave attack can generate longshore currents that baffled scientists and engineers up to 1970. The general principles and equations associated with the radiation stress theory are summarized in Chapter 3.

The local streamline curvature of rapidly varied, free-surface flows gives rise to vertical accelerations that also change the hydrostatic pressure distribution assumption. In 1872, Boussinesq derived expressions to account for this effect in the horizontal equations of motion for nearly horizontal free-surface flows, and an additional term (or terms depending upon the order of accuracy of the derivation) that permits frequency dispersion and wave propagation of permanent form. No time averaging is involved. Called the "Boussinesq Theory," it offers an alternative way to introduce the lateral momentum thrust due to gravity waves.

(2) **Mass Transport**. Time-averaging nonlinear waveforms result in a net drift velocity because particle orbits are not closed. The current that results is very small and can be considered negligible in the surf zone and beyond the breakers. After breaking, mass transport by translation of hydraulic bores through the surf can not be neglected.

The wave characteristics of interest are height, period, and angle of crest with the shoreline. The values at the first breaker line are reportedly the most significant. Surf zone transformations are discussed separately.

b. **Tides**. The tides create currents alongshore that are relatively small except near inlets. These currents have been omitted from this review. However, as mentioned by Sonu (1972), the slow water level changes induced by tides change the wave breaker location, hence the surf zone width, and ultimately affect the strength of wave-induced longshore currents. Also rip currents were found to be stronger at low tide and pulsated with a 25- to 50-second beat. The weaker rips at high tide fluctuated at the swell period.

c. **Wind Surface Shear**. The wind moving across the water surface has a vertical velocity distribution that gives rise to a surface shear stress. As a result the water surface layers move at a speed of about 3 percent of the mean windspeed above the boundary layer. Viscous processes (both molecular and eddy type) transport this momentum down into the water column. In large water bodies, Coriolis forces will cause the current to deflect to the right of the wind direction (facing downwind, Northern Hemisphere) and spiral away from the wind direction (Ekman motion). These classic deepwater oceanographic concepts can be

---

[8]DANISH TECHNICAL UNIVERSITY, ISVA, "Index to Reports," Report No. 20, Dec. 1969, Lyngby, Denmark (not in bibliography).

misleading in the surf zone when winds blow overland from the shore, and shallow depths allow bottom boundary layers to interact with wave breaking turbulence at the surface.

The importance of winds was mentioned by Shepard and Inman (1950). Field experimenters, however, find it difficult to differentiate effects of wind shear from short-period wind waves and the currents they generate. Linear multiregression analysis has been attempted to separate the relative importance of independent variables to generate the longshore current. Harrison and Krumbein (1964) found windspeed to rank ahead of offshore wave direction. If breaker angle was used instead, the result would be reversed which points out difficulties with regression studies if the wrong variables are employed. Sonu, McCloy, and McArthur (1967) found wind to be the second most important field variable influencing longshore current. Field tests of wind data should be recorded if comparisons are to be made. A recent study by Nummedal and Finley (1978) evaluated whether or not the inclusion of additional physical parameters (other than wave field characteristics) could significantly improve current predictions. More than 250 observations were made over 1 year at Debidue Island beach, South Carolina, using the Littoral Environmental Observation (LEO) program. Four, widely varied equations for longshore current prediction were used to evaluate the linear combinations of wave and other physical parameters, including the longshore component of wind velocity. It was invariably found that this wind component explained most of the observed variance in the current velocity. Consequently, their statistical data analysis suggested that wind stress is an important factor in longshore current generation.

Further strong evidence supporting this conclusion came when Dette and Fuhrboter (1974), in their North Sea experiments using EM current meters located at middepths, concluded that high longshore current velocities (up to 1.5 meters per second, means) could be expected during two different weather patterns:

(1) Heavy storms with high breakers (>3 meters) and small wave breaking angles (<25°).

(2) Winds blowing parallel to shore with low breakers (<1 meter) but large breaking angles (>25°).

When the wind blew parallel to the shoreline and shifted from south to north, the mean longshore current changed almost at the same time to create mean currents in opposite directions of more than 1 meter per second. Between these patterns winds blew from land to sea, small waves were present and longshore currents were near zero. Windspeeds were 5 to 10 meters per second.

Fox and Davis (1971, 1976) included the barometric pressure which causes the winds in their empirical analysis. They directly related local time variations (days) of barometric pressure to a longshore current velocity which varied in time (days) as well. The correlations

were based on experiments in Lake Michigan where local storm fronts
control the wave heights and windspeeds. This work made no effort to
separate the wave- or wind-generated currents.

Fundamental studies on boundary layer profiles and wind stress
in surf zones (e.g., Hsu, 1972) and wind-induced drift currents
(e.g., Tang, et al., 1978)[9] are available. Because of the significance of
winds as a forcing function, it is surprising that few specific investiga-
tions have been conducted.

d. _Planform and Bathymetry_. The shape of the coastline, the slope
of the beach face, the nearshore profile, bar formation, and offshore
bathymetry all influence longshore currents. These geometric features
primarily dictate the variation along the coast of the type, height, and
location of breaking waves. These are the primary mechanisms for near-
shore circulation and rip currents formation, as described in further
detail in the section on rip currents.

Beach-face slope and nearshore profile influence variations normal
to the coast and can be used to distinguish two broad extremes of beach
conditions. A reflective beach system is characterized by the typical
profile shown in Figure 13(a) (after Wright, et al., 1979). Much of the
incident wave energy is reflected from the beach face. Other distin-
guishing features summarized by Wright, et al. include: (1) surging
breakers with little setup, (2) well-developed beach cusps, and (3) the
rare appearance of inshore circulation cells and rip currents. Shore-
normal current spectra also have dominant peaks at incident wave periods
(T) or subharmonics (2T). Increasing breaker heights are accompanied by
an increase in the strength of seaward flows which pulse at the subhar-
monic period. This subharmonic resonance will also dominate longshore
current oscillations.

At the other extreme, a dissipative beach system has a wide surf
zone with complex and varied topography (Fig. 13, b). One or more bars,
three-dimensional features, and different scales of circulation cells and
rips are frequently present. Subregions with contrasting turbulent
mixing intensities can be present. Wright, et al. (1979) classified
dissipative beaches into six basic subtypes. Each is dominated by a
different combination of surf zone processes and by different scales and
frequencies of resonant phenomena.

The complexity of the nearshore planform and the bathymetry asso-
ciated with dissipative beach systems is partly the reason for the wide
number of hypotheses advanced as mechanisms for triggering rip currents
and circulation cells.

2. _Mechanisms Causing Nearshore Circulations and Rip Currents_.

These flows are treated together simply because they are physically
separate parts of circulation cells that occur in the nearshore zone.

---

[9]TANG, F.L.W., et al., "Wind-induced Water Surface Set-up and Drift
Currents," _Proceedings, 16th Coastal Engineering Conference_, Vol. I,
Hamburg, 1978 (not in bibliography).
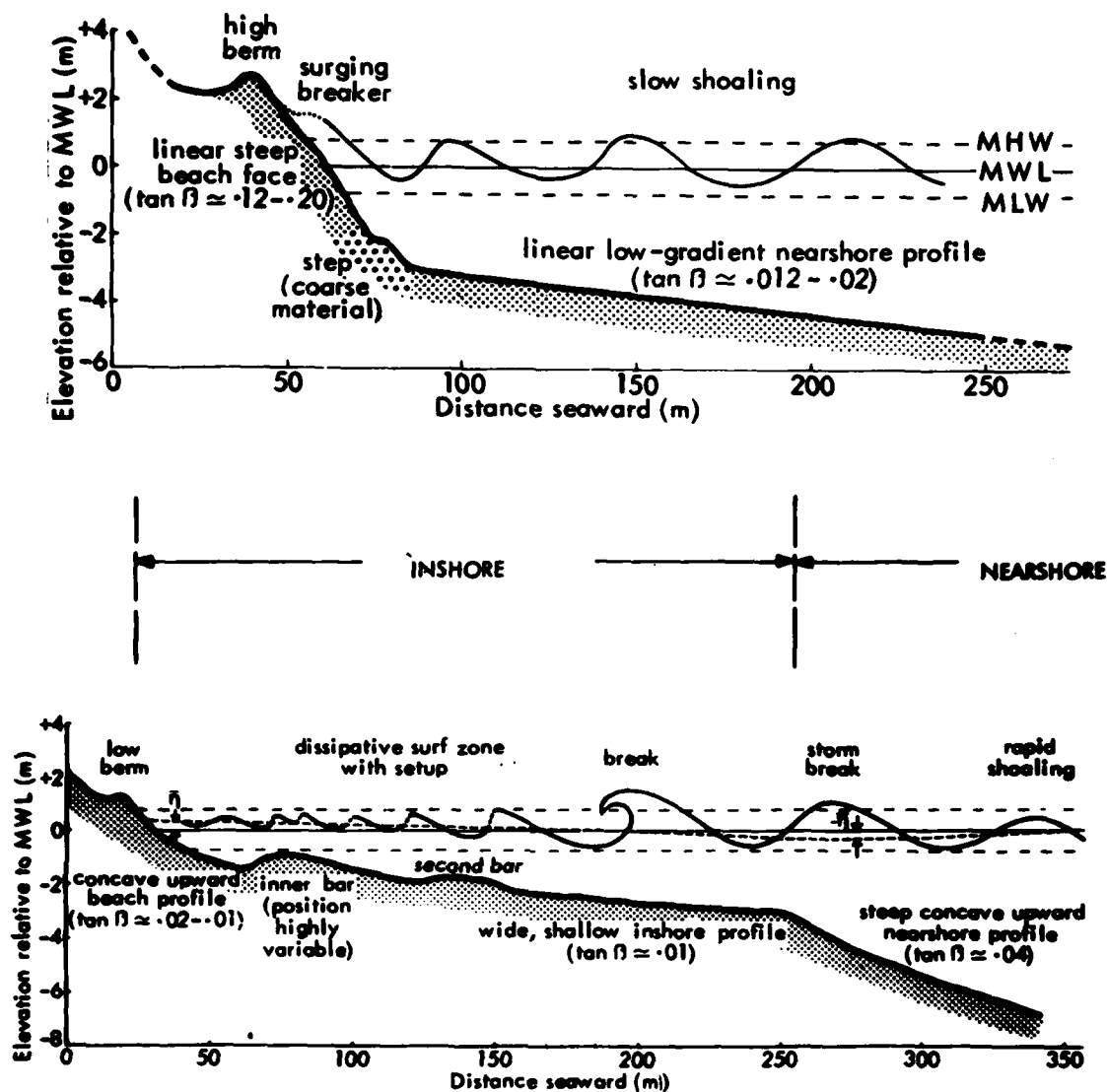
Figure 13. Beach classification system, showing (a) a reflective beach and (b) a dissipative beach (after Wright, et al., 1979).

Why do rip currents form? This question has been the subject of much debate for 40 years. The summary of various mechanisms proposed to date is taken from an excellent state-of-the-art report by Dalrymple (1978); also, Miller (1977) provides excellent summary. This section concentrates on the physics, although Dalrymple goes much further into the theory and equations supporting each model. Rip current spacing is a product of the theory.

There is no single theoretical model that can account for the presence of rip currents. Rip current generation mechanisms are divided into two main categories: (a) wave interaction and (b) structural interaction. The difference is that wave interaction mechanisms can occur on plain, infinite

46

beaches, and the second category mechanisms cannot. Table 1, as developed by Dalrymple (1978), lists these two categories and the major subclasses of mechanisms as first proposed in the literature.

Table 1. Proposed mechanisms for rip current generation and primary investigators since 1969 (after Dalrymple, 1978).

Wave Interaction Models	Primary Investigators
Incident edge wave	
Synchronous	Bowen (1969), Bowen and Inman (1969)
Infragravity	Sasaki (1975)
Intersecting wave trains	Dalrymple (1975)
Wave-current interaction	LeBlond and Tang (1974), Dalrymple and Lozano (1978)
Structural Interaction	
Bottom topography	Bowen (1969), Noda (1974)
Coastal boundaries	
Breakwaters	Liu and Mei (1976)
Islands	Mei and Angelides (1977)
Barred coastlines	Dalrymple, Dean, and Stern (1976)

a. **Structural Interaction.** The subclasses listed in Table 1 reveal that these structural interaction models are closely associated with the planform and bathymetry features previously discussed. Structural interaction probably accounts for the majority of rip currents present on the world's coastlines.

(1) **Bottom Topography.** Although Shepard and Inman (1950, 1951) correctly stated that rip currents could be related to variations in breaking wave height along the beach, it was Bowen (1969b) who explained why, using radiation stress principles. The excess momentum thrust of the waves normal to the beach produced a tilt or wave setup of the mean water surface from the breakers to the shore. Where the breakers were large the setup was large, and vice-versa. Longshore variations in breaker height created MWL gradients within the surf zone that produced currents flowing from positions of highest breaker height to positions of lowest breakers. Here, the longshore currents converge and turn seaward as rip currents, i.e., taking the path of least resistance and maintaining a mass and momentum balance. Outside the breakers a weak return flow is needed to complete a nearshore circulation pattern very similar to observed cell circulation. The bottom contours offshore causing wave

refraction was offered as one mechanism for producing the longshore varia-
tion in breaker height.

(2) Coastal Boundaries. Natural headlands or manmade lateral
barriers (breakwaters, jetties, groins) can also cause nearshore circula-
tions. The wave fields are diffracted and reflected by these structures
(some wave refractions also) causing wave breaking variations in complex
patterns. Rubble-mound structures also absorb wave energy present.
Figure 8 from Gourlay's (1978) laboratory study is a good example of a
circulation pattern in the lee of a breakwater.

(3) Barred Coastlines. From field observations and measurements
in an area with irregular bottom topography at Seagrove, Florida, Sonu
(1972) found that shoreward currents in a cell occurred over the shoals
while rips were observed over the troughs (Fig. 2). Paradoxically,
breaker heights were uniform down the coast so that the observed circula-
tion must be due to another mechanism. Over the shoals spilling breakers
were observed which continuously dissipated energy and created some setup
in the surf zone. Waves entering the rip current areas broke by plunging,
re-formed, and created little MWL change at the trough positions along the
beach. Thus, this difference in wave breaking type produced mean surface
gradients in the surf zone that were said to create the nearshore circula-
tions and rip currents present. Sonu (1972) took actual measurements and
used radiation stress theory to demonstrate theoretically that cell
circulations can be created by these conditions, i.e., a barred coastline
with seaward-directed troughs and no variation in breaker height.

An additional forcing for the circulation is suggested to stem from
wave reflection off the submerged bar (Dalrymple, 1978). Investigations
listed in Table 1 and not mentioned here will be discussed in Chapter 3.

b. Wave Interaction Models. The other major mechanism category in
Table 1 is more subtle. Circulation cells can exist on long, straight,
beaches with plain profiles as noted by Shepard and Inman (1950, 1951).
Three subcategories are presented by Dalrymple to explain how this may
occur.

(1) Incident Edge Wave. This was the earliest mechanism pro-
posed (Harris, 1967; Bowen, 1969) and first required an understanding of
edge wave modes (Eckart, 1951)[10], standing edge waves, and proof that they
actually existed on natural beaches. Waves propagating along the shore-
line or standing waves along the shoreline are termed *edge waves*. Huntley
and Bowen (1974) measured edge waves on the southern coast of England with
a period of 10 seconds that was twice (subharmonic) the incident wave
period. The theory states that incident swell waves can generate standing
edge waves of the same period or the moving type (synchronous) of the same
period on the beach. The linear superposition of these wave fields pro-
duces alternately high and low breakers along the shoreline. A regular

---

[10]ECKART, C., "Surface Waves in Water of Variable Depth," *The Theory
of Edge Waves*, Report No. 100, S10, Ref. 51-12 (not in bibliography).

pattern of equally spaced rip currents separating the circulation cells results from the same reasons as discussed for refraction.

A series of controlled laboratory test results was reported by Bowen and Inman (1969) and offered as confirmation of the theory. Regular, normally incident waves were made on a smooth concrete beach of slope 0.075. A 7.3-meter working section bounded by vertical barriers which extended seaward gave well-defined boundary conditions for the experiments. A standing edge wave was quickly formed in the basin. It was found for both swell-type waves, which did not break, and plunging-type breakers that the addition of these incident waves and the standing edge wave at the breaker position gave a longshore variation in observed breaker height. The net height was greatest where incident and edge waves were in-phase and lowest where they were 180° out-of-phase. Thus, every other edge wave antinode produced small breakers and rip currents appeared at these positions along the coast as shown in Figure 14 (from Komar, 1976a). The key aspect of these experiments and theory was that rip currents could not form unless both incident and edge waves have the same period. Their efforts to confirm the theory in the field at El Moreno Beach, Gulf of California, proved inconclusive. Synchronous edge waves could not be measured directly in the moving cell circulation system they observed (Bowen and Inman, 1969). Guza and Davis (1974)[11] showed theoretically, and Guza and Inman (1975) and Harris (1967) showed experimentally, that the most likely resonant edge wave is the subharmonic edge wave. It does not allow a rip current to form. But, Dalrymple (1978) points out that this model first proposed by Bowen (1969a) is only for steep, reflective beach systems with no wave breaking. It also requires some means such as reflection of the incident waves by a structure or headlands to create the synchronous edge wave mode.

As pointed out by Wright, et al. (1979), flat dissipative-type beaches have more circulation cells than the steep reflective-type. Tait (1970) and Tait and Inman (1969) showed that many of these beaches (east coast of the United States) have rip spacings far greater than the fundamental edge wavelength associated with the dominant, incident wavelength. Thus, there must be an additional mechanism that triggers longer rip spacing on flat dissipative-type beaches.

For wide surf zones and dissipative-type beaches (e.g., Silver Strand Beach, California), Bowen and Inman (1969) suggested that some type of surf beat phenomena of the incident waves could create longer period edge waves to produce the greater rip spacings observed. Sasaki (1977) made an extensive summary of the literature on rip current spacing including many field experiments conducted on Japanese beaches. Using surf zone width, beach slope, breaker type, and other parameters of the surf zone together with a number of empirical, dimensionless plots of the data, Sasaki defined three domains where he felt a hydrodynamically different mechanism produced the rip currents. At one extreme were the steep, reflective beaches dominated by synchronous edge waves. At the opposite extreme, for wide, flat

---

[11]GUZA, R.T, and DAVIS, R.E., "Excitation of Edge Waves by Waves Incident on a Beach," *Journal of Geophysical Research*, Vol. 79, No. 9, 1974, pp. 1285-1291 (not in bibliography).
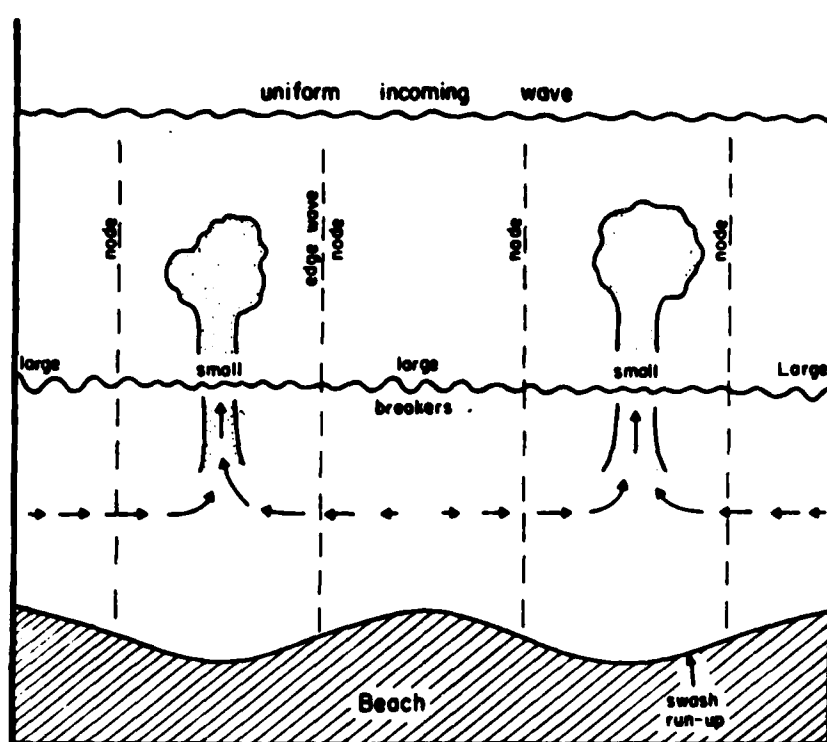
Figure 14. Positioning of rip currents at alternate antinodes of standing edge waves on a plain beach with regular incident swell waves (from Komar, 1976).

dissipative beaches, Sasaki (1977) proposed that infragravity waves 30-second to 5-minute periods) present in the surf zone trigger the rip currents with corresponding large spacings. In between, and in-stability domain was said to exist. This middle type of mechanism was classed as wave-current interaction by Dalrymple (1978).

Huntley (1976a) and Sasaki and Horikawa (1978) reported field obser-vations of edge waves with periods in the infragravity domain that are a major component of low-frequency energy. It remained to show where the edge waves with large periods come from. Gallagher (1971)[12] developed a

theory which suggested that surf beating between particular pairs of incoming waves led to the resonant growth of long-period edge waves. However, wave breaking was not permitted in this model. To study resonant interaction conditions in the presence of breaking waves, Bowen and Guza (1978) conducted a series of carefully designed laboratory tests. It was found that theoretical resonance can be produced in a wave basin with incident wave breaking present. When resonance conditions for edge wave growth from the theory were satisfied in the experiments, the response at the beat frequency was in the form of the theoretically predicted edge wave mode. It was concluded that these results suggest (strongly) that surf beat is predominantly an edge wave phenomenon. The reverse is also true to provide a mechanism for generation of long-period edge waves with resulting large rip spacings on :lat dissipative beaches.

(2) Intersecting Wave Trains. A second wave interaction mechanism to produce rips is the intersection of incident wave trains with the same periods, but from different directions (Dalrymple, 1975; Dalrymple and Lanan, 1976). Large rip spacings are possible from the theory (no maximum limit). However, as pointed out by Dalrymple (1978), the amount of time natural conditions (separate distant storms, refraction, diffraction, local reflection) produce wave intersections at real beaches is unknown. Synchronous, progressive cross-waves can also be excited in a wave basin with a sloping beach as demonstrated by the laboratory experiments of Maruyama and Horikawa (1977). The cross-waves are shown to be component waves, with angles different from 90° to the wave maker, and not edge waves. Numerical simulations, agreed well with observed flow patterns which included rip currents. It was concluded that the interaction of the incident and cross-waves produced the longshore variation in breaker height causing nearshore circulations and rip currents.

(3) Wave-Current Interaction. Finally, rip currents have been observed where there is no wave topography, wave wave, or wave structure interaction. There is no obvious external reason for a longshore variation in breaker height. Bowen and Inman (1969) stated this case clearly for perpendicular wave incidence on a plain noneroding beach:

> "In theory, the set-up at the beach can be in equilibrium
> with the momentum input of a uniform wave train over any
> width of beach, provided that the conditions are uniform
> in the longshore direction. However, as this condition
> is not observed in nature and not observed even in the
> laboratory unless the beach width is quite small, it has
> been suggested that the equilibrium might not be stable.
> That is, a small temporary disturbance might cause a com-
> plete breakdown of the two-dimensional equilibrium." (p. 5480)

They then presumed tha⁺ a small disturbance could excite edge waves in the region and their incident edge wave theory ensued. It is also conceivable

---

[12] GALLAGHER, B.,"Generation of Surf Beat by Non-linear Wave Interactions," *Journal of Fluid Mechanics*, Vol. 47, No. 1, Sept. 1971, pp. 1-20 (not in bibliography).

that a purely hydrodynamic instability, i.e., an initial disturbance (or perturbation) of the proper wavelength, can extract potential energy from the setup regime and convert it into horizontal circulation patterns and rip currents. Thus, perhaps a better title for Dalrymple's mechanism (Table 1) is hydrodynamic instability theory.

Hino (1974) was the first to postulate and use this mechanism to develop a theory of rip current spacing. Details of the theory are reviewed in Chapter 3. When the instability grew out of an allowed, movable bottom boundary, Hino found rip currents theoretically formed with an alongshore spacing about four surf zone widths apart. This was close to those observed in nature. However, when instabilities were purely hydrodynamic, the spacings were far too low and the analysis untenable. LeBlond and Tang (1974) using similar analysis procedures investigated the possibility that a wave-current feedback mechanism may cause a preferential spacing for rip currents (see also Iwata, 1976, 1978). But these models did not predict rip current spacings (Dalrymple and Lozano, 1978) unless an extra condition was introduced. LeBlond and Tang (1974) invoked the condition that rip currents will be found where the relative rate of energy dissipation is a minimum, i.e., a path of least resistance approach (Miller, 1977). Theoretical rip spacings were still far too small. Mizaguchi (1976) introduced (rather arbitrarily) a longshore variation in bottom friction as the extra condition. Dalrymple and Lozano (1978) showed that if the extra effect from current refraction of incident waves by the outgoing rip currents is included, reasonable rip current spacings are predicted. Finally, Miller (1977) and Miller and Barcilon (1978) postulated that the dominant rip current instability occurs at those wave numbers for which a balance can be steadily maintained between the kinetic energy dissipated by friction, wave breaking, and the potential energy released. Their model will be discussed further in Chapter 3 as will the key, empirical assumptions about the surf zone.

In retropsect, many of these arguments and theories about mechanisms are of the "chicken or egg" variety and somewhat academic. As summarized by Komar (1976), the rip currents probably come first as generated by some mechanism and cause sediment transport to produce the local bathymetry. (The analogy with popular "mechanisms" for winds to begin to generate surface water waves is appropriate.) These bottom irregularities probably maintain hydraulic control over the nearshore circulation and rip currents observed in today's field experiments. It is undoubtedly true that two or more factors could be present together and the unsteadiness of nature may prevent being absolutely sure. However, there is the need to sort out and understand the forced-type mechanisms (structural and wave intersection types) in relation to the free, intrinsic instability type for purposes of correct numerical modeling of nearshore systems.

(4) Other Factors. Fluid properties and sediment characteristics also play a role in wave interaction models. Water temperature changes its viscosity so that viscous shear effects are different on Alaskan versus Gulf of Mexico beaches. Density differences can create density currents. It is usually assumed homogenous fluids are present

at the coast. Also, density effects are generally ignored when comparing
test results from the Great Lakes (freshwater) with ocean (saltwater)
beaches. Surface tension plays a role when waves break, especially for
large-scale differences as found on laboratory versus natural beaches.
Turbulence intensity and resultant turbulent shear stresses must also be
considered. When generated by wave breaking, the type of breaker and the
scale of the observation (again, laboratory versus field) produce differ-
ent internal turbulence intensities. Boundary shear-generated turbulence
(oscillatory-type) can be significantly different over rigid versus mov-
able beds. Movable bottoms form rippled or duned beds that locally gener-
ate more vorticity. Sediment concentration distributions in the vertical
suppress turbulent fluctuation intensities near the bed. As discussed
in Chapter 3, both the bottom boundary resistance coefficient and lateral
turbulent mixing parameter play significant roles in theories on longshore
currents. They are both strongly influenced by the fluid properties.

It would be a mistake to assume that sediment characteristics (compo-
sition and weight, grain-size distribution, roundness, shape) are only of
interest for sediment transport studies. They play a role in coastal
currents that is yet to be fully understood or appreciated. For example,
the weight and size of the grains on the beach can influence the size of
ripples formed and the concentration distribution of suspended sediment.
Both properties thus change the turbulence intensity present in the water
column. If more wave energy is expended to keep sediment in suspension,
less is available to generate currents. Also many studies have shown how
grain size and beach slope are related (e.g., Bascom, 1951[13]). The major
differences between reflective- and dissipative-type beach systems and
their slope dependence are discussed earlier. Size, distribution, and
shape also affect beach porosity which, in turn, influences the extent
of backwash in the swash zone (Kemp, 1975). Wave energy is absorbed in
the surf zone by porosity effects as well as boundary resistance.

Finally, perhaps the key factor is the wave breaking phenomenon.
When, where and why do waves break? Because the physical understanding
is so weak, empirically based information is heavily relied upon. The
surf zone empirism that results plays a critical role in all theories of
longshore currents and nearshore circulations. Consequently, wave break-
ing processes are discussed in Chapter 3.

IV. INSTRUMENTATION AND MEASUREMENTS

A number of methods and problems have been discussed that relate to
making current measurements in the field and laboratory. This section
elaborates further on the instruments employed and on a number of measure-
ment systems devised for surf zone applications. The section concentrates
on the EM-type current meter and the so-called S_{xy} gage for estimating
momentum flux and wave direction. A number of other instruments are used

---

[13] BASCOM, W.H., "The Relationship Between Sand Size and Beach Face
Slope," *Trans. Am. Geophys. Union,* Vol. 32, 1951, pp. 866-874
(not in bibliography).

in the field to measure water surface variations, bottom pressures, winds, etc., but were felt outside the intended scope of this review (e.g., see Horikawa, 1978a; Gable, 1979). An additional method to develop steady uniform profile longshore currents in the laboratory is also discussed.

1.   Velocity Instruments.

The section relies primarily on the published literature of researchers making field measurements in the surf zone; useful information was also obtained from Teleki, Musialowski, and Prins (1976) and Woodward, Mooers, and Jensen (1978). The most recent source is the ongoing Nearshore Sediment Transport Study (NSTS) and publications from it (e.g., Gable, 1979).

a.   Lagrangian. Before 1968, currents were measured by timing the travel distance of dye, surface floats, or drogues. The main advantage is the simplicity of use. A mean current is obtained representative of the distance and traveltime used in the measurement. Most early researchers fail to mention these values in their publications. Surface floats give surface readings. Dye and drogues (weighted floats) give some type of depth-averaged value. The primary advantage of these methods is that when a series of photos are taken from overhead, nearshore circulation patterns, rip currents, and mean velocities (magnitude and direction) can be obtained. Such measurement systems are described in further detail below.

The Japanese (Horikawa and Sasaki, 1972; Sasaki, 1977) have continued the use of drogues as part of their tethered float technique (Sasaki, Igarashi, and Harikai, 1980). They began with polyurethane foam boxes (33 by 25 centimeters) as floats and evolved to the 20-centimeter cube drogue (Fig. 15). This size was found to be a minimum for viewing on ordinary color photographic film at 200- to 500-meter altitudes. Surfboarding can be a major problem with the drogue configuration when large spilling breakers are present (Sasaki, 1977). Larger and heavier drogues can be used but are not as readily nor swiftly deployed. Thus current magnitudes and directions are very questionable in the breakers but assumed to give reasonable estimates of depth-averaged longshore velocities and rip flows at other locations (Sasaki, 1977).

Dye also continues to be used. Breaking waves travel rapidly across the surf zone to quickly disperse a spot of dye in the onshore-offshore direction until it extends completely across the surf zone. The less intense longshore diffusion then spreads the patch laterally as it moves with the longshore currents (Bowen and Inman, 1974). What group of dyed water particles are used to measure longshore currents? Most researchers simply state that movement of the resulting dye-patch was measured and timed from shore. Clearly, the location of the dye-patch center or centroid is somewhat subjective and leads to errors. At what depth and when in the wave cycle the dye is released are also important factors. Laboratory researchers at the Delft Technical University (Visser, 1980) released the dye at three depths (repeated twice in middle) to obtain a depth-averaged value. They also released the dye at different phases in the wave cycle and made 20 independent measurements to arrive at one mean value. Such careful procedures would help to increase field accuracy but can be applied only under steady-state field conditions.
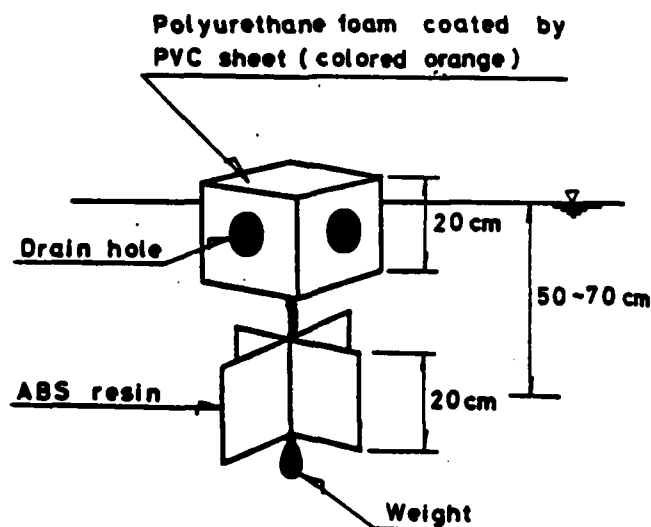
Figure 15.   Schematic of drogue used by Japanese (from Sasaki, 1977).

Further advantages and disadvantages of dye and float methods are discussed by Galvin and Savage (1966)[14].

b.   Eulerian.   Propeller-type current meters were first used in the surf zone by Sonu (1969b).   These bidirectional meters used a three-bladed impeller mounted within a duct.   Paired reed switches sensed both rotation speed and flow direction through magnetic coupling in the blades.   Threshold velocity was 5 centimeters per second.   The meter's response is non-linear near the threshold speed due to impeller inertia and thus not truly bidirectional.   This type of meter is also phase-dependent in that there is always a real timelag between forcing function and meter response.   In CERC's development of the Towed Oceanographic Data Acquisition System (TODAS), the ducted impeller type (mechanical sensor) was chosen over acoustic EM and force meters (Teleki, Musialowski, and Prins, 1976).   The reasons for this choice were the simple but rugged construction, zero drift, and antifouling characteristics (suspended sediments, seaweed etc.) of the propeller type (Teleki, Musialowski, and Prins, 1975). A 4-inch duct (8 inches long) directed the flow through a five-bladed impeller.   The measurement range was 0 to 2.6 meters per second (0 to 5 knots) with a threshold speed of 2 centimeters per second.   They found

---

[14] GALVIN, C.J., and SAVAGE, R.P., "Longshore Currents at Nags Head, North Carolina," Bulletin No. 2, U.S. Army, Corps of Engineers, Coastal Engineering Research Center, Washington, D.C., 1966 (not in bibliography).

considerable phase lag and much scatter depending on flow direction for 10- to 20-second swell. It would seem that this type is also readily fouled by kelp or seaweed.

Electromagnetic (EM) current meters are based on inductance principles. They are currently the most popular type since first being introduced for surf-zone measurements by Thornton (1969). A magnetic field (a.c.) is created by an electromagnet within the probe. Electrodes on the probe measure the voltage induced by the conductor (moving seawater) to generate the output signal. A popular brand is the two-axis, Marsh-McBirney EM current meter probe and electronics package. The Model 512 OEM has a 4-centimeter-diameter spherical probe with four middiameter electrodes, 90° apart and protruding 0.5 centimeter. The EM meter is rugged, has good cosine response, a wide frequency band width, and offers less chance for fouling than the propeller-type meter. During recent extensive use in the NSTS experiments at Torrey Pines, California (Gable, 1979), 22 EM meters withstood forces large enough to bend one support rod but not damage the probe. Entrapment of kelp and seaweed will alter the calibration, so EM probes must be frequently inspected and cleared of debris and marine fouling attachments.

Calibration problems have recently been reported for the EM probe under both steady-state and oscillatory-flow regimes. LaVelle, et al. (1978)[15] showed the meter to have a transition (change in slope) in steady flow (d.c. gain) at about 80 centimeters per second. This could possibly be due to nonlinear boundary layer effects including flow separation as suggested by Cunningham, Guza, and Lowe (1979) and also by Guza and Thornton (1980). Aubrey (NSTS Workshop, Scripps Institute of Oceanography, La Jolla, California, personal communication, February, 1981) found a break in the steady-flow calibration at 60 centimeters per second and attributed it to the electrodes jutting out from the sphere to disturb the boundary layer. This meter has a nominal output d.c. gain of 1 volt at 1 meter per second and calibration is usually made by towing in still water at this speed. Calibration of the 22 meters used in the NSTS experiment at Torrey Pines, California, made both before and after the experiment, showed less than 5 percent variation in d.c. gain for most meters (Gable, 1979).

But such meters deployed in the surf zone are subject to oscillatory motions over a wide range of frequencies and should be dynamically calibrated. For this purpose, the Shore Processes Laboratory of the Scripps Institute of Oceanography at La Jolla, California, has recently developed a hydraulically driven mechanical calibration device. A detailed description of the equipment can be found in Cunningham, Guza, and Lowe (1979). A horizontal arm with rack gear is driven back and forth by a hydraulic servo-controlled motor. The probe is rigidly positioned beneath the arm near its midpoint and kept about 20 centimeters below the water surface. Various types of arm motions were used to study

---

[15]LAVELLE, J.W., et al., "Near Bottom Sediment Concentration and Fluid Velocity Measurements on the Inner Continental Shelf, New York," *Journal of Geophysical Research,* Vol. 82, No. C12, 1979 (not in bibliography).

the dynamic response, including single-frequency sinusoids, broad band random noise, and asymetrical (ramp) functions, all with various amplitude-frequency combinations. No net flow rate was present in the basin during the tests.

The results were somewhat disconcerting as shown in Figure 16 (from Cunningham, Guza, and Lowe (1979). For the broad band response, the gain was found to be dependent upon both the frequency present and the spectral content. A random-noise generator running in three different modes was employed (curves I, II, and III) to vary the spectrums (Fig. 16). The black dots in the figure show results for the single-frequency tests where it was learned that the gain was also amplitude dependent. Recognizing these limitations and based on further experience gleaned from the Santa Barbara experiments for NSTS, Guza (Scripps Institute of Oceanography, La Jolla, California, personal communication, February 1981 stated that the uncertainty associated when using a single gain factor (d.c.) for all frequencies is roughly ±10 percent or ±5 centimeters per second, whichever is larger. Air bubbles in the water did not seem to alter this conclusion as stated by E.B. Thornton (Scripps Institute of Oceanography, La Jolla, California, personal communications, February 1981). Further research is needed to improve this accuracy, especially if velocity spectra are of interest.
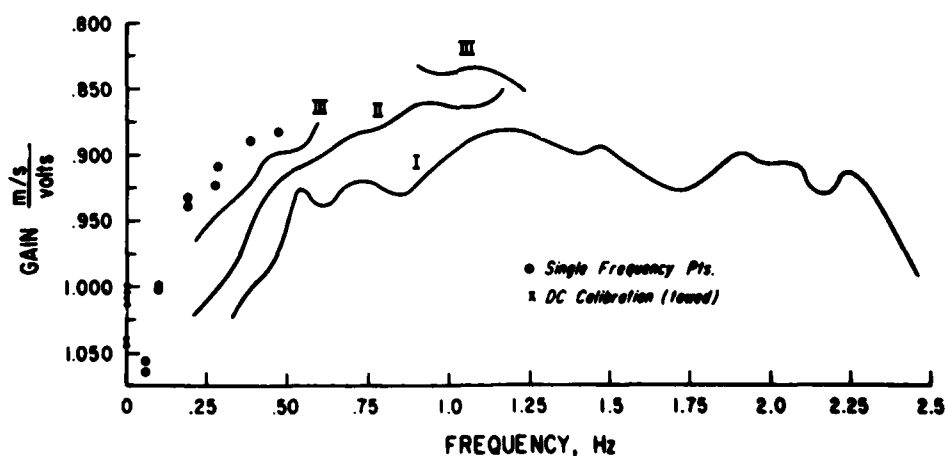
Figure 16.   Gain response of flow meters for pseudorandom noise runs, single-frequency runs, and towed (d.c.) values   (after Cunningham, Guza, and Lowe, 1979).

Because of these difficulties other meters for continuously record-ing current components in the surf zone are being developed and tested. These included the use of radar to track reflectors, doppler radar, and acoustic current meters (e.g., see Appell, 1978) such as the Neil Brown

system. These meters are not without their own problems. For example, the acoustic type is very sensitive to air bubbles in the water column to make it relatively intractable in the surf zone without further development (van der Graff, NSTS Workshop, Scripps Institute of Oceanography, La Jolla, California, personal communication, February 1981). All these types have not been extensively used in field experiments of surf zone currents, to date.

Articles by Kalaitis (1975), Appell (1977), and Mero and Appell (1977) provide further discussions of dynamic calibration tests. Turbulence effects are discussed by Bivins and Appell (1976). Other design shapes are also being developed for the EM type (Crump, 1976; Aubrey, personal communication, February 1981) that may lead to more uniform frequency response characteristics.

2.   Measurement Systems.

It can be reasonably argued that the scale of the phenomena observed (or perceived) at the coast depends on the observation method. Sasaki (1972) divided the coastal scale into (a) the spacing or rip currents, i.e. a unit cell scale, and (b) the velocity field within a cell. He then made (somewhat subjective) tables of desirable features and comparisons of observation methods for both scales. Color aerial photos taken at low tide were judged best for the larger scale phenomena. Horikawa and Sasaki (1972) also developed two measurement systems for taking successive overhead photos of flats to quantitatively describe the nearshore currents and rip currents at the smaller scales. One system, SHIELS, used two hovering helicopters to take successive stereo photos but was very expensive. The second, simpler and far cheaper method, BACS, uses a single balloon-borne, motor-driven camera but wave height determinations are impossible. This system is still used today by the Japanese. Figure 17 schematically illustrates the BACS system. The pier is used to tether the balloon and for workers to readily cross the surf zone while tossing the drogues. Wind drift of the balloon between pictures contributes measurement errors and limits use to calm days. They normally photograph rip currents usually expected near piers. This could be a valuable research tool but needs further development. Nonsurfboarding drogue shapes, tethering without piers, and electrical systems to precisely locate the camera at all times for position corrections must be developed. An excellent discussion of the use of these remote sensing systems can also be found in Sasaki (1977).

Sled systems have been used extensively in the surf zone. They can be instrumented heavily with wave staffs, pressure sensors, current meters, sediment concentration devices, etc. Also, they can be winched out into deeper water beyond the breakers and they follow the bottom contours. One of the first sleds developed is described by Lowe, Inman, and Brush (1972)[16]. Others that followed are reported by Teleki, Musialowski, and

---

[16] LOWE, R.L., INMAN, D.L., and BRUSH, B.M., "Simultaneous Data System for Instrumenting the Shelf," *Proceedings, 13th Coastal Engineering Conference,* ASCE, Vol. I., 1972, pp. 95-112 (not in bibliography).
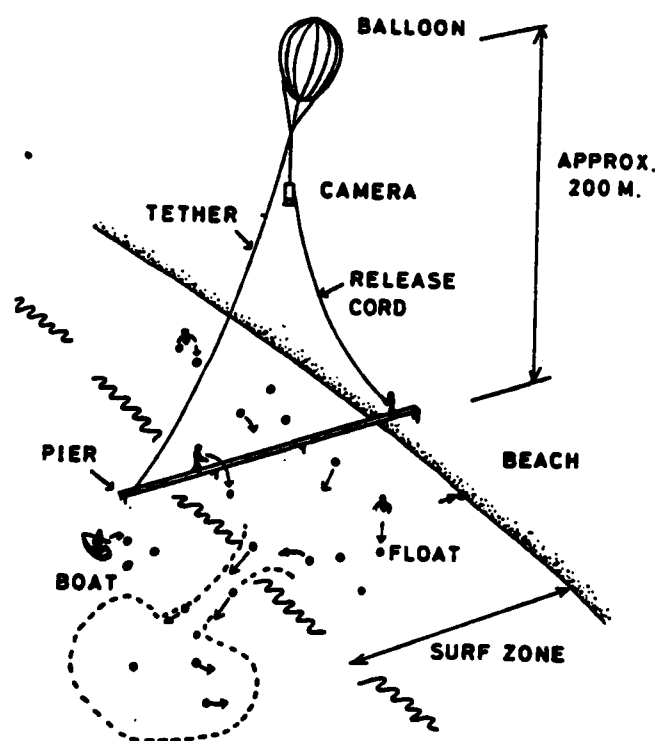
Figure 17. Schematic of BACS nearshore current system (from Sasaki, 1977).

Prins (1975, 1976), Coakley, et al. (1978), Bradshaw, et al. (1978), and Allender, et al. (1978). The newest U.S. sled has been developed for simultaneous bottom profiling, wave height, and two-axis current measurements with one EM meter (Sallenger, et al., 1980). Field tests of the latter device at Monterey, California, in 6-meter breakers over a 100-meter wide surf zone measured bottom current greater than 3.5 meters per second (Sallenger, et al., 1980).

The major problem with use of sleds is data interpretation. Some type of temporal stationarity of the currents must be assumed (Guza and Thornton, 1978, p. 768). If not continually moving, how long should the sled remain at each station to record information? Figure 6 showed considerable temporal variation between successive 17.1-minute ((1,024 seconds) averages at a plain beach for each gage location. If 17.1-minute records are taken at each station, it could be several hours between data taken at the outer and inner reaches of the surf zone. Can this data be combined to yield an instantaneous profile of the 17.1-minute mean longshore current?

To eliminate the need to make arbitrary assumptions regarding temporal stationarity, NSTS researchers choose to employ a large number of fixed

current meters in perpendicular arrays as shown in Figure 18 for the Torrey Pines Experiment. Twenty-two EM current meters were alined normal and along the beach with some bunching up in the surf zone. A similar configuration was established for the Santa Barbara experiments where a total of 25 EM current meters were employed. These alined arrays proved to be very successful in obtaining instantaneous and simultaneous longshore and cross-shore velocity time histories through and beyond the entire surf zone and down the beach near the midsurf position (Guza and Thornton, NSTS Workshop, Scripps Institute of Oceanography, La Jolla, California, personal communication, February 1981). All the raw data from both the Torrey Pines (Gable, 1979) and Santa Barbara, California (Gable, 1981[17]) experiments were made available on magnetic tape. Data were recorded at 64 samples per second, then later low pass-filtered and reduced to 2 samples per second. These then became the raw data tapes. They can be obtained for nominal cost from the National Oceanic Data Center (NODC) in Washington, D.C. Some of the early results will be discussed in Chapter 4. These data sets form an extensive and excellent data source for future analysis.

Unfortunately, however, no EM current meters were alined in the vertical for either of the NSTS field experiments. Plans to do so at Santa Barbara were scrapped due to the storm conditions encountered. Thus it was not possible to observe the vertical current structure nor know if circulations about horizontal axes were present.

3. Wave Direction.

Wave direction is an important parameter in surf zone current generation. It is also difficult to determine for irregular wave trains striking the coast. Linear arrays of pressure sensors have been quite successful in measuring directional wave data at the coast (e.g., Pawka, 1974). Other devices have been proposed (Hallermeier and James, 1974). The most practical and successful for measuring wave direction is the slope array, as developed by the Scripps Institute of Oceanography (Seymour, 1977; Seymour and Higgins, 1977; Higgins, Seymour, and Pawka, in preparation, 1981). Besides wave direction, pressure measurements from the device can also be used to calculate the longshore component of shoreward-directed momentum flux (S_{xy}) due to the waves. The device is also called an S_{xy}-meter. As such it provides a valuable tool for comparison with theories which use sea-surface variation and wave angle to calculate S_{xy}.

The slope array device is very simple. Four pressure transducers are mounted at the corners of a square frame, 6 meters on a side. The orientation of the sides on the bottom of the frame is determined relative to a reference longshore direction. Coordinate rotation yields the desired surface slope components from any array alinement. The real part of the cross-spectrum of the sea-surface slope components in the longshore and cross-shore directions is then used to compute a significant direction

---

[17] GABLE, C.G., Report on Data from the NSTS Experiment at Ledbetter Beach, Santa Barbara, California, Jan-Feb., 1980," IMR Ref. No. 80-5, Scripps Institute of Oceanography, Mail Code-A022, La Jolla, Calif., 1981 (not in bibliography).
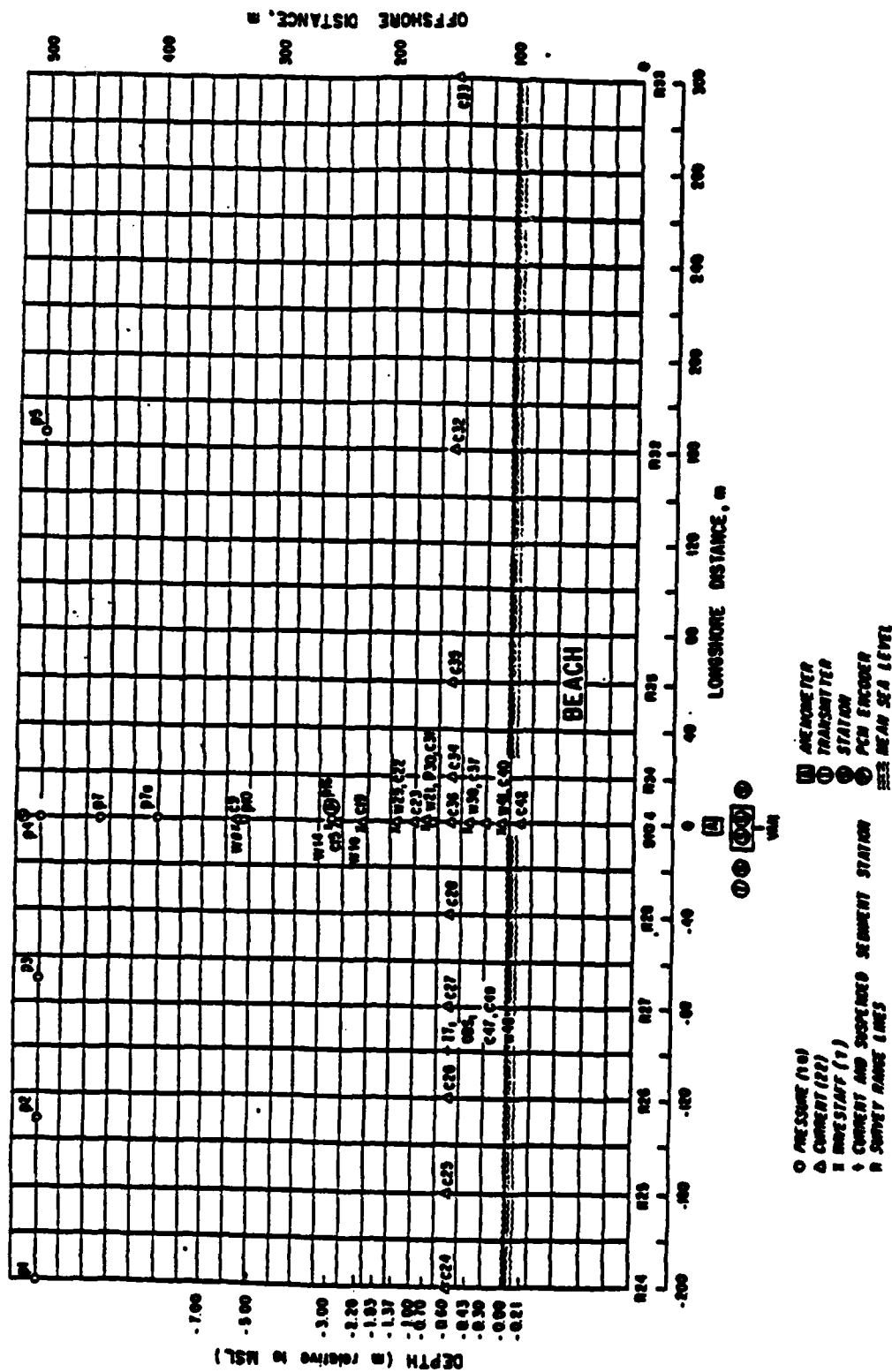
Figure 18. Location of EM current meters and other instruments in NSTS, Torrey Pines, California, experiment (from Gable, 1978).

61

and the spectrum of the momentum flux components, S_{xy}. Details are beyond the intended scope of this review. The calculation method stems from Longuet-Higgins, Cartwright, and Smith (1963)[18] and complete details can be found in Higgins, Seymour, and Pawka, in preparation, 1981.. They also made laboratory tests with irregular waves and field comparisons with a large linear array of five pressure sensors. Comparisons were judged to be excellent and quite good, respectively.

Use of the slope array device during the NSTS experiments showed its sensitivity to alinement errors along the coast relative to wave directionality. At Torrey Pines, California, alinement inaccuracy with the straight coastline was judged to be about 3° and greater than the wave directions observed (Seymour, 1981, NSTS Workshop, Scripps Institute of Oceanography, La Jolla, California, personal communication, February 1981). Consequently, a linear array of five pressure sensors more than 360 meters long was employed to measure the directional spectrum. The pronounced variability in bottom topography and large incident wave angles due to narrow wave windows present at Santa Barbara, California, made use of the slope array device ideal for this location.

4. Laboratory Systems.

There is another way to create a uniform longshore current profile (i.e., infinite beach) in the laboratory other than the method developed at the Delft Technical University (Visser, 1980). End effects are eliminated, and a zero mean slope in the longshore direction results. The technique, described by Dalrymple and Dean (1972), involves a spiral wavemaker generating waves in the center of a circular basin. A vertical right-circular cylinder oscillates in a small circle about its vertical axis to generate the waves. Wave crests move out in an Archimedian-type spiral and crests impinge on the circular beach everywhere at the same angle of incidence. A theory for the amplitude of generated waves based on shallow-water theory was confirmed in the laboratory. Dalrymple and Dean (1972) conducted littoral drift experiments with the device, and they recommend it for further sand transport studies. However, scale effects preclude obtaining quantitative results for this purpose. It could be an excellent tool, however, for confirmation of longshore current theory.

V. SUMMARY

More than 60 years of observations and measurements of longshore currents, nearshore circulations, and rip currents worldwide has been briefly reviewed. Magnitudes and directions of these currents depend upon the following factors:

---

[18] LONGUET-HIGGINS, M.S., CARTWRIGHT, D.E., and SMITH, N.D., "Observations of the Directional Spectrum of Sea Waves Using the Motions of a Floating Buoy," *Ocean Waves Spectra, Conference Proceedings,* Prentice-Hall, Englewood Cliffs, N.J., 1963 (not in bibliography).

(a) **Wave characteristics:**

    Evaluation point (usually the breaker line)
    Regular or irregular forms
    Height
    Direction (number of incident wave trains)
    Period
    Type of breaker (spilling, plunging, or surging)
    Wave energy transfer to other scales (nonlinear effects)
        Soliton formation (harmonic scales)
        Subharmonics (longer period scales)
    Breaker location
    Presence of edge waves or infragravity waves
    Wave-current interactions
    Surf zone wave energy decay

(b) **Wind characteristics:**

    Strength
    Direction
    Duration
    Atmospheric pressure gradients

(c) **Tidal influence**

    Mean water depths
    Width of surf zone

(d) **Planform and bathymetry**

    Coastal boundaries (natural headlands, jetties, breakwaters)
    Coastal planform
    Offshore bathymetry (refraction, diffraction)
    Local bathymetry (bars, troughs)
    Nearshore profile
        Beach face slope
        Reflections
    Bottom roughness (smooth, ripples, dunes)

(e) **Fluid**

    Gravity (density, saltwater, freshwater)
    Temperature (viscosity)
    Surface tension (air entrainment)
    Turbulence intensities (wave breaking, bottom shear,
      sediment effects)

(f) **Sediment**

    Size, gradation, shape, unit weight
    Porosity, permeability

Current variations in space and time result from the interplay of many of these features plus the fact that most are unsteady in nature. Many simplifications and assumptions are necessary to evolve theories from all these factors.

CHAPTER 3

THEORETICAL DESCRIPTION

I. HISTORICAL SUMMARY

1. Before 1967.

All the relevant theories proposed to predict longshore current velocity before 1967 have been thoroughly reviewed by Galvin (1967). At least 12 different equations existed and were derived by the following methods:

(a) Continuity of water mass,
(b) energy flux,
(c) momentum flux, and
(d) empirical correlations.

Galvin (1967) concluded that all were oversimplified models and the empirical methods lacked sufficient data. For example, the Inman-Quinn (1951) theory used momentum conservation principles modified by empirical data. It was shown to be based on an untenable assumption, supported by inappropriate data and found to be only a fair predictor for just one of the three data sets then available. No adequate theory was felt to exist at that time (Galvin, 1967).

A summary of most of these longshore current formulas is included as Appendix C (from Thornton, 1969). It lists an additional empirical equation based on multiregression analysis as found by Harrison (1968) at Virginia Beach, Virginia. Such equations are only roughly tenable for the location and range of variables observed. Equations based on the conservation laws of physics are much preferred for general usage. Additional analysis and discussion of the theories before 1967 can be found in Horikawa (1978a) who includes some Japanese formulas not previously referenced. The formula of Shadrin (1961), based on measurements at a barred coastline of the Black Sea (Anapa coast), is also discussed by Horikawa (1978). There are also recent original summaries by Komar (1976) and Gourlay (1978) of most theoretical attempts befor 1967.

In retrospect, all these theories were doomed to failure for a number of reasons. Those based solely on mass conservation and kinematics omitted the crucial dynamics and interplay among forces and fluid accelerations. The amount of energy dissipation in the surf zone is a significant percentage of the total available and difficult to estimate. Energy flux theories rely on that small fraction remaining which represents a second-order phenomenon (Galvin, 1967). Momentum conservation principles were simply not applied properly and neglected the influence of the streamline curvature present in short waves on the vertical pressure distribution. They all predicted one mean longshore current velocity for the entire surf zone width. They neglected important factors such as breaker type, beach profile, and bottom roughness. They were all for longshore current estimates and no theories to handle nearshore circulations and rip currents existed at that time.

64

2. Modern Approaches.

Since 1969, two fundamentally different yet related theoretical approaches to predict coastal hydrodynamics have emerged. Both rest on solid physical laws of mass (continuity) and momentum (motion) conservation that form the basis of Newtonian fluid mechanics. Most importantly, both assume the velocity profile to be uniform over the water depth for all points in the flow. No flow direction reversals with depth can be resolved (Fig. 9,b) so that circulations about horizontal axes are impossible.

a. Radiation Stress Theory. The equation of continuity and two horizontal momentum equations are depth-integrated and time-averaged to account for the excess lateral momentum thrust present in wind waves on the coast. Local net velocity components and the average MWL are the dependent variables of interest. The theory is now more than 12 years old and has undergone considerable development and refinement. It requires a priori specification of wave height fields throughout the area of interest. This is usually accomplished by normal wave refraction procedures (Snell's Law), combined with diffraction, reflection, and wave-current interaction estimates, as required. Most of this chapter (Secs. II to VI) is devoted to a thorough review of the extensive literature that has been published since 1969 on this subject. A key aspect is the time-averaging process inherent in the theory so that this could be labeled a time-average theory. For simple geometries, analytical (closed form) solutions are possible.

b. Boussinesq Theory. Based on ideas that go back much further (Boussinesq, 1872)[19], the vertical acceleration and streamline curvature effects in wind waves give rise to lateral momentum fluxes. They appear as additional, mixed and higher derivative terms in the horizontal, long wave momentum equations that are depth-averaged but not time averaged. Local instantaneous velocity components and the instantaneous water surface fluctuations are the dependent variables of interest. The first engineering applications to coastal swell wave propagation in two dimensions appeared in 1978, and only outside the breaker zone. Considerable research and development work remains to use the method for calculation of coastal currents, circulations, and rip currents. No additional wave field specifications are required since the waves propagate in space and time as a fundamental part of the solution. The limited amount of published information on this method is reviewed in Section VII. Numerical integration methods are required to obtain solutions.

For further insight into the physics and mathematics surrounding waves in the coastal zone, Lundgren (1976) is recommended. He refers to the Boussinesq approach as T-Methods (time-step methods).

---

[19] BOUSSINESQ, M.J., "Theory of Waves and Surges Which Propagate the Length of a Horizontal Rectangular Canal, Imparting to the Fluid Contained Within the Canal Velocities That Are Sensibly the Same from the Top to the Bottom," *Journal of Pure and Applied Mathematics*, Vol. 17 (2nd Series), Feb. 1872. For English translation, see VASTANO, A.C.J., and MUNGALL, J.C.H., Reference 76-2-T, Dept. of Oceanography, Texas A&M University, College Station, Tex., Mar. 1976 (not in bibliography).

II. PRINCIPLES OF RADIATION STRESS

In a series of papers beginning in 1960, Longuet-Higgins and Stewart (1962, 1964) laid down the principles and gave the physical meaning behind the concepts of radiation stress for water waves. About the same time, Lundgren (1962, 1963)[20] described how water waves can exert an extra wave thrust in the horizontal direction. The term radiation stress is borrowed from EM wave theory where a radiation pressure impinges on a surface. It is actually a misnomer in that depth integration gives a wave-induced excess pressure force per unit length (in excess of the hydrostatic pressure force) and not a true stress (force per unit area). However, the term stress implies a directional quantity which is true for this wave-induced thrust and radiation stress is now an accepted term in the literature. Transformations applicable to true stresses can be used. As will be shown later in this chapter, these radiation stresses resulting from time-averaging gravity wave orbital motions are also completely analogous to Reynolds stresses resulting from time-averaging turbulent flow motions.

The radiation stress principle has been used to develop theoretical, analytic expressions for the following coastal phenomena:

(a) Wave setdown and setup (Sec. III)
(b) Uniform longshore current profiles (Sec. IV)
(c) Nonuniform longshore current profiles (Sec. IV)
(d) Nearshore circulation systems and rip currents (Sec. V)

In addition, it is the basis for numerical integration schemes over variable bathymetry and boundaries (jetties, breakwaters) where analytic solutions are not available (Sec. V). Finally, principles of radiation stress theory have been extended to nonlinear and irregular waves as discussed in Section VI.

1. <u>Progressive Waves in Uniform Water Depths</u>.

a. <u>Radiation Stress Components</u>. The summary that follows is essentially that from the work of Longuet-Higgins and Stewart (1964). A monochromatic wave is shown propagating in the X-direction in Figure 19. A relatively standard set of nomenclature is adopted and defined at the beginning of this report.

(1) <u>Normal Stress</u>. The component S_{xx} of the radiation stress along a wave ray is defined as the time-average value of the total flux of horizontal momentum across a vertical plane minus the stillwater hydrostatic pressure force. Thus

$$S_{xx} \equiv \overline{\int_{-d}^{\eta} (p + \rho u^2) \, dz} \; - \; \int_{-d}^{0} p_o \, dz \tag{1}$$

---

[20]See some corrections in Danish Technical University, ISVA, Index to Reports, Rept. No. 20, Dec. 1969, Lyngby, Denmark (not in bibliography).
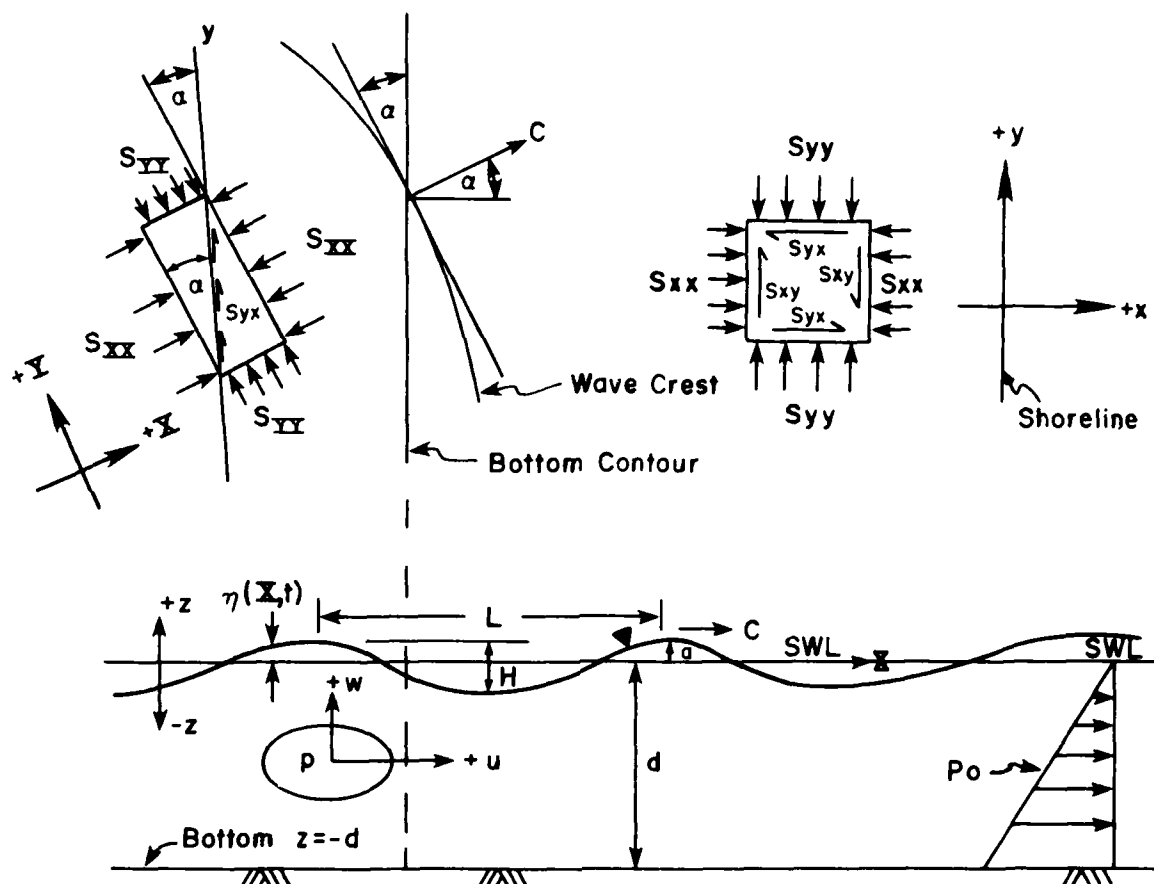
Figure 19. Definitions and nomenclature for radiation stress components.

where the overbar indicates a time-averaged mean. For convenience in further evaluation, S_{XX} is rearranged and divided into three parts as follows:

$$S_{XX} = \int_{-d}^{\eta} \rho u^2 dz + \int_{-d}^{o} (p-p_o)dz + \int_{o}^{\eta} pdz \qquad (2)$$

or

$$S_{XX} = S_{XX}^{(1)} + S_{XX}^{(2)} + S_{XX}^{(3)} \qquad (3)$$

The assumptions now begin. In the first term $S_{XX}^{(1)}$, the integration above the stillwater level to $z = \eta$ produces a third-order term (proportional to a^3) and is neglected. $S_{XX}^{(1)}$ is generally positive and can be considered a Reynolds stress integrated from the bottom to the stillwater level.

$$S_{XX}^{(1)} = \int_{-d}^{o} \overline{\rho u^2} dz \qquad (4)$$

The second term $S_{XX}^{(2)}$ can be shown equal to

$$S_{XX}^{(2)} = \int_{-d}^{0} \overline{-\rho w^2} \, dz \tag{5}$$

Longuet-Higgins and Stewart (1964) considered the time mean flux of vertical momentum across a horizontal plane balanced by the weight of water above that plane. This is equivalent to integrating and time averaging the vertical momentum equation over the stillwater column. This term is obviously generally negative. The third term $S_{XX}^{(3)}$ poses some difficulties when η is below $z = 0$. To get around this, Longuet-Higgins and Stewart (1964) assumed the pressure to fluctuate in-phase with the surface elevation, i.e., a hydrostatic distribution for pressure, p. This gave

$$S_{XX}^{(3)} = \frac{1}{2}\rho g \overline{\eta^2} \tag{6}$$

which is also generally positive. Combining gives

$$S_{XX} = + \int_{-d}^{0} \overline{\rho(u^2 - w^2)} \, dz + \frac{1}{2}\rho g \overline{\eta^2} \tag{7}$$

for the principle radiation stress. Equation (7) is completely general. Further simplification depends upon what classical wave theory is used for the three variables involved, η, u, and w and the averaging time employed. However, in deep water the particle orbits are almost circular so that the integral term approaches zero. Conversely, in shallow water $u \gg w$ so that the horizontal velocity stress dominates the integral term.

(2) Transverse Stress Component. Analogous to equation (1) the transverse radiation stress, S_{YY}, is defined

$$S_{YY} \equiv \overline{\int_{-d}^{\eta} (p + \rho u^2) \, dz} - \int_{-d}^{0} p_o \, dz \tag{8}$$

where v is the wave orbital velocity in the YY-direction parallel to the wave crests. For long-crested gravity waves, v equals zero. The transverse stress S_{YY} thus becomes

$$S_{YY} = \int_{-d}^{0} -\rho w^2 \, dz + \frac{1}{2}\rho g \overline{\eta^2} \tag{9}$$

if the same assumptions are the same as for S_{XX}.

68

(3) <u>Shear Component</u>. Since v is zero for long-crested waves, the shear component resulting from the cross products uv is identically zero everywhere, therefore

$$S_{XY} \equiv \overline{\int_{-d}^{\eta} \rho uv dz} \equiv 0 \tag{10}$$

for wave propagation in the X-direction. Consequently, S_{XX} and S_{YY} are principal stresses. It must be emphasized that S_{XX} and S_{YY} are horizontal forces per unit width acting normal to and parallel to the wave crests, respectively (see Fig. 19). Subsequently these principal radiation stresses will be transformed to a more convenient coordinate system oriented in the alongshore (y-coordinate) and shore-normal (x-coordinate) directions. In general, for waves making some angle, α with the shoreline, Sxy is not identically zero in this transformed coordinate system (Fig. 19). For additional physical interpretations of these stress components see Svendsen and Jonsson (1976).[21]

b. <u>Components Using Linear Wave Theory</u>. For small-amplitude waves of sinusoidal form,

$$\eta = a \cos(kx-\omega t) \tag{11}$$

where

$$a = \frac{H}{2} ; \quad k = \frac{2\pi}{L} ; \quad \omega = \frac{2\pi}{T}$$

and the particle orbital velocities u and w are defined in the usual manner[22]. Inserting this definition and equations for η, u and w into equation (7) for S_{XX} and equation (9) for S_{YY}, using the linear theory dispersion relation $\omega^2 = gk \tanh kh$, performing the integration, and time-averaging over one wave period yields

$$S_{XX} = E \left[\frac{2kd}{\sinh 2kd} \right] + \frac{1}{2} \tag{12}$$

$$S_{YY} = E \left[\frac{kd}{\sinh 2kd} \right] \tag{13}$$

where E is the usual total energy density of the waves given by

---

[21]SVENDSEN, I.A., and JONSSON, I.G., "Hydrodynamics of Coastal Regions," Den Private Ingenirfond, Technical University of Denmark, Lyngby, 1976 (not in bibliography).

[22]See, e.g., WIEGEL, R.L., Oceanographical Engineering, Prentice-Hall, Inc,, 1964, Englewood Cliffs, N.J., p. 15, for equations when equation (11) is in terms of the sine function (not in bibliography).

$$E = \frac{1}{2}\rho g a^2 = \frac{1}{8}\rho g H^2 \tag{14}$$

for linear theory. Use of the ratio n between group celerity, c_g, and wave celerity, c, defined as

$$n = \frac{c_g}{c} = \frac{1}{2}\left[1 + \frac{2kd}{sinh kd}\right] \tag{15}$$

gives the commonly found forms

$$S_{XX} = E(2n - \frac{1}{2}) \tag{16}$$

$$S_{YY} = E(n - \frac{1}{2}) \tag{17}$$

where the units of radiation stresses as force per unit length are now obvious.

In deep water, kd>>1 and $n \rightarrow \frac{1}{2}$ so that

$$S_{XX} = \frac{1}{2} E \tag{18a}$$

$$S_{YY} = 0 \tag{18b}$$

In shallow water, kd<<1 and $n \rightarrow 1$ so that

$$S_{XX} = \frac{3}{2} E \tag{19a}$$

$$S_{YY} = \frac{1}{2} E \tag{19b}$$

c. <u>Coordinate Transformations</u>. The usual strength of material method of plane stress analysis is applicable to transform the principle stresses into equivalent stresses on any other orthogonal coordinate system. The most convenient is a y-direction parallel to the coastline and positive to the right facing seaward, and the x-direction normal to the coast and positive toward the shoreline (Fig. 19). From either the Mohr's Circle or the stress element shown in Figure 20, the mathematical transformation equations become

$$S_{xx} = (\frac{S_{XX} + S_{YY}}{2}) + (\frac{S_{XX} - S_{YY}}{2}) \cos 2\alpha \tag{20}$$

70
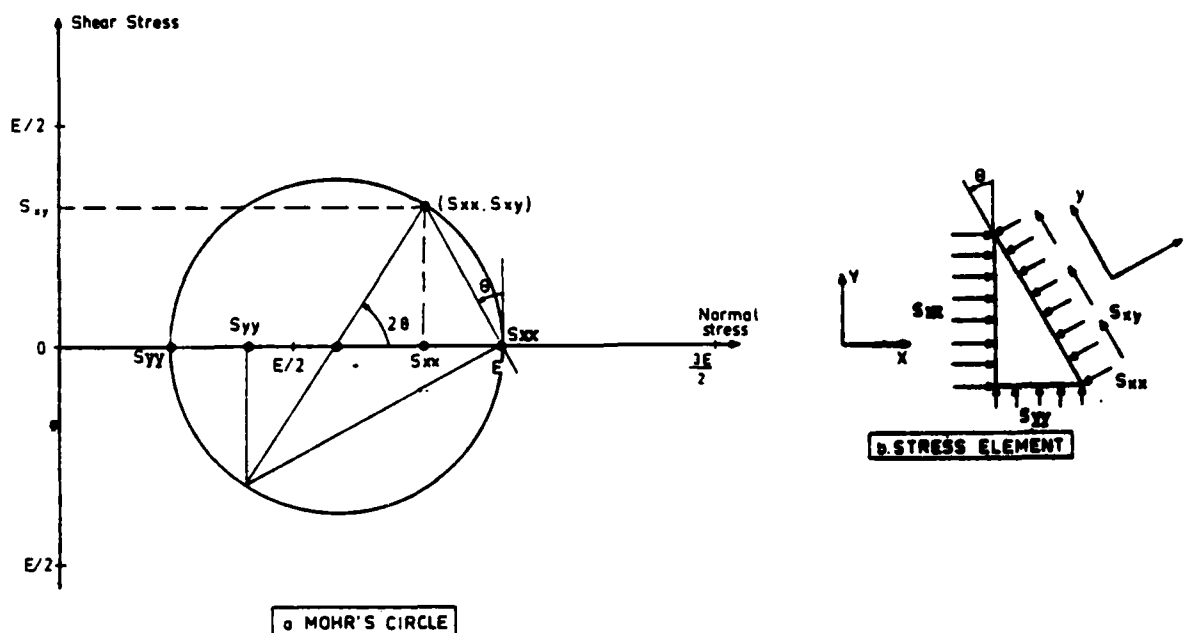
Figure 20. Mohr's Circle analysis.

$$S_{xy} = (\frac{S_{XX} + S_{YY}}{2}) - (\frac{S_{XX} - S_{YY}}{2}) \cos 2\alpha \qquad (21)$$

$$S_{xy} = (\frac{S_{XX} - S_{YY}}{2}) \sin 2\alpha \qquad (22)$$

where α is the angle between the wave crest and the shoreline. S_{xy} is the shear stress component in the longshore direction due to the excess momentum flux of oblique wave incidence. This shear stress is exerted in the $+ y$-direction on a fluid surface constant in x. The subscript nomenclature and order is consistent with that normally employed for shear stresses in fluid mechanics. An equal and opposite S_{xy} also exists.

For linear wave theory, the transformed components become

$$S_{xx} = E(\frac{3}{2}n - \frac{1}{2}) + E(\frac{n}{2})\cos 2\alpha \qquad (23)$$

$$S_{yy} = E(\frac{3}{2}n - \frac{1}{2}) - E(\frac{n}{2})\cos 2\alpha \qquad (24)$$

$$S_{xy} = En \sin\alpha \cos\alpha \qquad (25)$$

71

These equations form the basis for all subsequent applications of radiation stress principles that has been termed the first-order theory. The key assumptions are linear wave theory and a time-average over one wave period. If a steady state prevails, the averaging time can be over many wave periods.

2. Other Waveforms.

The principle stress equations (7) and (9) can be employed with other waveforms and expressions for η, u and w. For example, for standing waves in water of uniform depth and again using linear wave theory, Longuet-Higgins and Stewart (1964) obtained

$$S_{XX} = E(4n - 1) \tag{26}$$

$$S_{YY} = E[2n(1 + \cos 2kx) - 1] \tag{27}$$

for the principle stress components. S_{xy} is again identically zero. Although linear theory has been used extensively and forms the basic theory, various nonlinear wave theories and irregular waves with known spectral characteristics have also been studied. These special theories are discussed in Section VI of this chapter. The linear theory is reviewed in Sections III, IV, and V.

III. MEAN WATER LEVEL CHANGES

The radiation stress components are directly expressed in terms of the wave parameters: wave height H, wavelength L, crest angle α, and the still-water depth d. Waves approaching a sloping coastline or near structures will undergo modifications in these parameters resulting from shoaling, refraction, diffraction, reflection, and breaking processes. Spacial changes (gradients) in the radiation stress components must result. Under steady-state influence of the incident wave field and the modified wave field, a new time-averaged equilibrium will be established for the time-averaged water level and time-averaged currents present. For this steady-state situation, the equilibrium equations are the momentum balance equations perpendicular to and parallel to the shoreline and the continuity (mass conservation) equation. All forces and stresses in these equations are mean values over the wave period T. Forces are depth-integrated values per unit horizontal width.

1. Normal Wave Incidence.

When waves approach the coast at right angles with crests parallel to the coastline, the principles of radiation stress theory are readily demonstrated in terms of MWL changes. In this case for α = 0, the x-direction stress S_{xx} reduces back to principle stress S_{xx} and no shear-stress component exists.

a. Momentum Balance. Consider a plain sloping beach with bottom contours parallel to the wave crests as shown in Figure 21. For steady-state time-mean conditions, the rate of change of the radiation stress must create a rate of
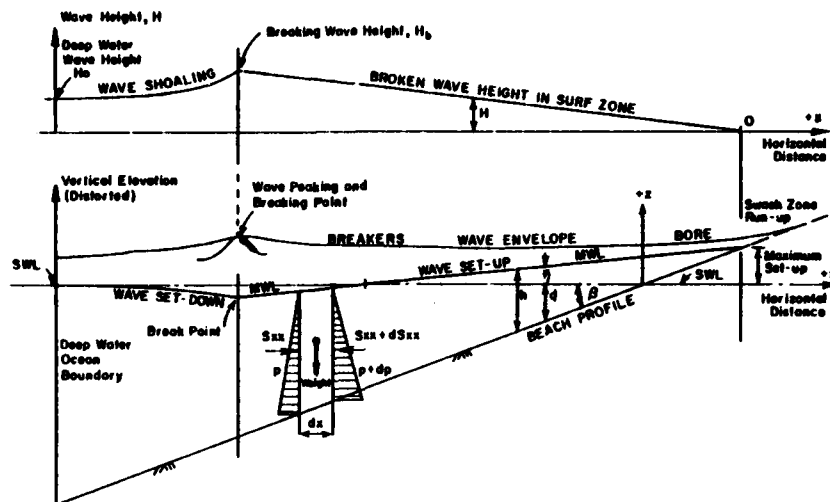
Figure 21. Schematic of wave setdown and setup due to normal wave incidence on a plain beach.

MWL change on a sloping bottom, β. If no net shear stresses are assumed at the bottom or on the free surface, the momentum balance gives

$$\frac{dS_{xx}}{dx} + \rho g h \frac{d\bar{\eta}}{dx} = 0 \qquad (28)$$

where $h = d + \bar{\eta}$, and $\bar{\eta}$ is the MWL change above or below the stillwater level (SWL). If S_{xx} is known, equation (28) can be integrated to yield a MWL setdown outside the breaker line and a MWL setup in the surf zone. Such an analysis was first conducted by Longuet-Higgins and Stewart (1963, 1964) and also by Bowen, Inman, and Simmons (1968) for plain sloping beaches and using S_{xx} from linear theory (eq. 23). However, equation (28) applies to an arbitrary bottom profile (still assuming straight and parallel contours) as long as the depth, d is monotonously decreasing.

b. Wave Setdown. Seaward of the breakers, it is reasonable to neglect wave reflections, percolation, bed-shear and internal turbulence dissipation so that the waves propagate with constant energy flux,

$$Ecn = Ecg = Constant. \qquad (29)$$

Using equation (29), Longuet-Higgins and Stewart (1963) integrated equation (28) over a plain sloping beach to obtain

$$\bar{\eta} = -\frac{1}{8} \frac{H^2 k}{\sinh(2kd)} \qquad (30)$$

73

Thus a lowering of the MWL below SWL takes place since $\bar{\eta}$ is negative and this wave-induced change is called setdown. The integration is not straightforward since all three variables k, d, and E can be dependent upon the horizontal coordinate x for this problem.

It is also possible to express $\bar{\eta}$ at a given depth d as a function of the deepwater conditions H_o and L_o (or a_o, k_o) as discussed by Gourlay (1978). His results are

$$\bar{\eta} = -\frac{1}{4} \frac{a_o^2 k_o}{n} \frac{coth^2 kd}{sinh\ 2kd} \tag{31}$$

or

$$\bar{\eta} = -\frac{H_o^2}{L_o} f(\frac{d}{L_o}) \tag{32}$$

with the form of the function $f(d/L_o)$ shown in Gourlay (1978) as plotted against a normalized setdown. Wave setdown is zero in deep water and increases rapidly as the depth increases. The maximum setdown is limited by wave breaking in shallow water which voids the assumption of constant energy flux. Using shallow-water approximations and a breaking criteria as discussed later, the maximum setdown at the breaker line is approximate 5 percent of the wave height at the breaker.

The most questionable assumptions in this theory are the use of S_{xx} based on linear wave theory and the neglect of bed shear in the region approaching wave breaking.

c. **Wave Setup.** Shoreward of the breakers, internal turbulence from wave breaking and bottom shear both drain energy from the waves in the surf zone. Since S_{xx} varies directly with E in shallow water (n → 1), or as H^2, the reduction of wave height toward the shoreline means a negative gradient of S_{xx} must be balanced by a positive gradient of $\bar{\eta}$ in the x-direction. This is called wave setup. The key question is how the wave height H varies from the first breakpoint to the shoreline.

(1) **Dissipative-Type Beaches.** Spilling-type breakers are found on wide, flat dissipative beaches. After breaking, the wave height continuously decreases as the waves and bores propagate shoreward as schematized in Figure 21. No truly satisfactory theory exists to explain when, where, and why waves break. Also, very little is known about energy dissipation rates in the surf zone for various types of breakers and beach profiles. Consequently, simplifying assumptions primarily based upon experimental evidence have been employed to develop wave setup theories. For spilling-type breakers on dissipative beaches, the assumption commonly employed is that the breaker index, γ (ratio of breaking wave height to mean depth at breaking) remains a

$$\gamma = \frac{H_b}{(\bar{\eta}+d)_b} = \frac{H_b}{h_b} = \frac{H}{h} \tag{33}$$

fixed ratio throughout the entire surf zone. This assumption is also important in longshore current theory. A complete review of surf zone empiricism will be presented in the section.

Now if it is again assumed (Longuet-Higgins and Stewart, 1964) that linear wave theory is applicable to compute S_{xx}, that shallow-water conditions prevail so $S_{xx} = 3/2E$, and that γ is constant in the surf zone, then

$$S_{xx} = \frac{3}{16} \rho g \gamma^2 (\overline{\eta} + d)^2 \tag{34}$$

Using equation (34) in the momentum balance equation (28), where $h = (\overline{\eta} + d)$ is retained in the second term, Bowen, Inman, and Simmons (1968) showed that for a plane beach of slope, $\tan \beta$

$$\frac{d\overline{\eta}}{dx} = \frac{1}{1 + 8/(3\gamma^2)} \tan \beta \tag{35}$$

For a given constant index γ, this meant that the mean water surface slope (setup) was proportional to the beach slope as illustrated in Figure 21.

Integration of equation (35) to find $\overline{\eta}$ on a plain beach reduces to a simple trigonometric analysis. All that must be specified is the magnitude of the breaker index γ, the location of the breakpoint, and the magnitude of the wave setdown at the breakpoint, $\overline{\eta}_b$. Again, using shallow-water theory and equations (30) and (33), $\overline{\eta}_b$ becomes

$$\overline{\eta}_b = - \frac{1}{16} \gamma H_b \tag{36}$$

For the maximum wave setup $\overline{\eta}_m$ at the shoreline, Battjes (1974a,b) used equation (36) and simple geometry to show that

$$\overline{\eta}_m = \frac{5}{16} \gamma H_b \tag{37}$$

This means that the MWL at the shoreline is predicted to rise about 25 percent of the breaker wave height due to wave setup. Horizontal distances to locate setup values of interest can easily be determined from the geometry involved. The key assumptions are use of linear theory for S_{xx} and a constant γ in the surf zone.

(2) Reflective-Type Beaches. Plunging-type breakers are found on steep reflective beaches with narrow surf zones. Most laboratory beaches are of this type. Two theories have been advanced for setup primarily based on

75

observations by laboratory researchers. Swart (1974)[23], for complete plunging, assumed that all the energy of the approaching wave immediately transformed at the outer edge of the breaker zone. An abrupt water level change occurs to balance the change in radiation stress at the breaker line and the mean water surface is assumed level across the surf zone. Maximum setup was found to be lower than for spilling breakers. This was cited as a limiting case for natural beaches which have some combination of plunging- and spilling-type breakers.

Gourlay (1974) made allowance for the effect of a plunge point distance X_p, between the breakpoint and plunge point of a curling breaker, where he postulated that energy dissipation began. Assuming a constant wave setdown n_b over this distance, no abrupt rise in setup at the plunge point and a constant index γ from the plunge point to the shoreline on a plain beach,

$$\bar{n}_m = \frac{5}{16} \gamma (1 - \frac{6}{5} (\frac{X_b}{H_b})\gamma\tan\beta)H_b \qquad (38)$$

For surging breakers, X_p was zero and equation (38) reduces to equation (37). The dimensionless plunge distance (X_p/H_b) must be found empirically, as by Galvin (1969), and is related to the beach slope. Maximum setup is again lower than for spilling breakers.

More assumptions are employed in the theory for plunging breakers. These points are discussed when comparing theories to the observations in Chapter 4.

2.   **Oblique Wave Incidence.**

The more general case is when waves approach the beach at an angle. Wave refraction causes changes in wave height and length. The magnitudes of theoretical setdown and setup can be shown to depend on wave angle and all other factors that influence surf zone wave heights such as the induced longshore current and resulting wave-current interaction processes.

All the analytic theories to date neglect the feedback of the current on the wave motion. The partial differential equations are decoupled in this way to become two ordinary differential equations. The momentum equation perpendicular to the shore (eq. 28) is solved independently so that calculation of $\bar{n}$ is independent of longshore current. Such a theoretical solution for a profile with straight and parallel bottom contours but arbitrary shape (monotonously decreasing depth toward shore) was given by Jonsson and Jacobsen (1973). The shore-normal radiation stress is found from equation (23).

a.   **Wave Setdown.** Outside the breaker line, the wave height is determined by assuming a constant energy flux between orthogonals and Snell's law ($c/\sin \alpha$ = constant) to reference conditions to deep water. Interestingly,

[23] SWART, D.H., "Offshore Sediment Transport an Equilibrium Beach Profiles," Publication No. 131, Delft Hydraulics Laboratory, The Netherlands, 1974 (not in bibliography).

wave setdown is identical to that given for perpendicular wave incidence, equation (30). In terms of deepwater wave height H_o, and deepwater wave angle α_o, this becomes

$$\bar{\eta} = -\frac{H_o^2}{16} \frac{k_o}{n} \frac{\coth^2 kh}{\sinh 2kh} \frac{\cos\alpha_o}{\cos\alpha} \tag{39}$$

Since the ratio $\bar{\eta}/h$ is very small outside the breakers, the stillwater depth d can replace h in equation (39) for ease in computation.

b. __Wave Setup.__ The solution for spilling-type breakers with γ constant across the surf zone follows closely to that outlined above with normal inci- dence. All the same shallow-water assumptions are employed. The solution for wave setup obtained by Jonsson and Jacobsen (1973) is

$$\frac{d\bar{\eta}}{dx} = \frac{1}{1 + 8/(3\gamma^2\cos^2\alpha)} \frac{dd}{dx} \tag{40}$$

The setup slope is no longer a constant proportion to the beach slope as with normal wave incidence. For a given set of deepwater conditions, H_o and T_o, refraction will cause less setup at a given x due to the $\cos^2\alpha$ term in equation (40) and the fact that waves break at a smaller water depth.

The theoretical maximum setup $\bar{\eta}_m$ was also determined by Jonsson and Jacobsen (1973) to be

$$\bar{\eta}_m = \frac{5}{16} \gamma H_b (1 - \frac{6\pi}{5} \frac{H_b}{\gamma L_o} \sin^2\alpha_o) \tag{41}$$

and verified by Gourlay (1978) who put it in this form. Here the subscripts b and o mean breaker point and deepwater conditions, respectively. Equation (41) was found by integrating equation (40) and use of the appropriate boundary conditions and not the trigonometric manipulations for a plain beach as before to obtain equation (37). Surprisingly, therefore, this model shows that maxi- mum setup is independent of the bottom profile in the surf zone. The oblique maximum setup is less than normal setup and equation (41) reduces to equation (37) for $\alpha = 0$. Further parameter study by Jonsson and Jacobsen (19/3) showed that wave steepness (H_o/L_o and γ have much less influence than wave angle on maximum setup which varied approximately as $(\cos \alpha_o)^{2/5}$.

All the above are based on linear wave theory and regular waves. Wave setdown and setup theories when nonlinear and irregular waves are present will be reviewed in Section VI.

3. __Other Factors.__

A tilt of the MWL at the coast can also be due to the wind stress over a long fetch distance inducing a wind setup. The horizontal distance involved

is much longer than wave setup which is a pure coastal phenomena. The direction, fetch distance, windspeed, and duration are all factors influencing the magnitude of wind setup. A quadratic wind-stress law is generally applied where surface stress is proportional to the square of some reference windspeed. The wind stress can be added to the momentum balance equations to theoretically predict its influence on mean water surface gradients and nearshore currents as discussed further in Section V.

For normal wave incidence to the coast, wave breaking also induces a vertical circulation current (about a horizontal axis) in the surf zone. This is due to a vertical distribution of radiation stress which is greater near the surface than near the bottom since it is proportional to orbital wave motion. The result is schematized in Figure 22 (from Bijker and Visser, 1978)[24], where it is theorized that a net shoreward force at the surface and a net seaward force near the bottom results. The hypothetical circulation pattern resulting is also shown in Figure 22. There is no known theoretical attempt to solve this wave-induced circulation problem using radiation stress principles.

IV. LONGSHORE CURRENTS

As summarized at the end of Chapter 2, there are a large number of factors influencing longshore currents. The complexity of the forcing field, geometry, and fluid must be reduced to an idealized level to allow theoretical treatment that permits analytic solution. The basic theory described in this section is for the longshore current induced by simple waves striking an infinite, plane
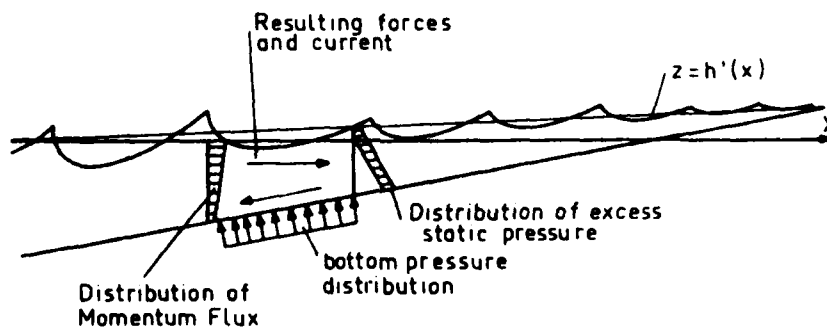
Figure 22. Circulation current in breaker zone (not to scale) (from Bijker and Visser, 1978).

---

[24] BIJKER, E. W., and VISSER, P.J., "Wave Set-Up, *"Coastal Engineering,"* W.W. Massie, ed., Vol. II, Harbor and Beach Problems, Department of Civil Engineering, Delft University of Technology, The Netherlands, 1979 (not in bibliography).

beach at an angle. Table 2 (modified from Ostendorf and Madsen, 1979) lists
the idealized environment along with those stresses and accelerations that
have been neglected. This list is long but many of these restrictions have
been relaxed in later generalizations of the basic theory, which will be re-
viewed separately, mostly in Sections V and VI. In addition, the basic theory
for uniform longshore current profile has undergone considerable modification
from the original models first introduced about 1970. These modifications
primarily reflect the influences of wave incidence angle, bottom shear stress,
and lateral turbulent mixing approximations and assumptions in the surf zone.
The original models and all subsequent modified theories for uniform longshore
current profile are reviewed in this section.

Table 2. Idealized environment for longshore current theory.

WAVE FIELD
    Simple, monochromatic gravity wave trains
    Steady-state, incident wave field
    Two-dimensional, horizontally propagating
    Linearized theory and radiation stresses
    Oblique angle of incidence, long wave crests
    Spilling-type breakers
    Constant breaker ratio in surf zone

BEACH
    Infinite length, straight and parallel contours
    Plane bottom slope
    Gentle slope
    Impermeable bottom

FLUID
    Incompressible
    Homogeneous (no air entrainment)

CURRENT
    Depth-integrated, parallel to coastline
    Time-average (one wave period)

NEGLECTED STRESSES AND ACCELERATIONS
    No surface wind stress
    No atmospheric pressure gradient
    No Coriolis acceleration
    No tides
    No local (time-average acceleration, i.e., steady flow
    No wave-turbulence interaction stresses
    No bed shear stress outside the surf zone
    No rip currents present
    No wave-current interaction stresses

79

1. Conservation Law Balances.

a. **Momentum.** Consider the idealized setting defined in Table 2. A schematic and definition sketch is shown as Figure 23, where the plan view shows two refracted wave rays a unit distance apart (exaggerated). The wave height and MWL variations shown are taken along any wave ray which are all identical for a plane, infinite beach. Clearly, there can be no gradient in S_{yy} in the y-direction for this case since time-average normal stresses are identical in the y-direction. The radiation shear stress S_{xy} (i.e., flux of y-direction momentum across plane perpendicular to the x-direction) is not the same on two sides of a differential element as shown in Figure 23. This is because all three factors (E, n, and α) in equation (25) for S_{xy} vary in the x-direction. The gradient dS_{xy}/dx thus becomes the driving stress in the y-direction momentum balance and is resisted only by the bed shear stress, $\bar{\tau}_B$. The overbar is for a time-averaged value. An additional y-direction stress is due to the gradient of the lateral shear force over the total depth, T_L due to turbulent mixing, i.e. wave orbital velocity interactions in the x- and y-directions. For the direction of wave incidence and coordinate system shown in Figure 23, the y-direction momentum balance becomes

$$\frac{dS_{xy}}{dx} - \bar{\tau}_B + \frac{dT_L}{dx} = 0 \tag{42}$$

The longshore current velocity, $\bar{v}$ appears in the time-averaged bed shear-stress term $\bar{\tau}_B$, and in the lateral shear force term T_L. With appropriate expressions for these quantities and for S_{xy}, it is possible to integrate equation (42) to derive an expression for the distribution of longshore current $\bar{v}(x)$ across the nearshore zone as schematized in Figure 23. This procedure again means a decoupling of the x-direction equation (28) from the y-direction equation (42).

b. **Energy Balance.** It is informative to also consider the energy balance equations in the nearshore zone. A good summary is found in Longuet-Higgins (1972a,b) for the idealized case in Figure 23. The general flux of energy per unit length of shoreline toward shore is given by

$$F_x = EC_g \cos\alpha = EC_n \cos\alpha \tag{43}$$

where E is the local energy density of the waves (eq. 14) and C_g, the group celerity. Assuming negligible wave reflection and no wave-current interactions, then the energy balance in the x-direction gives

$$\frac{dF_x}{dx} + D = 0 \tag{44}$$

where D is the local rate of energy dissipation per unit area.

But earlier, using linear wave theory, the shear component of the radiation stress was given by equation (25),

$$S_{xy} = E \, n \, \sin\alpha \, \cos\alpha$$

80
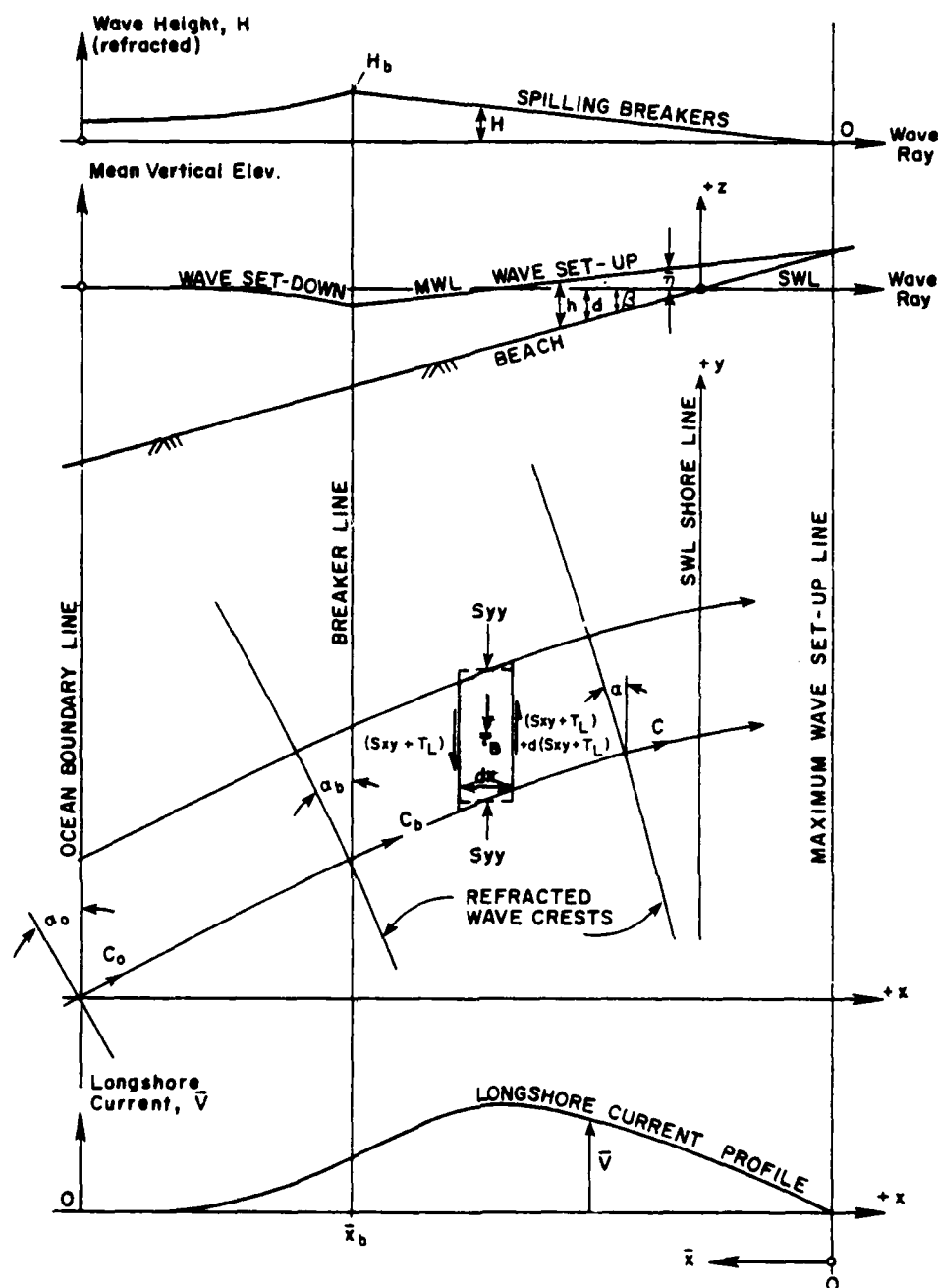
Figure 23. Schematic of refracted oblique wave incidence on a plane infinite beach showing resulting longshore current profile and MWL changes.

so that comparing equations (43) and (25) gives

$$S_{xy} = \frac{\sin\alpha}{c} F_X \tag{45}$$

where $\sin\alpha/c$ is also constant due to Snell's law. Longuet-Higgins (1972) proved that equation (45) is independent of the wave theory involved. Consequently, the driving force in the y-direction momentum balance equation (42) for longshore current becomes

$$\frac{dS_{xy}}{dx} = \frac{\sin\alpha}{c} \frac{dF_X}{dx} = -\left(\frac{\sin\alpha}{c}\right)D \tag{46}$$

and is thus directly proportional to the energy dissipation. "If there were no dissipation, there would be no current" (Longuet-Higgins, 1972).

Outside the breakers, if the energy flux is assumed constant, no energy is dissipated (D = 0) and consequently the longshore current must be identically zero. Inside the surf zone, continuous spilling-type breakers dissipate large amounts of wave energy to generate a longshore current. F_X is needed to be a continuous function of x in the surf zone to validate equation (44). Longuet-Higgins (1972) argued that most of the energy dissipation is due to wave breaking and not due to the bottom shear stresses. Thus, the shape of the wave height decay curve in the surf zone, as shown in Figure 23 and empirically determined from the breaker ratio, γ, plays a key role in the theoretical longshore current profile. Wave breaking, internal turbulent shears, and resulting energy dissipation as heat loss to the surroundings are the main mechanism driving the longshore current.

From the point of view of the momentum balance equation (42), the common belief is that the bottom shear stress dictates the strength of the longshore current. The lateral turbulent stresses only redistribute or smooth the velocity normal to the shore (e.g., see Horiwaka, 1978, p. 210). The question of the relative importance of internal turbulence dissipation and bottom shear is discussed further by examining their relative magnitude in the theoretical equations.

2. Original Model.

The use of radiation stress principles in the development of a theory for uniform longshore current profiles was first made by Bowen (1969a), Thornton (1969), Bakker (1970)[25], Iwata (1970), and Longuet-Higgins (1970). All used a longshore momentum balance as equation (42) but with some differences in the formulations for the three terms involved. Here the model by Longuet-Higgins (1970) has been designated as the original model primarily

[25]BAKKER, W.T., "Littoral Drift in the Surf Zone," Study Rept. WWK70-16, Directorate for Water Management and Hydraulic Research, Coastal Research Department Rijkswaterstaat, The Hague, The Netherlands, 1970 (not in bibliography).

because his results were put in dimensionless form, and further elaboration was presented by Longuet-Higgins (1972a).

It is convenient to introduce a new $\bar{x}$-direction coordinate system (after Bowen, 1969a) where the origin is taken at the maximum setup line and a positive $\bar{x}$ is facing seaward (Fig. 23). This simply gives the longshore current $\bar{v}=o$ at $\bar{x}=o$, and eliminates the uncertainty as to where the x-direction coordinate begins in deep water. The breaker position is $\bar{x}_b$. For the three terms in the y-direction momentum balance equation (42) Longuet-Higgins (1970, 1972a) derived the following.

a. <u>Driving Stress $dS_{xy}/d\bar{x}$</u>. Differentiating equation (25) or equation (45) in terms of energy flux gave

(1) <u>Outside the Surf Zone</u>

$$\frac{dS_{xy}}{d\bar{x}} = 0 \qquad (47)$$

(2) <u>Inside the Surf Zone</u>

$$\frac{dS_{xy}}{d\bar{x}} = \frac{5}{16} \rho \gamma^2 (gh)^{3/2} \left(\frac{\sin\alpha}{c}\right) \frac{dh}{d\bar{x}} \qquad (48)$$

where in equation (47) a constant energy flux is assumed. In equation (48) it is assumed that in the shallow-water surf zone, $n \doteq 1$; the wave angle is small, $\cos\alpha \doteq 1$; and Snell's constant is still applicable. Longuet-Higgins (1970) also neglected the effects of wave setdown and setup in further simplification of equation (48) although he recognized their effects. Wave setup is included in later modifications of this original theory. Therefore, within the surf zone he simply derived for a plane sloping beach

$$h^{3/2} \frac{dh}{d\bar{x}} \doteq d^{3/2} \frac{dd}{d\bar{x}} \simeq (\tan\beta)^{3/2} \bar{x}^{3/2} \tan\beta$$

so that equation (48) became

$$\frac{dS_{xy}}{d\bar{x}} \doteq \frac{5}{16} \rho g^{3/2} \gamma^2 (\tan\beta)^{5/2} \left(\frac{\sin\alpha}{c}\right) \bar{x}^{3/2} \qquad (49)$$

From equation (46), therefore

$$D = \frac{5}{16} \rho g^{3/2} \gamma^2 (\tan\beta)^{5/2} \bar{x}^{3/2} \qquad (50)$$

meaning the local rate of energy dissipation D due to wave breaking varies as $\bar{x}^{3/2}$ from zero at the maximum setup line (on a plane beach with constant γ). Other forms for equation (49) stem from using the celerity $C=\sqrt{gh}$ in the surf zone.

b. **Resisting Stress, $\bar{\tau}_B$.** For the time-average bottom shear stress, $\bar{\tau}_B$
Longuet-Higgins (1970) derived

$$\bar{\tau}_B = \frac{2}{\pi} C_f \rho |u_{Bm}| \bar{v} \tag{51}$$

where

> C_f = a boundary resistance coefficient due to both waves and longshore
>   current, $\bar{v}$
> $|u_{Bm}|$ = the absolute value, maximum wave orbital velocity near the bottom
>   for sinusoidal motion

Longuet-Higgins (1970) obtained equation (51) from the usual quadratic stress
law in real time for the vector value of $\vec{\tau}_B$

$$\vec{\tau}_B = \frac{1}{2} f_{wc} \rho |\vec{u}_B| \vec{u}_B = C_f \rho |\vec{u}_B| \vec{u}_B \tag{52}$$

where $\vec{u}_B$ is the wave orbital particle velocity just above the bottom boundary.

    To go from equation (52) for $\vec{\tau}_B$ to the time-average value in equation (51)
is not trival. Longuet-Higgins (1970) made the additional assumptions that

> (1) the longshore current velocity $\bar{v}$ is small in comparison with the
>   wave orbital velocity, u_B, and
> (2) the wave incident angle $\bar{\alpha}$ is very small in the surf zone so that
> $\bar{v}$ is roughly normal to u_B.

Taking the time-averaged mean value of $|u_B|$ over one wave period and assuming
C_f represents a constant mean value over this same period, the component of $\bar{\tau}_B$
in the y-direction becomes that given by equation (51). Assumption (1) above
essentially makes this a linearized bed stress term or a weak current theory.
Removal of assumptions (1) and (2) has been a significant achievement in
modifying the original theory as described below.

    Further approximations are needed to put equation (51) in a more usable
form. Using linear theory to obtain u_{Bm} in shallow water and taking $\gamma = H/h$
give

$$u_{Bm} = \frac{1}{2} \gamma \sqrt{gh} \tag{53}$$

so that equation (51) becomes if wave setup is again neglected

$$\bar{\tau}_B = \frac{1}{\pi} \rho C_f g^{\frac{1}{2}} \gamma (\tan\beta)^{\frac{1}{2}-\frac{1}{2}} x^{\frac{1}{2}} \bar{v} \tag{54}$$

This form clearly shows how the longshore current $\bar{v}$ is introduced and how the
bottom shear stress varies as $x^{-\frac{1}{2}}$.

c. Lateral Turbulent Mixing Stress, $dT_L/d\bar{x}$. For the time-averaged lateral mixing force over the water depth, T_L Longuet-Higgins (1970) derived

$$T_L = h\bar{\tau}_L = h\bar{\mu}_L \frac{d\bar{v}}{d\bar{x}} = h(Np\bar{x}(gh)^{\frac{1}{2}}) \frac{d\bar{v}}{d\bar{x}} \tag{55}$$

where

   $\bar{\tau}_L$ = the lateral turbulent eddy stress due to waves
   $\bar{\mu}_L$ = the lateral turbulent eddy viscosity due to waves
   N = a dimensionless, turbulent closure coefficient for lateral wave
        mixing proposed by Longuet-Higgins (1970) to be of the order $N\leq0.01$

The term τ_e is reserved for a true, turbulent Reynolds stress due to random turbulent velocity interactions at scales far less than the wave orbital velocity scale.

If wave setup is again neglected taking $h \cong d = x\tan\beta$ gives

$$\frac{dT_L}{d\bar{x}} = N\rho g^{\frac{1}{2}}(\tan\beta)^{3/2} \bar{x}^{5/2} \frac{d\bar{v}}{d\bar{x}} \tag{56}$$

so that the lateral turbulent mixing stress becomes

$$\frac{dT_L}{d\bar{x}} = N\rho g^{\frac{1}{2}}(\tan\beta)^{3/2} \frac{d}{d\bar{x}} [\bar{x}^{5/2} \frac{d\bar{v}}{d\bar{x}}] \tag{57}$$

d. <u>Dimensional Longshore Currents</u>. In summary, Longuet-Higgins (1970) derived the momentum balance equation (42)

$$\frac{dS_{xy}}{d\bar{x}} - \bar{\tau}_B + \frac{dT_L}{d\bar{x}} = 0$$

with equations (49), (54), and (57)

$$\frac{dS_{xy}}{d\bar{x}} = \frac{5}{16} \rho g^{3/2} \gamma^2 (\tan\beta)^{5/2} (\frac{\sin\alpha}{c})\bar{x}^{3/2} = r\bar{x}^{3/2}$$

$$\bar{\tau}_B = \frac{1}{\pi} \rho C_f g^{\frac{1}{2}}\gamma(\tan\beta)^{\frac{1}{2}}\bar{x}^{\frac{1}{2}}\bar{v} \cong q\bar{x}^{\frac{1}{2}}\bar{v}$$

$$\frac{dT_L}{d\bar{x}} = N\rho g^{\frac{1}{2}}(\tan\beta)^{3/2} \frac{d}{d\bar{x}}[\bar{x}^{5/2} \frac{d\bar{v}}{d\bar{x}}] = p \frac{d}{d\bar{x}} [\bar{x}^{5/2} \frac{d\bar{v}}{d\bar{x}}]$$

where we define three new constants

$$r = \frac{5}{16} \rho g^{3/2}\gamma^2 (\tan\beta)^{5/2}(\frac{\sin\alpha}{c}) \tag{58a}$$

$$q = \frac{1}{\pi} \rho C_f g^{\frac{1}{2}} \gamma (\tan\beta)^{\frac{1}{2}} \tag{58b}$$

$$p = N\rho g^{\frac{1}{2}} (\tan\beta)^{\frac{3}{2}} \tag{58c}$$

to give the second-order differential equation for $\bar{v}$

$$p\bar{x}^{5/2} \frac{d^2\bar{v}}{d\bar{x}^2} + \frac{5}{2} p\bar{x}^{-3/2} \frac{d\bar{v}}{d\bar{x}} - q\bar{x}^{-\frac{1}{2}}\bar{v} = -r\bar{x}^{-3/2} \tag{59}$$

with the right-hand side vanishing outside the surf zone. Thus $\bar{v}(x)$ is the solution of two second-order linear, ordinary differential equations which must match in magnitude and gradient of $\bar{v}(x)$ at the breaker line and vanish at $\bar{x}=0$ and the ocean boundary.

(1) <u>Neglecting Lateral Turbulent Mixing</u>. Taking p=0 greatly simplifies equation (59) to give as an approximate solution

$$\bar{v}* = \frac{r}{q}\bar{x} = \frac{5\pi}{16} \frac{\gamma}{C_f} g(\tan\beta)^2 (\frac{\sin\alpha}{C})\bar{x} \qquad \text{inside surf zone} \tag{60a}$$

$$v* = 0 \qquad\qquad\qquad \text{outside surf zone} \tag{60b}$$

On a plane beach with γ, C_f, and $(\sin\alpha/c)$, all constants in the surf zone, the longshore current profile is triangular in shape, reaching a peak at the breaker line and dropping to zero outside the breakers (see Fig. 24, P = 0).

(2) <u>Reference Longshore Current Velocity</u>. Again neglecting lateral turbulent mixing stresses, the longshore current velocity at the breaker line $\bar{v}_b^*$ can be used as a reference velocity. It becomes from equation (60a) after again taking $h_b = d_b = \tan\beta\bar{x}_b$

$$\bar{v}_b^* = \frac{5}{16} \frac{\gamma}{C_f} (gd_b)(\frac{\sin\alpha}{C})_b \tan\beta \tag{61}$$

Other forms result from taking $C_b = \sqrt{gd_b}$ in equation (61). In reality, the velocity discontinuity at the breaker line cannot occur so that the lateral turbulent mixing smooths the velocity profile. The solution with lateral mixing is simplified using dimensionless variables with $\bar{v}_b^*$ as the reference velocity.

e. <u>Dimensionless Longshore Currents</u>. Longuet-Higgins (1970) introduced the dimensionless variables, X and V as

$$X = \frac{\bar{x}}{\bar{x}_b} \qquad \text{and} \qquad V = \frac{\bar{v}}{\bar{v}_b^*} \tag{62}$$

into equation (59) to obtain

86
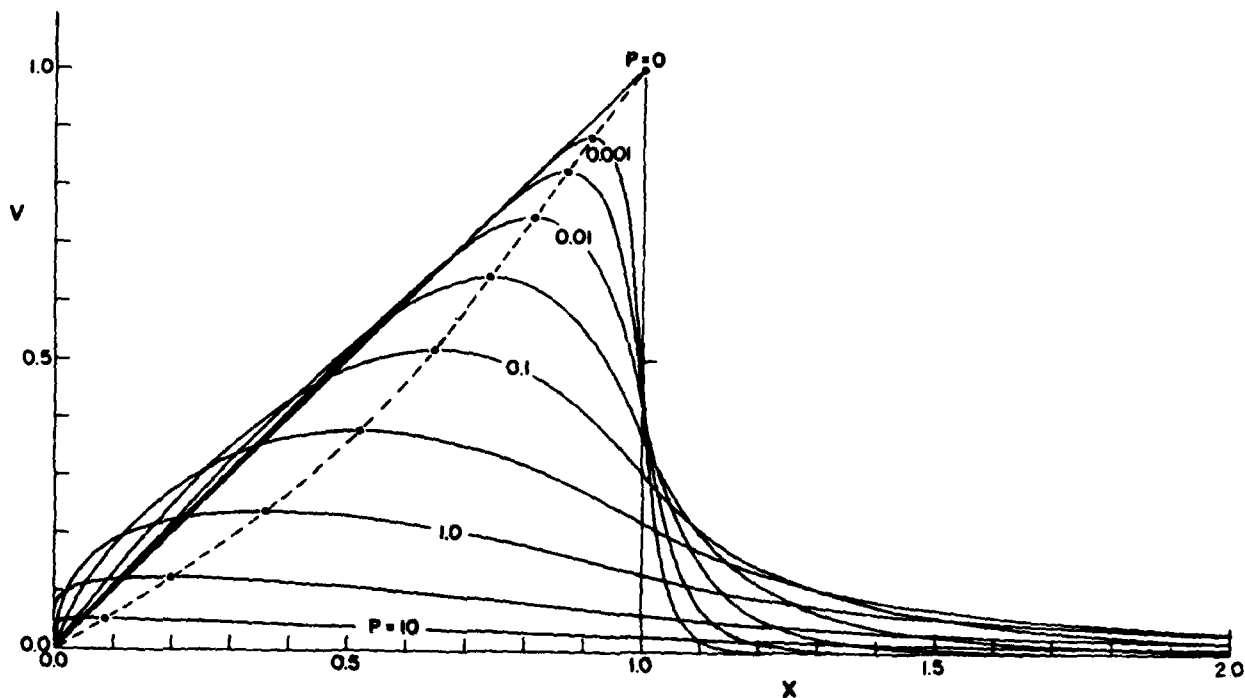
Figure 24. Dimensionless longshore current profiles as function of P-parameter (from Longuet-Higgins, 1970, 1972).

$$PX^{5/2} \frac{d^2V}{dX^2} + \frac{5}{2} PX^{3/2} \frac{dV}{DX} - X^{1/2}V = -X^{3/2} \qquad (63)$$

where again the right-hand side vanishes outside the surf zone and,

$$P = \frac{P\bar{v}_b^*}{\tau_b \bar{x}_b} = \frac{N\pi \tan\beta}{C_f \gamma} \qquad (64)$$

The dimensionless parameter P now represents the relative importance of lateral turbulent mixing of the wave orbital motion to the bottom frictional resistance. Taking P = 0 for no lateral mixing gives V = 1 at X = 1($\bar{x} = \bar{x}_b$) and the triangular solution as before with V = 0 outside the breakers.

Longuet-Higgins (1970) solved equation (63) using the boundary conditions that V→0 as X→0 and X→∞ and internally that V and dV/dX are continuous at X = 1. He obtained the following results.

(1) In general, P ≠ 0.4.

$$V = AX + B_1 X^{P_1} \qquad 0 < X < 1 \qquad \text{(inside breakers)} \qquad (65a)$$

$$V = B_2 X^{P_2} \qquad X > 1 \qquad \text{(outside breakers)} \qquad (65b)$$

where

$$A = \frac{1}{(1 - \frac{5}{2} P)} \qquad (66a)$$

$$P_1 = -\frac{3}{4} + \sqrt{\frac{9}{16} + \frac{1}{P}} \qquad (66b)$$

$$P_2 = -\frac{3}{4} - \sqrt{\frac{9}{16} + \frac{1}{P}} \qquad (66c)$$

$$B_1 = \frac{P_2 - 1}{P_1 - P_2} A \qquad (66d)$$

$$B_2 = \frac{P_1 - 1}{P_1 - P_2} A \qquad (66e)$$

so that all the constants (A, P_1, P_2, B_1, and B_2) in equation (65) depend upon P.

(2) Singularity, P = 0.4. The coefficient A becomes infinite for P = 0.4. For this singularity, Horikawa (1978a) gives the solution

$$V = \frac{10}{49} X - \frac{5}{7} X \ln X \qquad 0 < X < 1 \qquad \text{(inside breakers)} \qquad (67a)$$

$$V = \frac{10}{49} X^{-5/2} \qquad X > 1 \qquad \text{(outside breakers)} \qquad (67b)$$

The family of solutions for some representative P values is shown in Figure 24 (after Longuet-Higgins, 1972a). Taking larger P values gives more lateral turbulent mixing to smooth and spread the theoretical longshore current profile across the surf zone and beyond the breakers. Using lower P values shifts the maximum longshore current toward the breakers. The theory requires estimates for three parameters (γ, C_f, and N) for a solution on a given plane beach slope. It neglects wave setdown and setup effects in mean water depth but includes the maximum setup location as the new shoreline.

The radiation stress theory of longshore currents as summarized by equations (65), (66), and (67) provided the needed breakthrough in 1970. Since

then, many modifications attempting to improve the generality and accuracy of the original model have appeared in the literature. These are summarized in the next section along with the original contributions of Bowen (1969a) and Thornton (1969).

3. Modified Models.

The modified theories for longshore currents since 1970 are listed in Table 3. These theories still retain linear wave theory to calculate the radiation stresses for regular waves. Nonlinear and irregular wave theories are discussed in Section VI. In some cases, closed-form analytic solutions are no longer possible due to the beach profile or bed shear-stress formulation employed. Rather than discuss each model separately, the major modification areas involved are reviewed. In most cases, actual theoretical results will be discussed in Chapter 4 and compared with experimental measurements.

a. Beach Profile and Wave Setup. Those theories that are for a beach profile with straight and parallel bottom contours but with depth in the surf zone that is monotonously decreasing (arbitrary profile) require numerical integration methods for a solution. Thornton (1969) was the first to provide such an analysis.

Wave setdown effects on the MWL are neglected by all theories except the numerical integrations by Jonsson, Skovgaard, and Jacobsen (1974) and Skovgaard Jonsson, and Olsen (1978). However, the influence of wave-induced setup has been incorporated in most subsequent theories because of its influence upon γ.

Bowen (1969a) and Komar (1975) simply took the resulting wave setup slope equation for normal wave incidence on a plane beach (see eq. 35) which for the x-coordinate system becomes

$$\frac{d\bar{\eta}}{d\bar{x}} = - [\frac{1}{1 + 8/(3\gamma^2)}] \tan\beta = -K\tan\beta \tag{68}$$

Letting

$$m = \frac{d(d+\bar{\eta})}{d\bar{x}} = \frac{dd}{d\bar{x}} + \frac{d\bar{\eta}}{d\bar{x}} = \tan\beta - K\tan\beta$$

or

$$m = (1-K)\tan\beta = \frac{\tan\beta}{1+3\gamma^2/8} \tag{69}$$

then the following modified equations result, neglecting wave setdown.

For the driving stress term, equation (49) now becomes

$$\frac{dS_{xy}}{d\bar{x}} = \frac{5}{16} \rho\gamma^2 \frac{\tan\beta}{1+3\gamma^2/8} (gh)^{3/2} (\frac{\sin\alpha}{c})\cos\alpha \tag{70}$$

Table 3. Longshore current theories since 1969 based on radiation stress theory.

Researcher	Beach Profile	Wave Normal	Set-Up Refract.	Bed Shear Stress Form Strength	Angle	Lateral Mixing Formulation	Surf Zone Empirism	Analytic or Num. Soln.	Remarks
Bowen (1969)	Plane	Yes		Linear		Modified	Modified	Analytic	Oversimplified Bed Shear
Thornton (1969, 1970)	Plane & Arbit.	Yes		Weak*	Small*	Modified	"	Analytic & Numerical	Used wave motion friction factor
Jonsson, Skovgaard, & Jacobsen (1974)	Arbit.		Yes	Strong	Small	Modified	"	Numerical	Wave refraction included in wave set-up
Komar (1975, 1976)	Plane	Yes		Original eq. (51) Weak	Small	Original eq. (55)	"	Analytic	Neglects wave refr in wave set-up
Bijker & v.d. Graaff (1978)[26]	Plane	Neglected	Neglected	Strong**	Large**	Modified	"	Numerical	Numerical soln. required for strong currents
Liu & Dalrymple (1978)	Plane		Yes	Weak & Strong	Large	Neglected	"	Analytic	Numerical soln. required for strong currents
Madsen, Ostendorf & Reyman (1978)	Plane	Yes		Curve Fit with Available Data		Modified	.	Numerical	Empirical means used for strong currents to permit analytic soln.
Skovgaard, Jonsson, & Olsen (1978)	Arbit.		Yes	Strong	Small	Modified	"	Numerical	Mixing stresses different on each side of broken line.
Kraus & Sasaki (1979)	Plane		Yes	Weak	Large	Modified	"	Analytic	Weak current theory matches field data.

*Weak Current + Small Angle   linearized bottom friction model equation (51).
**Strong Current + Large Angle   non-linear bottom friction model.

"Original Model" Longuet Higgins (1970)	Plane	Omitted		Weak	Small			Analytic

[26]BIJKER, E.W., and GRAAFF, J., "Longshore Currents, *Coastal Engineering*, W.W. Massie, ed., Vol. II, Harbor and Beach Problems, Department of Civil Engineering, Delft University of Technology, The Netherlands, 1979 (not in bibliography)

where the incident wave angle is no longer assumed small. Using the same bed shear-stress formulation as before (eq. 54), except including wave setup, and neglecting lateral turbulent mixing stresses, the following modified equation is obtained

$$\bar{v}* = \frac{5}{16}\pi \frac{\gamma}{C_f} \, gh \, \frac{\tan\beta}{1+3\gamma^2/8} \, \frac{\sin\alpha}{C} \cos\alpha \tag{71}$$

for longshore currents. This reduces to equation (60a) inside the surf zone when h→d. Equation (71) is essentially that given by Bakker (1970)[25], Thornton (1969,1970a), and confirmed by Gourlay (1978) and others. At the breakpoint, it becomes the modified reference velocity (using $C_b = \sqrt{gh_b}$ for shallow linear waves)

$$\bar{v}*_b = \frac{5}{16}\pi \frac{\gamma}{C_f} \, (gh_b)^{\frac{1}{2}} \, \frac{\tan\alpha}{1+3\gamma^2/8} \, \sin\alpha_b \, \cos\alpha_b \tag{72}$$

For γ values from 0.5-1.2, the term $[(1/(1+3\gamma^2/8)]$ in equation (72) varies from 0.91 to 0.65, so that the wave setup modification is not insignificant. Komar (1975a, 1976b) obtained the additional term $1/(1+\gamma)^{\frac{1}{2}}$ in equation (72) that was shown to be inconsistent with previous assumptions for dS_{xy}/dx and τ_B by Gourlay (1978). Komar (1975a, 1976b) also had the term $(1+3\gamma^2/8)^2$ instead of the first power as in equation (72). The present report and Gourlay (1978) have been unable to verify Komar's form. Using this modified $\bar{v}*_b$ in equation (64) gives for Longuet-Higgins, P-parameter (modified)

$$P = \frac{N\pi}{C_f\gamma} \cdot \frac{\tan\beta}{1 + 3\gamma^2/8} \tag{73}$$

so that all of Longuet-Higgins' (1970) dimensionless results are still applicable (eqs. 65, 66, and 67) if $\bar{v}*_b$ and P are replaced by the modified versions (eqs. 72 and 73). However, it must be remembered that this setup correction assumes normal wave incidence and hence also neglects wave refraction effects in the surf zone.

All other modified models listed in Table 3 include some form of Snell's law refraction in the surf zone to additionally modify the wave setup. As shown earlier (eq. 40), the setup slope is no longer a constant proportion to the beach slope and refraction results in less wave setup. For the numerical solution methods, the decoupled motion equations (28) and (42) are solved together. The $\bar{\eta}$ solution from equation (28) includes effects of geometry refraction in the dS_{xx}/dx term and is in turn used in equation (42) to determine the longshore current profile. Numerical accuracy is important so that careful numerical integration procedures are needed (e.g., see Jonsson, Skovgaard, and Jacobsen, 1974). In all such models to date, current-refraction effects on the calculated $\bar{\eta}$ values have not been incorporated to make the equations a coupled set.

---

[25]Ibid.

Finally, Kraus and Sasaki (1979), following Liu and Dalrymple (1978), include wave refraction in their analytic development. Inside the breaker line they obtained the following result for the driving stress

$$\frac{dS_{xy}}{d\bar{x}} = \frac{5}{16} \rho \gamma^2 g \frac{\tan\beta}{1+3\gamma^2/8} \sin\alpha_b \left(\frac{h^3}{h_b}\right)^{\frac{1}{2}} [(1-\sin^2\alpha_b \frac{h}{h_b})^{\frac{1}{2}} -$$

$$\frac{\sin^2\alpha_b}{5} \frac{h}{h_b}(1-\sin^2\alpha_b \frac{h}{h_b})^{-\frac{1}{2}}] \qquad (74)$$

Note that neglecting wave setup, refraction and for small α_b, equation (74) reduces to that employed by Longuet-Higgins (eq. 48). These researchers also modified the form of the bed shear stress and lateral mixing terms, so their final results are deferred to the subsection on lateral mixing.

b. **Modified Bottom Shear Stress**. The most important modifications to the original model have been in relaxing the assumptions of a weak longshore current and small wave incidence angle. This is because the longshore current is inherently related to the bed shear-stress model employed. The major weakness of Bowen's (1969a) model was the overly simplistic, linearized, shear-stress term, $\tau_B = \rho C_f v$. All other models in Table 3 begin with a quadratic form as given by equation (52).

Bottom shear stress is a vector oscillating in both direction and magnitude. The major difficulty is to find an expression for the effective bed stress (and friction factors involved) in terms of a time-averaged current. The coordinate axes and velocity vectors are shown in Figure 25. The instantaneous bottom shear stress τ_B is assumed to be in the direction of the resultant velocity $\vec{U}$ of the vector sum of longshore current velocity v and bottom wave orbital velocity u_B (eq. 52).

$$\vec{\tau}_B = C_f \rho |\vec{U}|\vec{U} = f_{cw}\frac{1}{2}\rho |\vec{U}|\vec{U}$$

where $\vec{U} = \bar{v} + \vec{U}_B$, and C_f, f_{cw} are combined current and wave friction factors.

The ratio of theoretical breaker current with no lateral mixing to maximum wave orbital velocity near the bed, v_b^*/u_{Bm} has been shown to exceed unity except for small wave angles. This ratio was used to argue the inconsistency of the weak original model of Longuet-Higgins (1970) as discussed by Huntley (1976a), Madsen, et al. (1978), and Liu and Dalrymple (1978). But v_b^* is not a physical velocity. Therefore Kraus and Sasaki (1979) used the ratio $\bar{v}_m/u_{Bm}$ instead, where $\bar{v}_m$ is the maximum current from experiments or theory. Surprisingly, they showed that most laboratory experiments are invalid to test the Longuet-Higgins (1970) model since $\bar{v}_m/u_{Bm} \approx 1\text{-}3$, indicating strong longshore currents are present.

92
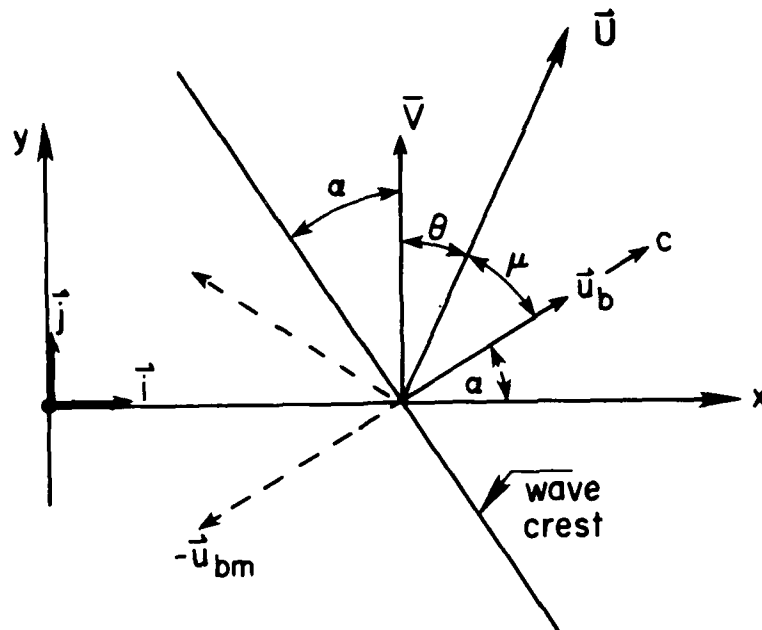
Figure 25. Schematic of wave and longshore current velocity vectors in bed shear-stress models.

(1) **Strong Currents at Small Angles**. Following the earlier work of Jonsson (1966a)[27] for waves and currents in the same direction, Jonsson, Skovgaard, and Jacobsen (1974) proposed a simple interpolation formula for the instantaneous friction factor f_{cw} when the waves are roughly normal to the current direction (i.e., $\alpha = 0$ in Fig. 25).

$$f_{cw} = f_w + (f_c - f_w)\sin\mu \qquad (75)$$

This made f_{cw} identical to the wave friction factor f_w with no current ($\mu = 0°$) and also made f_{cw} equal to the current friction factor f_c with no waves present ($\mu = 90°$). The combined friction factor f_{cw} is time dependent, since $\vec{u}_B$ varies over the wave period. Using linear wave theory for $\vec{u}_B$, Jo..son, Skovgaard, and Jacobsen (1974) derived the following expression using equation (75) in equation (52)

$$\bar{\tau}_{By} = f_s \tfrac{1}{2}\rho\bar{u}^2 \qquad (76)$$

for the time-averaged bottom shear stress parallel to the coast. The time-averaged friction coefficient f_s is found from

---

[27]JONSSON, I.G., "The Friction Factor for a Current Superimposed by Waves," Basic Research Program, Report 11, 2-12, ISVA, Technical University, Denmark, 1966a (not in bibliography).

93

$$f_s = f_c + (\frac{2}{\pi} \sqrt{1 + (u_{Bm}/\bar{v})^2} \cdot E(m) - 1) f_w \qquad (77)$$

The expression $E(m)$ is a complete elliptic integral of the second kind, i.e.,

$$E(m) = \int_0^{\pi/2} (1 - m\sin^2\mu)\, d\mu \qquad (78a)$$

with the parameter m given by

$$m = \frac{u_{Bm}^2}{u_{Bm}^2 + \bar{v}^2} \qquad (78b)$$

For weak currents ($\bar{v}_m \ll u_{Bm}$), equations (76) and (77) reduce to

$$\bar{\tau}_{By} = \frac{1}{\pi} f_w \rho |u_{Bm}| \bar{v} \qquad (79)$$

which is identical to equation (51) used by Longuet-Higgins (1970). The scientists' friction coefficient C_f could then be defined as fw/2 for the weak current-small angle theory. This form is also identical to that employed by Thornton (1969) who similarly began from the wave-current approach of Jonsson (1966a)[27]. Equation (77) requires determination of both f_w and f_c coefficients. For steady free surface flows, f_c depends on both water depth and bottom roughness. The experimental determination of fw in oscillatory water tunnels is still in progress. Details are beyond the intended scope of this review. The nonlinear nature of both $\bar{\tau}_{By}$ and f_s prevents simple analytic formulation of the current profile. Jonsson, Skovgaard and Jacobsen (1974) also included a different lateral mixing formulation (see below). The complete final results are discussed in Chapter 4.

Liu and Dalrymple (1978) gave a complete analysis for the strong current large-angle model with small angles as a special case. When $\bar{U}/u_{Bm} \gg 1$ they found

$$\bar{\tau}_{By} = \frac{1}{2} f_{cw} [\bar{v}^2 + \frac{u_{Bm}^2}{4}] \qquad (80)$$

but emphasized that to be applicable, u_{Bm} must also be very small if $\bar{v}$ diminishes for small α. They neglected lateral turbulent mixing stresses in all longshore current formulations. Their work is primarily of interest for the large-angle modifications on longshore current theory as described below.

---

[27]Ibid.
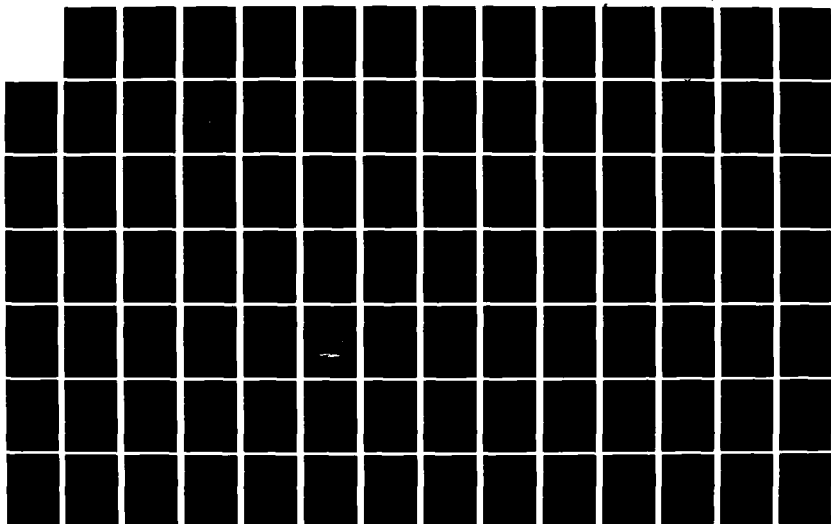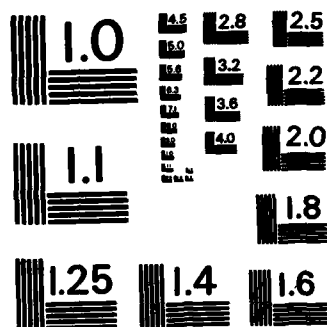
MICROCOPY RESOLUTION TEST CHART

NATIONAL BUREAU OF STANDARDS-1963-A

(2) <u>Weak Currents at Large Angles</u>. As observed in the laboratory and field (see Ch. 2), it is the occurrence of relatively large wave incidence angles that drives the longshore current (see Fig. 12). Liu and Dalrymple (1978) concluded from studies of available field data (Inman and Quinn, 1951; Balsillie, 1975; Komar, 1976a) that a weak current ($\bar{U}/u_{Bm} \ll 1$) large wave angle model for bottom shear stress was consistent with field observations. Using this assumption they derived the expression

$$\bar{\tau}_{By} = \frac{\rho C_f}{\pi} u_{Bm} [(\bar{v}\sin 2\alpha)\vec{i} + 2\bar{v}(1 + \sin^2\alpha)\vec{j}] \tag{81}$$

with $\vec{i}, \vec{j}$ the unit vectors in the x and y directions, respectively. For small angles α, the original model formulation of Longuet-Higgins (1970), equation (51) is recovered, as expected.

Of major interest was the theoretical longshore current velocity profile that resulted in comparison with that derived by Longuet-Higgins (1970), neglecting lateral mixing stresses and corrected for wave setup due to normal wave incidence, i.e., equation (71). Liu and Dalrymple (1978) derived the following complicated expression for the longshore current without lateral mixing

$$\bar{v}^* = \frac{5}{16}\pi\frac{\gamma}{C_f} gh\tan\beta(\frac{\sin\alpha}{c})[5-6(\frac{\sin\alpha}{c})^2 gh][1-(\frac{\sin\alpha}{c})^2 gh]^{-\frac{1}{2}}.$$

$$\{(1+3\gamma^2/8) + (1-5\gamma^2/16)(\frac{\sin\alpha}{c})^2 gh - \frac{3\gamma^2}{4}(\frac{\sin\alpha}{c})^4 g^2h^2\}^{-1} \tag{82}$$

Equation (79) uses Snell's Law to include wave setup from refraction. Consequently, the large-angle velocity profile that results from equation (82) is different from the small-angle modified form (eq. 71) for two reasons; namely, the bottom shear-stress formulation and the inclusion of wave refraction in the wave setup. Comparison of the results of the two theories must be viewed with this in mind.

The results of two comparisons made by Liu and Dalrymple (1978) for their weak current large-angle theory are shown in Figure 26. Here, X is the dimensionless surf zone distance such that X = 1 at the breaker. The symbol $\bar{v}^*_{LH}$ means the modified theory of Longuet-Higgins given by equations (71) in general and equation (72) at the breaker. Figure 26 (a and b) demonstrates a significant deviation between the two theories as incident wave angle increases. Even at $\alpha = 10°$, approximately a 20-percent difference is observed at the breaker line (Fig. 26,a) and across the surf zone (Fig. 26,b). It was also shown that the $\bar{v}^*/u_{Bm}$ ratio depended upon two factors, ($\tan\beta/C_f$) and wave angle α. When the ratio $\tan\beta/C_f$ was small (mild slopes or large bottom friction as usually found in the field), the $\bar{v}^*u_{Bm}$ ratio was also relatively low across the surf zone for $0 < \alpha < 45°$. This gives further credence to the weak current large-angle theory for dissipative-type beaches.

Liu and Dalrymple also developed a validity diagram (see Fig. 5 in Liu and Dalrymple, 1978) for longshore current theories that depended upon the ratio $\bar{v}^*/u_{Bm})_b$ at the breaker line to separate the weak and strong current

95
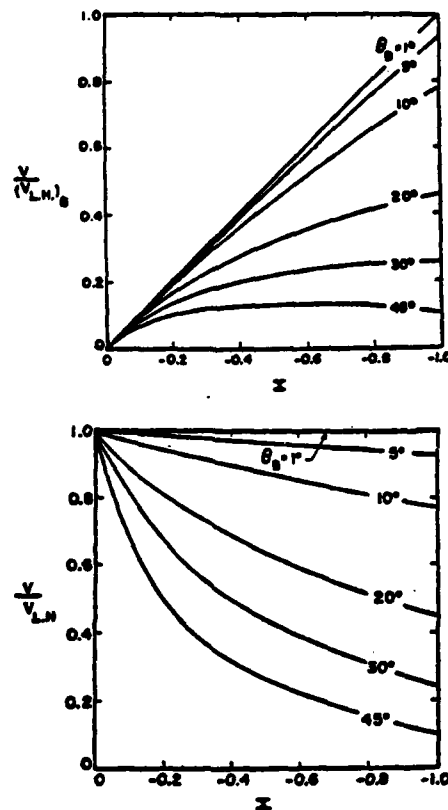
Figure 26. Comparison of theoretical longshore current velocity for weak currents, small- and large-angle theories (from Liu and Dalrymple, 1978).

theories. Although the effort is to be commended, the results are not very meaningful since lateral turbulent mixing stresses are neglected in the theories. The reference velocity $\bar{v}_b^*$ is not a true physical velocity as discussed above.

Kraus and Sasaki (1979) extended the weak current large-angle theory to include lateral mixing stresses. Their contributions are fully examined in the subsection on lateral mixing.

(3) Strong Currents at Large Angles. For steep (reflective) beaches with narrow surf zones (or smooth bottoms), a bed shear-stress formulation for both strong currents and large incidence angles is required. Complete expressions for $\bar{\tau}_{By}$ and $\bar{v}^*$ (neglecting lateral mixing) are given by Dalrymple and Liu (1978). The value of $\bar{v}^*$ is questionable. A constant $\gamma = H/h$ ratio is used in the surf zone even though plunging-type breakers are normally found on steep beaches. The theory is of interest for comparison of laboratory observations but requires modification by lateral mixing and plunging-type breaker formulations in the surf zone.

A different approach was suggested by Bijker (1966), modified by Swart (1974)[23] and fully discussed by Bijker and v.d. Graaff (1978)[26]. This theory is unique from those above in that the location above the bed where the wave orbital velocity and current velocity are specified is explicitedly defined. The elevation chosen was equal to the laminar sublayer thickness which is dependent upon the bed roughness height. In this way, modern turbulent boundary layer theory is incorporated into the bed shear-stress model. Expressions for the shear stress at this elevation used the resultant velocity $\vec{U}$ as defined in Figure 25. They then obtained the result

$$\bar{\tau}_{By} = \frac{2\rho g \bar{v}^2}{C_c^2 T} \int_{-T/4}^{T/4} \left\{ [1 + \xi \frac{u_{Bm}}{\bar{v}} \sin\omega t \sin\alpha] \cdot \right.$$

$$\left. [1 + (\xi \frac{u_{Bm}}{\bar{v}} \sin\omega t)^2 + 2\xi \frac{u_{Bm}}{\bar{v}} \sin\omega t \sin\theta]^{\frac{1}{2}} \right\} dt \tag{83}$$

where

    p = a dimensionless parameter found from wave orbital velocity experiments (e.g., Jonsson, 1966a)[28] relating the wave velocity at the bottom to that at the reference elevation

    κ = the von Karman constant $\doteq 0.4$

    C_c = the Chezy friction coefficient

    f_w = the wave friction coefficient from $\tau_w = \frac{1}{2} f_w \rho U_B^2$

    T = the wave period

Bijker (1966) numerically integrated equation (78) for a range of realistic values of $\bar{v}$, u_{Bm}, ξ and α. Curve fitting the results for $|\alpha| < 20°$ gave

$$\bar{\tau}_{By} = \frac{\rho g \bar{v}^2}{C_c^2} [0.75 + 0.45 (\xi \frac{u_{Bm}}{\bar{v}})^{1.13}] \tag{84}$$

For weak currents and small incident wave angles equation (80) can be integrated directly to yield a form identical with equation (51) taking

$$C_f = \frac{\sqrt{2 g f_w}}{C_c} \tag{85}$$

A numerical example is shown in Figure 27 adapted from Bijker and v.d. Graaff (1978). Here, turbulent mixing is neglected along with wave setup effects. The result labeled $\bar{v}_t^*$ is for weak current small-angle model but each velocity is calculated from a local friction term. This makes the profile

[23]Ibid.

[26]Ibid.

[28]JONSSON, I.G., "Wave Boundary Layers and Friction Factors," *Proceedings, 10th Coastal Engineering Conference* (Tokyo), Vol. I, Ch. 10, 1966b, pp. 127-148 (not in bibliography).
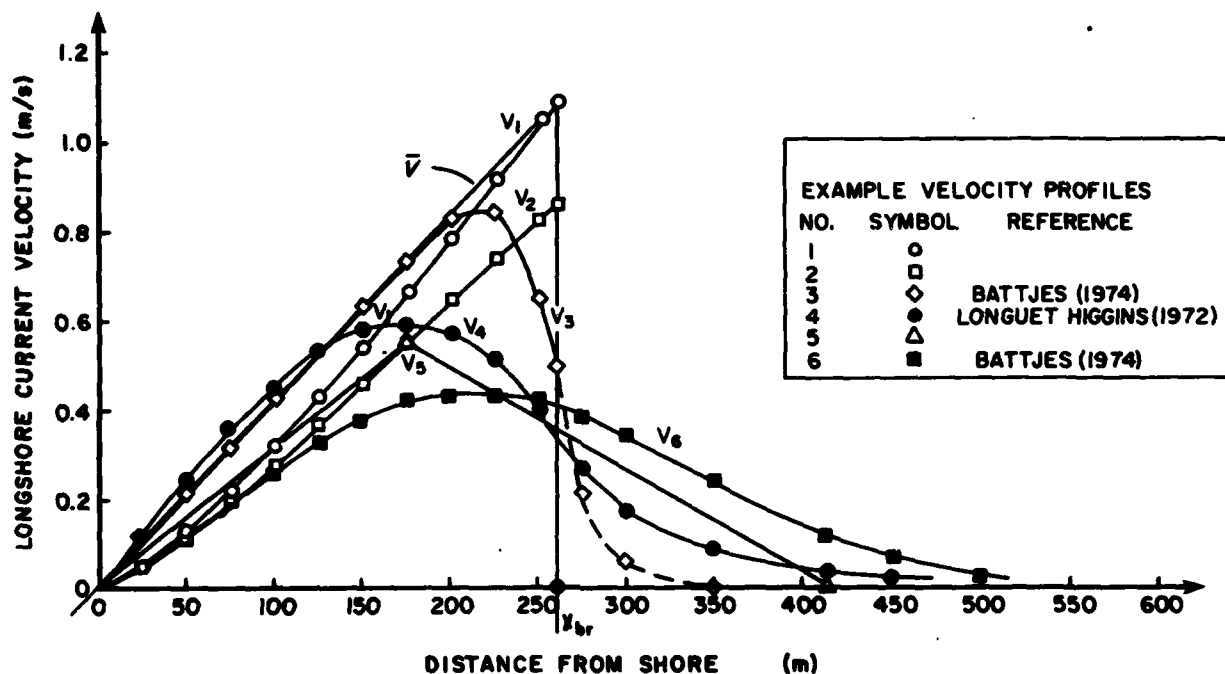
Figure 27. Effects of nonlinear bed shear stress on theoretical longshore current velocity profile neglecting lateral mixing (from Bijker and v.d. Graaff, 1978[26]).

deviate from an exact triangular shape where the bed friction factor is assumed constant in the surf zone (eq. 61). Profile $\bar{v}_2^*$ used the full nonlinear equation (80) for bed shear and full expression for dS_{xy}/dx with no shallow-water approximations. The results differ up to 20 percent near the breakpoint. Use of $\bar{v}_{2b}^*$ as a reference velocity in the dimensionless equation with lateral mixing would then reflect this difference in the magnitude of the longshore currents calculated.

(4) Empirical Formulation. Finally, in addition to the above theoretical modifications of the original bed-stress formulation by Longuet-Higgins (1970), the empirical, curve fit approach of Madsen, Ostendorf, and Reynolds (1978) must be included (see also Ostendorf and Madsen, 1979). To remove the weak current and small-angle assumptions, they first postulated that the form of the longshore current profile (with lateral mixing) is to remain that given by equations (65), (66), and (67) from the original model theory. A scaling factor is introduced between the characteristic reference velocity $\bar{v}_b^*$ (with setup) used by Longuet-Higgins (1970) and that for full nonlinear bottom stress proposed. This scaling factor is also proportional to the ratio $\bar{v}_b^*/u_{Bm}$. Curve-fitting procedures are used to obtain an expression for the scaling factor from a surf zone force balance. The modified model also includes new formulations for lateral turbulent mixing and the breaking criteria, γ. The resulting modified model requires appropriate values to be selected for the bottom stress coefficient and mixing parameter, as usual. Madsen, Ostendorf, and Reynolds (1978) used the laboratory data of Galvin and Eagleson (1965) to calibrate the model. It was recognized that plunging breakers present in these experiments did not match the γ = constant

98

assumption in the surf zone, but the data were used anyway. An explicit expression for the combined, nonlinear friction factor was obtained that properly reflected the weak and strong current theories. It is not clear how the effect of wave approach angle is included by this calibration approach.

The magnitudes of the bottom shear-stress coefficients required in all the above theories are discussed in Chapter 4.

    c.   <u>Modified Lateral Turbulent Mixing Shear Stresses</u>. Theoretical knowledge is very weak regarding the horizontal transfer of momentum due to turbulent mixing processes. Turbulence length scales represented here are on the order of the water depths, wave particle excursions, or surf zone widths, and generated by wave breaking shears, bore-bore interactions, and swash zone mixing. These processes in the surf zone are not sufficiently understood to permit detailed models of the effective stresses that result. Consequently, recourse has been universally made to some type of eddy viscosity model to linearly relate the time-averaged lateral mixing shear stress, $\bar{\tau}_L$ to the longshore current gradient $d\bar{v}/d\bar{x}$. If the velocity fluctuations ($\tilde{u}$, $\tilde{v}$) in the $\bar{x}$-y directions are considered respectively due to wave orbital motions and interactions, then for one-dimensional motion, as in equation (55) with $\bar{\mu}_L$ the time-averaged lateral eddy viscosity

$$\bar{\tau}_L = \overline{-\rho \tilde{u}\tilde{v}} = \bar{\mu}_L \frac{d\bar{v}}{d\bar{x}} = \rho \nu_L \frac{d\bar{v}}{d\bar{x}} \tag{86}$$

The tilde symbol here means velocity fluctuations on the scale of wave motion. The prime symbol is reserved for true, random velocity fluctuations due to turbulence, however generated. The kinematic eddy viscosity is $\bar{\nu}_L = \bar{\mu}_L/\rho$. Prandtl's mixing length hypothesis

$$\tilde{v} = \ell \frac{d\bar{v}}{dx} \tag{87}$$

could also have been employed giving

$$\bar{\tau}_I = -\overline{\rho \tilde{u}\ell} \frac{d\bar{v}}{dx} \tag{88}$$

so that the eddy viscosity is simply

$$\bar{\mu}_L = \rho \bar{\nu}_L = \rho |\bar{u}| \cdot \bar{\ell} \tag{89}$$

The eddy viscosity is related to the reference velocity $\tilde{u}$ and length scale $\bar{\ell}$ in some time-averaged sense. A rigorous and physically defensible derivation of equation (89) can be found in Battjes (1975).

Longuet-Higgins (1970, 1972a) chose to take the characteristic velocity proportional to the maximum bottom wave orbital velocity (u_{Bm}) and the reference length scale proportional to distance from shore (x). The closure coefficient N in his equation (eq. 55) incorporated both proportionality factors plus assumed that turbulence velocities $\tilde{u}$ were about 10 percent of mean velocities, as in normal turbulence (Longuet-Higgins, 1972a).

All other models for lateral mixing shear stress, $\bar{\tau}_L$, use some different combinations of characteristic velocity and length scales to approximate the eddy viscosity. They are summarized in Table 4 along with the resulting expression for ν_L. Three distinct categories of thought have emerged for both the velocity $\tilde{u}$, and length $\bar{\ell}$ scales employed.

(1) <u>Reference Velocity, $\tilde{u}$</u>. Thornton (1969, 1970a) and Jonsson, Skovgaard, and Jacobsen (1974) used time averaged (over one wave period) values of the maximum orbital velocity near the bottom u_{Bm} as the reference velocity $\tilde{u}$. To reduce its influence outside the breakers where turbulent mixing is smaller, Jonsson, Skovgaard, and Jacobsen (1974) used the mean overdepth, u_m, in place of the bottom value.

Madsen, Ostendorf, and Reynolds (1978) used the maximum orbital velocity predicted by linear long wave theory. For shallow water this reduces to equation (53) and is identical to the original model theory used by Longuet-Higgins (1970). It should be noted that

$$u_{Bm} = \frac{\gamma}{2} (gh)^{\frac{1}{2}} = \frac{\gamma}{2} C = \frac{\pi}{2} |\bar{U}_B| \tag{90}$$

and thus u_{Bm} is related to the surf zone celerity. Longuet-Higgins (1970, 1972a) never stated that the reference velocity taken was the wave celerity as reported by Thornton (1976, Table 3). Equation (90) also relates the time-averaged and maximum values of these two approaches. Kraus and Sasaki (1979) took slightly different models inside and outside the surf zone and followed the original model of Longuet-Higgins (1970).

A completely different approach was taken by Battjes (1975). He felt surf zone turbulence was generated by wave breaking so that the velocity scale chosen should reflect this fact. Since kinetic energy transport is proportional to velocity cubed, Battjes took the one-third power of the wave energy dissipation per unit area and per unit mass, i.e., $(D/\rho)^{1/3}$ as the reference velocity. Here, D, the rate of energy dissipation per unit area, was found from equation (50). Skovgaard, Jonsson and Olsen (1978) took the same result inside the surf zone but a simple proportion of $\bar{v}_b$ (at the breakers) to give less mixing outside the breakers.

Inman, Tait, and Nordstrom (1970) related the characteristic velocity to the breaker height and number of waves in the surf zone. The end result was simply H_b/T.

(2) <u>Characteristic Length Scale, ℓ</u>. Thornton (1969, 1970a) and Jonsson, Skovgaard, and Jacobsen (1974) used the excursion amplitude to get results for ν_L that were twice those derived by Thornton. The discrepancy is discussed by Jonsson, Skovgaard, and Jacobsen (1974), Nielsen (1977), and Gourlay (1978) but without resolution. Fortunately, such differences in ν_L produce relatively small (10 percent) changes in $\bar{v}$ magnitude and little shape change as indicated by Jonsson, Skovgaard, and Jacobsen (1974). Inman, Tait, and Nordstrom (1970) used solitary wave theory to calculate the horizontal excursion distance employed in their model. Further discussion can be found in Longuet-Higgins (1972a).

Table 4. Lateral turbulent eddy viscosity formulations and characteristic reference velocity and length scales.

Researcher	Kinematic Eddy Viscosity, L	Characteristic Velocity $\tilde{u}$	Characteristic Length Scale $\tilde{\ell}$	Remarks
Bowen (1969)	Constant	Constant	Constant	
Thornton (1969, 1970)	$\frac{H^2}{8\pi}\frac{gT}{h}\cos^2\alpha$	$\frac{H}{2}\frac{g}{h}\cos\alpha$	$\frac{HT}{4\pi}\frac{g}{h}\cos\alpha$	Time-averaged over one wave period $\bar{\ell}$ for one-half particle excursion
Inman, et al. (1971)	$K/X_b/\frac{H_b}{T}$	$\dfrac{\text{breaker height}}{\text{No. of surf waves}}$	ξB_m (solitary waves)	H_b is rms breaker height K is a coefficient about unity.
Jonsson, et al. (1974)	$\frac{4}{T}a_{Bm}^2\cos$	$\frac{2}{\pi}u_{Bm}\cos\alpha$	$a_{Bm}\cos\alpha$	Similar to Thornton (1970) except twice as large. Use a_{Bm} inside surf zone.
Battjes (1975, 1976)	$N x'\bar{x}/(gh)^{3/2}$; $M=M(5^2/16)^{1/2}\tan^{5/2}\beta$	$(D/\rho)^{1/3}$	h	0.3<M<1.8 theory, bed slope dependent D=local rate of energy dissip (eq. 50)
Madsen, et al. (1978)	$\Gamma/\bar{x}/u_{Bm}$	u_{Bm}	$/\bar{x}/$	Γ a constant similar to M in original model.
Skovgaard, et al. (1979)	$0.177^{2/3}\tan^{4/3}\beta/\bar{x}/(gh)^{1/2}$ inside ; $0.02 h_b\bar{v}_b$ outside breakers	$(D/\rho)^{1/3}$	h	Separate eddy viscosity models inside and outside breakers.
Kraus and Sasaki (1979)	$\Gamma/2/\bar{x}/(gh)^{1/2}$ inside breakers ; $\Gamma/2/\bar{x}/(gh)^{1/2} H/_h$ outside breakers	$u_{Bm}=\frac{(gh)^{3/2}}{}$	$/\bar{x}/$	Follows Madsen, et al.(1978) to lower mixing outside breakers.

a_m =maximum horizontal excursion amplitude of wave orbital motion $\doteq \frac{T}{2\pi}u_m$ in shallow water

a_{Bm} = at bottom

Researcher	Kinematic Eddy Viscosity, L	Characteristic Velocity $\tilde{u}$	Characteristic Length Scale $\tilde{\ell}$	Remarks
Original Model Longuet-Higgins (1970)	$N/\bar{x}/(gh)^{1/2}$	shallow water $u_{Bm}\doteq\frac{(gh)^{1/2}}{2}$ eq. (53)	$\bar{\ell}=k/\bar{x}/$ k=von Karman Constant(0.4)	Also applied outside surf zone and gives overly large values here (Longuet-Higgins, 1972)

The distance from shore $/\bar{x}/$ was used in all models that also used u_{Bm} as reference. Battjes (1975) again departed from the norm and used the water depth as the characteristic size of the eddies, i.e. the mixing length. In effect, this brought in the beach slope as an additional variable.

No single model for the lateral turbulent eddy viscosity has emerged as superior to the others. The tendency is to use separate formulations inside and outside the breaking zone. This recognizes the large differences present in mixing processes present in each. In almost all cases some type of closure coefficient is present that can be determined by calibration with field and laboratory data. Further discussion can be found under the Surf Zone Empiricism later in this section.

d. <u>Modified Theory of Kraus and Sasaki (1979)</u>. It is instructive to summarize here the latest and perhaps most complete modified analytic theory. Kraus and Sasaki (1979) extended the weak current-large wave angle theory to include lateral mixing. For plane, dissipative-type prototype beaches, it is possibly the best closed-form theory available at this writing. The many modifications incorporated into the theory when compared with the original theory of Longuet-Higgins (1970) are summarized in Table 4. Partial wave setup, refraction, angle-dependent bottom friction stress, and different lateral mixing formulations within and beyond the breakers are the primary changes. Near the breaker line, from the results of Longuet-Higgins (1970) (Fig. 24) and the results of Liu and Dalrymple (1978) (Fig. 26), the effects of both lateral mixing and large incident wave angle are comparable. Both effects have been isolated and studied independently as discussed below. New laboratory and field data presented to confirm the theory will be reviewed in Chapter 4.

Inside the breaker zone, the driving stress $dS_{xy}/d\bar{x}$ is given by equation (74) including refraction and partial wave setup (normal incidence). It is set to zero outside the breaker line. The time-averaged bottom shear stress is calculated from the expression

$$\bar{\tau}_b = \frac{1}{\pi}\rho C_f \bar{v}(gh)^{\frac{1}{2}} \begin{cases} \gamma(1+\sin^2\alpha_b \frac{h}{h_b}) & \text{inside breaker line} \\ \\ \frac{H}{h}(1+\sin^2\alpha_b \frac{h}{h_b}) & \text{outside breaker line} \end{cases} \tag{91}$$

This is essentially that derived by Liu and Dalymple (1978) for weak currents but large angles. Note that outside the breakers, the bottom stress is not assumed negligible. Also, the wave height outside the breakers is approximated from long wave theory to be

$$H \doteq (\frac{h_b}{h})^{\frac{1}{4}} H_b \tag{92}$$

and not assumed to increase linearly as implied in the Longuet-Higgins (1970) model. For lateral turbulent mixing stress $dT_L/d\bar{x}$, they used the eddy viscosity model given by equation (55) with kinematic viscosity as specified in

Table 4. Here again, equation (89) is employed to find H outside the breaker line. With these formulations analytic solutions of the basis momentum balance equations (28) and (42) are still possible by the decoupling concepts employed previously. However, it must be emphasized that only normal wave incidence effects on wave setup are incorporated in their procedure. This is done for mathematical convenience and produces different results than obtained by Liu and Dalrymple (1978) when lateral mixing is neglected.

(1) <u>No Lateral Mixing Stress</u>. Setting equation (74) equal to equation (88), taking a modified reference velocity $\bar{v}_b^*$ from equation (72) with $\cos\alpha_b$ assumed near unity, Kraus and Sasaki (1979) obtained the dimensionless longshore current velocity as

$$V = \frac{\bar{v}}{\bar{v}_b^*} = \frac{X}{(1+\sin^2\alpha_b X)}[(1-\sin^2\alpha_b X)^{\frac{1}{2}} - \frac{\sin^2\alpha_b}{5} X (1-\sin^2\alpha_b X)^{-\frac{1}{2}}] \qquad (93)$$

within the surf zone $0 < (X = \frac{\bar{x}}{\bar{x}_b}) < 1$. Outside, $V = 0$ for $X > 1$. Results

from equation (90) are shown in Figure 28. As $\alpha_b \to o$ (Note that $\alpha_b = o$ means theory reduces to original order (zero order) solution given by Longuet-Higgins, 1970, the triangular solution is regained. Increasing α_b causes the relative profile to be lowered across the surf zone. Figure 28 is directly comparable with the results of Liu and Dalrymple (1978) in Figure 26 since both normalized currents by equation (72) as reference velocity, $\bar{v}_b^*$. Although the general shapes are similar, the results of Kraus and Sasaki (1979) are generally 50 percent greater near the breaker line ($\alpha_b < 30°$). The only difference is in treatment of wave setup wherein Liu and Dalrymple (1978) included full setup effect for large wave incidence. Hydraulically, this trend for free surface flows is in the right direction. As shown by equation (40) oblique angle wave setup is léss than that caused by normal incident waves. For constant bed resistance and friction slope, velocity decreases as water depth decreases. The only surprise is in the magnitude of the difference. The full implications of the influence of wave refraction and wave setup on the longshore current theory need further research. Kraus and Sasaki (1979) argued that wave setup in the field was more complex than given by equations (35) or (40) to justify their result. Also, they point out that including the $\cos\alpha_b$ term in $\bar{v}_b^*$ would reduce the magnitude of their results.

(2) <u>General Solution With Lateral Mixing</u>. The y-direction momentum balance equation (42) with lateral mixing is solved by expanding $\bar{v}$ in a power series. The unknown coefficients are determined from the boundary conditions, namely $\bar{v}$ and $d\bar{v}/d\bar{x}$ continuous at the breaker line and finite within the bounds where $\bar{x} \to o$ and infinity. In the usual dimensionless terms, the longshore current profile is

$$V = \begin{cases} \sum_{n=o}^{\infty} (A_n X + B_n X^p) X^n, & \text{within surf zone } 0 < X < 1 \\[2em] \sum_{n=o}^{\infty} C_n X^{q-n}, & \text{outside the surf zone } X > 1 \end{cases} \qquad (94)$$
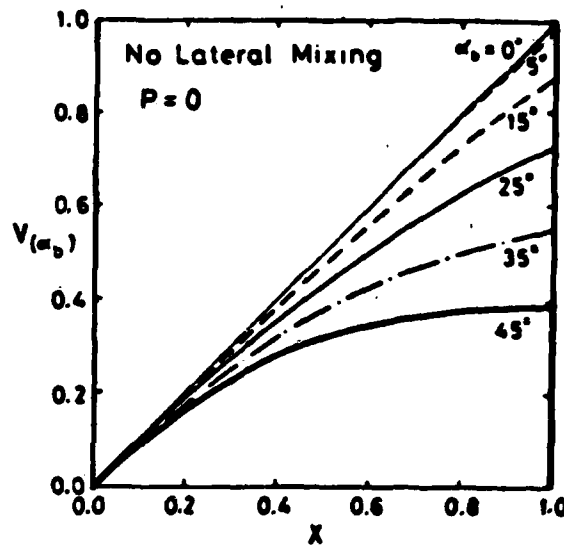
Figure 28. Dimensionless theoretical current profile inside the breaker
line as a function of incident breaker wave angle, neglecting
lateral mixing (from Kraus and Sasaki, 1979). Solution includes
refraction and angle-dependent bottom friction force. (α_b = 0
means angle correction to zero-order solution is zero.)

so that the solution form is consistent with the original model (eq. 65).
However, the coefficient expressions and definitions are quite lengthy and
involved, so they are included as Appendix D. The key dimensionless parameter
P* for this derivation is defined as

$$P^* = \frac{\Gamma\pi}{C_f^2} \frac{\tan\beta}{1+3\gamma^2/8} \tag{95}$$

where Γ is the closure coefficient for the kinematic eddy viscosity. P* is
slightly different than that defined by Longuet-Higgins (eq. 73); however,
this distinction is not fundamental and will be disregarded in the discussion.
The factor γ must now be specified along with P* to obtain a solution.

Dimensionless profiles with mixing parameter P* = 0.5, 0.1 and 0.05 (γ=
1.0) and various incident breaker angles ($o<\alpha_b<30°$) are shown in Figure 29
(after Kraus and Sasaki, 1979). The dashline (L-H) is the original theory
of Longuet-Higgins (1970) corrected for normal wave setup. Earlier Figure 24
showed how increasing the lateral turbulent mixing (larger P values) flattened

104
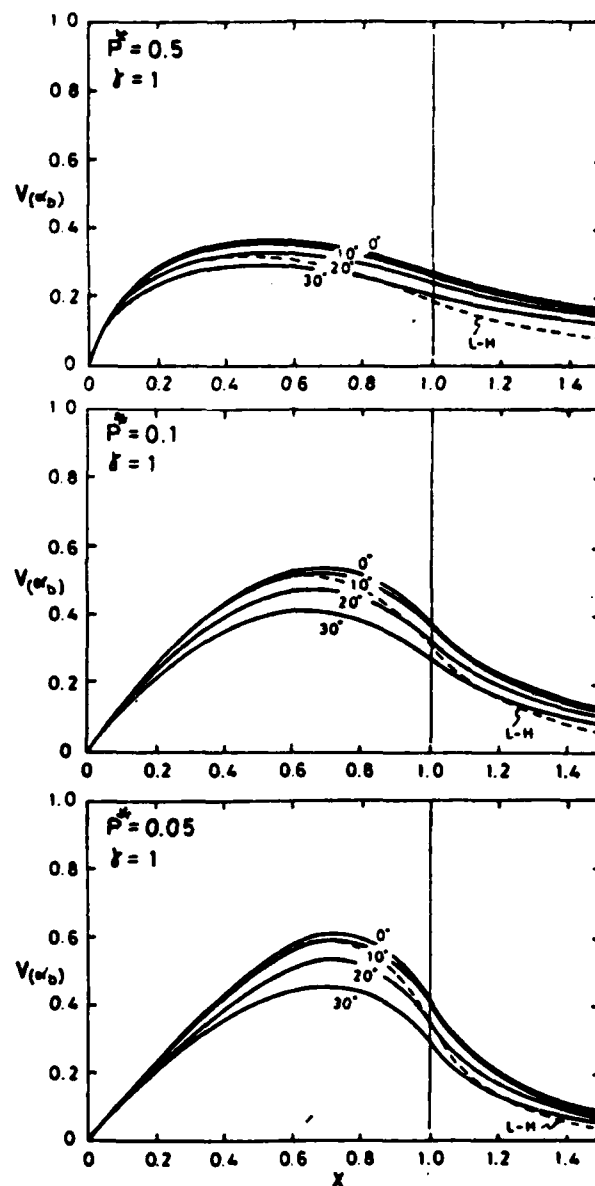
Figure 29. Dimensionless theoretical current profile with mixing
parameters P*= 0.5, 0.1, and 0.05 as a function of incident
breaker angle. Maximum velocity and its location decrease
with increasing angle (from Kraus and Sasaki, 1979).

and spread the current profile. Figure 29 reveals that larger breaker angles
have the same effect for a given P* value. The overall profile shape is still
maintained but lowered as α_b increases. At first glance this result (and
that above for no mixing) appears to contradict the original model theory
and intuition. The longshore current is expected to increase as α_b increases.
In fact, this does happen since the product $\sin\alpha_b \cos\alpha_b$ in the reference ve-
locity v_b^* increases much faster than the decrease in dimensionless V as α_b
increases.

105

To aid in the use of this theory for analysis, prediction, and calibration purposes, Kraus and Sasaki (1979) prepared the results shown in Figure 30. Here, V_{max} is a maximum velocity located at position X_{max}, V_b the breaker velocity, $V_{\frac{1}{2}}$ the midsurf velocity, and $\bar{V}$ a mean or average velocity across the surf zone. All are dimensionless and γ is taken as unity. For a fixed P*, the location of V_{max} is seen to move slightly shoreward as α_b increases.
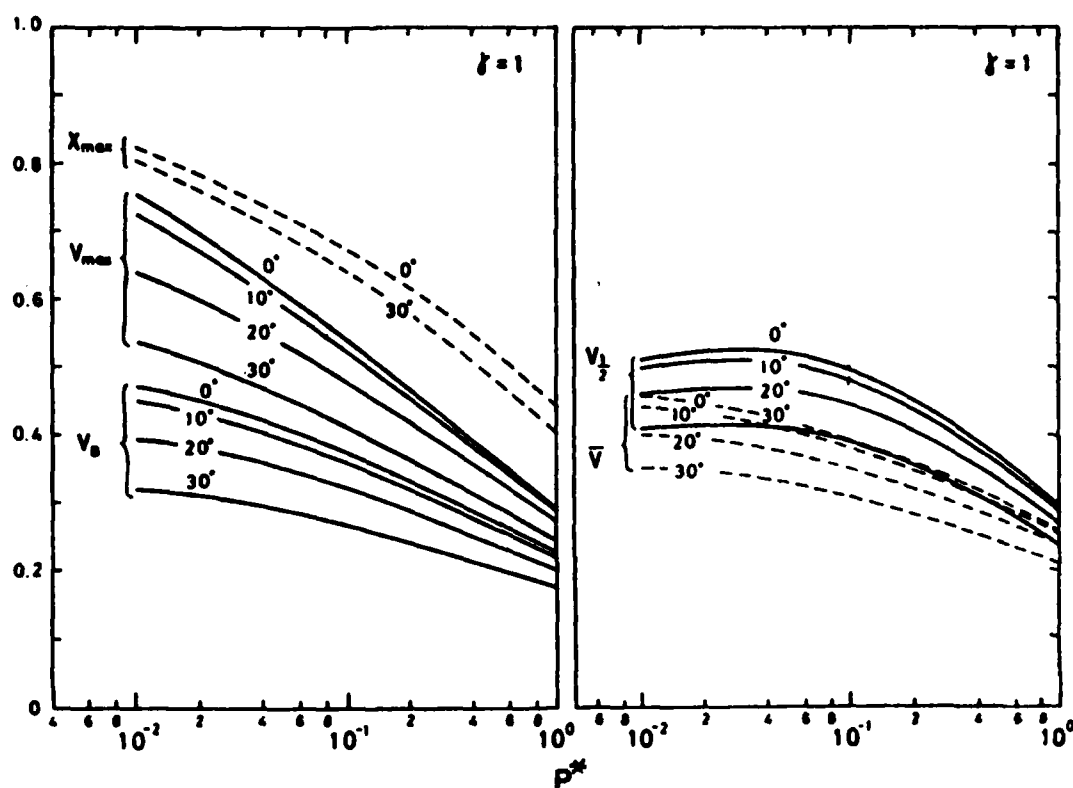
Figure 30. Calculated quantities as a function of mixing parameter P* and breaker wave angle (from Kraus and Sasaki, 1979).

All dimensionless velocities decrease as P* increases except $V_{\frac{1}{2}}$ at the midsurf position. In fact, $V_{\frac{1}{2}}$ is relatively insensitive to wide variations in P* and displays less variation to change in breaker angle than V_b or V_{max}. On the other hand, V_{max} displays the largest spread with α_b and greatest variation with P*. For this reason, V_{max} and X_{max} have been used by Kraus and Sasaki (1979) to fit and compare theory with observation as discussed in detail in Chapter 4.

e. <u>Parameter Studies</u>. In either the original or modified theories, the longshore current velocity at a given x depends upon six independent variables: γ, $\tan\beta$, C_f, α_b, h_b (or $C_b = \sqrt{gh_b}$), and N or Γ. The reference velocity $\bar{v}_b^*$ varies with the first four plus $C_b = (gh_b)^{\frac{1}{2}}$ to give the scale. The dimensionless

velocity V also varies with the first four and N (or Γ) to give the proper lateral mixing. Some examples of parameter studies have been discussed to determine the relative importance of the independent variables involved. Figure 30 from Kraus and Sasaki (1979) is an excellent example. More research is needed here especially regarding the relative importance of γ, C_f and N (or Γ) that appear together in the P - parameter.

For example, Jonsson, Skovgaard, and Jacobsen (1974) for their strong current small-angle model showed that bottom roughness (i.e., C_f) was more important than eddy viscosity (N or Γ) on current magnitude. The breaker height ratio γ had little influence on magnitude but greatly affected the location of the maximum velocity. Kraus and Sasaki (1979) concluded that for dissipative beaches, P*<0.1 (see Ch. 4). It would be very instructive to conduct sensitivity studies of the relative importance of γ, C_f and Γ in this range using their model. Ultimately however, more fundamental understanding of physical processes in the surf zone is needed to improve the theory.

4.   Surf Zone Empiricism.

Early in the 1970's, it became evident to many researchers in the field (e.g., Longuet-Higgins, 1972a; Battjes, 1974a) that the wave breaking and surf zone empiricism required was a major weak link in the longshore current theory. Long-range research began with the goal to ultimately provide more fundamental descriptions of wave shoaling processes, when and where waves break, flow separation at the crest, air entrainment effects, and the generation, transport and dissipation of turbulence across the surf zone. Numerical simulations have played an important role in both wave shoaling and breaking research, and only a bare outline for some of the important results is given here. The complexity of turbulent fluid motions also means some empirical models of surf zone hydrodynamics are still useful.

a.   Surf Similarity Parameter. Battjes (1974a,b, 1974) showed how a single surf similarity parameter ξ depending upon beach slope and incident wave steepness (H/Lo) is useful to quantify various aspects of waves breaking on a plane beach. The aspects considered were a breaking criterion, breaker type, number of waves in surf zone, wave runup and setup, and beach type (dissipative vs reflective). The similarity parameter is defined as

$$\xi = \frac{\tan\beta}{(H/Lo)^{\frac{1}{2}}} \tag{96}$$

and was based on the work of earlier investigators as solely a wave breaking criteria. Here, H is the wave height defined at the toe of the beach slope and Lo is the deepwater wavelength. Table 5 modified from Battjes (1974b) gives the results. The theory of longshore currents described above essentially holds for ξ<0.4. The criteria used to establish Table 5 were taken and modified from published research efforts at that time.

ξ	≈ 0.1	0.5	1.0	2.0	3.0	4.0	5.0
		breaking					no breaking
	spilling		plunging		collapsing/surging		
H_b/d_b	≈ 0.8	1.0	1.1	1.2			
N[a]	6-7 2-3	1-2	0-1		0-1		
τ	10^{-3}	10^{-2}	10^{-1}	4×10^{-1}	8×10^{-1}		
	absorption					reflection	
	progressive wave				standing wave		
	set-up predominant			run-up predominant			

[a] number of waves in surf zone

Recently, Ostendorf and Madsen (1979) defined a modified Battjes breaker
parameter as

$$\xi_b = \frac{\tan\beta \cos\alpha_b}{(H_b/L_o)^{\frac{1}{2}}} \tag{97}$$

for waves of oblique incidence and using the wave height evaluated at break-
ing, for convenience. It is then demonstrated that the longshore current
theory discussed above, which neglects such surf zone phenomena as wave runup,
wave reflection, edge waves and air entrainment but includes a linear γ ratio
inside the breaker line, is reasonable when $0.3 < \xi_b < 0.7$. The data employed are
somewhat different than that used to establish Table 5. Interestingly, they
conclude from laboratory data that for γ linear in the surf zone, $\xi_b > 0.3$, which
contradicts the belief, in this opinion, that the theory holds for all spilling-
type breakers.

b. **Wave Breaking Criteria.** The longshore current models simply take
$0.5 < \gamma_b < 1.2$ as a breaking criterion. The most common value employed is 0.8
(solitary wave theory gives 0.78). The actual MWL, $h_b = (d+\bar\eta)_b$, is employed in
the ratio (eq. 33). Many other variations are available some including the
wave steepness and beach slope in the formulation (e.g., Thornton and Smith,
1980[29]; Weishar and Byrne, 1978). Excellent reviews of wave breaking in shal-
low water can be found in Collins and Wier (1969), Galvin (1973), Battjes
(1974a), and Komar (1976a).

---

[29] THORNTON, E.B. and SMITH, R.M., "Breaking Wave Criterion on a Sloping Beach,"
Abstracts, *17th Conference on Coastal Engineering*, Sydney, Mar. 1980, pp.
28-29 (not in bibliography).

Modern developments in the study of breaking waves through 1976 are reviewed in Longuet-Higgins (1976). A new numerical method is revealed which uses a mixed Eulerian-Lagrangian technique in that both a velocity potential and marked particles are employed. This numerical method can follow the development of the jet in a plunging-type breaker, as shown in Figure 31 (from Cokelet, 1978). Details of the development of the simulation technique can be found in Longuet-Higgins and Cokelet (1976), and Cokelet (1978), and it continues to be researched in subsequent papers on the subject (e.g., Peregrine and Cokelet, 1980). Much of the initial effort has concentrated on deepwater wave breaking.

In July 1978 a research colloquim, *Euromech 102*[30], was held with the express purpose to present the latest developments in wave breaking research. Natural waves break for a large number of reasons: surface winds, shoaling, depth or current refraction, wave-wave interactions, wave energy concentration, reflections, and by relative motion between the water and a solid boundary. Peregrine (1979) stated that whatever the cause, the local motion of the water particles involved in the breaking process can be very similar. Thus for many applications, research can concentrate on the actual breaking process rather than the cause. It was also concluded that the theoretical study of breaking waves is in its infancy (Peregrine, 1979).

However, for longshore currents in the nearshore zone, wave breaking caused by nonlinear shoaling processes is of greatest interest. Sakai and Battjes (1980)[31] used Cokelet's (1978) theory to calculate two-dimensional shoaling of finite-amplitude waves on a gradual slope. The results were found to agree with laboratory experiments except near breaking where the theory predicted wave heights higher than the measured values. In the long run, numerical simulation of wave breaking processes is expected to provide much clearer empirical relations to determine when, where, and why waves break.

c. <u>Surf Zone Energy Dissipation</u>. After breaking, turbulent energy is produced at the expense of potential energy and wave height decay results across the surf zone. The longshore current models usually assume a constant value for the breaker index γ_b.

For large-amplitude waves with spilling-type breakers over gentle slopes, Divoky, LeMehaute, and Lin (1970)[32] derived theoretically (using energy balance principles) a wave height decay relationship which depended upon bottom slope, bottom friction, and the breaking ratio γ_b. Theories from

[30] *Euromech 102* (1978), "Breaking Waves; Surf and Run-up on Beaches," University of Bristol, England, July 18-21 (file copy of Abstracts Only in CERC Library, Fort Belvoir, Va.) (not in bibliography).

[31] SAKAI, T. and BATTJES, J.A., "Wave Shoaling Calculated from Cokelet's Theory," Abstracts, *17th Conference on Coastal Engineering*, Sydney, Mar. 1980, pp. 65-66 (not in bibliography).

[32] DIVOKY, D., LeMEHAUTE, B., and LIN, A. "Breaking Waves on Gentle Slopes," *Journal of Geophysical Research*, Vol. 75, No. 9, Mar. 1970, pp. 1681-1692 (not in bibliography).
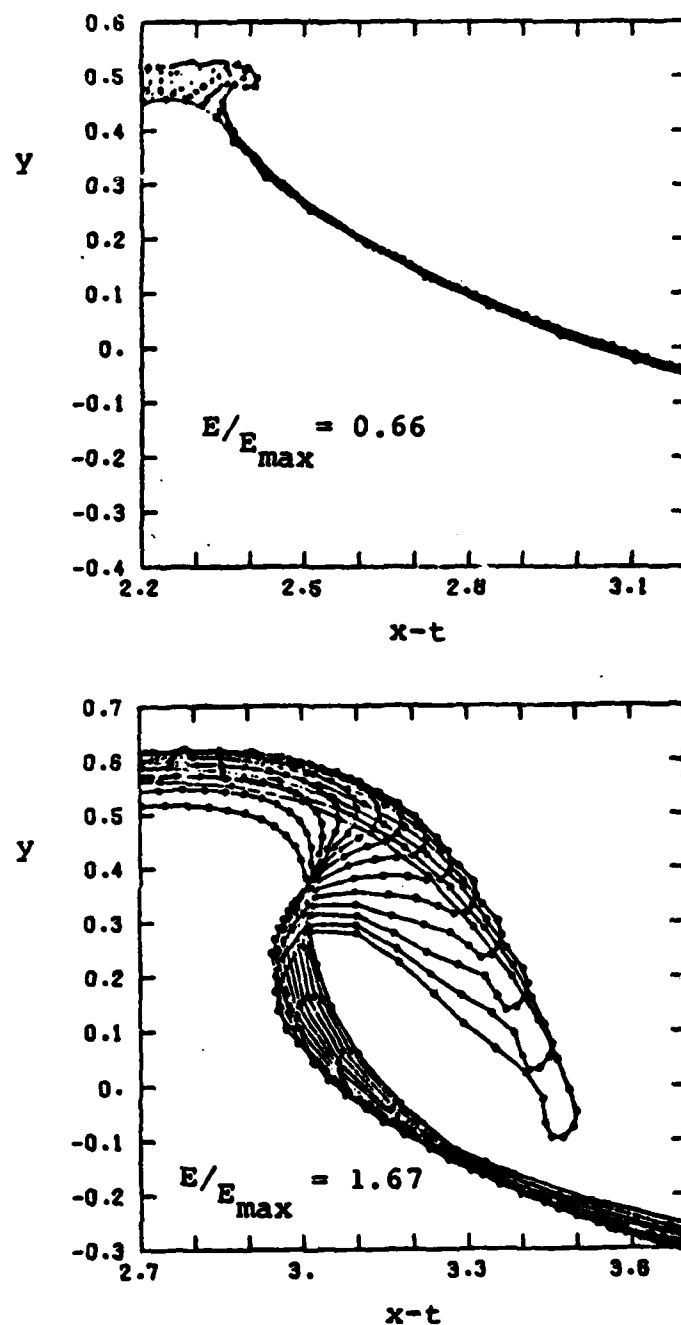
Figure 31.   Numerical simulation of a plunging-type breaker
(from Cokelet, 1978).

laboratory studies were reported by Horikawa and Kuo (1966)[33] and Sawaragi
and Iwata (1974).   It was concluded that the ratio γ is a function of dis-
tance from the breakpoint and ranges from 2.0 to 0.6.   Field investigations

[33]HORIKAWA, K., and KUO, C.T., "A Study on Wave Transformation Inside Surf
Zone," *Proceedings of the 10th Conference on Coastal Engineering*, Vol. I,
1966, Tokyo, pp. 217-233 (not in bibliography).

Battjes (1978) argued that a constant γ ratio across the surf zone introduces an unrealistically high sensitivity in all the longshore current models to variations in bottom profile. A constant γ is also not applicable for very gentle slopes or bar-trough profiles. Therefore, to model surf zone energy dissipation, the more fundamental conservation of energy equation (44)

$$\frac{dF_x}{dx} + D = 0$$

where F_x is the general flux of energy toward the shore, D is $EC_g\cos\alpha$, and D, the local rate of energy dissipation per unit area, is preferred. Thus local wave height in the surf zone is found by integration so that it depends on all preceding seaward depths in addition to the local depth. The energy balance equation can in principle be applied to bar-trough profiles, plus it provides a convenient way to incorporate other energy loss mechanisms besides wave breaking.

Thornton (1976) listed the following mechanisms for dissipation of wave energy in the surf zone:

(1) Breaking induced internal turbulence forming rollers, vortices, and eddies;

(2) air entrainment requiring energy to lower air beneath the surface and generation of more turbulence from rising air bubbles;

(3) boundary layer shear turbulence (bottom friction);

(4) energy cascade to higher frequencies due to nonlinear transfer processes and eventual dissipation as heat loss to surroundings;

(5) percolation; and

(6) work required to keep sediments in suspension and transport sediments.

Recent theoretical attempts to use equation (44) in the development of wave height distributions across the surf zone have concentrated on wave breaking induced turbulence as the primary mechanism.

Battjes (1978) estimated the dissipation rate per breaking wave from a bore (moving hydraulic jump) of corresponding height. The broken wave height was set equal to the water depth difference across the jump. The classic hydraulic jump theory was modified to calculate the energy (head) loss rate as an order of magnitude estimate. The results were incorporated in a model of random waves and applied to plane and bar-trough profile beaches. Further details are found in the Section VI of this chapter. Additional research using hydraulic jump theory in the surf zone has been reported by Svendsen, Madsen, and Hansen (1978a) and is continuing.

Recently, Mizuguchi (1980) suggested another theoretical model for the rate of energy dissipation in the surf zone. No physical explanation is offered for its origin. The model contained a kinematic eddy viscosity by Suhayda and Pettigrew (1977) confirmed these results. Thus the rate of energy dissipation decreases with distance from the breaker line.

coefficient that was not the same as that proposed by Battjes (1975), based on momentum principles. An expression is also hypothesized for the eddy viscosity that minimizes dissipation in wave re-forming areas (troughs) and relates dissipation to a ratio between the "...real and possible maximum wave heights at any location." The theory is found to simulate laboratory and field wave height distributions over uniform, plane, and step-type beach profiles as discussed in Chapter 4. The theory is extremely crude yet reflects the current primitive state of understanding concerning energy dissipation in the surf zone.

More detailed measurements of the velocity distributions and spectral characteristics are needed under laboratory and field conditions. Laboratory contributions toward this end have recently been reported by Battjes and Sakai (1980) and Stive (1980). The field effort of Thornton (1977, 1979), Thornton and Schaeffer (1979), and Thornton, et al. (1976) to understand the kinematics of breaking waves is a major step in this direction. Kinematic energy spectra made from field velocity measurements in the surf zone reveal the highly nonlinear transfer processes resulting in energy transfer to both higher and lower frequencies from the primary incident wave frequency. Higher frequency harmonic peaks appear indicative of the peaked crests and broad troughs of shoaling waves. The spectrum then tails off at a -3 slope because breaking induces a saturation region where energy transfer is constrained. Finally, the highest frequency region of the spectrum decays at a -5/3 slope as found in all isotropic turbulence. Better surf zone energy dissipation models will result from this type of information and ultimately lead to improved methods to estimate wave height distributions across all types of beach profiles. Refined theoretical models of longshore current profiles will be the end result.

5. Nonuniform Longshore Current Profiles.

The analytic theory of longshore currents described in this report is for steady, uniform wave conditions on an infinite beach. As observed in the field (see Ch. 2) variations in breaker height can readily occur along the coast for various reasons (Table 1) but usually due to offshore bathymetry. The alongshore gradient of breaker height produces additional stresses in the y-direction momentum balance (eq. 42). As can be deduced from Figure 23, an alongshore gradient of wave height establishes a gradient in wave setup to produce a net hydrostatic force in the y-direction. In addition, the gradient of radiation stress, dS_{yy}/dy is no longer zero, but also plays a role in the y-direction momentum balance.

Using these two additional stress components, Komar (1975a, 1976) extended the original theory of Longuet-Higgins (1970) to include the alongshore variation in wave height. Convective acceleration terms and variations in surf zone width are neglected. Komar used the same weak current small-angle bed shear stress and lateral turbulent mixing stress formulations as Longuet-Higgins (1970) but included the normalized wave setup. A series of examples of longshore current profiles for various wave setup gradients in the alongshore direction is shown in Figure 32, where the data for the computation are also shown (after Komar, 1975a). A negative surface slope gradient in the +y-direction contributes an additional driving force to create a stronger current than when $\partial \bar{\eta}/\partial y = 0$. For this example, a positive MWL slope
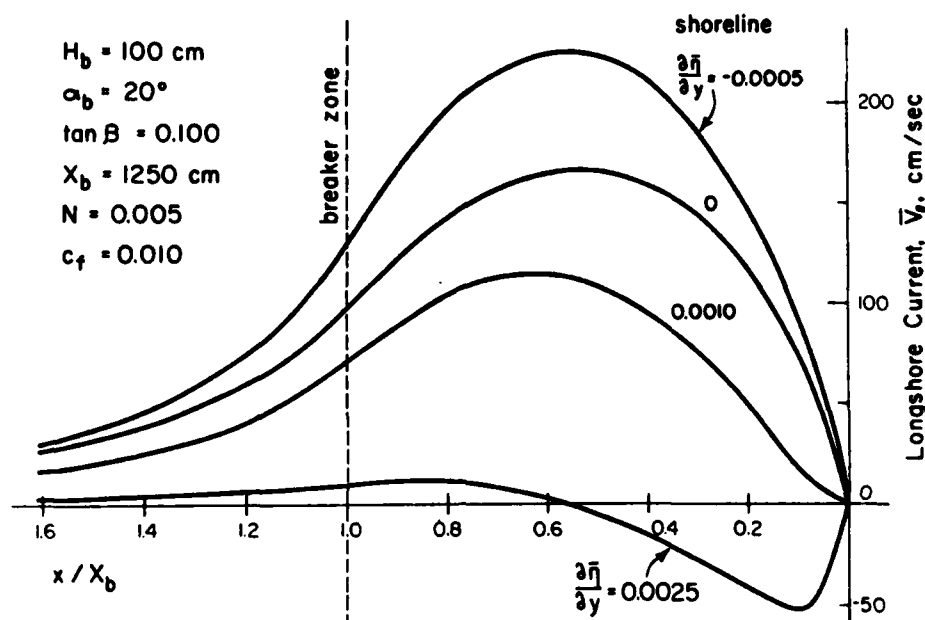
Figure 32. Examples of complete solutions of the distribution of longshore current
velocities through the surf zone for a series of values for the longshore
variation in the wave setup ($\partial\bar{\eta}/\partial y$). With $\partial\bar{\eta}/\partial y$ = 0.0025, the setup slope
in the longshore direction nearly opposes and balances the thrust due to
the oblique wave approach, and the velocities are greatly weakened (from

of about $\partial\bar{\eta}/\partial y$ = 0.0025 nearly balances the wave-induced thrust so that long-shore currents are greatly diminished. A net circulation flow is possible with nearshore currents in the opposite direction from those near the breaker line. Additional examples are given in Komar (1975a).

One final application of the decoupled quasi-one-dimensional theory must be mentioned. For the wave-generated current system behind an offshore breaker (Fig. 8), Gourlay (1978) used principles of radiation stress to develop analytic expressions for the longshore current profiles at various sections. Two basic regions were identified for the analysis. An inflow region of spatially varied flow in the exposed area extended up to the geometric shadow of the breaker, and the eddy circulation region within the sheltered area which drains momentum from the primary longshore current system. Painstaking means were devised to compute the wave breaking heights and locations, wave-induced setup, and to incorporate bottom friction stresses. Lateral mixing stresses were neglected in establishing the velocity distributions. A number of other limitations were imposed in order to derive the final theory. The results, although useful to verify the experiments as discussed in Chapter 4, are not readily generalized to other geometries. Gourlay (1978) demonstrated the practical limitations for extending a one-dimensional analysis to truly two-dimensional flows. The two coupled momentum balance equations are now needed plus the mass balance equation to solve for the three time-averaged unknowns $\bar{v}$, $\bar{u}$, and $\bar{\eta}$ as described in the next section.

113

V. NEARSHORE CIRCULATION SYSTEMS

No theoretical methods existed before 1969 to predict mean water sur-
face and current variations in the nearshore region when circulation cells
and rip currents were present. Only a relatively crude model of rip currents
was available as devised by Arthur (1962). For steady flow, neglecting bot-
tom frictional resistance, lateral mixing, and the driving force terms (ra-
diation stress gradients), Arthur (1962) showed that the nonlinear, convection
acceleration terms in the vorticity transport equation increase with increase
in water depth. This translated into a narrowing and strengthening of a sea-
wind current, i.e., a rip current model near the root. Bowen (1967, 1969b)
followed many of the general assumptions suggested by Arthur (1962), except
he included the resistance and driving force terms. The analytic model of
nearshore cell circulation and rip currents incorporating radiation stress
principles as devised by Bowen (1967, 1969b) became the forerunner for all
subsequent efforts. Central in the theory are the equations employed.

1. Fundamental Equations of Motion in Two Dimensions.

The conservation of mass, momentum, and energy equations for waves super-
imposed on a current was first given by Whitham (1962)[34]. The complete
derivations can be found in Liu and Mei (1975) or Phillips (1977)[35]. The
water is assumed homogeneous and incompressible of constant density. Coriolis
accelerations are neglected. The velocity field is assumed independent of
the water depth so that only two-dimensional (horizontal) motion is allowed.
Most importantly, the velocity field is considered as the sum of the mean and
wave-induced variation. Turbulence due to random velocity fluctuations at
scales far below the wave motions is neglected.

The applicable equations are derived by averaging the Navier-Stokes dif-
ferential motion equations and the mass equation over depth and over time, in
that order. Battjes (1974a) has a detailed discussion of the averaging pro-
cess. A key ingredient is the Liebnitz rule for differentiation of a definite
integral. The resulting equations have appeared in two different forms in the
literature.

a. Eulerian Form. As used first by Bowen (1967, 1969b), the equations
are written in terms of the depth-averaged Eulerian mean velocities $\bar{u}$, $\bar{v}$, and
mean water surface deviation, $\bar{\eta}$. The accelerations form to the total or sub-
stantive derivative, meaning the equations are in Eulerian form.

Mass

$$\frac{\partial \bar{\eta}}{\partial t} + h \frac{\partial \bar{u}}{\partial x} + \bar{u} \frac{\partial h}{\partial x} + h \frac{\partial \bar{v}}{\partial y} + \bar{v} \frac{\partial h}{\partial y} = 0 \qquad h = d + \bar{\eta} \qquad (98)$$

---

[34]WHITMAN, G.B., "Mass, Momentum and Energy Flux in Water Waves," *Journal
of Fluid Mechanics*, Vol. 12, 1962, pp. 135-147 (not in bibliography).
[35]PHILLIPS, O.M., *The Dynamics of the Upper Ocean*, Cambridge University
Press, Cambridge, Mass., 2d ed., 1977 (not in bibliography).

Motion

x-direction:

$$\frac{\partial \bar{u}}{\partial t} + \bar{u} \frac{\partial \bar{u}}{\partial x} + \bar{v} \frac{\partial \bar{v}}{\partial y} = + \frac{1}{\rho h} (\bar{\tau}_{sx} - \bar{\tau}_{Bx})$$

$$- \frac{1}{\rho h} (\frac{\partial S_{xx}}{\partial x} + \frac{\partial S_{xy}}{\partial y}) - \frac{1}{\rho h} (\frac{\partial h \bar{\tau}_{Lxx}}{\partial x} + \frac{\partial h \bar{\tau}_{Lxy}}{\partial y})$$

(99)

y-direction:

$$\frac{\partial \bar{v}}{\partial t} + \bar{u} \frac{\partial \bar{v}}{\partial x} + \bar{v} \frac{\partial \bar{v}}{\partial y} = + \frac{1}{\rho h} (\bar{\tau}_{sy} - \bar{\tau}_{sy})$$

$$- \frac{1}{\rho h} (\frac{\partial S_{yy}}{\partial y} + \frac{\partial S_{xy}}{\partial x}) - \frac{1}{\rho h} (\frac{\partial h \bar{\tau}_{Lxy}}{\partial x} + \frac{\partial h \bar{\tau}_{Lyy}}{\partial y})$$

(100)

where $\bar{u}, \bar{v}$ = the depth-averaged and time-averaged velocity components

$\bar{\tau}_{sx}, \bar{\tau}_{sy}$ = the time-averaged surface wind shear-stress components

$\bar{\tau}_{Bx}, \bar{\tau}_{By}$ = the time-averaged bottom shear-stress components

S_{xx}, etc. = the radiation stress components

$\bar{\tau}_{Lxx}$, etc.= the effective lateral stress components.

In this Eulerian form, the mass equation neglects the small contribution of mass transport due to finite-amplitude wave orbital motion. The motion equations include a possible surface wind shear stress for completeness. For steady, uniform motion, with no wind and no coupling with the y-direction momentum terms, equation (99) reduces to the simple momentum balance for wave setdown and setup derivations (eq. 28). Similarly, equation (100) reduces to the y-direction momentum balance (eq. 42) used to derive the longshore current profile.

The motion equations (99,100) are equivalent to those for nearly horizontal free-surface flows if the radiation stress gradients are neglected. Then, all variables and the stresses are no longer time-averaged quantities and the pressure distribution is assumed hydrostatic. The radiation stress gradients, by definition, account for the deviation from hydrostatic pressure resulting from the streamline curvature present in short waveforms. Consequently, the pressure distribution is nonhydrostatic in the motion equations. The radiation stresses effectively arise from time-averaging the mean velocity plus the wave orbital velocity fluctuation in analogy with Reynolds stresses.

Horizontal momentum flux is due to the convective acceleration terms, radiation stress gradient terms, and the effective lateral stress terms. The latter effective stresses combine momentum fluxes due to both horizontal mixing of wave scale motions and deviations of the local velocity from its depth-averaged value (Vreugdenhil, 1980). As before, the effective lateral

115

stresses are usually described in terms of an eddy viscosity coefficient due
to the weak understanding of the surf zone. Care is required to ensure that
the results are independent of the coordinate system chosen and consistent
with surf zone turbulence. For example, Vreugdenhil (1980) has shown that
the contribution of the pressure fluctuations to the normal stresses is rela-
tively small so that the following expressions result for the effective
lateral stresses:

$$\bar{\tau}_{Lxx} = \bar{\mu}_{Lx}(\frac{\partial \bar{u}}{\partial x} - \frac{\partial \bar{v}}{\partial y}) \tag{101a}$$

$$\bar{\tau}_{Lxy} = \bar{\mu}_{Lxy} (\frac{\partial \bar{u}}{\partial y} + \frac{\partial \bar{v}}{\partial x}) \tag{101b}$$

$$\bar{\tau}_{Lyy} = \bar{\mu}_{Ly} (\frac{\partial \bar{v}}{\partial y} - \frac{\partial \bar{u}}{\partial x}) \tag{101c}$$

where the eddy viscosity coefficients are direction dependent. For homo-
geneous, horizontal, time-averaged wave scale turbulence

$$\bar{\mu}_L = \bar{\mu}_{Lx} = \bar{\mu}_{Ly} = \bar{\mu}_{Lxy} \tag{102}$$

and only in this case do the cross gradient terms $\partial/\partial xy$ disappear. Finally,
it is also common for the mean water depth h, in the effective, lateral stress
gradient terms to be mistakenly removed from the differentials. Since h is
a function of x and y it must also be differentiated. If the water depths
are canceled, forms often found in the literature (e.g., Bowen, 1967, 1969b)
result, i.e.,

x-direction:

$$\cdots -\bar{v}_L (\frac{\partial^2 \bar{u}}{\partial x^2} + \frac{\partial^2 \bar{u}}{\partial y^2}) \tag{103a}$$

y-direction:

$$\cdots -\bar{v}_L (\frac{\partial^2 \bar{v}}{\partial x^2} + \frac{\partial^2 \bar{v}}{\partial y^2}) \tag{103b}$$

that can only be considered as approximations of the true expressions for
the effective lateral stress terms. Here $\bar{v}_L = \bar{\mu}_L/\rho$ is the kinematic eddy
viscosity, and only the last terms of the full motion equations are shown.

If the motion equations are dimensionless, it can be seen that the re-
lative importance of the effective lateral stress terms compared with the
convective acceleration terms is given by a time-averaged lateral Reynolds
number

116

$$\bar{R}_L = \frac{\tilde{u}\bar{\ell}}{\bar{v}_L} \tag{104}$$

where $\tilde{u}$ and $\bar{\ell}$ are reference velocity and length scales for the velocity gradients as previously discussed (see eq. 86). Expressions for $\bar{v}_L$ commonly employed are given in Table 4.

b. _Conservation Form_. For the combined motion of waves and currents, it is far more convenient and exact to use the conservation form of the mass and motion equations. By averaging over depth and over time, in that order, we define the following averaged quantities:

$$p \equiv \overline{\int_{-d}^{\eta} u\,dz} \qquad u(x,y,z,t) \tag{105a}$$

$$q \equiv \overline{\int_{-d}^{\eta} v\,dz} \qquad v(x,y,z,t) \tag{105b}$$

so that p and q are the discharges per unit width at any x, y, and t. Now, the transport components p and q include mass transport induced by finite-amplitude waves; e.g.,

$$p = \int_{-d}^{\bar{\eta}} \bar{u}\,dz + \overline{\int_{\bar{\eta}}^{\eta} u\,dz} \tag{106}$$

and the second term on the right-hand side is not generally zero (Vreugdenhil, 1980). Note that generally $\bar{u} \neq p/h$ and $\bar{v} \neq q/h$. Some authors choose to re-define $U = p/h$ and $V = q/h$ as "...mean horizontal velocities" (e.g., Ebersole and Dalrymple, 1979, 1980). This serves no useful purpose, particularly for numerical solution methods where the following physical conservation laws are preferred (Vreugdenhil, 1980):

Mass

$$\frac{\partial h}{\partial t} + \frac{\partial p}{\partial x} + \frac{\partial q}{\partial y} = 0 \tag{107}$$

Motion

x-direction:

$$\frac{\partial p}{\partial t} + \frac{\partial p^2/h}{\partial x} + \frac{\partial (pq/h)}{\partial y} + gh\left(\frac{\partial h}{\partial x} + \frac{\partial Z_b}{\partial x}\right) =$$

$$+ \frac{1}{\rho}\left(\bar{\tau}_{sx} - \bar{\tau}_{Bx}\right) - \frac{1}{\rho}\left(\frac{\partial S_{xx}}{\partial x} + \frac{\partial S_{xy}}{\partial y}\right) - \frac{1}{\rho}\left(\frac{\partial h\bar{\tau}_{Lxx}}{\partial x} + \frac{\partial h\bar{\tau}_{Lxy}}{\partial y}\right) \tag{108}$$

117

y-direction:

$$\frac{\partial q}{\partial t} + \frac{\partial (pq/h)}{\partial x} + \frac{\partial (q^2/h)}{\partial y} + gh(\frac{\partial h}{\partial y} + \frac{\partial Z_b}{\partial y}) =$$

$$+ \frac{1}{\rho} (\bar{\tau}_{sy} - \bar{\tau}_{By}) - \frac{1}{\rho} (\frac{\partial S_{xy}}{\partial x} + \frac{\partial S_{yy}}{\partial y}) - \frac{1}{\rho} (\frac{\partial h\bar{\tau}_{Lxy}}{\partial x} + \frac{\partial h\bar{\tau}_{Lyy}}{\partial y}) \qquad (109)$$

where Z_b is the vertical distance of the bed above an arbitrary datum and always positive (see Fig. 23), and all other terms are as previously defined. Arbitrary beach profiles are readily handled using the gradient of Z_b terms. The dependent variables are now p, q, and h as function of x, y, and t.

c. **Other Forms.** The equations above are derived by assuming the motion is composed of mean components plus fluctuations at the scale of the short wave motions on the coast. The latter two terms in the motion equations result from the interactions of the mean flow and the wave-induced oscillations. Harris and Bodine (1977)[36] extended this approach by recognizing that two different scales of perturbations exist in coastal hydrodynamics:

(1) the generally organized oscillations due to wind-generated waves (indicated by a tilde), and

(2) the generally random fluctuations called turbulence produced by either the mean flow or the waves (indicated by a prime).

Each primary variable was divided into three components:

$$u(x,y,z,t) = \bar{u} + \tilde{u} + u'$$

$$v(x,y,z,t) = \bar{v} + \tilde{v} + v'$$

$$w(x,y,z,t) = \bar{w} + \tilde{w} + w' \qquad (110)$$

$$p(x,y,z,t) = \bar{p} + \tilde{p} + p'$$

These expressions are substituted into the incompressible continuity equation and Navier-Stokes equations (with Coriolis terms) and averaged over some space and time interval. As expected, products of perturbation variables arise that reveal interactions between the large- and small-scale flows. For wave and mean flow interactions, the vertical integrations over the water depth are performed first, and then the time-averaging operation is performed. This is identical to the procedures described above. For the random turbulence interactions, the time-averaging process is conducted first followed by vertical depth intergration. Thus the averaging methods employed lack complete mathematical exactness but serve to demonstrate the physical interactions of nature (Harris and Bodine, 1977). For example, when the waves are omitted, the Reynolds equations of motion are recovered.

[36]HARRIS, D.L., and BODINE, B.R., "Comparison of Numerical and Physical Hydraulic Models, Masonboro Inlet, North Carolina," GITI Report 6, U.S. Army, Corps of Engineers, Coastal Engineering Research Center, Fort Belvoir, Va., and U.S. Army Engineer Waterways Experiment Station, Vicksburg, Miss., June 1977 (not in bibliography).

Of interest here are the equations obtained when both wave and random turbulent fluctuations are present together. The derivation is quite lengthy and involves further simplifications and assumptions. The resulting horizontal motion equations are almost identical to equations (108) and (109), except as follows:

(1) At the true scales of random turbulence, additional Reynolds stress terms appear,

(2) the component of effective stress due to the deviation of the local velocity from its depth-averaged value appears as a separate stress component,

(3) the lateral stress terms due solely to wave scale interactions with the traditional radiation stresses, and

(4) a number of additional new interaction stress terms appear that have never been studied in detail before.

All these new stress terms are proportional to the square of the wave amplitude. Harris and Bodine (1977) postulated that all these terms are generally smaller than the radiation stresses and can generally be neglected because of uncertainties in the radiation and turbulence stresses. No reasons are given. It will undoubtedly prove necessary to lump these additional interaction stresses (4) with the others until vastly improved data are available. Those due to vertical velocity profile variations (2) could become important within and near rip currents and could be incorporated as momentum correction factors (β) in the convection terms. The bed friction and lateral eddy viscosity will continue to serve as closure coefficients to absorb these unknown stresses.

The question of form of conservation equations for waves in the surf zone including turbulence is an active research area (e.g., see Madsen and Svendsen, 1978). But in all cases, the solution first requires the a priori specification of the wave height field to evaluate the radiation stress gradients.

2. Specification of Wave Height Fields.

The wave heights outside and within the surf zone must be known before a solution of the mass and motion equations can begin. This is implied in all time-averaged methods using radiation stress gradients where the local wave heights appear in the total energy density, E. In addition, wave orbital velocities needed in the bottom shear-stress terms require local wave height information. For this purpose, standard wave refraction, diffraction, and reflection computation procedures are normally employed outside the breaker line. Within the surf zone wave height variations in space are found using the surf zone empirical relations discussed above. For complicated beach profiles with bar-trough bathymetry and near groins, offshore breakwaters, or other structures, the detailed specification of the wave height fields throughout the entire nearshore zone of interest can be a tedious and difficult task. Many numerical computation systems are available for this purpose (e.g., see Noda 1972a, 1974) or have been specially adapted for use with nearshore circulation solution techniques (e.g., Liu and Mei, 1975). All the systems have limitations and special problems that develop at caustics with soliton formation and are usually based only on linear wave theory. In addition, percolation, bottom friction, and, most importantly, current-refraction effects on the specified wave height fields are usually neglected.

119

The overall importance of the accuracy of specified wave heights on the resulting nearshore circulation and rip current models should not be underestimated.

3.   Analytic Solutions.

Bowen (1967, 1969b) was the first to analytically solve the two-dimensional motion equatio.s (Eulerian form, eqs. 98, 99, and 100). Of interest at that time was theoretical proof that nearshore circulations and rip currents could be produced by variations in breaker height along the coast. Steady regular waves of normal incidence on a plane beach with a periodic wave height variation alongshore were specified. Convective acceleration and wind stresses were neglected. In a first approximation, by also neglecting the lateral mixing stresses, an analytic solution was obtained in terms of the mass transport stream function, Ψ. As a second approximate solution, only convective acceleration, radiation stress, and lateral mixing terms were considered. This case produced a nonlinear problem requiring numerical integration methods, employing successive, overrelation procedures. In both cases, oversimplified bed shear and eddy viscosity models reduced the accuracy but not the general, qualitative nature of the results (Fig. 33).

The vertical axis in terms of wavelength of the alongshore wave height variation reveals that in both cases, rip currents form in regions of low wave height. The rip currents also strengthen (narrow streamlines) as the eddy viscosity decreases (increasing Reynolds number). It is not clear what Re = 0 means (Fig. 33,b) since by definition, $Re \equiv UL/\bar{\nu}_L$. Also these same figures show the maximum current outside the breaker line. The solution with only bottom friction (Fig. 33,a) is more realistic in this regard by showing the strongest longshore currents in the surf zone (left of the breaker line). Since specification of the alongshore wavelength for alongshore wave height variation fixed the circulation cells, Bowen solved a forced circulation problem. However, these shortcomings do not diminish the pioneering importance of Bowen's efforts.

Sonu (1972) repeated the theoretical analysis with only bed shear stress for the case when wave height variation alongshore is created by bottom topography. Here, rip currents returned offshore where water depths were large, as expected. Other solutions followed for different initial or boundary conditions and by making assumptions that were analytically tractable. O'Rourke and LeBlond (1972) investigated the circulation currents induced by oblique waves in a semicircular bay. They neglected the convective acceleration and lateral stress terms. Similar analyses were reported by Noda (1972a, 1972b, and 1974).

LeBlond and Tang (1974) also recognized that the resulting current patterns interact with the wave heights initially specified. Bowen's work was extended to include wave-current interaction effects. More importantly, LeBlond and Tang also sought to solve a free oscillation problem and hypothesized that the wave-current feedback mechanism would create a preferential spacing for rip currents. But, as discussed in Chapter 2, it became necessary to invoke an additional condition in their eigenvalue formulation which turned
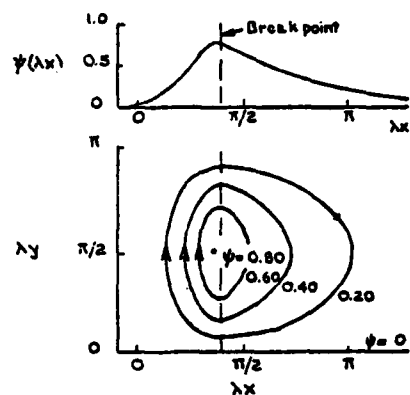
(a) Solution considering bottom friction

$R_\psi = 0$

$R_e = 0.20$
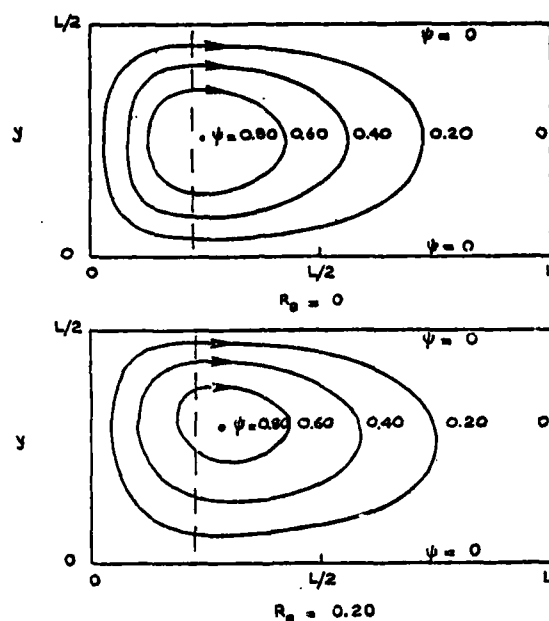
(b) Solution considering lateral mixing

Figure 33. Bowen's solutions for nearshore current circulations.(from Bowen, 1969b).

out to give incorrect cell circulation sizes. It was also learned that coupling the equations by including the wave-current interactions reduced the magnitude of the rip currents.

Most of the analytic solutions have been made by researchers interested in theoretical means to predict rip current spacing. The eigenvalue free oscillation problem to determine rip current spacing is generally conducted as outlined below. It was first made by Hino (1974). The latest efforts have been by Dalrymple and Lozano (1978) and Miller (1977) (see also Miller and Barcilon, 1978). The time-averaged horizontal motion equations and continuity,

as given above, along with the energy equation for steady-state conditions, are expressed in terms of an equilibrium state plus a small perturbation of the steady state. The four dependent variables, Ψ, $\bar{\eta}$, h and E, are often employed. After normalization of the resulting perturbation equations, they are subjected to small disturbances in each of the four perturbation dependent variables involved. These perturbation variables are expressed as components of a Fourier series periodic in wave number in the longshore direction and in time. The eigenvalues of the resulting system of equations are determined after specification of sufficient boundary conditions. The solution techniques at this stage are quite involved and normally involve polynomial expansion methods and numerical methods to determine the eigenvalues. The resulting eigenvalues λ are related to the eigenvalue wave numbers of rip current spacing $2\pi/\lambda$, i.e., lower eigenvalues mean larger wave numbers. Wave numbers normalized by the surf zone width, x_b are usually employed. Consequently,

$$\lambda x_b = \frac{2\pi}{L_r} x_b = \text{a dimensionless eigenvalue wave number} \qquad (111)$$

where L_r is the rip current spacing. The lowest possible eigenvalues obtainable (of an infinite number of possibilities) are of principal interest since they represent the fundamental modes of instability (and largest rip current spacings) possible in the surf zone. Parameter studies are then conducted to determine the relationships between the independent variables involved (e.g., tan β, γ, C_f, etc.) and the eigenvalue wave numbers that result. Because of the mathematical complexities, only regular waves of normal incidence on plane beaches are usually involved. Also the lateral mixing stresses are neglected.

Under these conditions, Dalrymple and Lozano (1978) showed that

$$\lambda x_b \doteq \frac{1}{A_D} + 2.8 \qquad (112)$$

where

$$A_D = \frac{\tan\beta\gamma}{8f} \qquad (113)$$

f = a Darcy-Weisbach type friction coefficient
$= 8C_f$ (as defined in eq. 52)

and A_D lumps the key independent parameters. They included wave-current refraction by rip currents in their analysis and showed that by doing so no extra conditions were needed to predict rip current spacing.

As pointed out by Dalrymple (1978), all such free-oscillation eigenvalue solutions rely heavily upon γ and how energy dissipation is modeled in the surf zone. It is tacitedly assumed that the form for γ (constant or x-dependent) holds for all orders of perturbation. Miller (1977) and Miller and

Barcilon (1978) used various models for the variation of γ through the surf zone including one similar to that described above by Battjes (1978) based on bore theory. Their case B = 32 gave

$$\lambda x_b = \frac{0.03}{A_D} + 0.6 \qquad (114)$$

Dalrymple (1978) concluded that no real progress in eigenvalue methods to determine rip current spacings can be made until better surf zone energy loss models are available. Also the use of time-average equations voids the possibility to study real instability mechanisms, except those that evolve slowly. Finally, it is also noted that neglect of the lateral shear-stress gradient terms in the fundamental equations also reduced the physical meaning of the results.

The primary motivation for solution of the fundamental equations is the determination of nearshore currents, circulation patterns, rip currents, and MWL variations. It quickly became obvious that for realistic bottom contours, coastal planforms with manmade structures, and arbitrary incident wave conditions, numerical solution methods were required.

4. Numerical Models.

Beginning with Noda (1972a), 11 efforts to build two-dimensional numerical models of nearshore circulation systems were uncovered. These are numbered in Table 6 along with two other studies discussed below. Researchers at Tetra Tech, Inc., Massachusetts Institute of Technology, University of Delaware, and in Japan (Sasaki, 1977) and Holland (Vreugdenhil, 1980) have made major contributions. Most of the models employed the finite-difference method with some recent finite-element method efforts.

a. Tetra Tech, Inc. As part of a research effort from 1968 to 1977 (summarized by Collins, 1977), researchers at Tetra Tech, Inc., Pasadena, California, have developed a wave-induced circulation model (Noda, 1972a; Noda, et al., 1974) for regular waves. Wave-current interactions and shoaling were included by a relaxation technique and the current refraction effects produced by even small currents resulted in major changes in the surf zone driving forces and entirely different rip current patterns. The full motion equations were not employed. For steady flows, the convective accelerations and lateral turbulent mixing stresses were neglected. Tidal variations were incorporated by making separate steady-state calculations every 3 hours. Coastal flooding and water level setup were neglected. The pioneering efforts of Noda, et al. (1974) are more valuable today for the refraction program developed as part of the study. Because the study includes wave-current interaction effects and is computationally efficient, it continues to be employed by coastal circulation modelers (Birkemeier and Dalrymple, 1976; Ebersole and Dalrymple, 1979).

b. Massachusetts Institute of Technology (MIT). Liu and Mei (1975, 1976b) developed a finite-difference model to study the effects of offshore and shore-connected breakwaters on nearshore circulation. A major part

123

Table 6. Two dimensional numerical models of surf zone hydrodynamics.

Authors (reference)	Terms Included in Motion Equations						Wave Field Methods				Surf Zone		Numerical Methods					Remarks
	Accelerations		Surf. Grad.	Rad.-Stress	Lateral Mixing	Wind Shear	Refrac-tion	Diff.	Type	Current Inter	Y	Set-up	Met-hod	Explicit or Imp.	Rad. B.C.	Coastal Fixed	Coord. Syst.	
	Local	Conv.																
(1)	(2)	(3)	(4)	(5)	(6)	(7)	(8)	(9)	(10)	(11)	(12)	(13)	(14)	(15)	(16)	(17)	(18)	
Noda (1972) Tetra Tech (TC-149-3)			M	M			M		I		-		FDM	E			R	For ONR, Coastal Geography Prog. (CGP).
Noda et al. (1974) Tetra Tech (TC-149-4)			M	M			M		I	M	c*		FDM	M			R	For ONR
Sasaki (1977) U. of Tokyo		M					M		M		c		FDM	M			M	U. of Toyko, Ph.D. Diss.
Liu and Mei (1957) MIT TN No. 57			M	M			M	M	M		c	M	FDM	M			M	For CERC MIT Ph.D. Diss.
Birkemeier and Dalrymple (1976) Delaware			M	M		M	M		M	M	c*	M	FDM	M		M	M	For ONR, Coastal Geography Prog. Delaware, Ph.D. Diss.
Fox and Davis (1976) Williams College	Not Applicable. Empirical Procedures Employed, See Text.																	For ONR. (CGP)
Allender et al. (1978) Argon Labs.			M	M		M	M		M	M	c*	M	FDM	E		M	R	For Nuclear Regulatory Comm.
Betten et al. (1978) U. College of Wales, U.K.		M	M	M					M		c	M	FEM	-	M			
Liu and Lennon (1978) Cornell U.			M	M					M		c	M	FEM	-				For NSF, ONR Cornell U., Ph.D. Diss.
Ebersole and Dalrymple (1979) Delaware	M	M	M	M	M		M		M	M	c*	M	FDM	E	-	M	M	For ONR. (CGP)
Vreugdenhil (1980) DHL, Holland	M	M	M	M	M		M		M	M	v	M	FDM	I		M	T	For Rijkswaterstaat.

Remarks legend:
I = irregular waves   I = implicit
M = monochromatic   E = explicit
c = constant   R = rectangular
c* = equation   T = transformed
v = varies

124

of the effort was the wave field determinations for both refraction and diffraction (Liu and Mei, 1976a). Wave-current interactions, convective accelerations, and lateral mixing stresses were neglected, as were wind and flooding effects. However, the governing equations remained nonlinear in the surf zone since the solution permits a large wave setup relative to the stillwater depth. Bottom shear stresses are calculated from the weak current small-angle model.

The solution was facilitated by use of the transport stream function and a coordinate transformation to get finer resolution nearshore. The finite-differencing techniques employed were equivalent to a Gauss-Seidel relaxation technique. Iteration procedures are needed to first calculate the stream functions, then $\bar{\eta}$ and a new shoreline, and then to repeat this process to convergence of a specified amount. Example results for one test case of the offshore breakwater are shown in Figure 34. Besides needed improvements in the many empirical approximations, it was also concluded that future efforts must include the convective accelerations, lateral turbulent mixing stresses, and wave-current interactions. Future improvement would also come from nonlinear refraction and diffraction models, inclusion of breakwater energy absorption properties, and location of the breaker line. Controlled laboratory experiments were requested to confirm the theory since incomplete experimental data (such as Gourlay, 1978) were then unavailable.

Mei and Angelides (1977) applied the model to study currents on a beach of constant slope around a circular island. Liu and Lennon (1978) at Cornell University employed the finite-element (weighted residual) method to essentially model the same set of simplified equations with neglected terms as discussed above. In addition, the equations were linearized in the alongshore direction by assuming $\bar{\eta}$ small compared to local water depth in this direction. No iteration procedure was consequently required. The finite-element method was claimed to be "...more efficient and powerful than the existing finite-difference models." This statement is not substantiated, however.

c. <u>University of Delaware</u>. The shortcomings of the model developed by Noda, et al. (1974) have been addressed in a series of developments by Birkemeier and Dalrymple (1975, 1976) and Ebersole and Dalrymple (1979, 1980). The 1976 model included a different wave breaking ratio γ, wave setup effects, the Longuet-Higgins (1970) bed-shear model, coastline flooding, and wind-shear shears. The final motion equations employed were in Eulerian form and included the unsteadiness but neglected the convective accelerations and lateral stress components. A staggered, explicit finite-difference scheme was devised to solve the system of equations. Wave height fields were found using the refraction program of Noda, et al. (1974) modified to include calculation of the time dependency by a finite-difference routine. This, in turn, gave the radiation stresses from the linear wave theory for all depths. The major difficulty was the large number of time steps dictated by the stability requirements for two-dimensional explicit schemes. No accuracy analysis of the finite-difference method utilized is presented. Only a limited number of tests were performed. Most were for steady-state conditions so that the local acceleration terms became iteration steps in the steady-state solutions. A one-dimensional unsteady wave setup computation demonstrated how setup lagged the deepwater wave height due to traveltime of the wave toward shore.
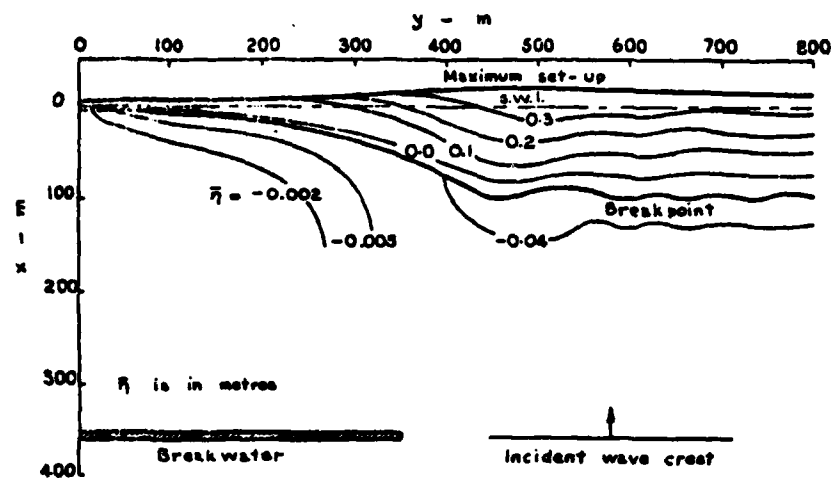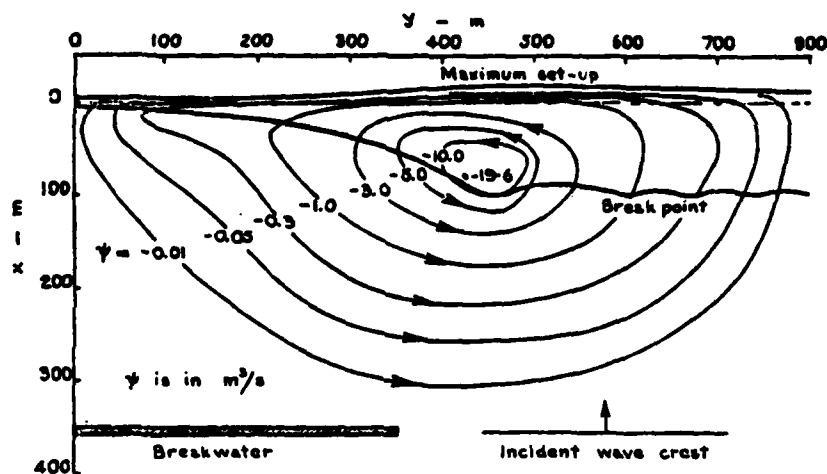
Figure 34. Solution for an offshore breakwater (from Liu and Mei, 1975).

The model was improved in 1979 by including the convective accelerations and lateral mixing stress terms (Ebersole and Dalrymple, 1979, 1980). In addition, the full, strong current large-incidence angle bed-stress model (Liu and Dalrymple, 1978) was employed. Eddy viscosity was calculated by equation (55) and from Longuet-Higgins (1970) for the shore-normal direction. In the alongshore direction, a constant coefficient $\bar{\nu}_y$ was employed.

Numerical integration was by the finite-difference method. The explicit three level leapfrog-type scheme employed required a special starting routine to generate the initial conditions at two time levels. In addition, special

126

smoothing procedures were needed every 10th time step to dampen the time-splitting instability inherent with three level schemes. Considerable averaging of all dependent variables was incorporated within the difference formulations which were essentially centered for all space derivatives. The lateral mixing stress gradients were evaluated at the lowest time level (n-1) for stability reasons.

The numerical model results for longshore current profile under oblique wave attack on a plane beach with and without lateral mixing are shown in Figure 35(a) (Ebersole and Dalrymple, 1980). The analytic model results for the same example are given in Figure 35(b) using the Longuet-Higgins (1970) model. A significant difference is apparent. With no lateral mixing, the large difference between the analytic and numerical results is completely due to numerical "viscosity," i.e., truncation error terms stemming mainly from the local and convective accelerations that give numerical dispersion. The dotted line in Figure 35(a) is from the 1976 model which omitted the convective acceleration term. The difference can be attributed to additional numerical dispersion associated with the truncation error from finite-differencing the convective term. Decreasing the grid scales will help but it is apparent that the physical mixing desired will generally be dominated by the undesirable numerical mixing inherent in the scheme employed. Use of the model to quantify longshore current profiles, nearshore circulations, and rip currents is questionable for this reason. Circulation cells will be generated and rip currents form but how certain can the magnitudes of the results be when the numerical information losses dominate the physical processes?

Ebersole and Dalrymple (1979, 1980) recognize the importance of including the convective acceleration and lateral mixing terms for accuracy in the physical processes being modeled. They also noted the numerical mixing present in Figure 35 (a and b). However, the time step was selected "...to be significantly lower than the two-dimensional Courant stability criterion..." and no discussions of numerical accuracy are presented.

d. Others in United States. Allender, et al. (1978) used the numerical model developed by Birkemeier and Dalrymple (1975, 1976) to compare field observations in Lake Michigan (see Ch. 4). Hudspeth (1979)[37] describes extensions to the MIT model (Liu and Mei, 1975) to include tide-induced currents. The finite-element method is being implemented.

Two other U.S. computer-based models are included in Table 6 for completeness. These were developed by Fox and Davis (1971, 1976). In the 1971 simulation model for eastern Lake Michigan, longshore current is computed as the first derivative of the local barometric pressure variation with time. For small water bodies where local storms generate the wind waves at the coast, this approach is physically defensible. The scaling parameters are found experimentally and are not generally transferable to other locations. The 1976 Coastal Storm Model (Fox and Davis, 1976) forecasts or hindcasts longshore current conditions for a given storm size, shape, intensity, and path. Standard wave height forecasting procedures are used to compute period, breaker

---

[37]HUDSPETH, R., "Effects of Jetties in Steady Currents," *Research in Ocean Engineering*, Massachusetts Institute of Technology, Cambridge, Mass., Vol. 1, No. 3, 1979 (not in bibliography).
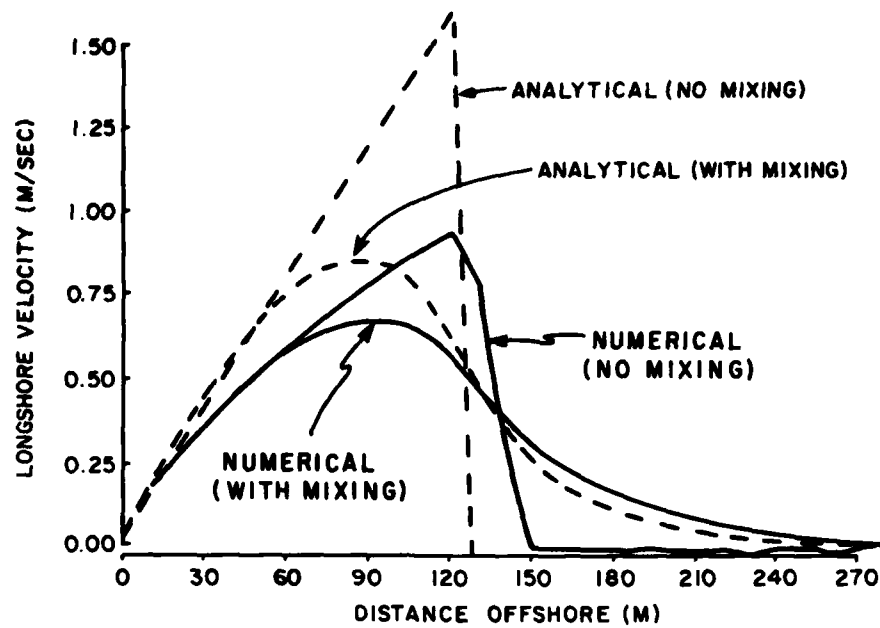
a. Numerical model results (Ebersole and Dalrymple, 1980).
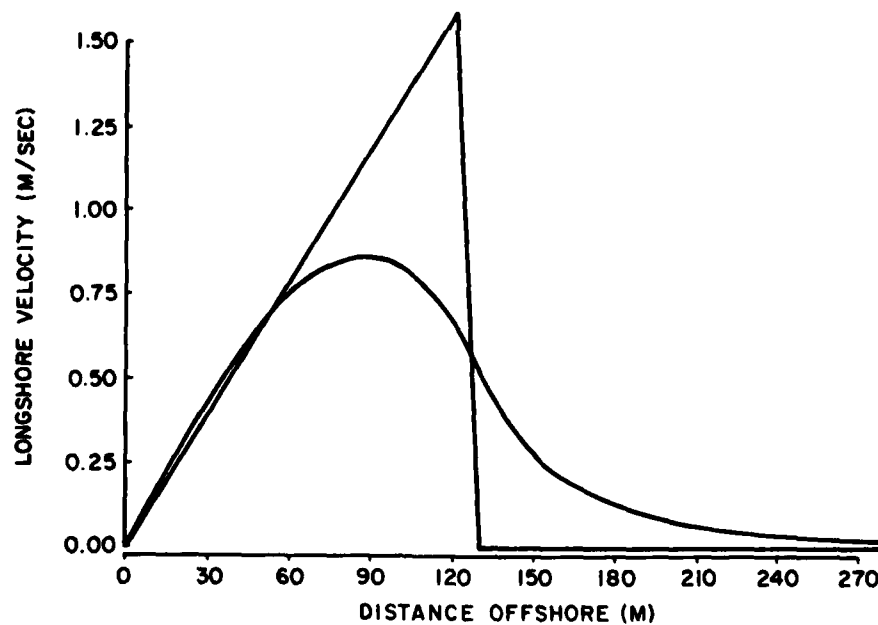
b. Analytical model results (Longuet-Higgins, 1970).

Figure 35. Numerical and analytical model results for longshore current, with and without mixing.

128

height, and angle at the shoreline. The original model of Longuet-Higgins (1970), modified by U.S. Army, Corps of Engineers, Coastal Engineering Research Center, (1977)[38] is then used to calculate a mean longshore current. Although local winds are a dominant feature of the field data displayed, no term to include surface wind shear-generated currents is included.

    e. **Others Outside the United States.** In Japan, Sasaki (1977) essentially followed the efforts of Noda, et al. (1974) and neglected all the terms in the basic equations except mean water surface gradient, radiation stress gradient, and bottom shear. The weak current small-angle friction model is employed. The wave height field is calculated numerically but neglects wave-current interactions. A successive overrelaxation (SOR) numerical method solved the resulting equations after first being put in transport stream-function form. Because of the large number of omitted terms and neglect of wave setup, the model is only valuable as a general indicator of trends (see Ch. 4).

    In response to the need to investigate currents near a proposed cooling water intake basin on the coast, Bettess, et al. (1978), in England, developed a steady-state finite-element model. It included all terms in the motion equations plus the Coriolis accelerations. Wave-current refraction effects in the wave height field calculations were neglected. Wave height fields were also calculated using the finite-element method for solution of Berkhoff's (1972)[39] modified form of the shallow-water equations. An example of their results for currents calculated using a constant eddy viscosity coefficient is shown as Figure 36. The size and strength of the large eddy in the lee of the breakwater compares favorably with physical model results (dotted lines). The authors call for an improved means to simulate surf zone energy decay, radiation stresses with standing waves, and lateral mixing eddy coefficients in order to improve the numerical simulation.

    Finally, Vreugdenhil (1980) carefully outlines methods presently being implemented at the Delft Hydraulics Laboratory to develop a numerical model for unsteady wave-driven currents. The primary purpose of this model is to better understand physical processes such as migrating rip currents. The equations employed are written in conservation form (eqs. 107, 108, and 109) with all terms included. Modules are introduced to permit easy variation or suppression of submodels for lateral mixing stress, bottom friction, the wave theory in the radiation stress, wave breaking, and the surf zone energy loss criteria. Wave height fields are computed from linear theory to include refraction from both depth and current variations, and diffraction effects can also be included.

    The numerical method selected as the finite-difference method of the implicit type. Together with a transformed coordinate system to readily handle curved breaker lines and boundaries, the finite-difference method was felt superior to the finite-element method where little is known about

---

[38]U.S. ARMY, CORPS OF ENGINEERS, COASTAL ENGINEERING RESEARCH CENTER, *Shore Protection Manual*, Vol. I, U.S. Government Printing Office, Washington, D.C., 1977 (not in bibliography).

[39]BERKHOFF, J.C.W., "Computation of Combined Diffraction-Refraction," *Proceedings of the 13th Coastal Engineering Conference*, Vancouver, 1972 (not in bibliography).
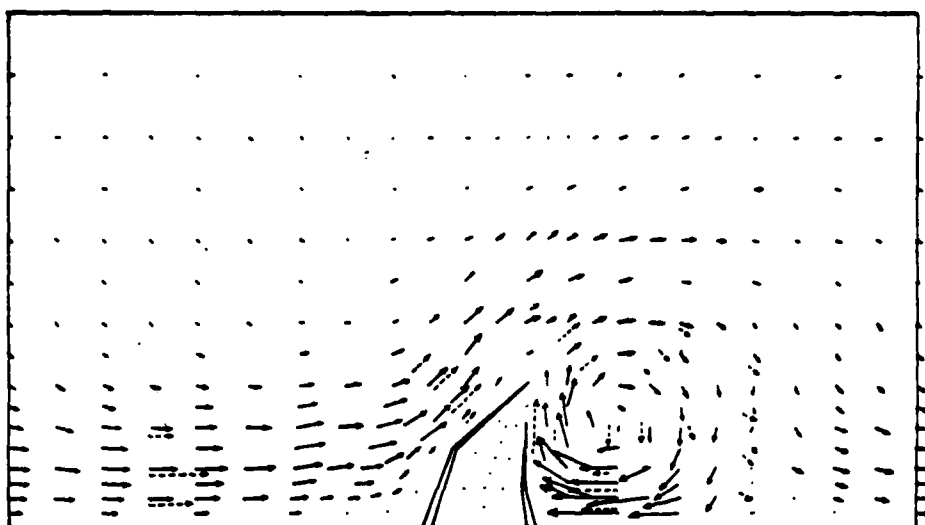
Nearshore Circulation Pattern, constant viscosity
Physical Model Pattern shown dotted

Figure 36. Nearshore circulation pattern, constant
viscosity; physical model pattern shown
dotted (from Bettess, et al., 1978).

accuracy for propagation-type problems. The locally one-dimensional implicit
method (Mitchell and Griffiths, 1980)[40] was employed to efficiently and numeri-
cally integrate the equations. The weighting coefficient between upper and
lower time levels θ of the two level scheme is adjustable for efficient steady-
state solutions ($\theta = 1$) or accuracy ($\theta = \frac{1}{2}$) in unsteady flows. All the
space derivatives are centered.

Considerable discussion is presented by Vreugdenhil (1980) regarding
stability, numerical accuracy, and the boundary conditions. Complete details
are beyond the scope of this report but such analyses are critical to the
quantitative success of any numerical simulation. For example, the direction-
al nature and repetition of the solution procedure for the x-direction and
y-direction sweeps (using either locally one-dimensional or alternating direc-
tion implicit methods) will affect the amount of numerical viscosity or dif-
fusion generated. Numerical viscosity can easily be much greater than the
eddy viscosity even for schemes using centered space derivations for the con-
vective acceleration terms. For steady-state solutions, spatially oscillating
solutions (wiggles) in the velocity fields can be generated even in linearly
stable schemes. These come from the nonlinear convective acceleration terms
and can be artificially damped by using large eddy coefficients at the expense
of numerical accuracy. The relationships between boundary conditions, bed
friction, internal, lateral eddy viscosity, numerical viscosity (truncation

---

[40]MITCHELL, A.R. and GRIFFITHS, D.R., *The Finite Difference Method in Partial
Differential Equations*, Wiley-Interscience, J. Wiley and Sons, New York,
1980 (not in bibliography).

errors), and boundary geometry for the proper simulation of flow vorticity, circulations, eddies, etc. in numerical models are still an active research area. The modeling effort described by Vreugdenhil (1980) is by far the best effort to model nature because it includes all the physically important terms and simulates them numerically with the most accuracy.

VI. NONLINEAR AND IRREGULAR WAVES

All the analytic and numerical methods described previously in this chapter were with radiation stresses computed from linear wave theory for regular sinusoidal waves. The stress components are then simply given by equations (23), (24), and (26) or first-order theory. Because of the relatively crude assumptions needed for modeling the surf zone energy dissipation, it could be argued that higher order radiation stress terms were not warranted. On the other hand, since irregular waves naturally occur and break at different offshore locations, the stochastic approach to longshore current modeling may be more realistic. Both nonlinear and irregular wave theories of MWL change and longshore currents are reviewed in this section. Differences and similarities with the linear regular wave theories are noted.

1. Nonlinear Waves.

a. **MWL Change.** James (1973, 1974a) used third-order Stokes theory in deep water and a modified (Iwagaki, 1968)[41] cnoidal wave theory nearshore to compute the higher order radiation stress needed to define wave setdown and setup for spilling breakers on plane, gentle slopes. Wave setdown was less than that found by linear theory especially near the breaking point. Theoretical wave setup is·also less and the gradient is not a constant proportion of the beach slope as in linear theory. Numerical methods are employed to integrate the resulting ordinary differential equations.

The theory for cnoidal waves over a gently sloping bottom (Svendsen, 1974)[42] is used by Svendsen and Hansen (1976) to derive analytic expressions for wave setdown. Near breaking both nonlinearity and vertical acceleration effects must be included in the wave theory. Using the actual bottom velocity in cnoidal waves given by

$$u_b = c \frac{\eta}{d} (1 - \frac{\eta}{d}) + \frac{1}{6} cd \frac{\partial^2 \eta}{\partial x^2}$$ (115)

setdown became

---

[41] IWAGAKI, Y., "Hyperbolic Waves and Their Shoaling," *Coastal Engineering in Japan*, Vol. II, 1968, pp. 1-12 (not in bibliography).

[42] SVENDSEN, I.A., "Cnoidal Waves Over a Gently Sloping Bottom," ISVA, Series Paper No. 6, Technical University of Denmark, Lyngby, 1974, (not in bibliography).

$$\bar{\eta} = -\frac{c^2}{2g}\left[(2\frac{c}{\sqrt{gh}} - 1)\frac{\bar{\eta}^2}{d} - \frac{7}{2}\frac{\bar{\eta}^3}{d^3}\right] \tag{116}$$

where c is cnoidal theory celerity, and η is wave surface variation based on second-order cnoidal theory. The results again give less wave setdown than linear theory and are closer to experiments in this regard as discussed in Chapter 4 where other even closer approximations are also shown.

Maximum wave setup, $\bar{\eta}_m$, is determined by Jonsson and Buhelt (1978), using a series of solitary waves just outside the breaker line to calculate the mean water depth at the breakers,

$$h_b = 0.344\gamma^{-\frac{1}{2}}(H_o/L_o)^{-\frac{1}{3}}H_o \tag{117}$$

When inserted into equation (37) using $H_b = \gamma h_b$ they obtained the result

$$\frac{\bar{\eta}_m}{H_o} = 0.107\gamma^{\frac{3}{2}}(H_o/L_o)^{-\frac{1}{3}} \tag{118}$$

This expression includes setdown effects and holds for any beach profile where depth decreases continuously. These results are for normal wave incidence and have been found to explain how beach slope and wave steepness influence maximum setup in experimental data (Ch. 4).

b. **Uniform Longshore Current Profile.** James (1973, 1974b) was primarily interested in how a nonlinear wave theory for the radiation stresses would affect the longshore current profile. The same wave theories as reviewed for wave setup were employed. He took the full nonlinear bed friction expression (eq. 52) and Longuet-Higgins (1970) expression for lateral mixing stress (eq. 55) in his numerical solution methods. All results are for plane, flat beaches with spilling breakers and $\gamma = 0.85$. A comparison between the linear and nonlinear theories is shown in Figure 37 (after Gourlay, 1978) where it is important to recognize that the nonlinear solutions include both the nonlinear bed stress and wave setup effects while the linear solution does not (original model, Longuet-Higgins, 1970). With this in mind, it is observed that the linear theory required significantly larger bottom friction values (to match experimental surf zone currents) and is more sensitive to eddy viscosity variations than the nonlinear theory.

James (1974b) concluded that the results for longshore current in the surf zone are of the same order of magnitude for both linear and nonlinear theories. Perhaps this is the reason his research remains the only one known of this nature. All such efforts require numerical solution methods which, in light of their use for two-dimensional solutions, is not an additional problem. Dutch researchers are planning to vary the wave theory in the radiation stress terms of their numerical model (Vreugdenhil, 1980). Their future results and others of a similar nature will be of considerable intere

(a) $f_{wc} = 0.004$, N = 0.016 $f_{wc} = 0.004$, N = 0.01

——————— nonlinear theory ——— — ———

— — — — linear theory ·····················

(b) Linear theory

	f_{wc}	N	P
·············	= 0.004,	= 0.01,	= 2.09
—— ··· ——	0.005	0.01	1.67
— — — —	0.004	0.016	3.34
—— · —— ·	0.014	0.01	0.60
—— —— ——	0.004	0.05	10.44
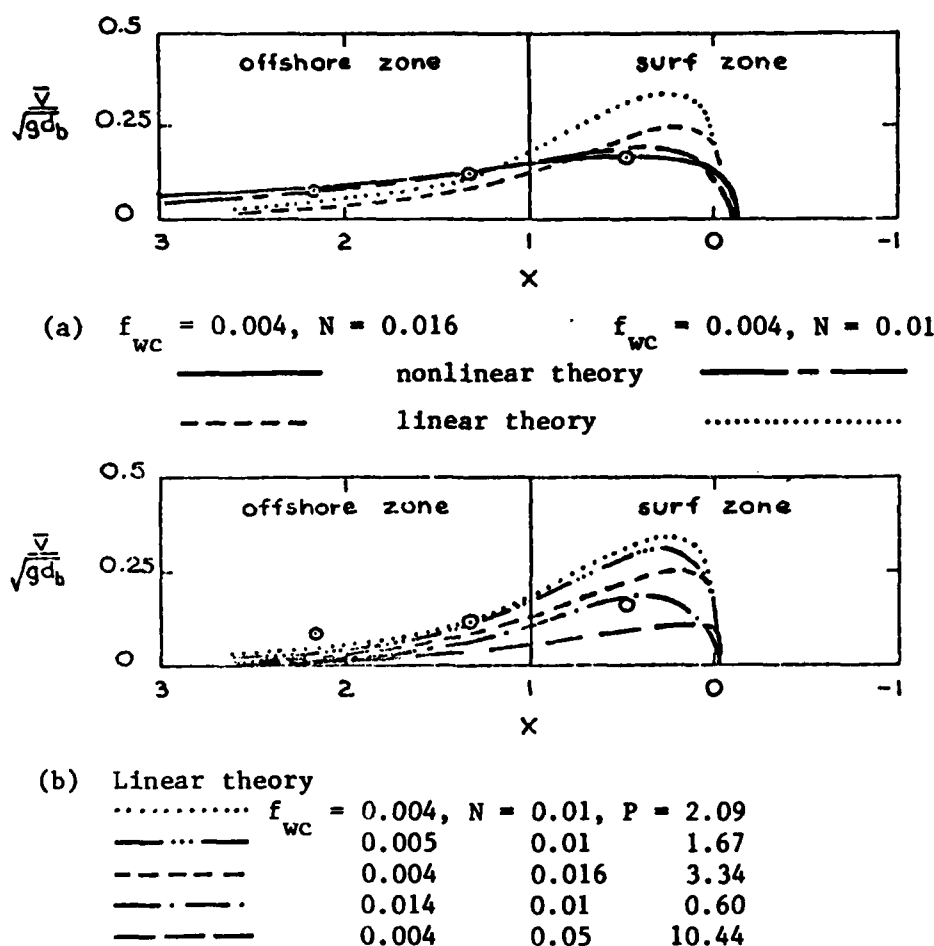
Figure 37. Comparison between linear and nonlinear
theories of uniform longshore current
profiles (from Gourlay, 1978).

2. Irregular Waves.

In a wide range of circumstances, wave breaking is a local phenomenon in
an irregular (random) wave field that is qualitatively similar to individual
wave breaking. Both the type of breaker and the wave height at breaking are
similar. However, in the irregular wave surf zone there is no one given
breaker line since at each location only a percentage of waves passing have
broken, and this percentage varies gradually toward the shore giving rise to
average gradual variations of energy density, energy flux, momentum flux, and
other wave parameters. The dissipation of wave energy and resultant decrease
in radiation stress for irregular waves that break in the surf zone has been
the subject of extensive research by Collins and Wier (1969), Collins (1972),
and Battjes (1972, 1974).

133

Two approaches to mathematicaly describe irregular waves in shallow water exist. Ijima, Matsuo and Koga (1972)[43] used an equilibrium linear spectral model (frequency domain) related to the deepwater spectrum. McReynolds (1977) used a two-component frequency spectrum to simulate a narrow spectrum. Battjes (1974a) argued that this approach gives an upper saturation limit on the spectral density values which depends on the width of the spectrum -- this is not realistic. Also, wave breaking is highly nonlinear and occurs to individual waves in physical space (space domain) and not to individual spectral components. For these reasons, Collins (1972) and Battjes (1974a) both adopted irregular models based on a wave-by-wave height theoretical and empirical probability distribution for individual waves in the space-time domain. In this model, it is the integral of the spectrum which has an upper bound in shallow water and not the spectral density. No rigor is claimed, only a rational approach where nonlinear processes are important.

Collins' (1972) approach was to consider the irregular sea as the ensemble average of periodic components, each with its own H_o, L_o, and α_o in deep water. The energy, energy flux, momentum flux, radiation stresses, and longshore current velocities are assumed expressible in terms of H_o, L_o, and α_o for regular waves. The mathematical expectation of these quantities is then calculated assuming that the joint probability density function of the stochastic ensembles of H_o, L_o, and α_o is known. Suitable functions for the joint probability density function are determined by empirical means from field data. Implied in this approach is the assumption that various nonlinear interactions between the waves and the mean motion (e.g., wave setup changes, wave characteristics) are properly represented by ensemble averages of individual waves. Battjes (1974a) presents arguments to show that this assumption is incorrect. In the highly nonlinear surf zone, the contribution of a wave with certain characteristics to wave setup, longshore current velocity, etc. is affected by the presence of waves of different characteristics. Therefore, Battjes took a different approach.

For irregular waves on gentle slopes with spilling breakers, Battjes made the basic assumption that

"...at each depth a limiting wave height H_b can be defined (which may also depend on the wave period), which cannot be exceeded by the individual waves of the random wave field, and that those wave heights which in the absence of breaking would exceed H_b are reduced by breaking to the value H_b."
(Battjes, 1974a, p. 125).

The energy variation in the surf zone thus results from clipping a fictitious wave height distribution which is present (theoretically) if breaking did not occur. This upper bound is found from the regular wave breaking ratio γ. In this way, energy varies gradually due to shoaling, refraction, bottom friction, and because of the increasing number of breaking waves in shallow water.

---

[43] IJIMA, T., MATSUO, T., and KOGA, K., "Equilibrium Range Spectra in Shoaling Water," *Proceedings, 12th Coastal Engineering Conference*, Vol. I, Washington, D.C., 1972, pp. 137-149 (not in bibliography).

The fictitious wave heights H_f are assumed to follow the Rayleigh probability distribution. Battjes (1974a) presented additional arguments and empirical evidence to support this choice even where waves are definitely nonlinear and do not possess a narrow spectrum. Clipping this fictitious wave height distribution at $H = H_b$ gave the following approximation to the true height distribution, $F(H)$

$$F(H) \equiv P\{\underline{H} \leq H\} = \begin{cases} 0 & H < 0 \\ \{1-\exp(-H^2/\bar{H}_f^2) & 0 \leq H \leq H_m \\ 1 & H \geq H_m \end{cases} \quad (119)$$

where
$\underline{H}$ = the stochastic wave height
$\bar{H}$ = the wave height of interest
$\bar{H}_f^2$ = the mean square value of the fictitious wave height
H_m = the maximum possible wave height in the surf zone, i.e., H_b.

In the shallow-water surf zone, it is further assumed that the effects of variability of wave period and wave direction on breaker heights are negligible. These factors are important, however, in calculations of the fictitious wave heights from the complete two-dimensional spectrum. The mean energy per unit area at a fixed location, taking breaking into account is then calculated from linear theory as

$$\bar{E} = \frac{1}{8}\rho g\bar{H}^2 \quad (120)$$

where

$$\bar{H}^2 = \int_{-\infty}^{\infty} H^2 dF(H) \quad (121)$$

The radiation stresses which can be found (to second order) as the weighted integral of the two-dimensional spectral density are of interest. But again, in the shallow-water surf zone, the only frequency-dependent weighting factor is η which is approximately unity. Consequently, Battjes (1974a) assumed that the radiation stresses are reduced by breaking in the same proportion as the total energy

$$S_{ij} = \frac{E}{E_f} S_{ij_f} = \{1-\exp(-H_b^2/\bar{H}_f^2)\} S_{ij_f} \quad (122)$$

where
S_{ij} = components of the radiation stress tensor
S_{ij_f} = components of the fictitious radiation stress tensor without breaking

such that

135

$S_{11} = S_{xx}$ = transformed component in x-direction
$S_{22} = S_{yy}$ = transformed component in y-direction
$S_{12} = S_{21} = S_{xy}$ = transformed shear stress component

and given by equations (23), (24), and (25), respectively. The validity of this approach improves for narrow frequency and directional spectra.

Another model for predicting irregular wave height distributions near-shore on continuously decreasing depths was proposed by Goda (1975). The following assumptions are made: (a) the equivalent significant wave height and peak spectral period in deep water are known; (b) the Rayleigh distribution applies in deep water for wave heights; (c) average beach slope is known; (d) empirical formulas for wave setup, breaking limits, etc. are applicable; (e) wave shoaling is nonlinear; and (f) broken waves can reform at smaller heights. A numerical procedure to use this model to predict nearshore conditions, maximum wave heights, and critical water depths has recently been developed (Seelig and Ahrens, 1980[44]; Seelig, 1980[45]). Goda's model is similar to Battjes (1974a) but provides a smoother cutoff at breaking by use of a varying probability for the breaking ratio, γ.

Finally, as briefly mentioned earlier in Section IV of this chapter, Battjes and Janssen (1976) used hydraulic jump bore theory to calculate the energy loss rate in the surf zone for irregular waves. The same probability theory as described above (Battjes, 1974a) is utilized except the probabilities (Q_b) are expressed in terms of H_{rms} and H_m to give a clearer physical meaning. The local value of H_{rms} is found by integrating the fundamental surf zone energy equation (44)

$$\frac{\partial F_x}{\partial x} + D = 0$$

with $F_x = ECg\cos\alpha$

and $E = \frac{1}{8}\rho g H_{rms}^2$ (123)

To close the system of equations for H_{rms}, the rate of energy dissipation per unit width D was determined from classical hydraulic jump theory with the depth across the jump approximately the local wave height. This gave

$$D = K\frac{1}{4}Q_b\bar{f}\rho g H_m^2$$ (124)

for irregular waves with $\bar{f}$ the mean frequency of the energy spectrum and K, a constant, near unity if the model is acceptable.

---

[44]SEELIG, W.N., and AHRENS, J., "Estimating Nearshore Conditions for Irregular Waves," TP 80-4, U.S. Army, Corps of Engineers, Coastal Engineering Research Center, Fort Belvoir, Va., June 1980 (not in bibliography).
[45]SEELIG, W.N., "Maximum Wave Heights and Critical Water Depths for Irregular Waves in the Surf Zone," CETA 80-1, U.S. Army, Corps of Engineers, Coastal Engineering Research Center, Fort Belvoir, Va., Feb. 1980 (not in bibliography).

Equation (124) is the key result of Battjes' (1978) paper and when inserted into equation (44) permitted H_{rms}, to be calculated across the surf zone for sloped or bar-type beach profiles. The closure parameters are K and γ, and it is important to point out that γ is only used as a breaking criteria and not to estimate the wave height decay. The main interest is in the resulting mean water surface changes calculated from the momentum balance as discussed below.

a. **Wave Setdown and Setup**. Figure 38 displays example theoretical mean water surface profiles for two beach profiles using the theory of Collins (1972). Less wave setdown is evident for the irregular waves than regular (monochromatic) waves with the same energy content. The wave setup profile is also highly nonlinear in the surf zone and maximum setup is less for irregular waves.

Similar results are shown in Figures 39 from Battjes (1974a) for a plane beach. Note the horizontal axis is stillwater depth, d, normalized by deep-water wave height, H_o, and could be related to horizontal distance offshore. Details of the solution method are omitted here but include shoaling and bottom refraction effects. Numerical integration procedures are employed and the results reduced to the regular wave setup as a check (eq. 35) for normal wave incidence. Figure 39(a) shows how wave refraction reduces wave setup, as expected and the mean water surface profile is almost linear near the
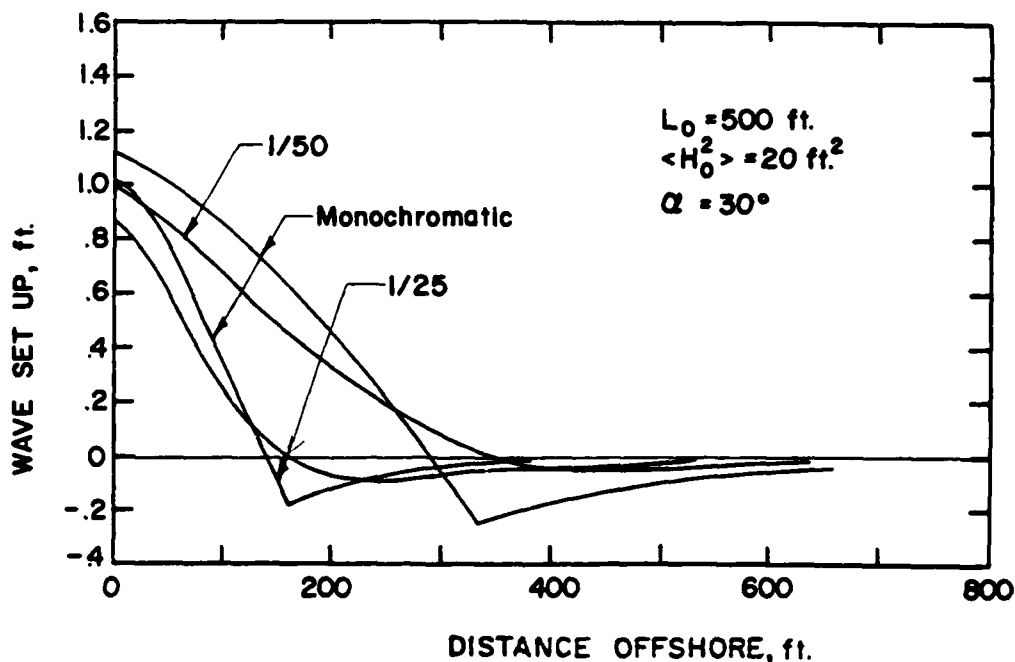

Figure 38. Illustration of wave setup on offshore slopes of 1:25 and 1:50, broken lines indicate results for periodic waves having the same energy content (from Collins, 1972).
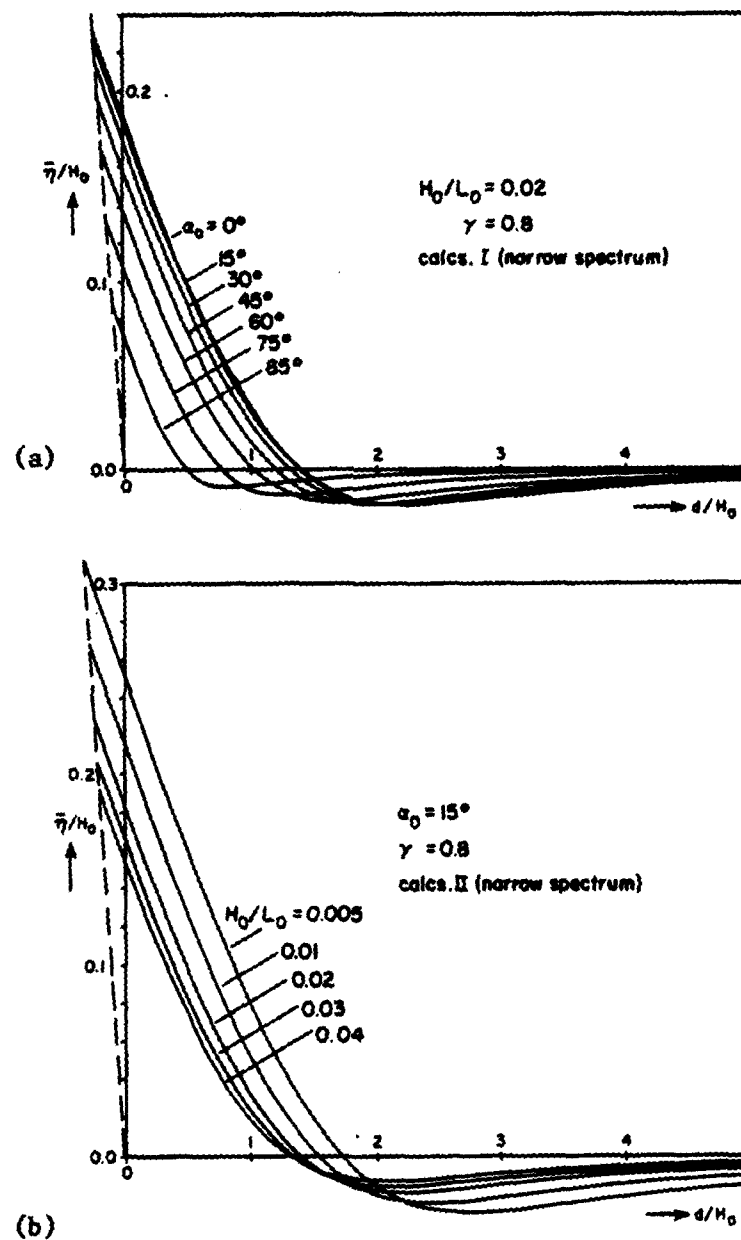
137

Figure 39. Calculated setup curves for (a) various
mean angles of incidence and (b) various
wave steepnesses (from Battjes, 1974a).

the maximum setup line, in contrast to Collins (1972). Wave steepness effects are shown in Figure 39(b). Battjes (1974a) used the breaking criterion of Miche (1951)[46] which included wavelength effects so that decreasing steepness (longer waves) made a wider surf zone to increase setup. In both these examples, $\gamma = 0.8$

In Goda's (1975) model, the effect of wave steepness on setup is similar to that obtained by Battjes (1974a). However, the magnitudes of both setdown and setup are relatively greater and depend more on beach slope since γ is variable and increases as beach slope increases. This causes a greater maximum setup than the Battjes (1974a) model.

The more sophisticated hydraulic jump model of the surf zone by Battjes and Janssen (1978) produced the MWL variations shown as Figure 40. In all cases the theoretical wave height variation across the surf zone is also shown, The steep plane beach (Fig. 40,b) has less setup than the flatter profile (Fig. 40,a). A smooth transition from setdown to setup is again evident. The results for two bar-trough profiles are given in Figure 40 (c and d). In one case (Fig. 40,c) two wave setdown regions are apparent while in another case (Fig. 40,d) a broad flat setup region is created. The crosses (x) indicated laboratory measurements, and a detailed discussion of the comparison is given in Chapter 4.

Finally, based on extensive measurements in the field off the Isle of Sylt (Germany) in the North Sea, Hansen (1978b) offered the following empirical relations for the maximum wave setup due to irregular waves on a flat plane beach

$$\bar{\eta}_{max} = 0.3\ H_{o,s}$$

$$\tag{125}$$

$$\bar{\eta}_{max} = 0.5\ H_{b,s}$$

where $H_{o,s}$ is the deepwater significant wave height and $H_{b,s}$ is the same but at the breakers.

b. Longshore Current Profile. Collins (1972) and Battjes (1974a) were primarily interested in the effect of irregular waves on longshore currents. In a random sea the breaking line for regular waves becomes a zone for irregular waves since the higher steeper waves break farther offshore than the gentle waves which break near the beach. The stochastic description of a real sea state (either spectral or probablistic) will find waves breaking in different locations at slightly different angles and with a range of wave heights and lengths. The net result is that irregular waves provide a degree of lateral mixing to distribute the longshore currents and produce a smooth profile across the surf zone similar to that found in the theory of regular waves when the lateral turbulent mixing stress term is included (see

---

[46]MICHE, R., "Le Pouvoir Réfléchissant Des Ouvrages Maritimes Exposés á L'action De La Houle," *Ann. des Ponts et Chaussées*, 121 é Année, 1951, pp.285-319 (not in bibliography).
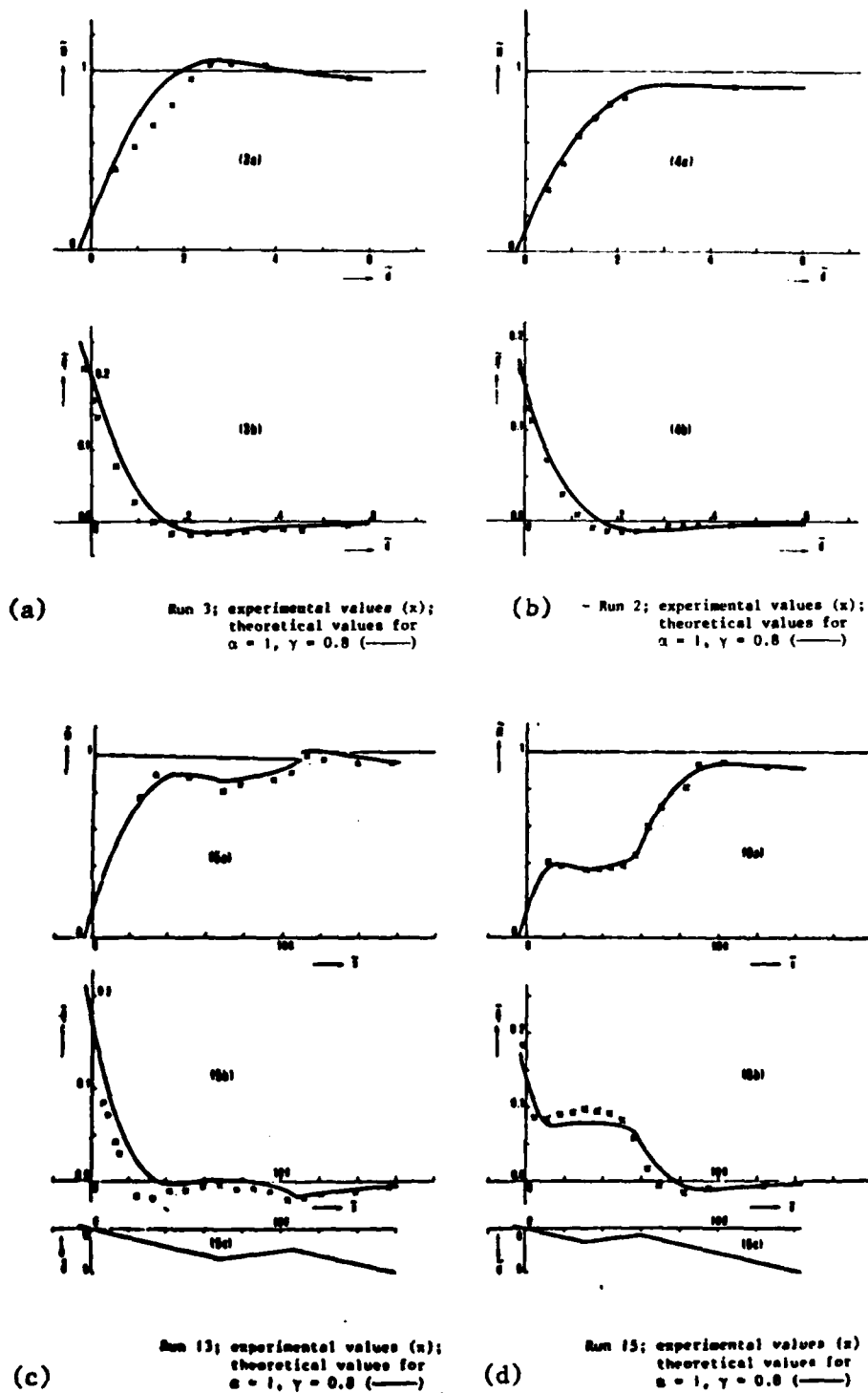
Figure 40. MWL variations for irregular waves (a),(b) plane beach (c),(d) bar-trough profiles (from Battjes and Janssen, 1978).

Fig. 24). In their original contributions, both Collins (1972) and Battjes (1974a) chose to omit the lateral mixing term since their irregular wave theories provided the same effect. They recognize, however, that such a term should also be included in future analysis.

Some example results from Collins (1972) are presented in Figure 41 for two beach profiles. The flatter slope produces a wider surf zone and broader longshore current profile. The dashlines are for regular waves with the same total energy content from the original theory of Longuet-Higgins (1970). No lateral mixing stress terms are involved. The extent and magnitude of the longshore current outside the breaker line is excessive and perhaps due to the lack of nonlinear interactions in Collins' approach.

The results obtained by Battjes (1974a) are more realistic in this regard. A weak current small-angle bed shear-stress model (eq. 51) was employed. For irregular waves with a narrow spectrum, Battjes took the time mean wave orbital velocity near the bottom, $\bar{u}_B$ rather than the maximum. This gave

$$\bar{u}_B = \frac{\bar{H}}{\pi} \left[\frac{\omega}{kh}\right] \tag{126}$$
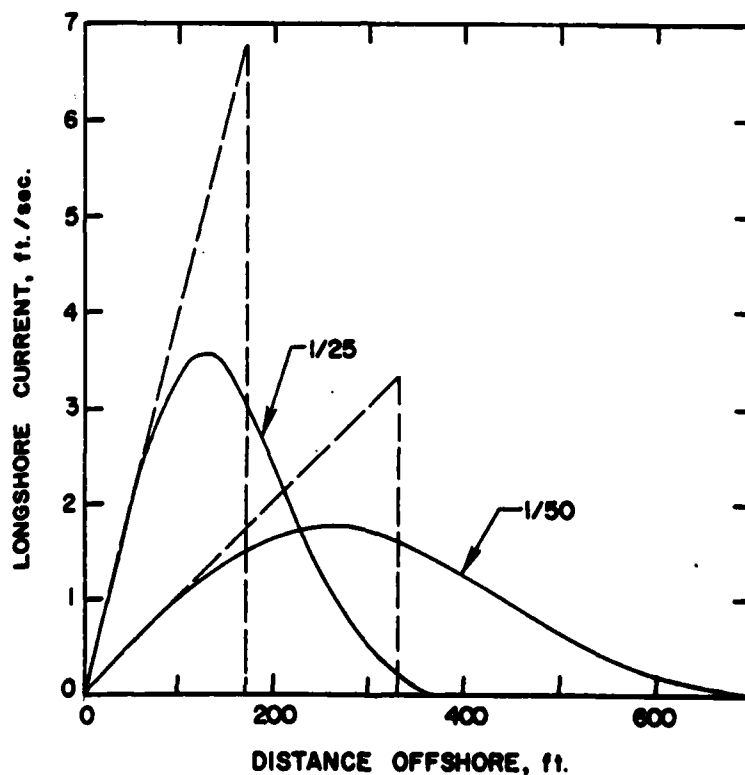
Figure 41. Illustration of the effect of offshore bottom slope on longshore currents, deepwater wave angle = 30°, deep-water wavelength = 500 feet, broken lines show longshore currents for periodic waves having the same total energy content (from Collins, 1972).

141

where $\omega = \dfrac{2\pi}{T_o} = (g\bar{k} \tanh \bar{k}h)^{\frac{1}{2}} =$ a mean frequency

$T_o =$ the deepwater mean wave period (i.e., peak period for narrow spectrums)

and $\quad \bar{H} =$ the mean wave height

$$\bar{H} = \frac{\sqrt{\pi}}{2} H_{f_{rms}} \ \ \text{erf}(\frac{H_b}{H_{f_{rms}}}) \tag{127}$$

with $H_{f_{rms}} =$ the fictitious root mean square wave height

$\quad\quad H_b =$ the local breaker height

$\quad\quad \text{erf} =$ the error function.

Small errors (<10 percent in deep water) result if $\bar{H}$ is replaced by H_{rms} in equation (126). Using a bed shear-stress model of the form

$$\bar{\tau}_{By} \doteq c_f \rho \bar{u}_B \bar{v} \tag{128}$$

in the longshore momentum balance equation (42) without lateral mixing gave

$$\bar{v} = + \frac{T_o}{2\, c_f\, \bar{H}} \sinh \bar{k}h \frac{dS_{xy}}{d\bar{x}} \tag{129}$$

with $\bar{x}$ again defined a positive in the ocean direction. When the wave setup is included as expressed in terms of the bottom slope for a plane beach (i.e., see eq. 68) this expression for $\bar{v}$ becomes

$$\bar{v} = \frac{T_o}{2\rho c_f \bar{H}} \tan\beta \sinh \bar{k}h \frac{dS_{xy}}{dh}(1 + \frac{1}{\rho g h} \frac{dS_{xx}}{dh})^{-1} \tag{130}$$

where the wave setup has yet to be determined.

Battjes (1974a) defined a normalized current velocity

$$\bar{v}^* = \frac{c_f T_o}{\tan\beta\pi H_o} \bar{v} \tag{131}$$

to give

$$\bar{v}^* = \frac{\bar{L}_o h}{H_o \bar{H}} \sinh \bar{k} h \frac{dS_{xy}}{dh} (\rho g h + \frac{dS_{xx}}{dh})^{-1} \tag{132}$$

which required numerical evaluation. As a check, the dimensional expression in equation (130) for a narrow spectrum in shallow water reduced to the modified Longuet-Higgins model (eq. 71) including setup.

Sample calculation results are presented in Figure 42 where the horizontal axis is the normalized mean water depth including setup. In Figure 42(a) for a narrow spectrum with mean wave steepness 0.02 and γ = 0.8, the effects of mean deepwater approach angle $\bar{\alpha}_o$ are shown. Some optimum angle ($\bar{\alpha}_o \pm 60°$) will produce a maximum current. For regular waves α_b = 45° gave the maximum. This result is in direct contrast to the large-angle theory for regular waves of Kraus and Sasaki (1979) (see Fig. 29).
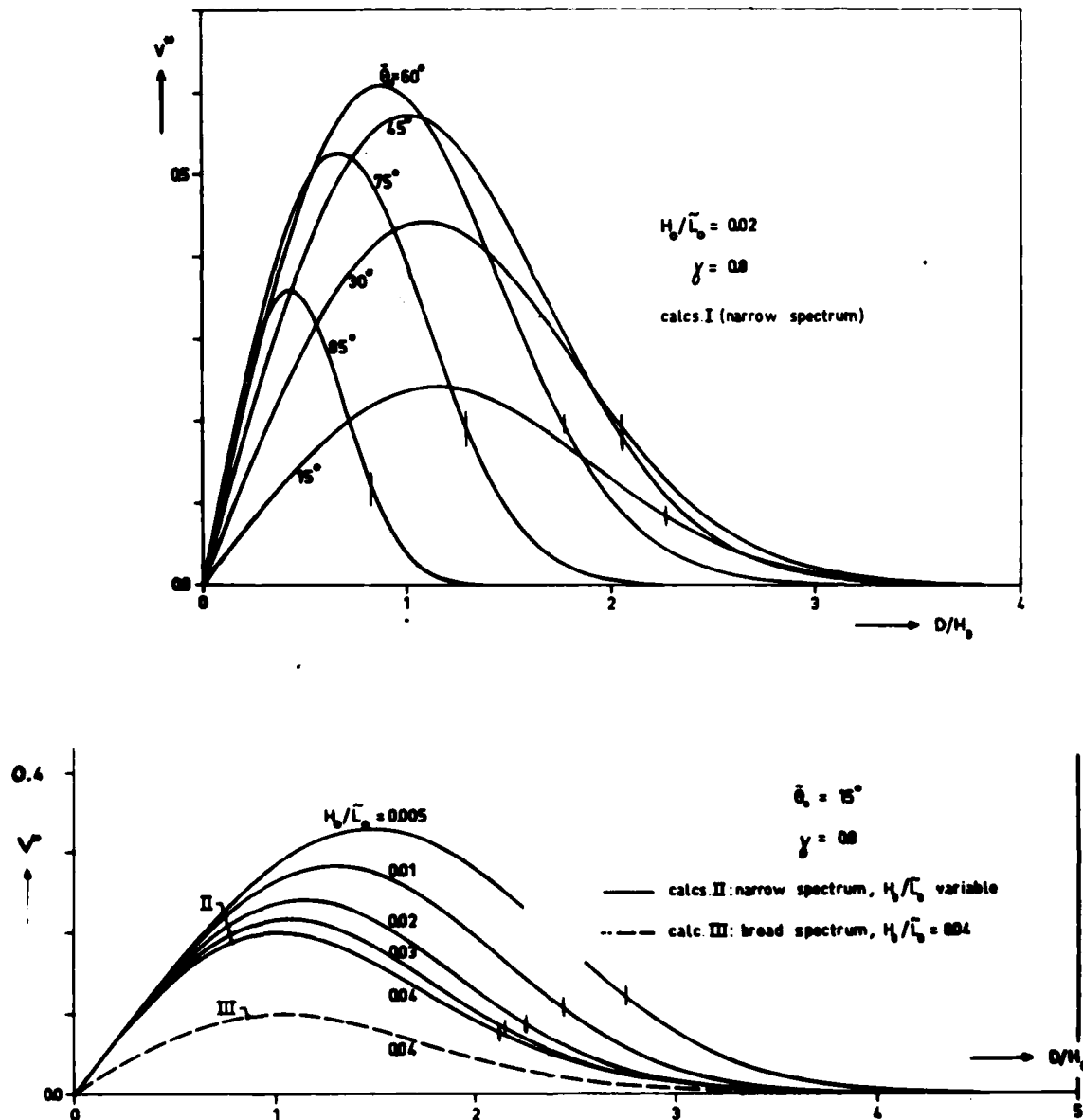
Figure 42. Calculated longshore current velocity profiles for (a) various mean angles of incidence and (b) various wave steepness (from Battjes, 1974a).
a).

The small vertical mark on these profiles indicates approximately where maximum wave setdown occurs, as determined from Figure 40. This would be the location of the breaker line in the periodic theory. The extent and magnitudes of the longshore currents outside this breaker line are more realistic (than Collins, 1972) in that the current drops off rapidly.

Figure 42(b), the solid lines, shows the influence of wave steepness for narrow spectra when $\tilde{\alpha}_o$ = 15° (γ = 0.8). Steeper wave decrease both the width and magnitude of the longshore current. This is because mean value length is included in the breaking criterion and long waves create a wider surf zone for a given H_o.

The dashline in Figure 42(b) is the longshore current profile for a broad spectrum of the Pierson-Moskowitz type and a $cos^2\alpha$-type spreading. Battjes (1972, 1974a) derived the theoretical expressions for radiation stresses in short-crested waves in deep water to prove that, in general, short-crestedness reduces all the radiation stress components. In shallow water, S_{xy} is 50 percent smaller for short-crested waves and a $cos^2\alpha$-type spreading of the directional spectrum. This result manifests itself in roughly the same percentage reduction in longshore current magnitude as illustrated by this one example in Figure 42(b). After further study of the complicated relationships between short-crested radiation stresses, bottom shear stress, and longshore currents, Battjes (1974a), in fact, concluded that

> "...for the purpose of longshore (current) calculations...the wave energy can be lumped into a very narrow frequency-and-direction interval (and)...the velocities so obtained are afterwards reduced by a factor equal to the ratio of the deep-water radiation shear stresses corresponding to the actual spectrum and the lumped, narrow spectrum." (p. 151)

This procedure eliminated the need to carry out a number of numerical integrations over the two-directional broad band spectrum.

It is not clear why additional theoretical work with irregular waves has not been pursued since 1974. The effects of more realistic strong current large-angle bed stress models, inclusion of lateral mixing stress terms, and incorporation of more sophisticated energy dissipation models for the surf zone would all be extremely interesting modifications. Perhaps with the recent availability of detailed field test results from the NSTS experiments to use as comparison, such computations are now warranted. Two-dimensional circulation and rip current computations for irregular waves have yet to be attempted.

VII. BOUSSINESQ METHODS

The time-averaged approach using radiation stress theory is the fundamental basis behind the theoretical results summarized in Sections II to VI. It has become the accepted theory of coastal hydrodynamics.

A new approach which employs the Boussinesq equations of motion that are depth-integrated but not time-averaged is emerging. Vertical accelerations resulting from streamline curvature of swell-type wind waves (periods down to 6 seconds) create a nonhydrostatic pressure distribution. Additional terms appear in the real-time motion equations that effectively account for the excess horizontal momentum flux in much the same way as the radiation stress terms. These terms are higher order differentials of the dependent variables (velocity and depth) so that equation solution determines the instantaneous currents and water surface variations as the waves propagate near the coast. Wave shoaling, refraction, diffraction, reflection, and current interactions are automatically part of the solution.

The theory can adequately describe nonlinear, nonpermanent form wave propagation over variable bathymetry to near the breaking limit. The equations required and some initial engineering applications outside the breaker zone are described below. Research and development is currently taking place to extend the theory to include wave breaking and energy dissipation in the surf zone. The instantaneous currents and water surf variations that result could then be time-averaged if it was desired to compute mean longshore currents, circulations, and setup. However, because of the highly nonlinear response of sediment to near-bottom velocities, the direct use of the instantaneous results coupled with sediment transport equations is expected.

The present situation is roughly analogous to tidal hydraulic and mass transport understanding in estuaries in the 1950's. The motion equation was time-averged over the tidal period to present a view of the net velocity distribution and circulations in the estuary. Much effort went into reformation of bed shear, turbulence dispersion, and sediment transport based on the time-averaged flows. The entire approach was abandoned when the numerical computation of the exact unsteady-flow equations became economical and realistic on the computer. This has subsequently led to much clearer understanding of mass, momentum, and energy transport processes for unsteady river and estuarine flows.

The ratio of tide-to-wind wave period is about 5000:1. Although significant improvements in size and speeds of computers continue, the simple fact remains that vast numbers of grid points and time steps are needed to accurately resolve wind waves in the coastal zone. Real time methods will remain a research tool for the near future.

1. Boussinesq Theory.

The theory that incorporates vertical accelerations, to a limited extent, in the horizontal motion equations is called Boussinesq theory (Boussinesq, 1872). Many forms of the equations attributable to Boussinesq are found in the literature and are possible due to the order of accuracy of terms retained and methods of derivation. They will still be referred to as Boussinesq equations or theory. Simplification of the equations by limiting wave propagation to one direction (no reflections) gives the

145

Korteweg and de Vries (1895)[47] equations (KdV). These are of less generality and will be omitted in what follows. However, exact solution of the KdV equations are termed first-order cnoidal waves. The solitary wave is a limiting case of a cnoidal wave. Thus these classical wave theories which are found to duplicate experimentally determined surface profiles and velocity distributions of real waves in shallow water have their roots in Boussinesq theory, or vice versa.

The basic Boussinesq equations in one dimension on a horizontal bottom can be written (neglecting surface or bed stresses) in Eulerian form

$$\underline{\text{Mass}} \qquad \frac{\partial h}{\partial t} + h \frac{\partial u}{\partial x} + u \frac{\partial h}{\partial x} = 0 \tag{133}$$

$$\underline{\text{Motion}} \qquad \frac{\partial h}{\partial t} + u \frac{\partial u}{\partial x} + g \frac{\partial h}{\partial x} = + \frac{1}{3} d^2 \frac{\partial^3 u}{\partial x^2 \partial t} \tag{134}$$

where $h = \eta + d$ with d the stillwater depth and η the instantaneous water surface variation. The velocity u is a depth-averaged instantaneous value. The equations are identical to the long wave equations except for the mixed derivative Boussinesq term on the right-hand side of equation (134). It is instructive to briefly review various theories which omit certain terms in equation .(134).

a. <u>Waves of Permanent and Nonpermanent Form</u>. If the convective acceleration and Boussinesq terms are neglected, a wave of permanent form moving with speed $c = (gd)^{\frac{1}{2}}$ results. Without only the Boussinesq term, each part of the solution travels at a speed $c = u \pm (gh)^{\frac{1}{2}}$ so that the high parts tend to overtake the low sections with time. The wave travels with nonpermanent form, continually steepens, and eventually breaks. This tendency is termed amplitude dispersion. If, however, only the convective acceleration term is omitted, a linearized version of the Boussinesq equations results which includes vertical acceleration of the wave orbital motion. The celerity is of the form

$$c = (gd)^{\frac{1}{2}} / (1 - 4\pi^2 d^2 / 3L^2)^{\frac{1}{2}} \tag{135}$$

where L is the wavelength of any wave component in the solution. Thus each wave component travels at its own speed depending on its length. This tendency is termed frequency (or wavelength) dispersion. The full equations with all terms maintain a balance between amplitude and frequency dispersion only for the limiting case of the solitary wave. They also simulate a progressive wave of permanent form (first order, cnoidal) without excessive dispersion as long as the wave does not propagate indefinitely (Peregrine, 1972).

---

[47]KORTEWEG, D.J., and de VRIES, G., "On the Change of Form of Long Waves Advancing in a Rectangular Canal and on a New Type of Long Stationary Waves," Phil. Mag., 5th Series, Vol. 39, 1895, pp. 422-443 (not in bibliography).

Ursell (1953)[48] devised the following criterion, the Ursell number U, for applying the Boussinesq equation or special cases with terms omitted. When

$$U \begin{cases} \gg 1 & \text{Nonlinear long wave equations} \\ \theta(1) & \text{Boussinesq equations} \\ \ll 1 & \text{Linear wave equations} \end{cases} \tag{136}$$

where

$$U = \frac{(\text{wave amplitude/depth ratio})^3}{(\text{wave steepness})^2} = \frac{(\eta_{max}/d)^3}{(\eta_{max}/L)^2} = \frac{\eta_{max} L^2}{d^3} \tag{137}$$

The region where U is comparable to unity is often cited as applicable to cnoidal wave theory.

No waves of permanent form can exist on a sloping beach. By comparison with experiments, Madsen and Mei (1969)[49] concluded that the Boussinesq equations given by equations (133) and (134) give reasonable shoaling solutions for H/d up to about 0.5. Waves break when H/d $\doteq$ 0.8-1.0. As discussed further below, even this limit is approachable when the Boussinesq equations are expanded to include sloping bottom terms and more accurate numerical solution techniques are employed.

b. **Derivation of Boussinesq Equations.** The Boussinesq equations are normally derived (Peregrine, 1972) by expanding all dependent variables as polynomials in terms of scaling parameters

$$\epsilon = \frac{\eta_{max}}{d} \tag{138}$$

$$\sigma = \frac{d}{L} \tag{139}$$

with ϵ = on the order of (θ) σ^2, substitution in Euler's equation of motion for inviscid flow, and integration over the vertical water column. Retaining all terms up to order σ^2 (or ϵ) results in equation (134) for a horizontal bottom.

[48]URSELL, F., "The Long-Wave Paradox in the Theory of Gravity Waves," *Proceedings of Cambridge Philosophical Society*, Vol. 39, London, 1953, pp. 685-694 (not in bibliography).

[49]MADSEN, O.S., and MEI, C.C., "The Transformation of a Solitary Wave Over an an Uneven Bottom," *Journal of Fluid Mechanics*, Vol. 39, Pt. 4, 1969, pp. 781-791 (not in bibliography).

In terms of the scaling parameters it can readily be shown that the normalized Boussinesq equations for horizontal bottom become (Whitham, 1974)[50]

Mass $\quad \dfrac{\partial \eta^*}{\partial t} + \dfrac{\partial}{\partial x}[(1 + \epsilon\eta^*)u^*] + \theta(\epsilon\sigma^2, \sigma^4) = 0 \qquad (140)$

Motion $\quad \dfrac{\partial u^*}{\partial t} + \epsilon u^* \dfrac{\partial u^*}{\partial x} + \dfrac{\partial \eta^*}{\partial x} - \dfrac{1}{3}\sigma^2 \dfrac{\partial^3 u^*}{\partial x^2 \partial t} + \theta(\epsilon\sigma^2, \sigma^4) = 0 \qquad (141)$

where the star indicates normalized terms and all higher order terms of order $\epsilon\sigma^2$, σ^4, ϵ^2, etc. have been neglected. The Ursell parameter simply becomes

$$U = \frac{\epsilon}{\sigma^2} = \frac{\text{Importance of nonlinear term}}{\text{Importance of Boussinesq term}} \qquad (142)$$

so that when $U \doteq 1$, the relative importance of both dispersion terms in equation (141) is apparent.

Other forms for the Boussinesq term have appeared in the literature (e.g., Abbott, 1979)[51] and result from using the linearized mass equation to transform the term into a mixed derivative in h.

c. Boussinesq-Type Equations for Variable Water Depth. The derivation of Boussinesq-type equations over variable depths remains an active research area. The derivation by Peregrine (1967)[52] and summarized in Peregrine (1972) is for propagation of arbitrary long waves over slowly-varying bathymetry. A new length-scale parameter associated with depth variations is needed and the local bottom slope, β is used. Peregrine assumed $\sigma \geq \beta$ to be consistent with the order of approximation for surface boundary conditions. He obtained for the one-dimensional motion equation (Peregrine, 1972)

$$\frac{\partial u}{\partial t} + u\frac{\partial u}{\partial x} + g\frac{\partial h}{\partial x} = \frac{1}{2}d\frac{\partial}{\partial x}\left[\frac{\partial}{\partial x}\left(d\frac{\partial u}{\partial t}\right)\right] - \frac{1}{6}d^2\left[\frac{\partial}{\partial x}\left(\frac{\partial}{\partial x}\left(\frac{\partial u}{\partial t}\right)\right)\right]$$

or

$$\frac{\partial u}{\partial t} + u\frac{\partial u}{\partial x} + g\frac{\partial \eta}{\partial x} = \frac{1}{3}d^2\frac{\partial^3 u}{\partial x^2 \partial t} + \frac{1}{2}d\frac{\partial d}{\partial x}\left(\frac{\partial u}{\partial t} + \frac{\partial^2 u}{\partial x \partial t}\right) \qquad (143)$$

which reduces to equation (134) for a horizontal bottom. Peregrine (1972) states:

[50] WHITHAM, G.B., *Linear and Nonlinear Waves*, Wiley Interscience, New York, 1974 (not in bibliography).

[51] ABBOTT, M.B., *Computational Hydraulics*, Pitman, London, 1979, p. 52.

[52] PEREGRINE, D.H., "Long Waves on a Beach," *Journal of Fluid Mechanics*, Vol. 27, 1967, pp. 815-827 (not in bibliography).

"The existence of β means that it is possible to use difference scalings of variables by incorporating β and thus get different equations of motion, especially for small beach slopes." (p. 116)

Other derivational methods exist (e.g., Green and Naghdi, 1976)[53] which avoid using scaling parameters, but an assumed velocity field instead. For a uniform vertical velocity profile, their derived equations after linearization reduce to those derived by Peregrine (1967). An alternative derivation has been reported by Mass and Vastano (1978)[54] using variational techniques to minimize the total energy of the system. Assumptions regarding scaling of parameters are necessary. When both large wave amplitude and bottom variations are permitted, a total of 19 terms appear in the one-dimensional motion equation. Most terms are small and should disappear for practical coastal engineering applications. Engineering derivations can be found in Abbott and Rodenhuis (1972)[55], Liggett (1975)[56], Abbott (1979), and others.

d. Two-Dimensional Equations in Conservation Form. For practical engineering applications, Abbott, Petersen and Skovgaard (1978a,b) took the equations derived by Peregrine (1967) but in terms of depth-integrated flows and in conservation form. This gave for disturbances of small to moderate amplitude over slowly varying bathymetry

$$\frac{\partial \eta}{\partial t} + \frac{\partial p}{\partial x} + \frac{\partial q}{\partial y} = 0 \tag{144}$$

$$\frac{\partial p}{\partial t} + \frac{\partial}{\partial x}\left(\frac{p^2}{h}\right) + \frac{\partial}{\partial y}\left(\frac{pq}{h}\right) + gh\frac{\partial \eta}{\partial x} = \frac{1}{2} hd\left[\frac{\partial^3}{\partial x^2 \partial t}\left(\frac{pd}{h}\right) + \frac{\partial^3}{\partial x \partial y \partial t}\left(\frac{qd}{h}\right)\right]$$

$$- \frac{1}{6} d^2 h\left[\frac{\partial^3}{\partial x^2 \partial t}\left(\frac{p}{h}\right) + \frac{\partial^3}{\partial x \partial y \partial t}\left(\frac{q}{h}\right)\right] \tag{145}$$

$$\frac{\partial q}{\partial t} + \frac{\partial}{\partial y}\left(\frac{q^2}{h}\right) + \frac{\partial}{\partial x}\left(\frac{pq}{h}\right) + gh\frac{\partial \eta}{\partial y} = \frac{1}{2}hd\left[\frac{\partial^3}{\partial y^2 \partial t}\left(\frac{qd}{h}\right) + \frac{\partial^3}{\partial x \partial y \partial t}\left(\frac{pd}{h}\right)\right]$$

$$- \frac{1}{6} d^2 h\left[\frac{\partial^3}{\partial y^2 \partial t}\left(\frac{q}{h}\right) + \frac{\partial^3}{\partial x \partial y \partial t}\left(\frac{p}{h}\right)\right] \tag{146}$$

[53]GREEN, A.E., and NAGHDI, P.M., "A Derivation of Equations for Water Propagation in Water of Variable Depth," *Journal of Fluid Mechanics*, Vol. 78, Pt. 2, 1976, pp. 237-246 (not in bibliography).

[54]MASS, W.J., and VASTANO, A.C., "An Investigation of Dispersive and Nondispersive Long Wave Equations Applied to Oceans of Variable Depth," Reference 78-8-T, Department of Oceanography, Texas A&M University, College Station, Texas, July 1978 (not in bibliography).

[55]ABBOTT, M.B., and RODENHUIS, G.S., "On the Formation and Stability of the Undular Hydraulic Jump," Report Series No. 10, International Courses in Hydraulic and Sanitary Engineering, Delft, Netherlands (not in bibliography)

[56]LIGGETT, J.A., "Basic Equations of Unsteady Flow," Ch. 2, *Unsteady Flow in Open Channel*, Vol. I, K. Mahmood and V. Yevjevish, eds., Water Resources Publications, Fort Collins, Colo., 1975 (not in bibliography).

where p = uh and q = vh are the volumetric flow rates per unit width. Numerical integration methods, testing, and some application examples of these equations are reviewed below.

Recently, Hauguel (1980) obtained somewhat different results by assuming that the vertical velocity increases linearly through the water column and averaging the Navier-Stokes equations over this depth. It should be noted here that such an assumption for the vertical velocity, w is equivalent to assuming a uniform horizontal velocity profile based on continuity principles. If the bed stress term is neglected, the x-direction motion equation is

$$\frac{\partial p}{\partial t} + \frac{\partial}{\partial x}(\frac{p^2}{h}) + \frac{\partial}{\partial y}(\frac{pq}{h}) + \frac{\partial}{\partial x}[(\frac{g+b}{2} + \frac{a}{3})h^2]$$

$$= (g + b + \frac{a}{2})h \frac{\partial z}{\partial x} \tag{147}$$

where p, q, and h are as previously defined, z is the bed elevation above an arbitrary datum, and the new terms a and b characterize the vertical accelerations due to wave steepness and bed-slope variations. They are defined as

$$a = \frac{d^2h}{dt^2} \tag{148}$$

$$b = \frac{d^2z}{dt^2} \tag{149}$$

where the total or substantive derivative is given by

$$\frac{d}{dt} = \frac{\partial}{\partial t} + \frac{p}{h}\frac{\partial}{\partial x} + \frac{q}{h}\frac{\partial}{\partial y} \tag{150}$$

The derivation is said to follow that given by Serre (1953)[57] for cnoidal waves. A similar expression is given for the y-direction momentum. This approach may permit steeper waves to propagate farther over irregular bathymetry.

e. **Limitations of Boussinesq Theory.** The range of application of equations (144), (145), and (146), based on a comparison with first-order cnoidal-wave theory and Dean's stream-function wave theory (Dean, 1974)[58],

[57]SERRE, F., "Contribution a letude des ecoulements permanents et variables dans les canaux," *La Houille Blanche*, 1953, pp. 374-388, 830-872 (not in bibliography).

[58]DEAN, R.G., "Evaluation and Development of Water Wave Theories for Engineering Application," SR-1. Vols. I and II, U.S. Army, Corps of Engineers, Coastal Engineering Research Center, Fort Belvoir, Va., 1974 (not in bibliography).

as determined by Abbott, et al. (1978), is presented in Figure 43. In
shallow water, the wave celerity approaches the group velocity or speed of
energy propagation. Hence celerity is a good indicator of usefulness of
the theory. An error of 2 percent is indicated for a wide range at the
breaking limit.

The expected application limit shown is for $d/L = 0.2$ ($d/L_0 = 0.17$).
This is in the intermediate wave theory range and near the engineer's limit
of $d/L_0 = 0.25$ for deepwater waves. Even near this limit, the assumption
of a uniform velocity profile is still reasonable as shown in Figure 44.
The U_{max} profile based on classical linear wave theory for $d/L = 0.22$ is
shown for comparison. The vertical w_{max} profile is very close to a linear
variation with depth. The exponential decay of the horizontal velocity com-
ponent is roughly analogous, in some respects, to the fully developed log-
arithmic boundary layer profile of open channel flows which are routinely
modeled as depth-averaged flow.
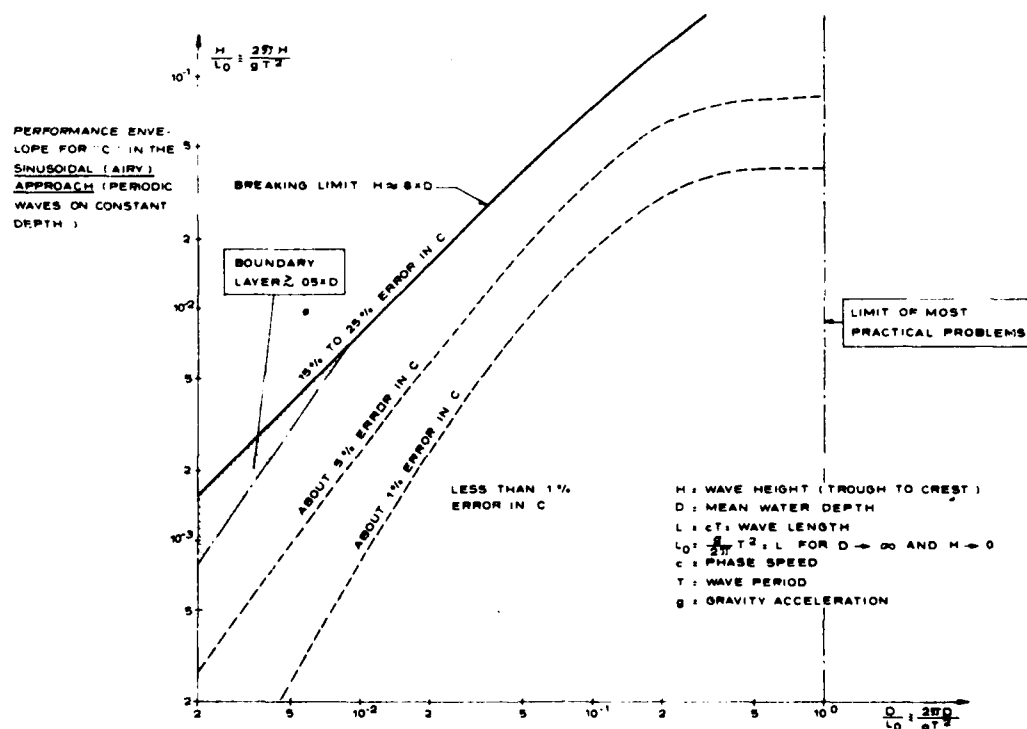
Figure 43. Range of application of the mass and Boussinesq equation system
(from Abbott, et al, 1978).

151
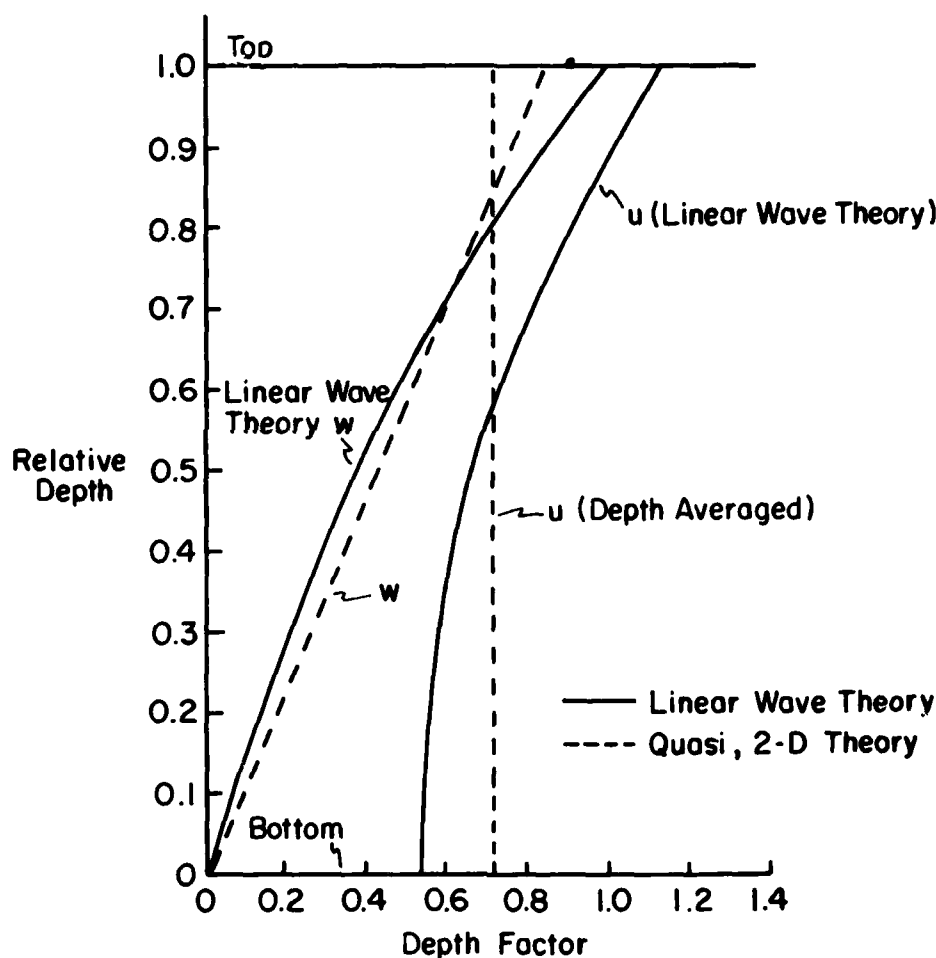
Figure 44. Comparison of horizontal and vertical maximum
velocity profiles between quasi, 2-D, and
linear wave theories for d/L = 0.22.

The practical limitations for engineering purposes of the Boussinesq
theory are still open to question and require further research. This is
because for variable bathymetry, the precise form of the continuum equations
involved is not known. In addition, accuracy errors in the numerical solu-
tion procedures produce additional numerical amplitude and frequency disper-
sion effects. Numerical integration procedures are very important in use
of the Boussinesq theory.

2. Numerical Solution.

The finite-difference method has been the only numerical integration
method employed to date to solve the Boussinesq equations. Early numerical
efforts to study one-dimensional wave shoaling and transformations over

steps (e.g., Peregrine, 1967, Camfield and Street, 1969[59], Madsen and Mei, 1969[49], Chan and Street, 1970[60]) must be reviewed with caution since the numerical accuracy of the results is questionable. This is because the truncation errors from the acceleration terms were of the same order or lower order than the Boussinesq terms and essentially masked its effect. These researchers were interested in the physical aspects of wave transformations which were qualitatively simulated so that the value of these early efforts from this aspect is not diminished.

In addition, all numerical methods must use only a discrete number of points per wavelength (N) to define each wave. Finite-amplitude (cnoidal) waves when decomposed by Fourier analysis consist of many, superimposed sinusoidal components. All harmonic components are described by fewer and fewer grid points, and this coarse description can lead to amplitude and phase errors. Thus, solutions of the Boussinesq equations are extremely sensitive to numerical errors (Abbott and Rodenhuis, 1972[55], Hauguel, 1980).

a. **Abbott, Petersen, and Skovgaard (1978a, 1978b)**. These researchers of the Danish Hydraulics Institute were the first to successfully develop a two-dimensional numerical model to accurately propagate quasi-long waves over variable bathymetry to near the breaking limit. They integrated equations (144), (145), and (146) using a staggered, implicit finite-difference scheme. One key aspect of their contribution (see also Abbott, 1978, 1979) is the method to remove all truncation error terms of order comparable to the Boussinesq term so the resulting finite-difference equations are third-order accurate. This was done (following the observations by Long, 1964[61]) by rewriting all higher order truncation error terms using the linearized wave equations with no loss of accuracy or generality. In one dimension these linearized equations are

$$\frac{\partial \eta}{\partial t} + \frac{\partial p}{\partial x} = 0 \tag{151}$$

$$\frac{\partial p}{\partial t} + gd \frac{\partial \eta}{\partial x} = 0 \tag{152}$$

In this way, the truncation errors are finite-differenced, combined with the finite-difference Boussinesq term and subtracted out of the equations together in an efficient manner. It is theoretically possible to use higher order accurate finite-differences initially to accomplish this goal but Abbott, Petersen, and Skovgaard (1978a) claim this leads to "...algorithmically intractable difference forms of the Boussinesq equations."

[59]CAMFIELD, F.E., and STREET, R.L., "Shoaling of Solitary Waves on Small Slopes," *Journal of the Waterways and Harbors Division*, Vol. 95, No. WW1, Feb. 1969, pp. 1-22 (not in bibliography).

[60]CHAN, R.K.C., and STREET, R.L., "Shoaling of Finite-Amplitude Waves on Plane Beaches," *Proceedings of the 12th Coastal Engineering Conference*, American Society of Civil Engineers, 1970 (not in bibliography).

[61]LONG, R.R., "The Initial Value Problem for Long Waves of Finite Amplitude," *Journal of Fluid Mechanics*, Vol. 20, Pt. 7, 1964, pp. 161-170 (not in bibliography).

A number of performance envelope tests were conducted on the numerical scheme to determine the extent to which it came close to the continuum limitation shown in Figure 44. These were all for nonbreaking waves and included the following one- and two-dimensional tests:

(1) One-dimensional:

    (a) Finite-amplitude, periodic wave propagation on a horizontal bottom;

    (b) Full and partial wave reflections (transmission);

    (c) Wave shoaling on plane beach.

(2) Two-dimensional:

    (a) Wave diffraction, and

    (b) Comparison with physical model results of harbor resonance.

An example perspective view of two-dimensional short wave propagation on the computer is shown in Figure 45. A comparison of the numerical results with physical experiments and other theories is presented in Chapter 4. For practical applications, 1-second time steps and 10-meter space steps are estimated to give reasonable results for engineering purposes.
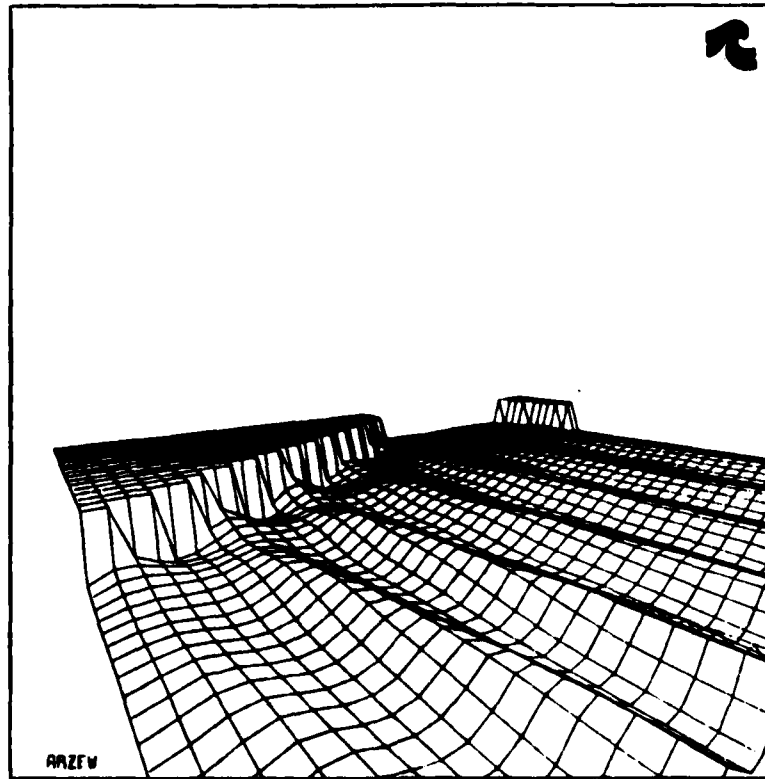

Figure 45. Numerical propagation of quasi-long waves in two dimensions using Boussinesq equations (from Abbott, 1979[51]).

b. <u>Others</u>. Hauguel (1980) employed a different numerical solution strategy with the finite-difference method for equations (147) to (150). A predictor-corrector scheme which uses the method of characteristics in the prediction phase and a three time level implicit scheme in the corrector phase is employed. Complete details are forthcoming since only the abstract is presented in Hauguel (1980).

Additional efforts in one dimension using the techniques developed by Abbott, Petersen, and Skovgaard (1978a) for truncation error removal but with an implicit three level box or Preissmann[62] scheme have been made by McCowan (1978)[63] or are in progress by Jensen (personal communication, 1981).

3. Simulation of Surf Zone Hydrodynamics.

Research is currently in progress to extend the Boussinesq approach to include wave breaking, surf zone energy dissipation, and lateral turbulent mixing effects in an effort to simulate the hydrodynamics of the surf zone. The main features of the flow are of interest which will be the instantaneous depth-integrated velocity components and water depth. Time-averaging these results would produce longshore currents, nearshore circulations, rip currents and MWL changes, if desired to compare with the many radiation stress theories. Such numerical results are a few years in the future.

In summary, the primary advantages of the Boussinesq approach are (a) the insight into physical processes taking place within each wave period, and (b) the elimination of the need to specify the wave height field by other calculation procedures throughout the area of interest. On the other hand, the approach still requires empirical surf zone simulations that are just being developed plus large efficient computers for the extensive computations.

VIII. SUMMARY: THEORETICAL ASPECTS

A comprehensive review and summary of relevant theories since 1967 has been presented. The time-averaged radiation stress approach has been extended in considerable detail since first introduced. Mean water level variations and net currents are linked together by the conservation laws of mass and momentum. The primary driving force is created by the excess momentum flux due to the waves, i.e. the radiation stress gradients. Major modifications to the original theory have taken place primarily in three areas:

---

[62]PREISSMANN, A., "Propagation des Intumescenses Dans Les Canaux et Rivieres," Cer Congres de l'Assoc., Francaise de Calcul, Grenoble, 1961, pp. 433-442 (not in bibliography).

[63]McCOWAN, A.D., "Numerical Simultation of Shallow Water Waves," *4th Australian Conference on Coastal and Ocean Engineering,* Adelaide, Nov. 1978, pp. 132-136 (not in bibliography).

(a) Bed shear-stress formulations,
(b) extensions to irregular waves, and
(c) use of two-dimensional numerical models.

Extensive use of empirical surf zone models remains a weak link in the
theory, expecially in determining, when, where, and why waves break. Use
of the method also requires prior specifications of wave heights throughout
the region of interest. This aspect poses difficulties in its own right
due to wave shoaling, refraction, diffraction, reflection, transmission,
and wave-current interaction computations required. Additional research
is needed; e.g., the modified bed shear-stress and lateral mixing stress
models used with an accurate two-dimensional numerical formulation to study
both regular and irregular wave conditions.

Time-averaging masks the physical processes that occur at scales within
each dominant wave period. The Boussinesq approach unlocks this information
and allows finite-amplitude waves in the nearshore zone to propagate and
interact with the surroundings in a fundamental way. Solutions to the gov-
erning equations are only possible with the aid of large high-speed computers
A new research tool is thus emerging to perhaps raise the level of theoreti-
cal understanding above that obtainable from radiation stress theory.

In either case, only depth-integrated flow characteristics are consid-
ered. No truly three-dimensional model of coastal hydrodynamics has been
attempted.

Which theory is correct? All the physical observations (Ch. 2) have
purposely been separated from the theory (Ch. 3) and left for a comparison
of each in Chapter 4. It will become apparent that the number, extent, and
detail of the theory far exceed the number of good data sets available for
comparison and verification.

CHAPTER 4

EXPERIMENTAL VERIFICATION OF THEORY

Again, all theory before 1967 which has been thoroughly discussed by Galvin (1967) has been omitted in this report. Results of comparisons between laboratory and field measurements and theory as original presented in the literature are reviewed. No new analysis of the available data base is attempted. Only those equations from Chapter 3 that have experimental backing or are seriously questioned are repeated in this chapter.

I. WAVE SETDOWN AND SETUP

1. Regular Linear Waves.

Some classic results of MWL change as determined in a 0.5-meter-wide by 0.75-meter-deep by 40-meter-long wave flume by Bowen, Inman, and Simmons (1968) are shown in Figure 46. The wave height in deep water was 6.45 centimeters and the beach slope 1 on 12. For normal wave incidence on a plane beach, wave setdown is shown to match the theory given by equation (30), except near the breaker line. Wave setup was found to be almost linear over the entire surf zone and proportional to the beach slope as expected from equation (35), repeated here

$$\frac{d\bar{\eta}}{dx} = \frac{1}{1 + 8/3\gamma^2} \tan \beta = K \tan \beta$$

and letting

$$K = \frac{1}{\tan \beta} \, (\bar{\eta}_{max} - \bar{\eta}_b)/\bar{x}_b \tag{153}$$

K versus γ as plotted in Figure 47. Included are data from Putnam, Munk and Traylor (1949) for other slopes and the agreement was characterized as ". . . quite good."

Gourlay (1978) reanalyzed the Bowen, Inman, and Simmons data and concluded that values of maximum wave setup $\bar{\eta}_{max}$ in equation (153) were overestimated (see App. A4.43 in Gourlay, 1978) due to inclusion of wave runup effects. Both plunging- and spilling-type breakers were produced in the tests of Bowen, Inman, and Simmons (1968).

Similar results were obtained by Smith (1974) for breaking waves of the same types. Gourlay (1978) also adjusted these data to account for total water volume and include a discussion of the results.
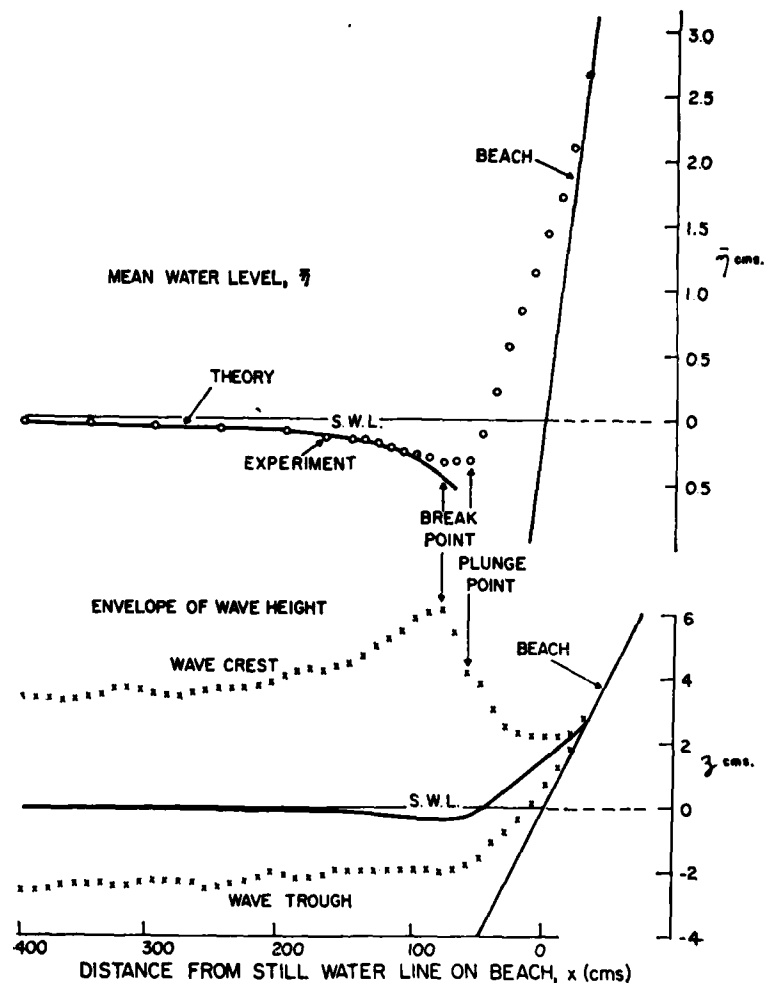
Figure 46. Wave setdown and setup, comparison of experiment and theory
(eqs 3 and 8) for regular waves on a plane beach (after
Bowen, Inman, and Simmons, 1968).

Additional experiments in the same wave basin as originally used by
Bowen, Inman, and Simmons (1968) but with three different beach slopes
(tan β = 0.022, 0.040, 0.083) have been reported by van Dorn (1976). The
object was to distinguish wave setup from the dynamic shoreline motions
called runup due to partial reflections. The empirical result was that
the setup slope was found approximately linear across the surf zone (as
before) but proportional to the square of the beach slope. This relation

158
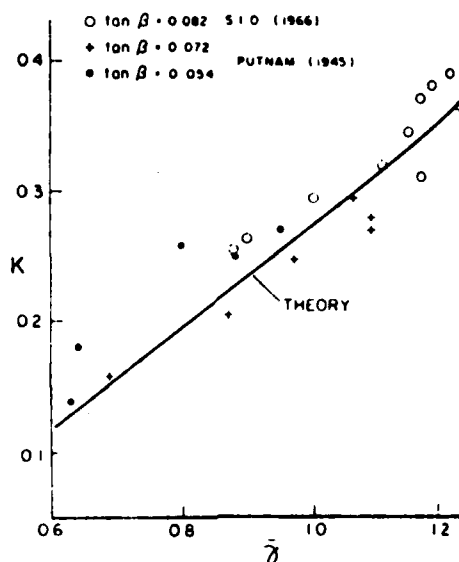
Figure 47. Ratio of wave setup slope to beach slope (K) versus γ (after
            Bowen, Inman, and Simmons, 1968).

is shown in Figure 48 (after Gourlay, 1978) with the equation

$$\frac{d\bar{\eta}}{dx} = 3.4 \tan^2 \beta \tag{154}$$

given as line of best fit to the data. The vertical error bar lines
indicate possible variation due to wave periods of the experiments. Results
of all experimenters, including that by Gourlay (1978) are also shown.

      Van Dorn (1976) concluded that on relatively steep beach slopes
(tan β ≳ 0.1), with some reflection present, setup slope increased with wave
period. Conversely, for tan β ≤ 0.04 the setup was independent of wave
frequency (within experimental error). The reason offered by van Dorn
(1976) for this difference is the assumed constant breaker ratio γ in the
theory. Data are presented to approximately confirm this assumption on the
0.083 slope, but the flatter slopes show a nonlinear variation with abrupt
wave height decay near the breaker point and little frequency correlation.
Thus, Bowen, Inman, and Simmons (1968) may have reached different conclusions
if flatter beach slopes had been tested.

      Gourlay (1978) based on his own data and a thorough reanalysis of Bowen,
Inman, and Simmons (1968) and Smith (1974) also concluded that experimental
data do not show very good agreement with equation (35) as shown in Figure
49. All data here are for relatively steep beaches (tan β > 0.083) and a
wide range of wave periods.

159
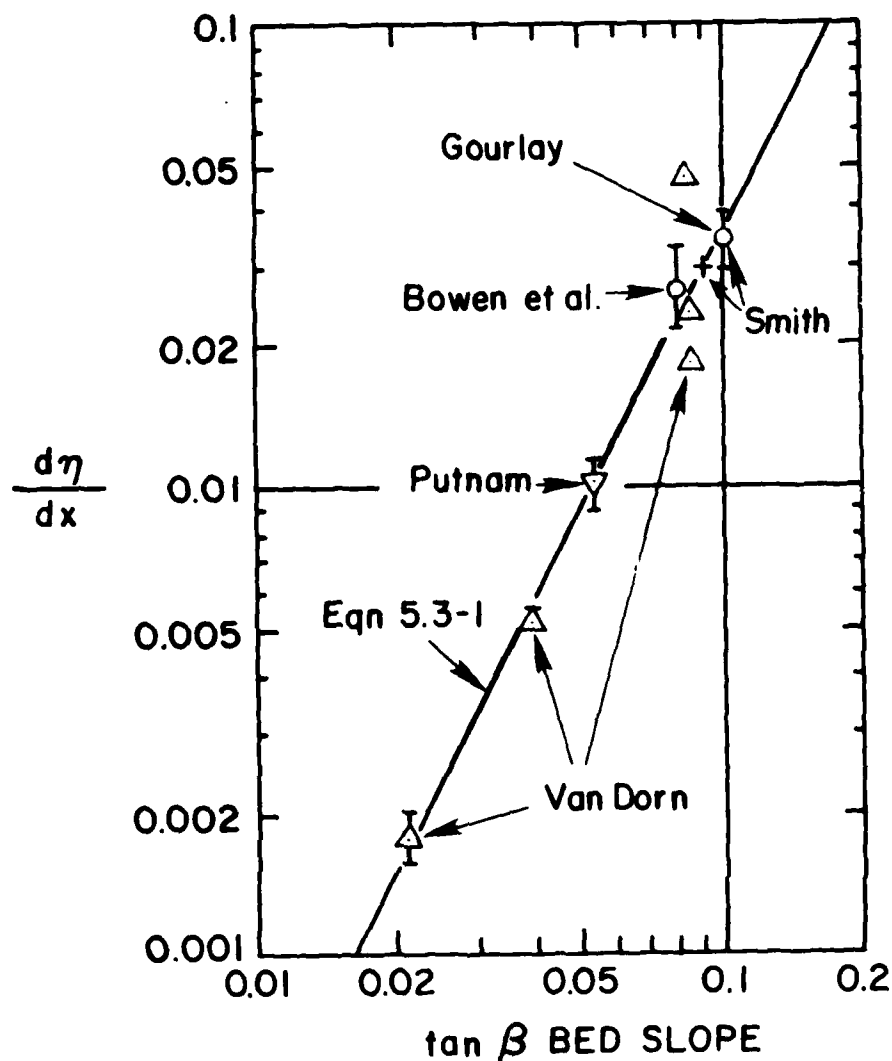
Figure 48. Wave setup versus bed slope: all experiments versus theory of van Dorn (1977) (after Gourlay, 1978).

Because of these observed differences between theory and observation, the assumptions for the theory are now being studied further. Wind (1978) used 23 MWL readings on a 1:40 slope in the laboratory to compute S_{xx} by direct integration of equation (28) from the shoreline toward deep water. In the horizontal (deepwater) section, linear wave theory gives radiation stress levels about 10 to 20 percent greater than found from the data. On the slope, in the surf zone, the linear wave theory was found to give estimates for $S_{xx}^{(1)} + S_{xx}^{(2)}$ (i.e., the orbital velocity components) about three times smaller than measured values, found by subtracting the observed potential energy density, $S_{xx}^{(3)}$ from the total radiation stress, S_{xx}.
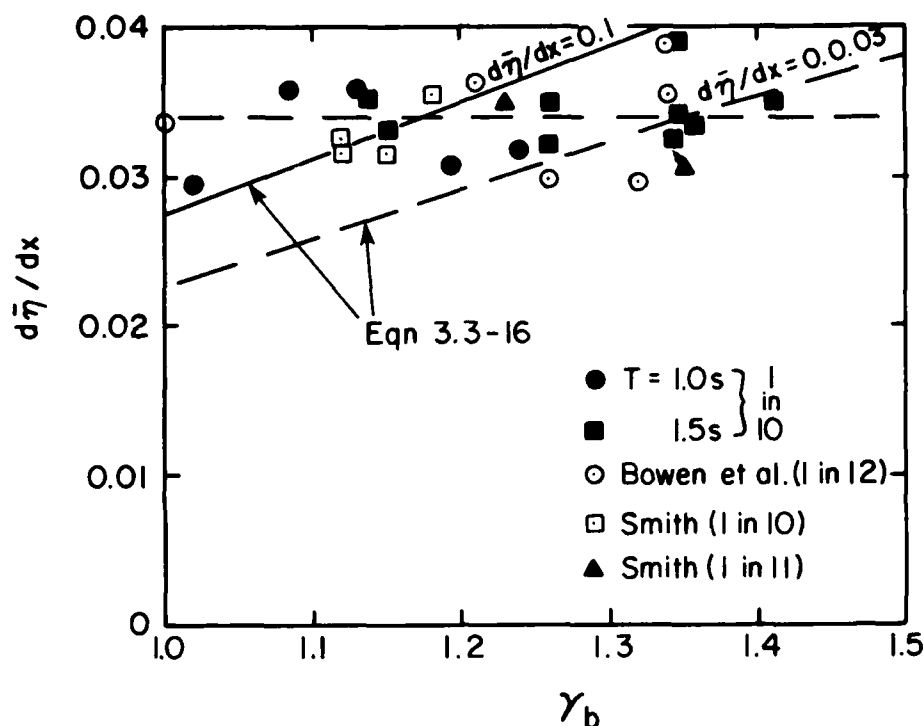
Figure 49. Wave setup versus breaker ratio, γ_b: Theory from equation (8) versus experiments on slopes around tan $\beta \doteq 0.1$ (after Gourlay, 1978).

A large difference in observed and calculated wave setup was also reported. It was concluded that the linear wave theory only roughly followed the trend of the observed results.

Finally, Stive (1980) briefly discusses preliminary results of the first known direct laboratory measurements of internal velocity and pressure fields to directly calculate momentum and energy flux in breaking waves. All previous experimental studies of the surf zone were literally on the surface, i.e., wave gage surface variations or MWL readings. The use of a two-component laser-Doppler velocity system, minature pressure transducers, and electronic data recording and analysis systems greatly facilitated the work. A sample from one experiment is summarized in Figure 50. The radiation stress for a number of surf zone locations was directly calculated from equation (1), and the values used in equation (28) are close but slightly above the measured $\bar{\eta}$ values. Use of linear wave theory and H_{rms} measured gave excessive wave setdown and setup. It will be extremely helpful to study the published results of these experiments.

In summary, it can be concluded that wave setup for normal wave incidence of regular waves on plane beaches as given by equation (35) is
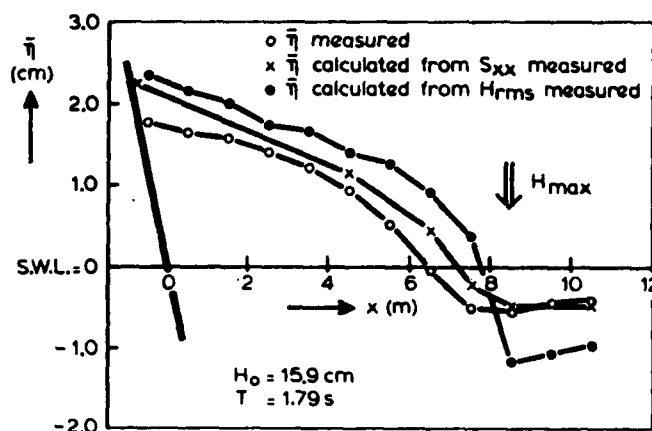
Figure 50. Comparison of measured and calculated mean water level varia-
tions using laser-Doppler velocity meter (after Stive, 1980).

questionable. The use of linear wave theory for S_{xx} and constant γ across
the surf zone is a major assumption being addressed. Wave setdown based
on the same theory is definitely incorrect at the breaker line. These
results are important in that investigators have used this theory to correct
for setup effects in the longshore current theory.

Experiments to verify the theory for oblique wave approach (eqs. 39
and 4) are not known. They reduce to the normal incidence forms and hence
are based on the same questionable assumptions.

2. Nonlinear and Irregular Waves.

James (1974a) only included the two comparisons of his nonlinear theory
and experiments shown in Figure 51. No real conclusions can be drawn from
this limited comparison. Predicted setup is sometimes greater and sometimes
less than measured by Galvin and Eagleson (1965), and of the correct order
of magnitude. Setdown is much less near the breaker line and more in agree-
ment with observations by Bowen, Inman, and Simmons (1968) than linear
theory. James' model is said to be limited to spilling breakers on gently
sloping beaches and for the case of large P values ($P = T/\sqrt{gd_b}$) where non-
linear effects are more pronounced.

The cnoidal theories for wave setdown (Svendsen and Hansen, 1976) were
compared with experimental results on a 1:35 slope using a regular wave
generator that eliminates free second harmonics. Example results are
reproduced in Figure 52 where the dark line is experimental data. Linear
wave theory (eq. 30) is shown to greatly overestimate the magnitude of set-
down (labeled eq. 4 in figure). The curve (eq. 9 in figure) does a better

162
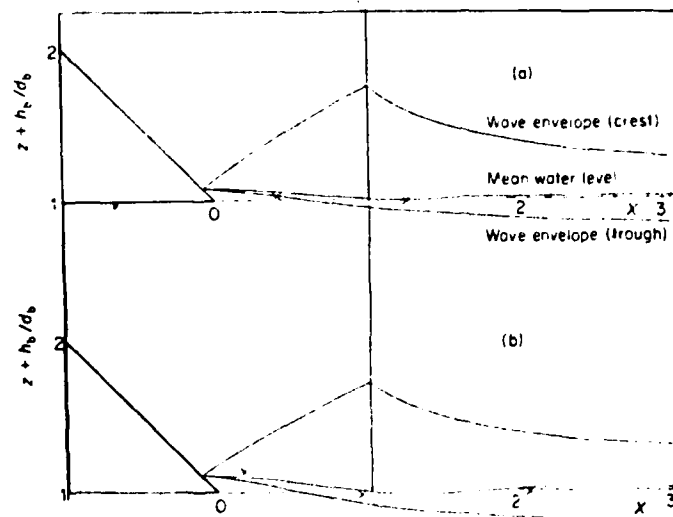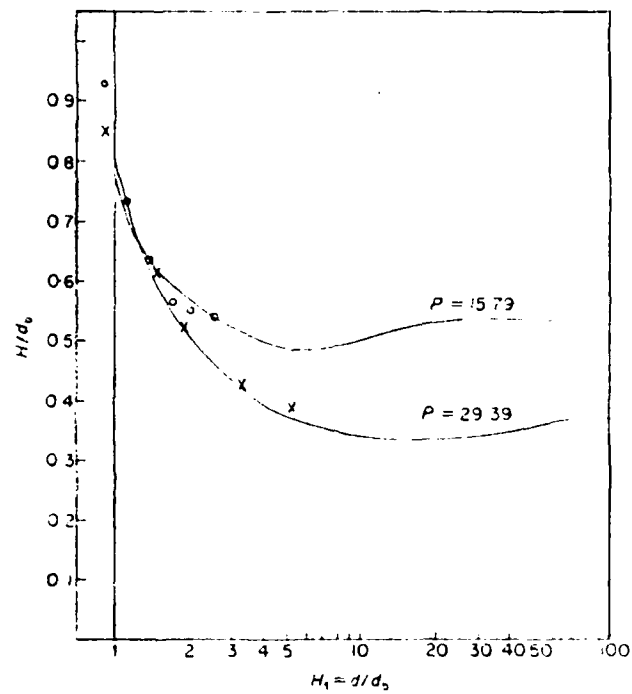
Figure 51. Some comparisons of nonlinear theory for wave setdown and setup with experimental data (after James, 1974a).
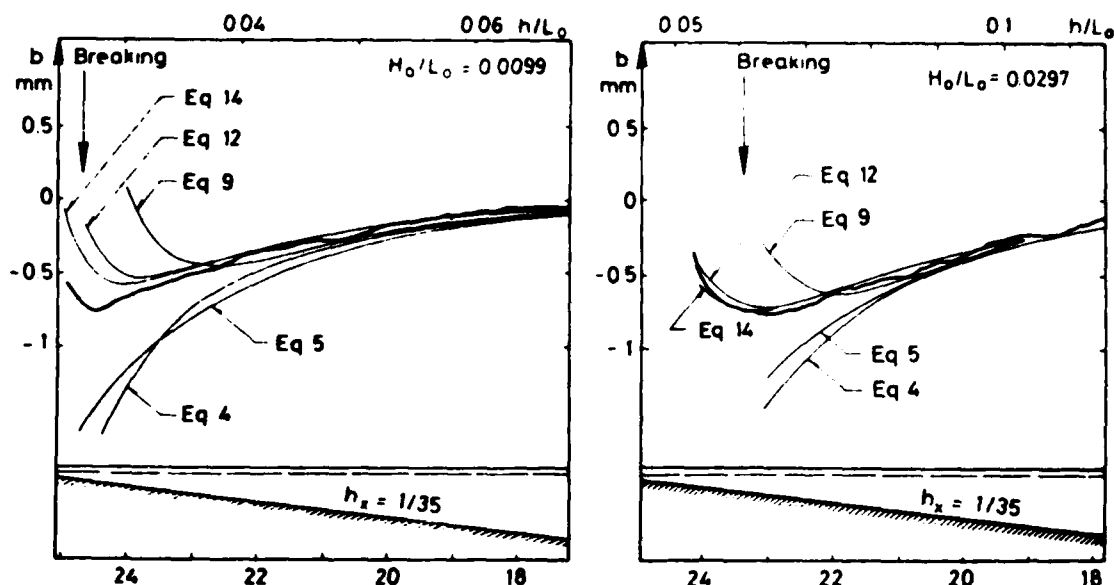
Figure 52. Comparison of cnoidal theory of wave setdown with experiments for regular waves (after Svendsen and Hansen, 1976).

job but also gives incorrect values (too small) near breaking. These results are from the theory given in equation (116). This poor fit near breaking is greatly improved by modifying the approximation employed $(1-\eta/d)$ in the bottom velocity u_b as given by equation (115). The result, consistent with all other cnoidal approximations, is

$$\bar{\eta} = - \frac{c^2}{2g} \left[\left(\frac{c^2}{gh} - 0.35 \right) \frac{\bar{\eta}^2}{h^2} - 1.9 \frac{\bar{\eta}^3}{h^3} \right] \qquad (155)$$

where both c and η are determined from second-order cnoidal wave theory. Equation (155) (shown as eq. 14 in Fig. 52) gives excellent results right up to the breaker limit.

Finally, the work of Jonsson and Buhelt (1978) on maximum wave setup has been included here since the motion just outside the breaker line is calculated as a series of solitary waves. Figure 53 compares the results of equation (118) with some experimental results. Maximum setup does indeed vary with deepwater wave steepness to the one-third power. Also, γ (calculated values shown as constant across the surf zone and values in parentheses with setdown neglected) increases with beach slope as expected from Battjes' (1974a) analysis (see Table 5). Unfortunately, due to other assumptions involved, Figure 53 cannot alone justify whether γ is a constant in the surf zone.
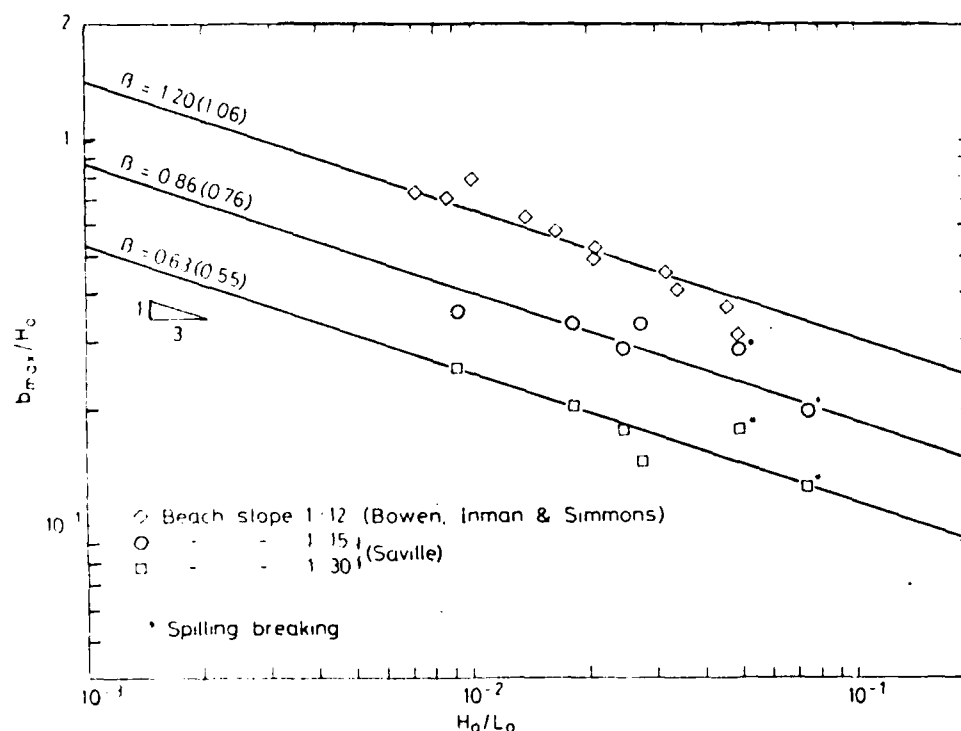
Figure 53. Maximum wave setup dependent upon deepwater wave steepness and beach slope (after Jonsson and Buhelt, 1978).

In summary, for nonlinear regular wave theory, it is tentatively concluded that excellent results are attainable for wave setdown calculated by equation (155) from cnoidal theory, and that the theory of James (1972, 1974a) requires further comparison with experimental results. All wave setup theories still require assumed values for the wave breaking ratio, γ.

Only the laboratory scale experiments by Battjes (1972, 1974a) and Goda (1975) are available to test the theory for irregular waves. The theory of Collins (1972) has never been compared with measured values.

Battjes used a 100-meter-long and 2-meter-wide basin with a water depth of 0.55 meter in the horizontal section. Beach slope was 1:20. Two examples of measured and computed wave setup (based on theory of Battjes, 1972, 1974a) are shown in Figure 54. A systematic difference between theory and measured laboratory data was observed in both cases, (a) mean period T_O = 1.2 s; rms, incident height, H_O = 8.2 centimeters, (b) mean period T_O = 2.0 s; rms, incident height, H_O = 8.5 centimeters, with the theory always giving too high a wave setup. Wave setdown values were very close

165
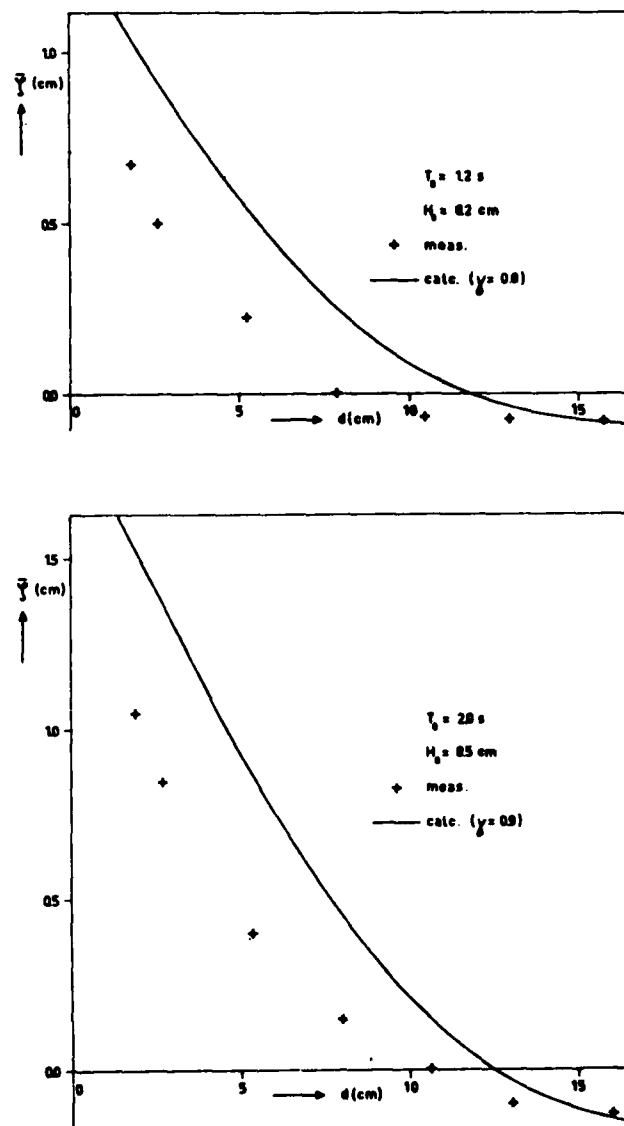
Figure 54. Comparison of wave setup for irregular waves and theory of Battjes (after Battjes, 1974a).

to measured data. A thorough investigation of possible reasons for the discrepancy was made by Battjes (1974a). Air entrainment was ruled out after separate tests proved this effect was not significant. Battjes concluded that because of the uncertainty regarding the laboratory system to measure the setup, it is not known whether the differences are real or apparent.

166

In addition, Battjes (1974a) obtained the field measurements of Dorrestein (1962) to verify his theory. Differences between measured and calculated values for two separate cases when averaged over the surf zone proved to be less than experimental error. It was concluded that the field measurements lend support to the computational model.

Goda's (1975) model for irregular waves is very similar except it uses a varying probability function for the wave breaking criteria. It was checked against experiments in a 30-meter basin with a 1:50 slope and a water depth of 35 centimeters in the uniform end. Also on 1:10 slope where the H_O = 50 centimeters in constant depth region. However, no comparison of theory versus experimental results was presented by Goda (1975) for wave setdown or setup.

Finally, in support of the purely empirical relations for $\bar{\eta}_{max}$ (eq. 125) put forth by Hansen (1978a), Figure 55 presents the field data (black dots) along with some measured or theoretical values. Generalizations for other locations are pure speculation.
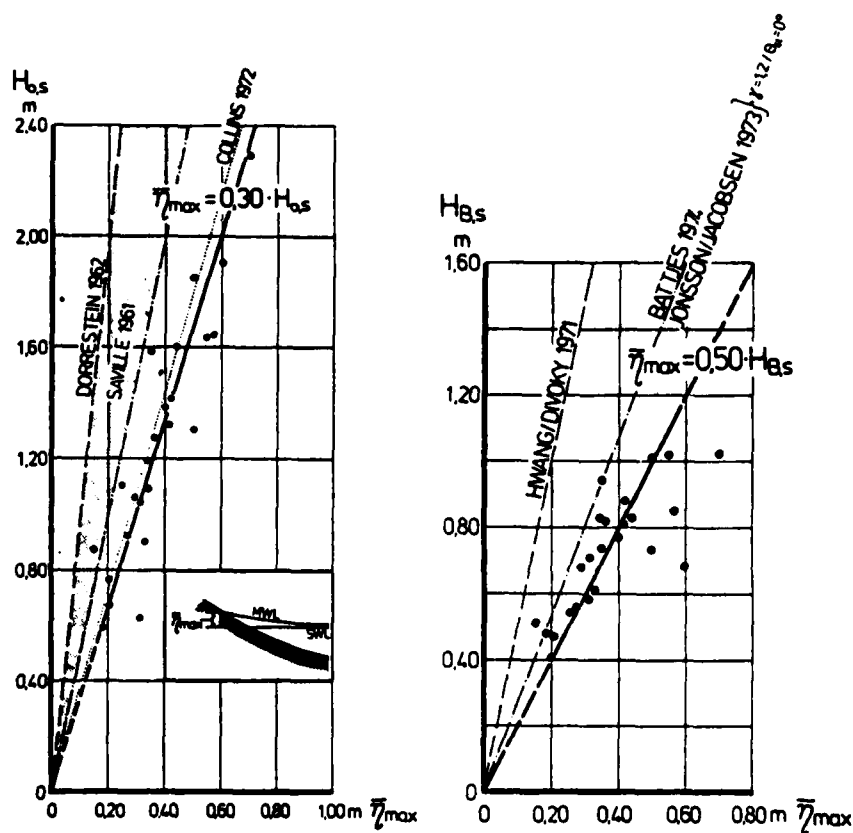
Figure 55. Empirical data for maximum wave setup (after Hansen, 1978).

In summary, it is concluded that all irregular wave theories for MWL change in the nearshore area suffer from a lack of concrete experimental confirmation of their validity. This situation is unfortunate since the theories of Battjes and Goda show much promise in this regard. If successful comparisons exist in the published literature, they have escaped the review in this study.

Several possible reasons have been offered to explain why the experimental measurements of wave setup disagree with the theory. Air entrainment by breaking waves is one possibility since the mixture has a lower density. Another is the neglect of the instantaneous bed shear stress resulting from the asymetrical wave orbital motion which can produce a nonzero average stress (Bijker and Visser 1978).[24]

II. LONGSHORE CURRENTS

Of primary interest is a comparison of laboratory and field measurements with radiation stress theory for uniform longshore currents. In most cases the accuracy of both laboratory and field data is relatively low due to observational difficulties in measurement of breaker heights and wave angles. Also, nonuniform boundary conditions, alongshore variations in breaker height, winds, etc. can contribute to the uncertainties in the measured values. Current variation with water depth is another factor to be considered regarding the available data base.

1. Mean Currents.

Before 1967, all theories were for a mean longshore current (Galvin, 1967). Horikawa (1978a) provides a more recent summary which includes Japanese research efforts. What was meant by mean velocity in the theory and what was measured is not always clear. For example, Komar (1976b, p. 184) used $\bar{v}_1$ for the average longshore current in a review of all theories and also the current at midsurf (p. 190) when referring to data in Figure 56. The data by Harrison et al. (1968) in Figure 56 were said to plot higher than the others because the data were measured just shoreward of the breakers as a maximum longshore current (Komar, 1976b).

In the theory (Ch. 3), the following time-averaged longshore currents are defined:

$\bar{v}_b$ = velocity at breaker line

$\bar{v}_m$ = maximum current velocity

$\bar{v}_{\frac{1}{2}}$ = the midsurf velocity

[24]BIJKER and VISSER, op. cit.
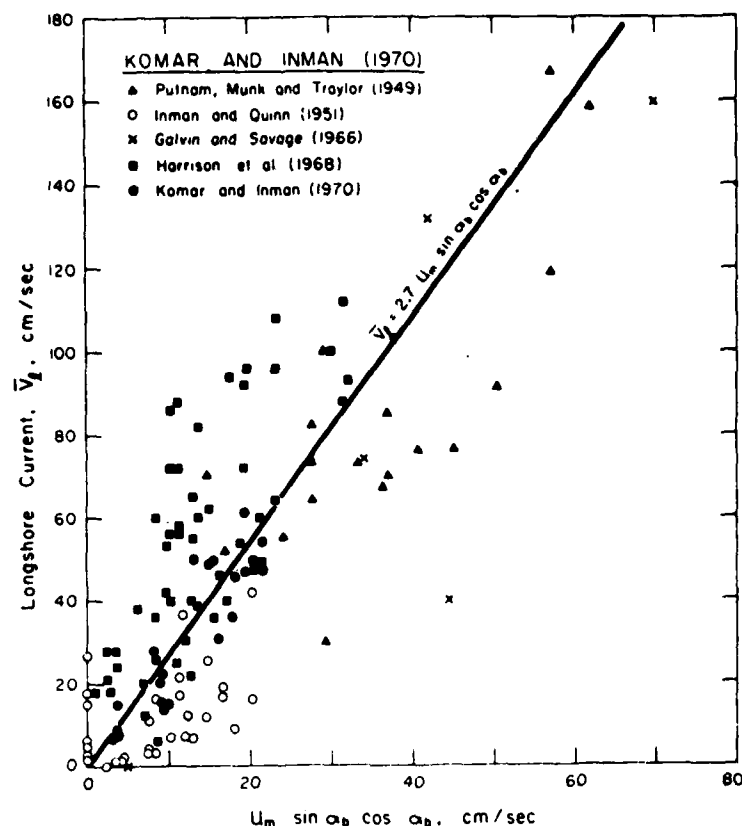
Figure 56. The empirical longshore current at midsurf position as deduced by Komar and Inman (1970) based upon sand transport studies (after Komar and Inman, 1970).

$\bar{v}$ = the mean or average velocity across the surf zone. Even here the meaning is somewhat ambiguous since the mean could be determined by including that portion seaward of the breaker line (also a local value when profile is given)

and their dimensionless counterparts (using V). It is assumed here (following Komar, 1969, 1975b, 1976b) that all field data, except as noted, were for the midsurf position, $\bar{x}_{1_{2}}$.

A comprehensive discussion and detailed analysis of all available laboratory and field data led Komar and Inman (1970),[64] and Komar (1975b, 1976b)

---

[64]KOMAR, P.D., and INMAN, D.L., "Longshore Sand Transport on Beaches," *Journal of Geophysical Research,* Vol. 75, No. 30, 1970, pp. 5914-5927 (not in bibliography).

169

to propose the following empirical equation (see Fig. 57)

$$\bar{v}_{\frac{1}{2}} = 2.7 \, U_{bm} \sin \alpha_b \cos \alpha_b \qquad (156)$$

Considerable discussion of equation (156) can be found in Longuet-Higgins (1970). Gourlay (1978) reanalyzed the same data using higher average values of γ estimated from the wave breaking criterion of Weggel (1972)[65] which includes beach-slope effects. He obtained the empirical resu`t

$$\bar{v}_{\frac{1}{2}} = 3.72\sqrt{gH_b} \, \tan \beta \sin 2\alpha_b \qquad (157)$$

When using new data by Lee (1975) from western Lake Michigan, the coefficient in equation (157) was 2.87 and the differences attributed to the coarser materials present to give a rougher bed. The empirical expression by Komar (eq. 156) in revised form (using eq. 53 and taking $\gamma = 0.78$) could be written

$$\bar{v}_{\frac{1}{2}} = 0.60\sqrt{gH_b} \, \sin 2\alpha_b \qquad (158)$$

Komar argued that the ratio of beach slope-to-bed friction coefficient was essentially constant so that $\tan \beta$ did not appear in his result.

Dette (1974a) measured longshore currents on the west coast of the Island of Sylt in the North Sea for comparison with all the available formulas at that time, including those based on radiation stresses. He concluded that the best agreement was obtained with the relation (in dimensionless form)

$$\bar{v} = 0.32\sqrt{gH_b} \, \sin 2\alpha_b \qquad (159)$$

If it is assumed this average longshore current is equivalent to the mid-surf velocity, then these empirical results for sand beaches (like Komar's) are also independent of beach slope.

Kraus and Sasaki (1979) analyzed why equation (156) or (158) satisfied the field data over a wide range of beach slopes, breaker angles, and beach materials. As demonstrated in Figure 30 based on their radiation stress theory for large wave angles, it is seen that the midsurf velocity, $\bar{v}_{\frac{1}{2}}$ remains almost constant for $0.01<P^*<0.1$. Here $P^* = \frac{\pi}{2} \, \Gamma \, \dfrac{\tan \beta}{1+3\gamma^2/8}$ is different than Longuet-Higgin's P. Also, $\bar{v}_{\frac{1}{2}}$ varies less than 20 percent for α_b up to 20° and is about 0.5 over a broad range. Kraus and Sasaki show why (for both laboratory and field data) $P^*<0.1$ so that the empirically determined, single factor of 2.7 in equation (156) can describe longshore

[65] WEGGEL, J.R., "Maximum Breaker Height," *Journal of Waterways, Harbors, and Coastal Engineering Division,* Vol. 98, No. WW4, 1972, pp. 529-548 (not in bibliography).
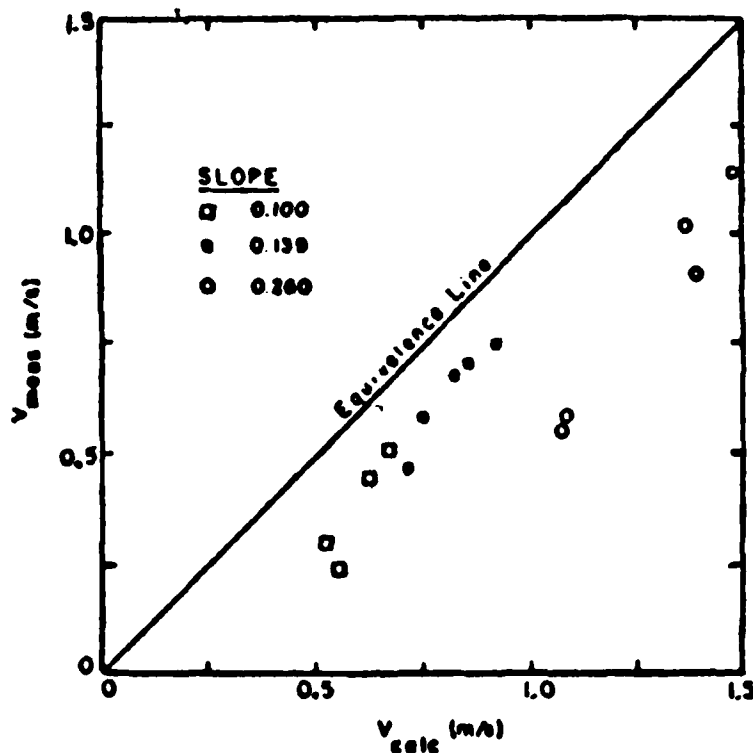
Figure 57. Comparison of laboratory mean currents with integrated currents obtained from strong current theory (after Liu and Dalrymple, 1978).

current data over a wide range of variables. Stated in another way, the field data and radiation stress theory both demonstrate that the midsurf velocity is insensitive to changes in independent variables. It is a poor choice to compare theory and experiment for this reason. Consequently, Kraus and Sasaki (1979) used the maximum longshore current velocity, $\bar{v}_m$ in their analysis, which will be discussed later.

Theoretical results of the large-angle strong current theory of Liu and Dalrymple (1978) were compared with the data set of Putnam, Munk, and Traylor (1949) which had large breaking angles. An average longshore current velocity was computed from the theoretical profile by intergrating over the surf zone and dividing by the surf zone area. Their results (Fig. 57) show computed values consistently larger than measured for all three bed slopes tested when a friction factor, $f_{cw} = 0.01$ was employed. The friction factor could be adjusted to improve the agreement. Liu and Dalrymple (1978) concluded that their large-angle strong current model is primarily valid for steep beaches and large incidence angles as commonly occur in laboratory studies. Comparisons with other data sources were not made. Similar comparisons of integrated mean theoretical values and observations can be found in Thornton (1969, p. 88), Sasaki (1977, p. 147), and Sonu (1975, p. 63).

2. Longshore Current Profile.

The original model of Longuet-Higgins (1970) for longshore current profile in dimensionless form was compared with the experiments by Galvin and Eagleson (1965). Figure 58 reproduces the results. The small numbers in Figure 58 represent different wave periods tested (e.g., plotted point 2 = 1 second wave period; see Longuet-Higgins, 1972b for key). The laboratory observations generally lie between $P = 0.1$ and $P = 0.4$ which corresponded to a lateral mixing coefficient, N in the range between 0.0024 and 0.0096, respectively. The bottom friction coefficient, C_f was assumed constant at 0.01. As shown, large variations in P produce relative small changes in longshore current velocity; however, it is very dependent upon C_f which directly influences the reference velocity $\bar{v}_b*$. Longuet-Higgins (1972b) felt the lateral mixing and bottom friction effects were too large outside the surf zone. In addition, the neglect of wave setup and use of $\gamma = 0.82$ in the theory when the experiments by Galvin and Eagleson (1965) were on a steep beach (tan $\beta = 0.11$) must be noted when analyzing these results.
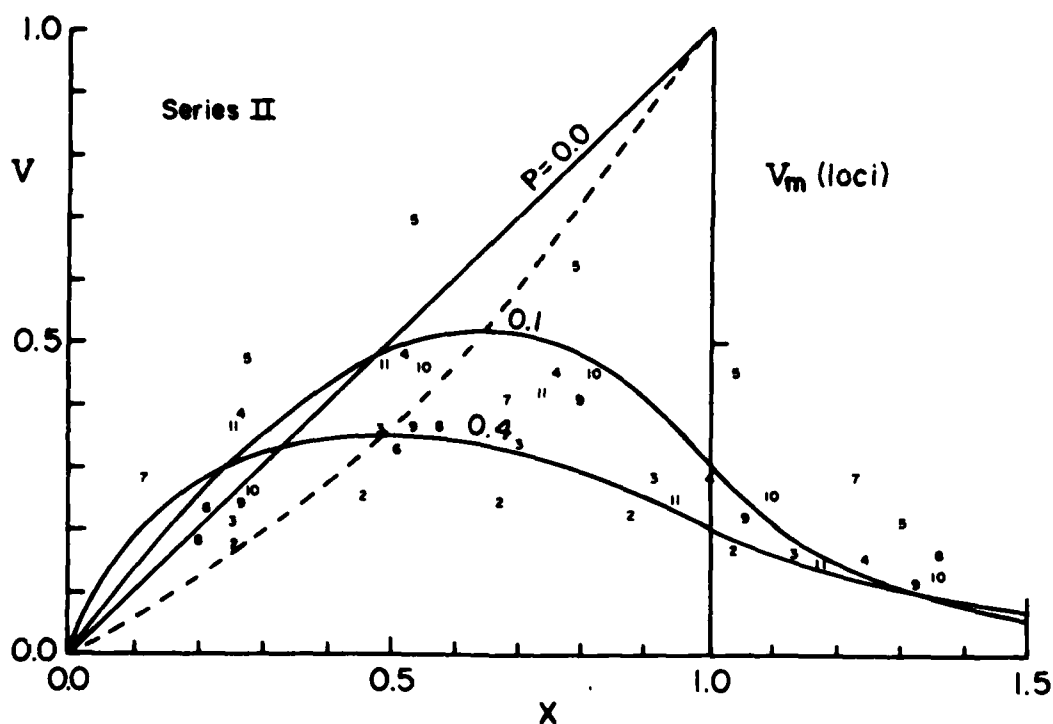
Figure 58.   Original longshore current profile theory versus laboratory
             data of Galvin and Eagleson, 1965 (after Longuet-Higgins, 1970).

Table 3 provides a list of modified theories and additional details. Bowen (1969a) also compared his theory against the experiments of Galvin and Eagleson (1965), as shown in Figure 59. The θ parameter here related mixing coefficient, friction, etc., but in a different manner than P. B is a grouping of independent variables to give a dimensionless, relative longshore current velocity. The results shown are for K = 0.4 (eq. 68) and include normal wave incidence and setup effects. Because of the relatively simplistic shear stress and lateral mixing models employed, Bowen's theory has not been subjected to further analysis.
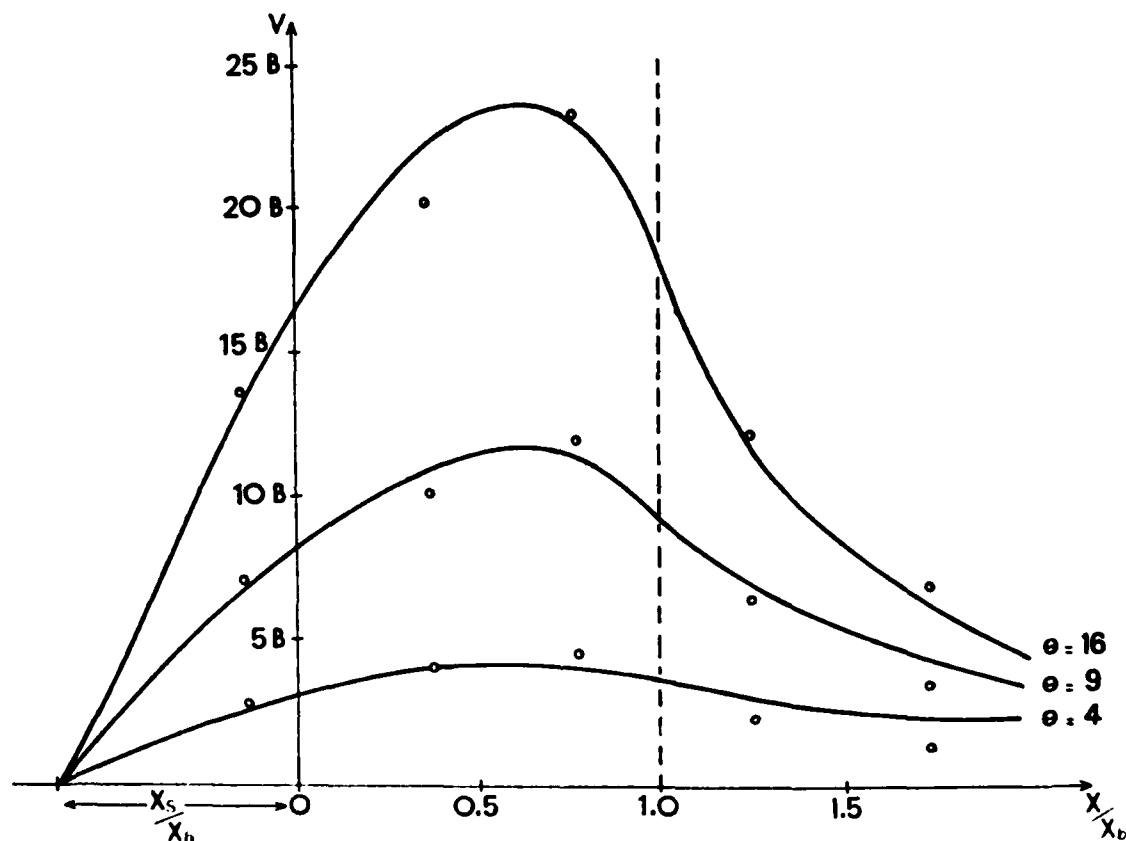
Figure 59.   Bowen's longshore current profile theory versus laboratory data of Galvin and Eagleson, 1965 (after Bowen, 1969).

Thornton (1969, 1970a) included wave setup in his theory that in all aspects except lateral mixing was very similar to Longuet-Higgins (1970). A comparison with one experiment of Galvin and Eagleson (1965) is shown in Figure 60. Also shown are distributions of lateral mixing

173
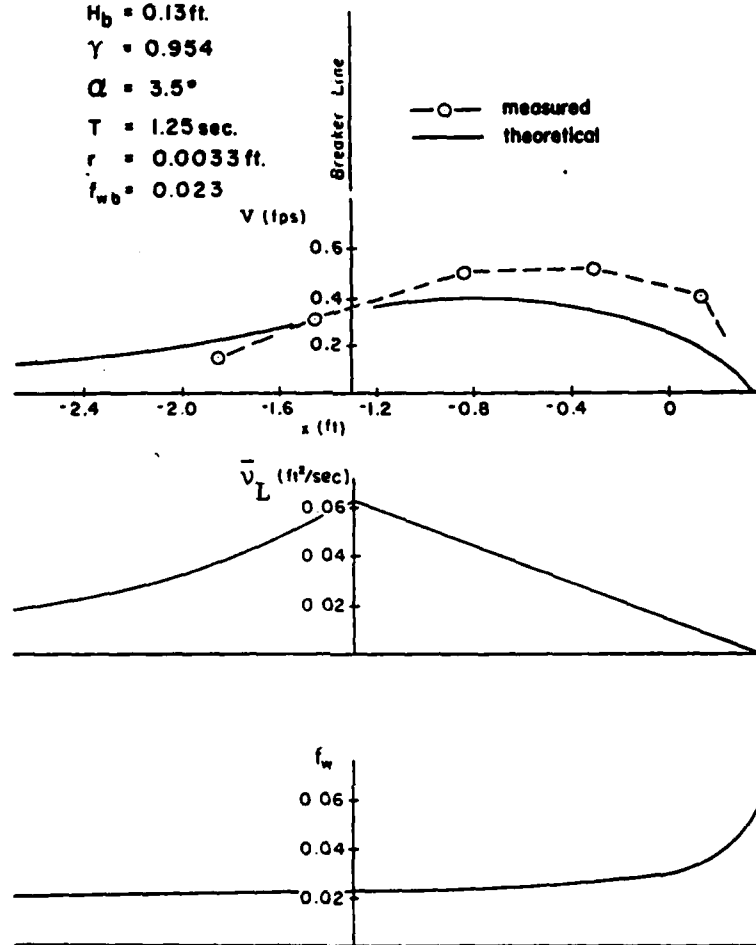
Figure 60. Thornton's longshore current profile theory versus laboratory data of Galvin and Eagleson, 1965, test II-4 (after Horikawa, 1978).

coefficient ($\bar{v}_L$) and bed friction coefficient (f_w) employed in his theoretical analysis. Only bottom roughness (here $r = 0.0033$ foot for a concrete beach) is chosen in Thornton's model. Comparisons for two other cases with larger waves at greater angles are shown in Figure 61. In all cases, the theory predicts too strong a current outside the breaker line. Some field data by Ingle (1966) taken at Trancas Beach, California, are used to compare the theory as shown in Figure 62. The beach profile was represented by a fourth degree polynomial. The magnitude of the eddy viscosity is much larger in the field than in the laboratory but values employed are too large and overly smooth the profile.

174
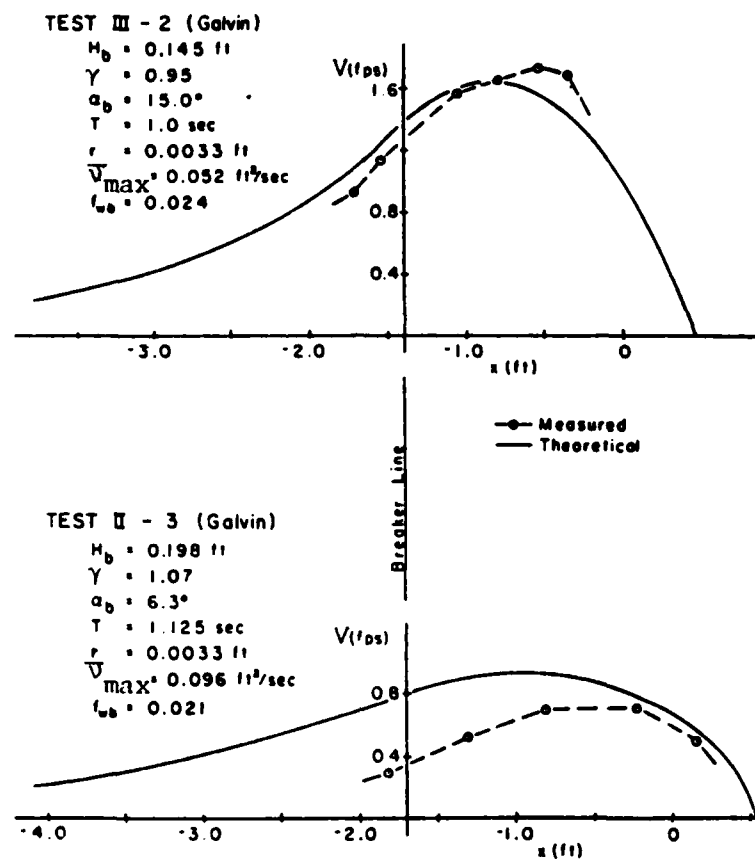
Figure 61. Thornton's longshore current profile theory versus laboratory
data of Galvin and Eagleson, 1965, tests II-2 and II-3 (after
Thornton, 1969).

Jonsson, Skovgaard, and Jacobsen (1974) were the first to include
a strong current formulation for bed shear in the theory. Depth refraction
and a different lateral mixing formulation was also incorporated. Some
numerical results are compared in Figure 63 against (a) the laboratory
data of Galvin and Eagleson (1965) and (b) some limited field measurements
of Ingle (1966). The theory with $\gamma = 1.42$ gave a better fit within the
surf zone and also matched the breaker location for the laboratory data.
A poor comparison outside the breaker line was possible due to an exces-
sively large eddy viscosity in this region. The field data shown in Figure
63(b) are too incomplete to make a true analysis possible. Jonsson,
Skovgaard,and Jacobsen (1974) chose to use $\gamma = 0.8$ for the field comparison
which gave a rather good agreement for the $\bar{v}_m$ value. In one example, the
combined bed friction coefficient, f_{cw} across the surf zone was about
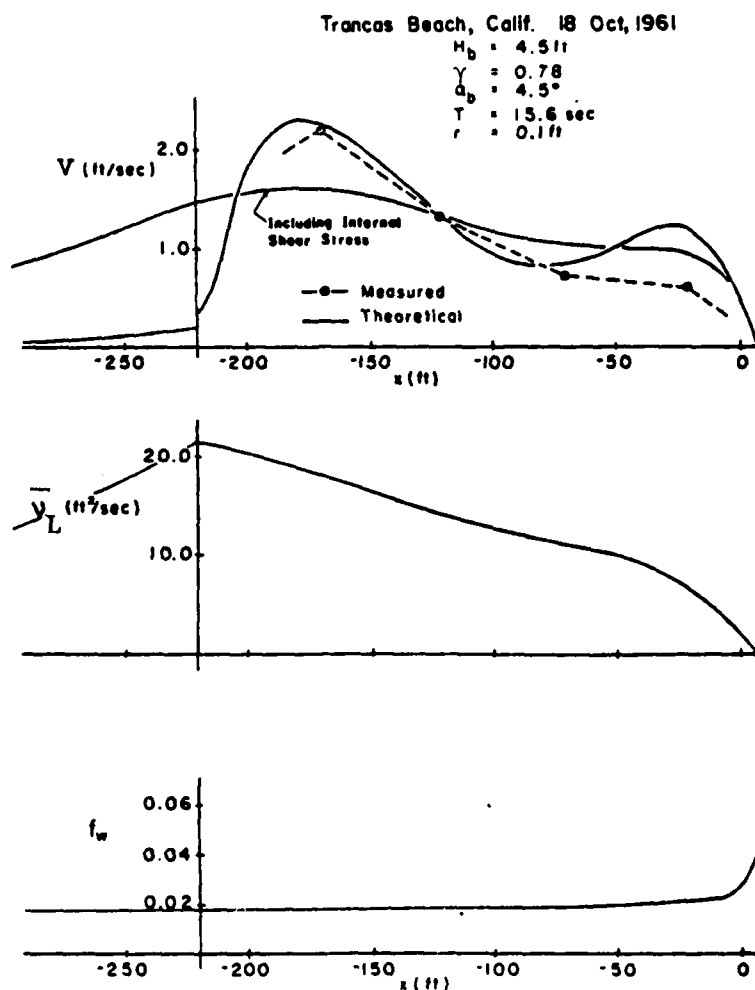
Figure 62. Thornton's longshore current profile theory versus field data by Ingle, 1966 (after Horikawa, 1978).

$f_{cw} \doteq 0.05$ and rose rapidly nearshore and beyond the breakers as the current approached zero.

The nonlinear longshore current profile model developed by Madsen, Ostendorf, and Reynolds (1978) (see also Ostendorf and Madsen, 1979) used the laboratory data of Gavlin and Eagleson (1965) to determine appropriate values for bed friction and lateral mixing coefficients. An explicit empirical equation for f_{cw} resulted with average $f_{cw} \doteq 0.01$ and decreased as $\bar{v}$ increased for the calibration runs on smooth concrete ($\varepsilon = 0.001$ foot). The lateral eddy viscosity parameter, Γ was found to be 0.013. To test this model a parameter, δ, defined as

176
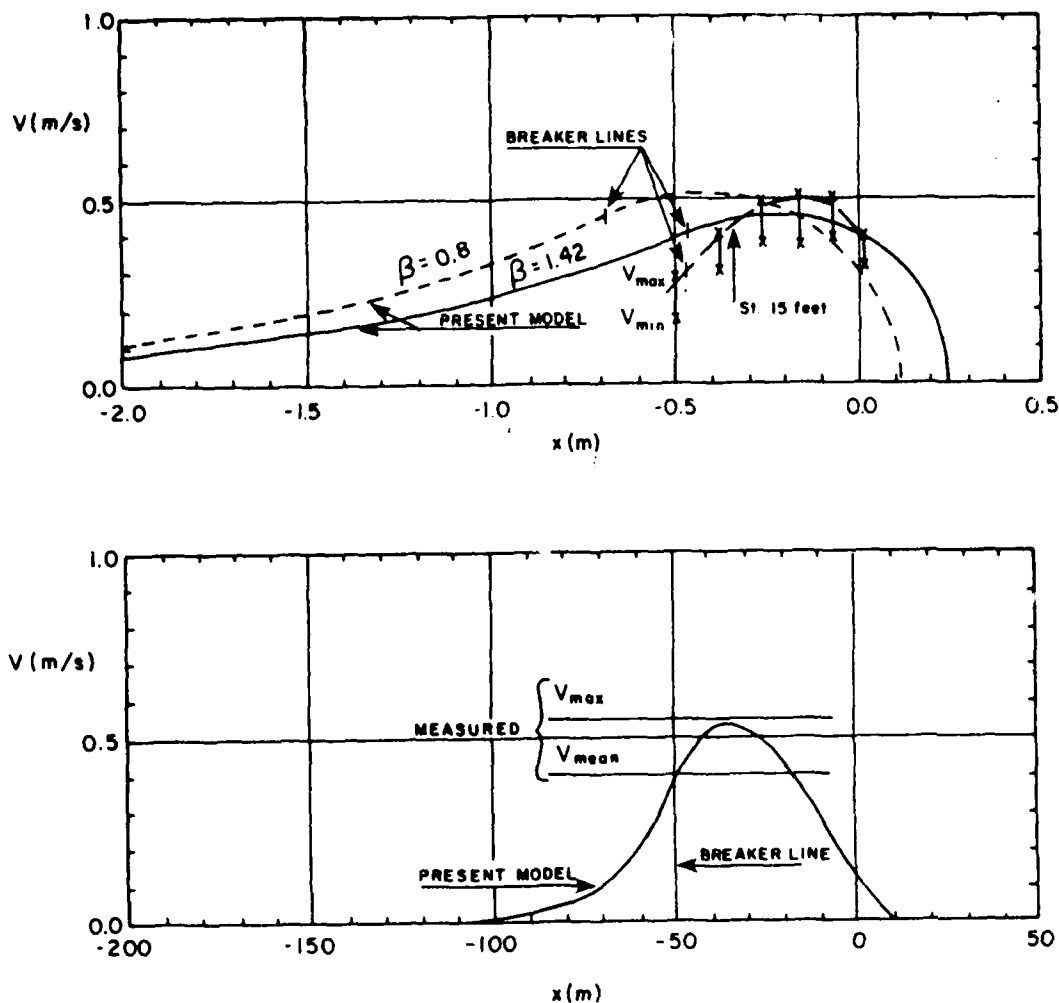
Figure 63. Jonsson, Skovgaard, and Jacobsen's longshore current profile versus laboratory and field data (after Jonsson, Skovgaard, and Jacobsen, 1974).

$$\delta = \frac{\bar{v}(measured) - \bar{v}(predicted)}{\bar{v}(predicted)} \tag{160}$$

was employed and its mean and standard deviation used in the analysis. For the Putnam, Munk, and Traylor (1949) data $\bar{v} = \langle\bar{v}\rangle$, the average over the surf zone; for the data for Brebner and Kamphuis (1963) $\bar{v} = \bar{v}_m$, the maximum longshore current; and for Galvin and Eagleson (1965) data, only the denominator was $\langle\nabla\rangle$. In all cases tested, the standard deviation was such that an accuracy of ± 15 percent was expected for their nonlinear longshore current model (Ostendorf and Madsen, 1979, p. 147). The model tended to underpredict current magnitudes for beach slopes flatter than 1 on 10. A weak current small-angle (linear) model was also tested and and found to be less accurate.

177

The eddy viscosity model in Jonsson, Skovgaard, and Jacobsen (1974) was improved by Skovgaard, Jonsson, and Olsen (1978). Different models and lateral mixing coefficients were employed within and outside the breaker line. An example of the result is shown in Figure 64 for two different cases of lateral mixing. Both show much smaller tails beyond the breaker zone which is closer to reality where " . . . observations indicate a virtually complete absence of turbulent mixing outside the breaker zone" (Battjes, 1978). The experimental data are again from Galvin and Eagleson (1965). The tail was found to diminish further as bed slope decreased.
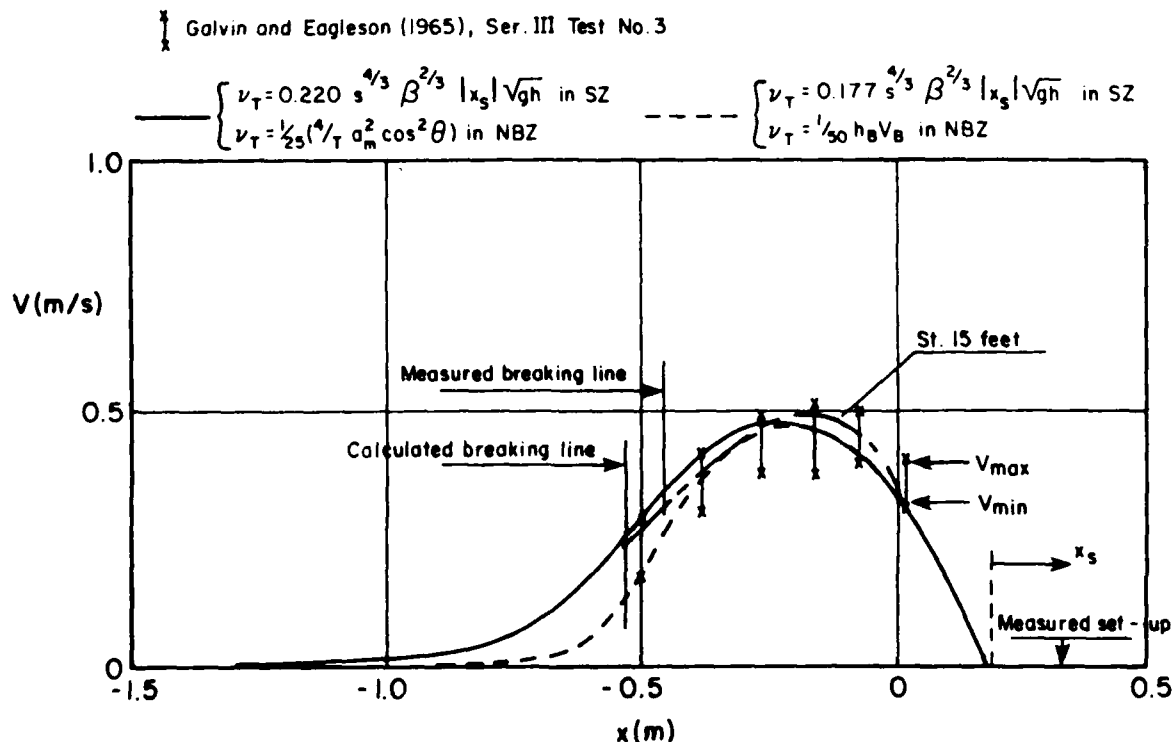
Figure 64. Skovgaard, Jonsson, and Olsen's longshore current profile versus laboratory data (after Skovgaard, Jonsson, and Olsen, 1978).

The most recent longshore current profile model by Kraus and Sasaki (1979) was verified with new laboratory and field measurements taken in Japan. The theory is discussed in complete detail in Chapter 3 and essentially extends the weak current large-angle theory to include lateral mixing stresses. A key dimensionless parameter in the theory is P* which indicates the relative importance of the lateral mixing stress to the bed stress and also includes wave setup effects. Laboratory measurements of

of Mizuguchi, Oshima, and Horikawa (1978)[66] were performed in a 15- by 15-meter wave basin with a 9-meter beach section of slope 1:10.4. Table 7 summarizes the results for four separate test cases. Current measurement was by propeller-type meter and values recorded represented averages taken in the vertical direction. A test section with no systematic acceleration in the longshore direction was found to exist and data reported for this location. The intersection of the mean setup and setdown lines was used to define the breaking point. The wave breaking ratio, γ was described as approximately linear in the surf zone.

Results of the laboratory experiments when compared with the theory (solid line) are presented in Figure 65. Velocities are normalized by the maximum current $\bar{v}_m$ and distance by $\bar{x}_b$. By requiring the theoretical location of the maximum velocity to match the experimental results, all curves were fitted to the data in this regard. Agreement for profile shape is excellent in the region shoreward of $\bar{v}_m$ in all four cases. The dotted line is the original model of Longuet-Higgins (1970) which gives very similar results in this region since small angles are present. The model of Kraus and Sasaki (1979) gives better agreement beyond $\bar{v}_m$ and the breaker line where large wave angles are present. In two cases (1 and 4) the theoretical tail dropped off too rapidly to fit the data.

In three of the four cases studied, P* values were less than 0.1. The eddy viscosity coefficient, Γ ranged from 0.0062 to 0.037 with higher values associated with large wave angles. The bed friction coefficient, c_f was in the range between 0.011 and 0.024. All these values were computed and were not initially specified since fitting the maximum velocity was used in their determination. To do this, γ and α_b must also be initially specified. Thus by adding the extra condition available through $\bar{x}_m$, all parameters of the theory not usually obtainable by measurement, i.e., P*, Γ and C_f, can be obtained by fitting the theoretical and experimental maximum velocities. The model is made predictive by inputting expected values of $\bar{x}_m$, γ, tan β, and α_b.

Results of the plane beach theory compared with limited observations in the field (near Niigata, Japan) on a step-type beach are presented in Figure 66 which also shows the beach profile with average slope of 1 to 40. Each velocity is the average of five measurements for the same location. Reasonable agreement is now found seaward of $\bar{v}_m$ but the stepped beach profile produced secondary breaking and a nonlinear γ ratio to give the disparity of results shown shoreward of $\bar{v}_m$. Kraus and Sasaki stated that a refined wave height description (requiring numerical solution) in this shoreward region should produce better agreement. For this one field observation, P* = 0.072, Γ = 0.015 and C_f = 0.0061. Other field data also give P* < 0.1 and such low values are in agreement with observed rapid decrease in longshore current profile tails outside the breaker zone. Kraus and Sasaki (1979) also use this as evidence in support for their weak current model.

---

[66]MIZUGUCHI, M., OSHIMA, Y., and HORIKAWA, K., "Laboratory Experiments on Longshore Currents," *Proceedings of the 25th Conference on Coastal Engineering,* Japan (in Japanese) (not in bibliography).

Table 7. Summary of the preliminary laboratory data of Mizuguchi, Oshima, and Horikawa (1978). The last six rows contain parameters calculated from theory; subscript "L" refers to the model of Longuet-Higgins (1970); other calculated values from the present work.

Quantity	Symbol and Units	CASE 1	CASE 2	CASE 3	CASE 4
Breaker Angle	α_b (deg)	4.5	4.8	15.4	11.4
Mean water line	x_a (cm)	– 18	– 11	– 15	– 15
Breaker distance	x_b (cm)	59	37	60	42
Depth at breaking	h_b (cm)	3.8	2.4	4.2	2.5
Maximum velocity	v_m (cm/s)	16.4	15.2	22.0	20.0
Nondim. location of maximum velocity	X_m $[= \frac{(x_m - x_a)}{x_b}]$	0.71	0.72	0.63	0.70
Beach slope, including setup	$\tan\beta*$	0.064	0.065	0.070	0.060
Mean wave height to water depth ratio	$\bar{\gamma}$	1.15	1.12	0.99	1.28
Wave steepness	H_0/L_0	0.044	0.027	0.052	0.033
Wave period	T (S)	0.80	0.80	0.80	0.81
Mixing parameter	P_L	0.049	0.043	0.12	0.055
(including wave angle)	P	0.067	0.058	0.17	0.077
Friction coefficient	$c_{f,L}$	0.013	0.012	0.026	0.021
(including wave angle)	c_f	0.012	0.011	0.024	0.020
Lateral viscosity coefficient	N_L	0.0024	0.0019	0.010	0.0049
(including wave angle)	Γ	0.0080	0.0062	0.037	0.017
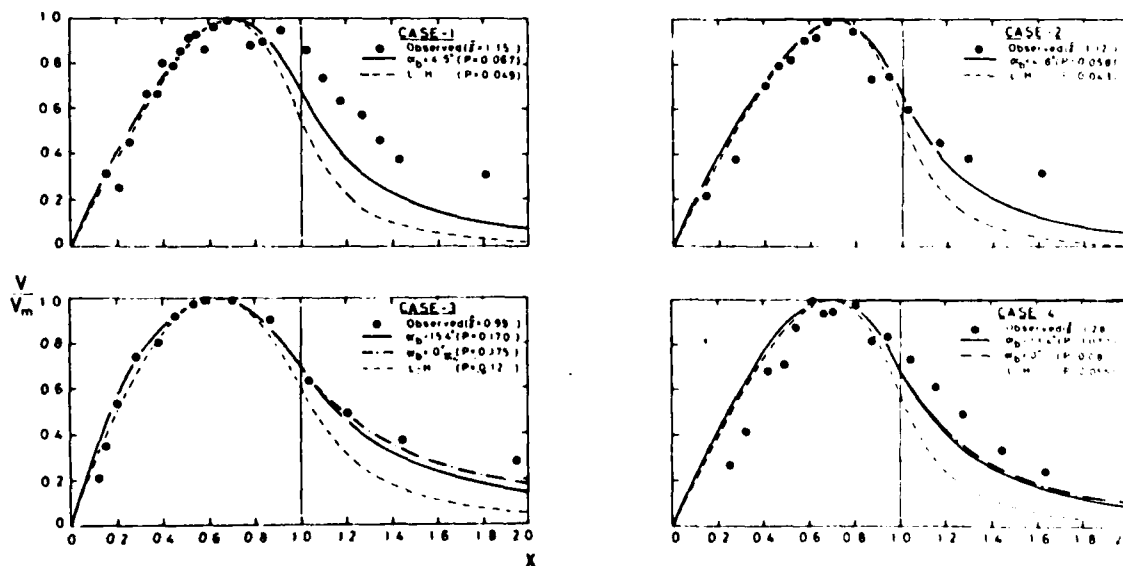
Figure 65. The model of Kraus and Sasaki compared with laboratory data of Mizuguchi, Oshima, and Horikawa, 1978.

180
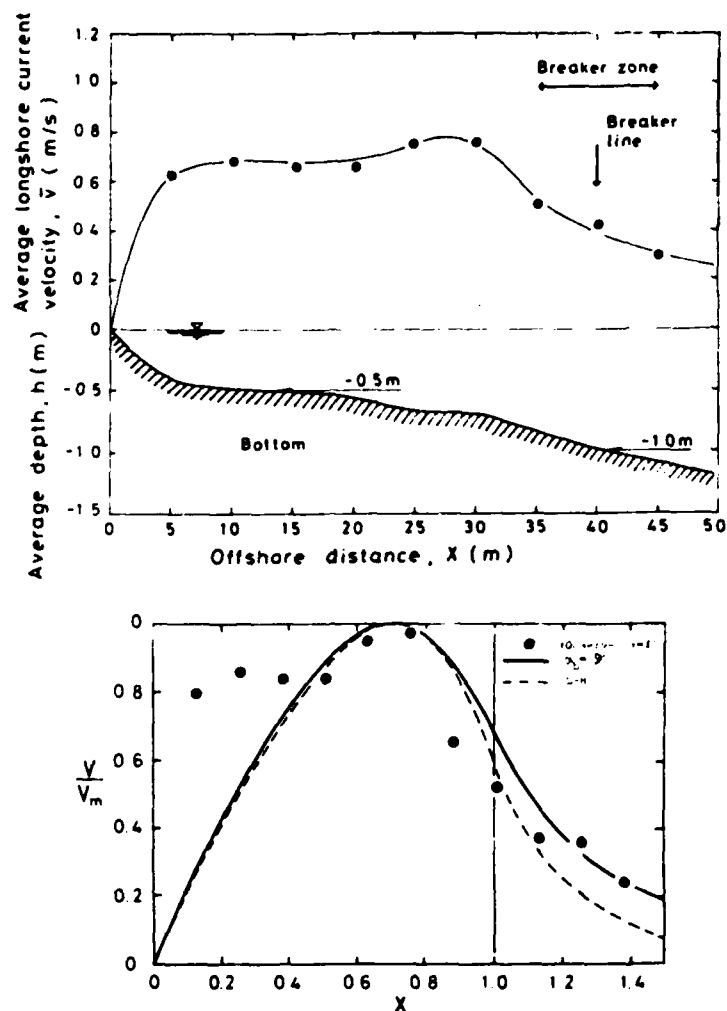
Figure 66. Kraus and Sasaki model compared with field data (after Kraus and Sasaki, 1979).

Finally, some preliminary data from the NSTS field study at Torrey Pines, California, have been presented by Guza and Thornton (1980). Vectors of 17.1-minutes average currents are shown in Figure 67 for one shore-normal section and along the coast. Also shown is the theory of Longuet-Higgins (1970) by putting the measured offshore radiation stress into an equivalent regular, unidirectional wave at the measured spectral peak. The dashline includes lateral mixing stress. Complete details regarding this and other extensive comparisons were not available but said to be forthcoming.

Bijker and Visser (1978)[24] and Liu and Dalrymple (1978) did not make comparisons of their longshore profile theoretical results with the data available. The NSTS field data, the laboratory data of Mizuguchi, Oshima, and Horikawa (1978)[66], and the ongoing extensive laboratory data sets

---

[24]BIJKER and VISSER, *op. cit.*
[66]*Ibid.*

181
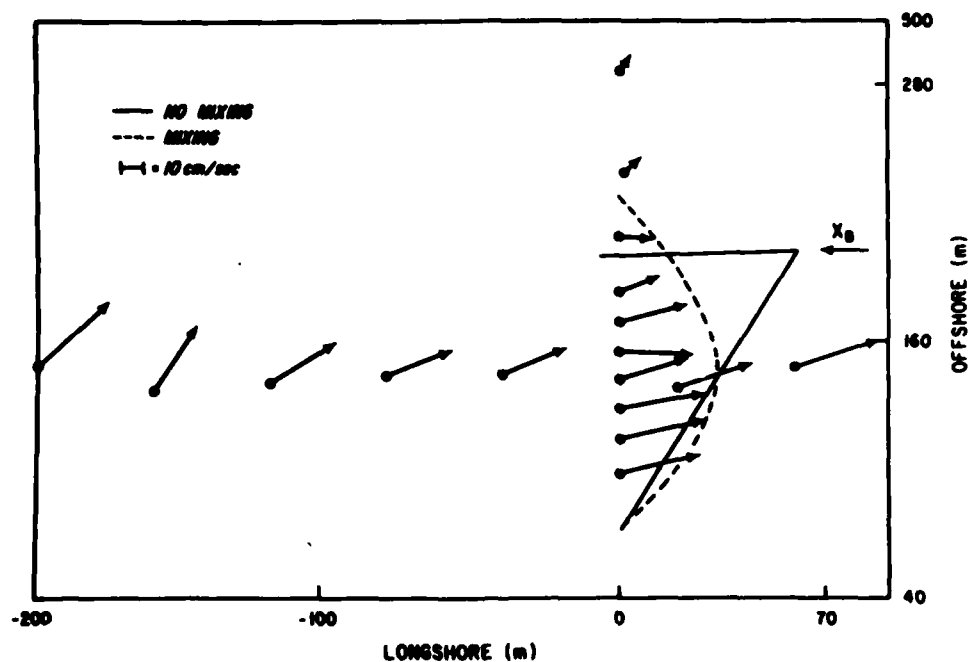
Figure 67. Typical vectors of 17.1-minute average currents at Torrey
Pines, California, from NSTS experiments (after Guza and
Thornton, 1980).

currently being obtained at the Delft Technical University (see Visser,
1980) should provide the needed information to verify the theory in the
near future. The data of Galvin and Eagleson (1965) and others are simply
inadequate for this purpose. This is true for both regular (linear and
nonlinear) and irregular theories.

3. **Nonlinear and Irregular Waves.**

The nonlinear theory of James (1974b) is shown in Figure 68 along
with four experiments from Galvin and Eagleson (1965) and their data.
Transition between the hyperbolic and Stokes wave theories is indicated
by the arrow. Various combinations of friction coefficient C_f and eddy
coefficient N are presented. The values indicated for these coefficients
give relatively small variations in velocity and are said to give good
agreement with the measured velocity shown by crosses. Friction coefficients
varied between 0.001 and 0.0025 and eddy coefficients between 0.01 and
0.016 in these cases. Figures 38 and 59 showed how the original linear
theory required significantly larger bottom friction values ($C_f = 0.01$)
to match the surf zone measurements. The nonlinear theory is also apparen-
tly less sensitive to variations in eddy coefficient.

Collins (1972) and Battjes (1974a) did not attempt any comparisons
with laboratory or field data for their irregular wave theories. Sonu
(1975) prepared the results presented here as Figure 69 where the random
sea model (heavy solid line) is from Collins (1972). It was assumed that
the monochromatic wave height is equal to a rms wave height in the irregular
sea. For comparison, the original model theory of Longuet-Higgins (1970)
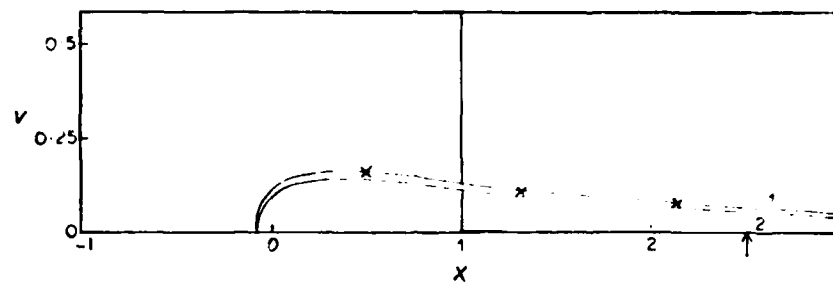
Longshore current profiles for the conditions of experiment (a), 1 for
$C = 0.002$, $N = 0.016$; 2 for $C = 0.0025$, $N = 0.016$.
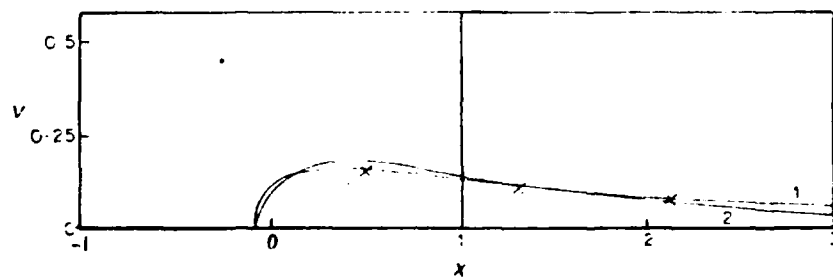
Longshore current profiles for the conditions of experiment (a), 1 for
$C = 0.002$, $N = 0.016$; 2 for $C = 0.002$, $N = 0.01$.
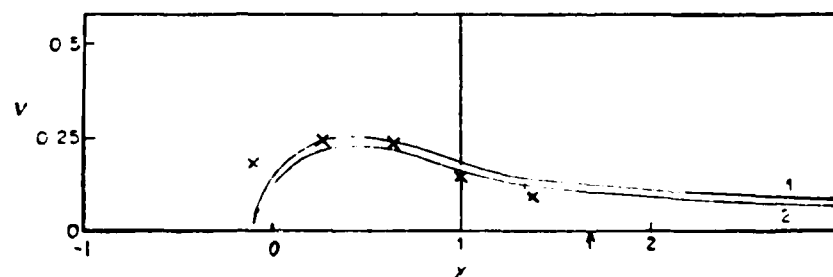
Longshore current profiles for the conditions of experiment (b), 1 for
$C = 0.002$, $N = 0.01$; 2 for $C = 0.0025$, $N = 0.01$.
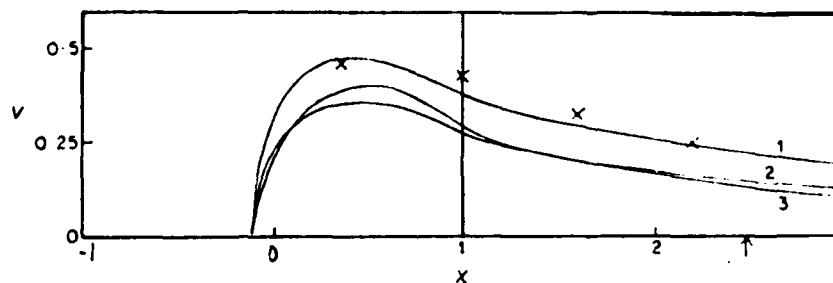
Longshore current profiles for the conditions of experiment (c), 1 for
$C = 0.001$; $N = 0.016$; 2 for $C = 0.002$, $N = 0.016$; 3 for $C = 0.002$, $N = 0.01$.

Figure 68. Comparison of nonlinear theory of James (1974b) with laboratory
data (after James, 1974b).

183
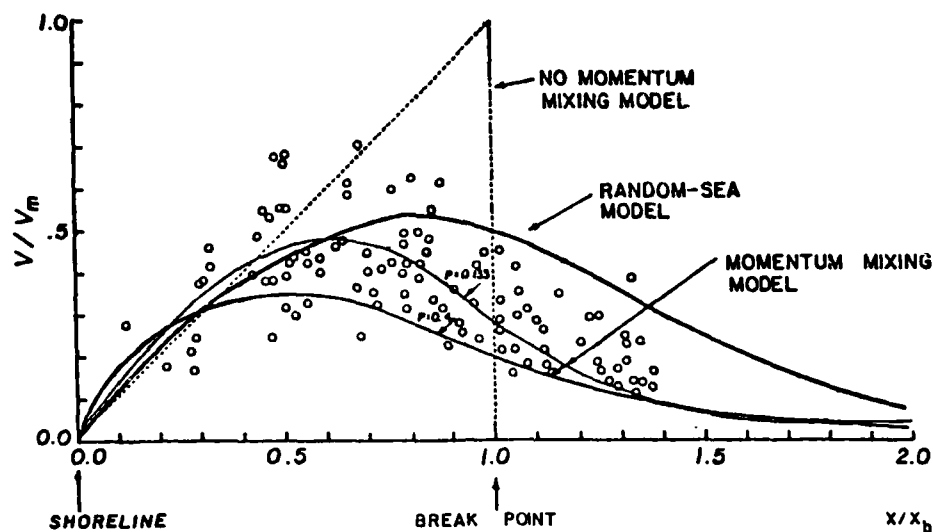
Figure 69. Comparison of irregular theory of Collins (1972) with
original model of Longuet-Higgins (1970) and laboratory
data for regular waves (after Sonu, 1975).

at $P = 0.4$ and 0.135 is plotted along with the experimental data of Galvin
and Eagleson (1965). It is stated that the irregular wave model represents
more closely the mean trend of the experimental data in the surf zone.
This conclusion is debatable and the irregular wave theory clearly over-
estimates the laboratory data outside the breakpoint.

As discussed in Chapter 2, field measurements of longshore currents
generated by irregular waves also show time variations. To illustrate
this fact, Meadows prepared the results shown in Figure 70 where the theory
is by Collins (1972) for various deepwater approach angles. The error
bars indicate the magnitudes of the variations in currents measured. It
was therefore concluded that time-averaged theories for plane beaches,
based upon radiation stress principles, are inappropriate for expressing
natural surf zone water motions that are three dimensional and unsteady
(see also Wood, 1976; Wood and Meadows, 1975).

These are the only known comparisons between nonlinear and irregular
wave theories and experiments available in the literature.

4. Bed Friction and Eddy Coefficients.

Different coefficients of bed friction and eddy viscosity appear in
these investigations. Comparisons are complicated by the use of different
stress models, laboratory and field data sets, theories of longshore
current profile, and different methods of analysis including time-averaging.
For example, most researchers selected C_f (or f_{wc} or f) and N (or Γ or M)

184
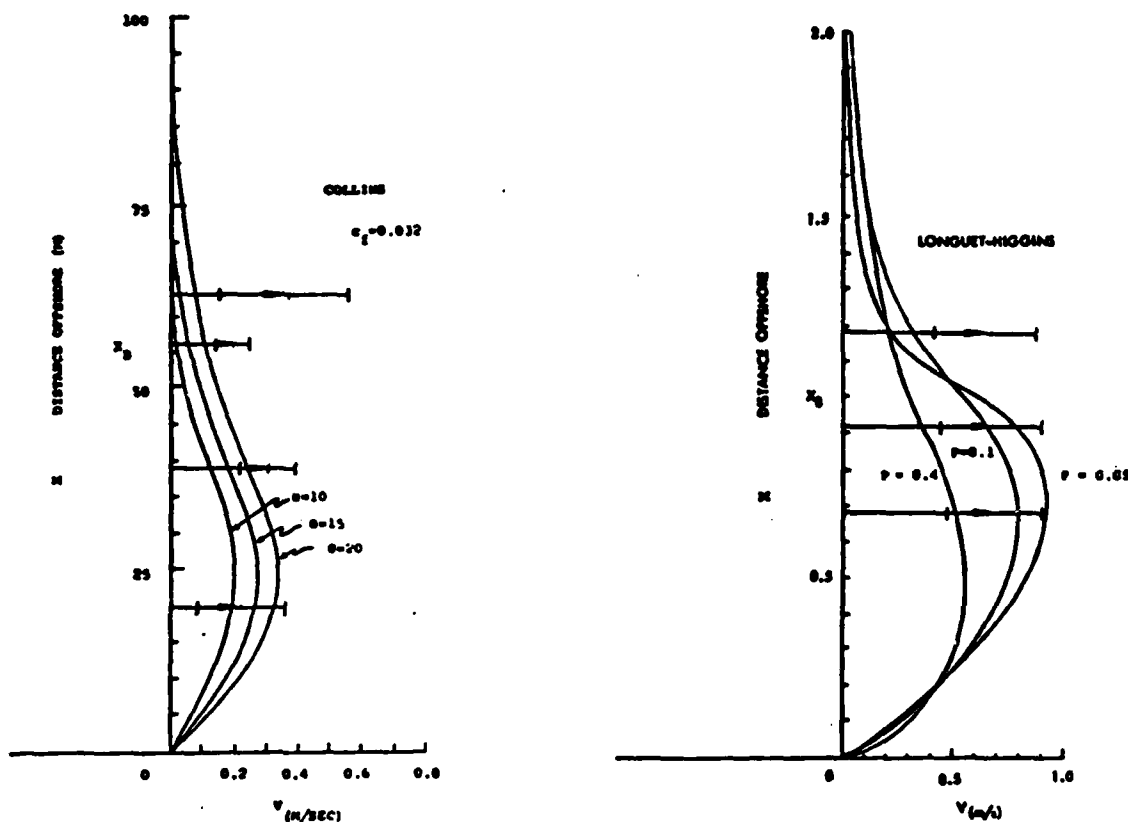
Figure 70. Comparison of irregular theory of Collins (1972) with unsteady
field data (after Meadows, 1977).

to fit the data set employed, whereas Kraus and Sasaki (1979) matched
$\bar{v}_m$ so that C_f and Γ could be computed. Some previous efforts to summarize
values have appeared in the literature. Table 8 lists the major formu-
lations and results.

    a.   <u>Bed Friction Coefficients</u>. The coefficients found for bed shear-
stress models must be approached with caution. No satisfactory formulation
exists and the user must apply coefficients consistent with the model type,
beach slope, laboratory or field situation, etc. under consideration. In
any event, values ranging from 0.001 to 0.06 have been applied. For the
weak current small-angle (linear) model used in early investigations, it
is generally true that C_f decreased with flatter beach slopes as found
in the field. In fact, Komar (1975b, 1976b) argued that the ratio tan β/C_f
is approximately constant. This argument has been attacked on physical
grounds by Longuet-Higgins (1972b) and also experimentally by Huntley (1976)
and Kraus and Sasaki (1979).

Table 8. Summary of bed friction and eddy viscosity coefficients.

Researcher	Experiments (L or F) By	Bed Friction Coefficient				Eddy Viscosity Closure Coefficient				γ ratio	P (or P°) values	Remarks
		Symbol	Equation	Model	Value	Closure Symbol	Equation	Model	Value			
Longuet-Higgins (1970)	Galvin and Eagleson (1965) (L)	C_f	(51)	Weak $\bar{v}$/ small α_b	0.01 estimated	N	(55)	Same	0.0024-0.0096	0.02	0.1-0.4	
Thornton (1969)	Galvin and Eagleson (1965) Ingle (1966)(F)	C_f C_f	Jonsson (1966) Jonsson (1966)	weak $\bar{v}$/ small α_b Bed roughness	(varies) 0.02-0.04 (varies) 0.02-0.6	None	See Table 4		1		N.A.	
Jonss (1972)	Galvin and Eagleson (1965) (L)	C_f	(51)	weak/ small	0.001-0.0025	N	(55)	Different			N.A.	
Jonsson, Skovgaard, and Jacobsen (1974)	Putnam, Munk, and Traylor (1949)(L) Galvin and Eagleson (1965)(L) Ingle (1966)(F)	f_w	(77)	Strong/ small angle	(varies) 0.05-0.1	None	See Table 4		1	0.8 0.8-1.62 0.8	N.A.	Bed friction coefficient function of f_c and f_w for uniform currents and waves, respectively.
Komar (1975b, 1976b)	Others prior to 1967	C_f	(156)	Empirical	0.0172 0.0225	N	(55)	Same	0.01-0.016		0.1-0.4	
Battjes (1975, 1978)	None made	C_f	(127)	weak/ small	none specified	N	See Table 4		0.3-1.8 (Lab) 21-45 (Field)		N.A.	N depends upon bed slope.
Huntley (1976)	Own experiments Devon, England	C_f C_f	(51) non-linear	S_{xy} measured directly in field	0.0026 1.0006 0.0019 1.0006	NOT APPLICABLE						tan β ≈ 0.01 Includes lateral mixing in bed stress coefficient.
Liu and Dalrymple (1978)	Putnam, Munk, and Traylor (1949)	f	non-linear	strong/ large	0.04	NOT APPLICABLE						
Skovgaard, Jonsson, and Olsen (1978)	Galvin and Eagleson (1965)(L)	f_w	Same as Jonsson, Skovgaard, and Jacobsen (1974)			C N	See Table 4	Outside Surf Zone Inside Surf Zone	0.02-0.06 0.177-0.220	1.13	N.A.	Same as Battjes (1975) in surf zone.
Madsen et al. (1978) Ostendorf and Madsen (1979)	Galvin and Eagleson (1965)(L)	f_{es}	Empirical	curve fitting	(varies) 0.01	P	See Table 4		0.013		P°	
Kraus and Sasaki (1979)	Mizuguchi, Oshima, and Horikawa (1978)	C_f C_f	(78) (78)	Weak $\bar{v}$ Large α_b Weak $\bar{v}$ Large α_b	0.011-0.024 0.0061	P	See Table 4	Different	0.0062 0.037 0.015	0.99 1 20 ±1.0	P° 0.050-0.17 0.072	Different formulation for $\bar{v}_L$ in and outside surf zone.
Thornton (1980)	Own experiments, Torrey Pines, Calif. (1978) (F)	C_f	(42) neglecting T_L	S_{xy} measured directly in field	0.006± See Fig. 71	NOT APPLICABLE						$\tau_b = \rho C_f |\bar{u}| \bar{v}$ tan β ≈ 0.023±

186

Huntley (1976) showed that the assumption for using equation (51) based on $\bar{v} \ll u_{Bm}$ is invalid for his data so that C_f values so deduced are not a true bottom friction coefficient. He defined another C_f^* in the equation of motion (neglecting lateral mixing stress) as

$$\frac{\partial}{\partial x} [\rho \overline{uv} \, (\bar{\eta} + h)] = - \rho C_f^* |\vec{U}| \bar{v} \tag{161}$$

where u, v include both wave orbital velocities and turbulence. It must be noted here that the right-hand side of equation (161) is not the same as equation (52) where $\vec{U}$ is the total velocity vector. A two-component current meter on a relatively flat beach (tan β = 0.01) was employed to directly measure u and v, and hence $\vec{U}$ and $\bar{v}$. From equation (161) Huntley directly computed the values of C_f^* shown in Table 8. By the same procedure, C_f values were calculated using u_{Bm} in place of $\vec{U}$ in equation (161). It is not clear why the term $2/\pi$ in (eq. 5) was dropped from the later calculation by Huntley. The value of C_f is generally larger than C_f^* found from equation (161). The difference was found to vary across the surf zone and with approach angle. It is fairly clear that the wide range of C_f values deduced in the literature is partly due to the incorrect weak current small-angle model employed.

Finally, C_f^* values based upon equation (161) must also be considered somewhat questionable for the following reasons. The left-hand side of equation (161) is also an approximation of the true gradient of the radiation stress in that (a) the mass flux term is neglected, and (b) the term $\overline{uv}$ is assumed independent of water depth. Only single position measurements were made with a meter in the water column. In addition, lateral turbulent mixing stresses are combined into C_f^* and steady uniform flow conditions must be present in the field. Huntley (1976) presented methods and arguments in support of his contention that wave-induced turbulence effects were relatively small compared with the wave orbital interactions.

Recently, Thornton (1980) overcame some of these questions by directly measuring the radiation stress component, S_{xy}, offshore and by indirectly computing it inshore (in the surf zone). Thus, a simple steady-state wave-induced current model for a straight and parallel contour beach is employed to estimate C_f^*.

$$\frac{dS_{xy}}{dx} = - \bar{\tau}_{By} = - \rho C_f^* |\vec{U}| \bar{v} \tag{162}$$

The right-hand side is identical to equation (161) but the left hand side is not.

Outside the breakers, a linear array of five pressure sensors (in 10-meter water depth) was used to measure S_{xy} for a series of experiments at Torrey Pines Beach, California (tan β ≅ 0.023), in connection with the NSTS (see Guza and Thornton, 1979, for details). In the surf zone, wave angle measurement directional errors made this procedure inaccurate

for Torrey Pines Beach. Consequently, inshore S_{xy} was computed from a version of equation (10), i.e.,

$$S_{xy} = \overline{\int_{-d}^{0} \rho u(f,z) v(f,z) dz} = \int_{-\pi}^{\pi} E(f,\theta) n(f) \sin\alpha \cos\alpha \, d\alpha \qquad (163)$$

where n is given by equation (15);.f, frequency; and E, the energy density per unit frequency and direction. Further details are beyond the intended scope of this review. The method relies heavily upon the fact that linear wa theory can be employed to relate velocity measured at a single elevation to the energy density spectrum for u (see Guza and Thornton, 1980).

The bed shear-stress coefficient, C_f^* found in this fashion from equation (162) is shown in Figure 71 for various locations in November 1978. Seventeen-minute averaging times were used for each point and eight such values when averaged produced the solid line. The average of all such calculations gave $C_f^* \approx 0.006$. Considerable scatter occurs outside the breakers due to the onshore velocity variability in space and time. In the surf zone, less scatter was observed because the variability is related to local water depth. Thornton (1980) also found that C_f^* was consistently less inside the surf zone when comparing the results of other days. It should be noted that this single value of 0.006 is consistent with that deduced by Kraus and Sasaki (1979) from Japanese field data and their model.

Some negative C_f^* values are noted in Figure 72 outside the breaker line. Thornton (1980) believes this means the currents are driven in the wrong direction. However, Huntley (1976) states that C_f^* can possibly become negative beyond the surf zone due to neglect of the lateral turbulent mixing stress gradient in equation (161) or (162). Electromagnetic current meters with a gain response cutoff around 2 hertz (see Fig. 16) behave as filters to distort all higher fre₄ ᵔncy turbulence signals. Their use is limited for studying wave breaking turbulence and wave-turbulence interactions.

The methods described by Thornton (1980) and applied to additional field data in the NSTS from Santa Barbara, California, will be of considerable interest in the near future. Estimates of the bed roughness patterns, heights, etc., both beyond and within the surf zone, are needed to correlate the data for future applications.

b. **Eddy Viscosity Closure Coefficients**. Even less is formally known about magnitudes and variability of eddy viscosity closure coefficients. As discussed in Chapter 3, eddy viscosity is normally calculated from the expression (eq. 86)

$$\bar{\mu}_L = \rho \bar{\nu}_L = \rho |\bar{\tilde{u}}| \bar{\ell}$$

where considerable disagreement exists as to the proper expressions to
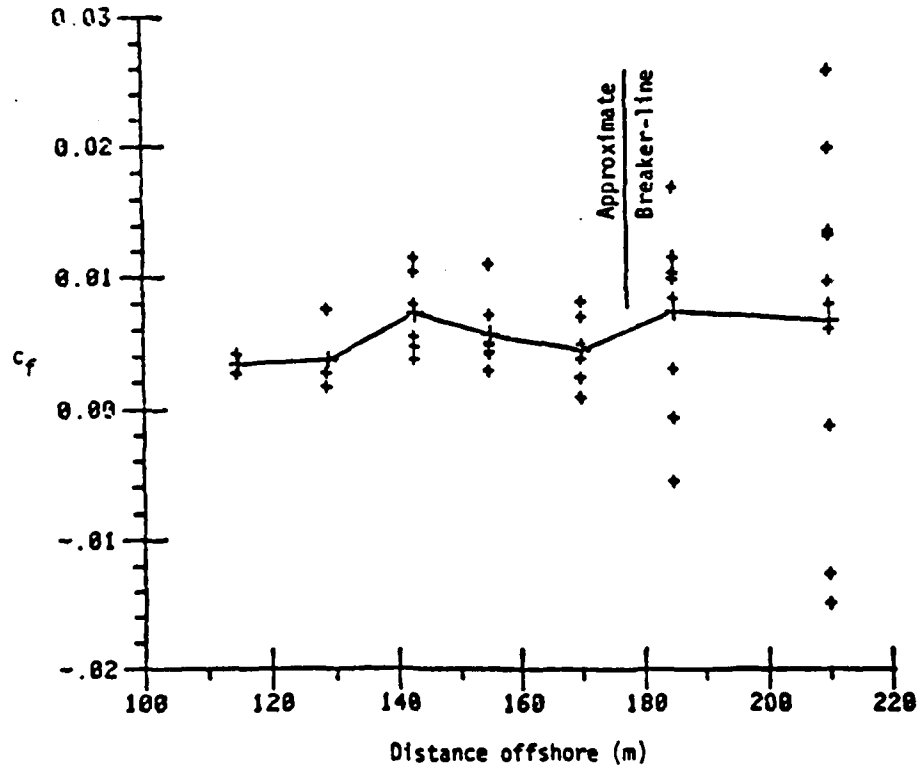
Figure 71. Bed shear-stress coefficients computed from equation (162) and data taken at Torrey Pines Beach, California, November 1978 (after Thornton, 1980).

employ for the characteristic reference velocity $\tilde{u}$ and reference length scale, $\tilde{l}$. A closure coefficient (N, Γ, M, etc.) then is inserted in some expressions (see Table 4) such as that first proposed by Longuet-Higgins (1970)

$$\bar{v}_L = N\bar{x}\sqrt{gh} \tag{164}$$

or later by Madsen, Ostendorf, and Reynolds (1978)

$$\bar{v}_L = \Gamma |\bar{x}| U_{Bm} \tag{165}$$

Consequently, comparisons of various theories of turbulent mixing in the surf zone and beyond must be in terms of $\bar{v}_L$ (or $\bar{\mu}_L$) and not the closure coefficients involved.

189

The earliest effort to compare nearshore mixing theories was by Bowen and Inman (1974). Table 9 presents estimates of $\bar{v}_L$ (A_H) from the limited available field and laboratory studies by Inman, Tait, and Nordstrom (1970) and Harris, et al. (1962). Also included are $\bar{v}_L$ values that Thornton (1970a) used to reproduce longshore current observations with his theory. Although the eddy viscosity varies over almost four orders of magnitude from laboratory to field, the closure coefficient N shows a relatively small range of variation from 0.009 to 0.065 with an average N $\approx$ 0.03 across the surf zone. This value is considerably larger than that used by Longuet-Higgins (1970) to verify his profile theory ($N = 0.0024$ to 0.0096 from Galvin and Eagleson, 1965, see Table 8). One explanation is that his model overestimates $\bar{v}_L$ beyond the surf zone (Longuet-Higgins, 1972a) so that if much smaller $\bar{v}_L$ values are used outside the breakers, a larger mean coefficient is needed to reproduce observed profiles (Bowen and Inman, 1974). Paradoxically, because direct measurements of eddy viscosity by dye diffusion in the field are difficult, Bowen and Inman (1974) state that estimates of $\bar{v}_L$ by fitting observed velocity distributions to theory may be a more accurate method.

Nielsen (1977) used the available field and laboratory data in Table 9 to test four different theories for $\bar{v}_L$. These were by Longuet-Higgins (1970) and Jonsson, Skovgaard, and Jacobsen (1974), and were similar to Thornton (1969, 1970a), Inman, Tait, and Nordstrom (1970), and Battjes (1975, 1978). The comparison is summarized in Table 10 and only for surf zone mixing. Based on Nielsen's analysis of mean values of eddy viscosity across the surf zone $\bar{v}^*$, the model by Longuet-Higgins is preferred. The resulting empirical constant of 0.007 gives N = 0.018 which is near the maximum value of 0.016 predicted by Longuet-Higgins (1970, 1972a). It is not clear why these results by Nielsen for N, using essentially the same data, differ from those by Bowen and Inman (1974) who obtained N $\approx$ 0.03. Also, the average eddy viscosity ($\bar{v}^*$) is not indicative of how the $\bar{v}_L$ variation across the surf zone and beyond produces the proper longshore current profile. Figures 61 and 62 give an idea of how widely $\bar{v}_L$ can change in this regard.

Finally, as discussed by Nielsen (1977), $\bar{v}_L$ is not a true eddy viscosity for turbulent diffusion. It is really a combined transport-dispersion coefficient since much fluid is advected shoreward in the upper layers by the reference celerity for breaking waves. An excellent summary of all models before 1978 can be found in Gourlay (1978).

The trend since 1978 is to use separate models and coefficients within the surf zone and beyond the breaker line (Skovgaard, Jonsson, and Olsen, 1978; Kraus and Sasaki, 1979). Completely different closure coefficients result in each region (see Table 8). It will be extremely beneficial in the future to use the newly available field data on longshore currents (NSTS) to estimate separate $\bar{v}_L$ and closure coefficients by fitting the data. It will also be appropriate to consider new ways to analyze the available velocity time histories across the surf zone. One possibility is to use auto- and cross-correlation techniques to estimate Lagrangian length scales from which Eulerian length scales and local eddy viscosities

END
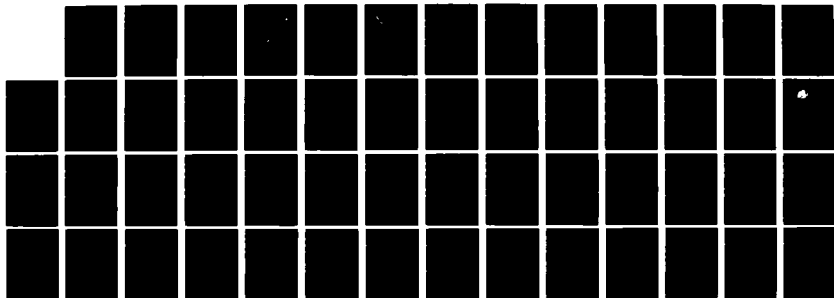
FILMED

DTIC
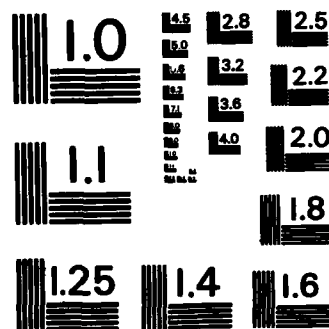
MICROCOPY RESOLUTION TEST CHART
NATIONAL BUREAU OF STANDARDS-1963-A

Table 9. Estimates of eddy viscosity across the surf zone from laboratory and field experiments (after Bowen and Inman, 1974).

Date	Exp. No.	x_b (m)	h_b (m)	$\overline{gh_b}$ (m/s)	A_H (m²/s)	N
Inman, Tait and Nordstrom (1970)						
Scripps	129	83	0.80	2.7	5.9	0.064
	109	80	0.60	2.4	2.8	0.037
	112	68	0.60	2.4	2.0	0.030
	107	70	0.66	2.5	2.0	0.027
El Moreno	55	5.5	0.45	2.1	.30	0.065
	97	4.7	0.45	2.1	.12	0.030
	95	4.8	0.40	2.0	.11	0.026
	104	4.8	0.35	1.8	.12	0.034
	97	3.8	0.30	1.7	.08	0.039
Harris et al. (1962)						
field	1	18	1.4	3.7	1.1	0.041
	2	14	1.1	3.3	0.24	0.013
	3	12	0.9	3.0	0.26	0.018
	4	16	1.2	3.4	0.42	0.020
	5	8	0.6	2.4	0.28	0.036
laboratory	–	0.70	0.068	0.82	0.0051	0.022
	–	0.80	0.072	0.85	0.0054	0.020
	–	0.80	0.072	0.85	0.0050	0.018
	–	0.50	0.043	0.66	0.0051	0.038
	–	0.60	0.056	0.75	0.0028	0.016
	–	0.50	0.045	0.67	0.0023	0.018
	–	0.50	0.041	0.64	0.0019	0.015
	–	0.30	0.027	0.52	0.0022	0.036
	–	0.50	0.043	0.65	0.0012	0.010
	–	0.35	0.032	0.57	0.0007	0.009
Thornton (1970a)						
lab (Galvin, 1965)	–	0.52	0.043	0.65	0.0029	0.021
field (Ingle, 1966)	–	70	1.5	3.8	1.4	0.013

Table 10. Comparison of four surf zone theories for mean eddy viscosity across the surf zone (after Nielsen, 1977).

Author	Equation for Average $\overline{U}_L^2$ Across Surf Zone	Kn, Empirical Constant	Closure Coefficient	Relative Scatter	Remarks
Longuet-Higgins (1970).	$(0.4N)|x_b|\sqrt{gh_b}$	0.007	0.018	0.5	$K_{L-H} = 0.4N$
Inman, Tait, and Nordstrom (1970).	$(K_I)H_b x_x/T$	0.46	0.46	0.80	K_I = Coeff. by Inman
Jonsson, Skovgaard, and Jacobsen (1974).	$(K_J)T\rho g H_b \cos^2\alpha_b$	0.017	0.017	1.12	K_J = Coeff. by Jonsson
Battjes (1975).	$(K_B)(\tan\beta-\tan m)^{4/3} \cdot |x_b|\sqrt{gh_b}$	8	0.3-1.8	1.8	$N = H\left(\frac{5\gamma^2}{16}\right)^{1/3}\frac{dh}{dx}^{1/3}$

191

can be deduced (Baldwin, and Johnson 1972).[67] Much additional work remains to determine which model for $\bar{v}_L$ is best and to pin down the appropriate closure coefficient associated with it.

All the above discussion is for onshore-offshore mixing where the characteristics length scale is the surf zone width. A model for turbulent mixing in the alongshore direction (longshore dispersion) has been developed by Lin and Horikawa (1978). It assumes the surf zone as an open channel with triangular cross section and that the lateral variation of longshore current as the primary mechanism for longshore dispersion. Rip current effects are ignored. The theory when compared with observed field and laboratory measurements is found to agree reasonably well. The model follows concepts originally developed by Fischer (1967)[68] for longitudinal dispersion in natural water courses. Results are of interest for use in two-dimensional numerical models where different cross-shore and longshore dispersion processes are possible. Rip current effects must be included in future efforts in this regard.

5.   Surf Zone Empiricism

The final closure coefficient needed in all theories for comparisons with measured data is the wave height to total water depth ratio, γ. It is often used to estimate both the breaker height and the energy decay in the surf zone. An extensive discussion is presented in Chapter 3; however, this section concentrates on surf zone energy dissipation and those attempts to compare actual measurements with theory.

All the longshore current theories listed in Table 3 and reviewed in this chapter assume a const $_\text{ant}$ γ ratio across the surf zone. Is this correct for all breaker types, beach slopes, wave steepnesses, etc.? Collins and Weir (1969) summarized the results of four experimental investigations on plane beaches as shown in Figure 72. With the coordinates shown, a 45° line would give constant γ in the surf zone. In general, as beach profile decreased the γ ratio departed further and further from being constant across the nearshore area. On flat dissipative-type beaches (spilling breakers as found in the field) the γ ratio changed continuously as the rate of energy dissipation decreased with distance from the breaker line. Distance from the breaker line is also important for determining wave heights in the surf zone. This result was confirmed by laboratory

[67]BALDWIN, L.V., and JOHNSON, G.R., "The Estimation of Turbulent Diffusivities from Anemometer Measurements," submitted to *Journal of Fluid Mechanics* Jan. 1972 (no record of JFM publication) (not in bibliography).

[68]FISCHER, H.B., "The Mechanics of Dispersion in Natural Streams," *Journal of Hydraulics Division*, Vol. 93, No. HY6, 1967, pp. 187-216 (not in bibliography).
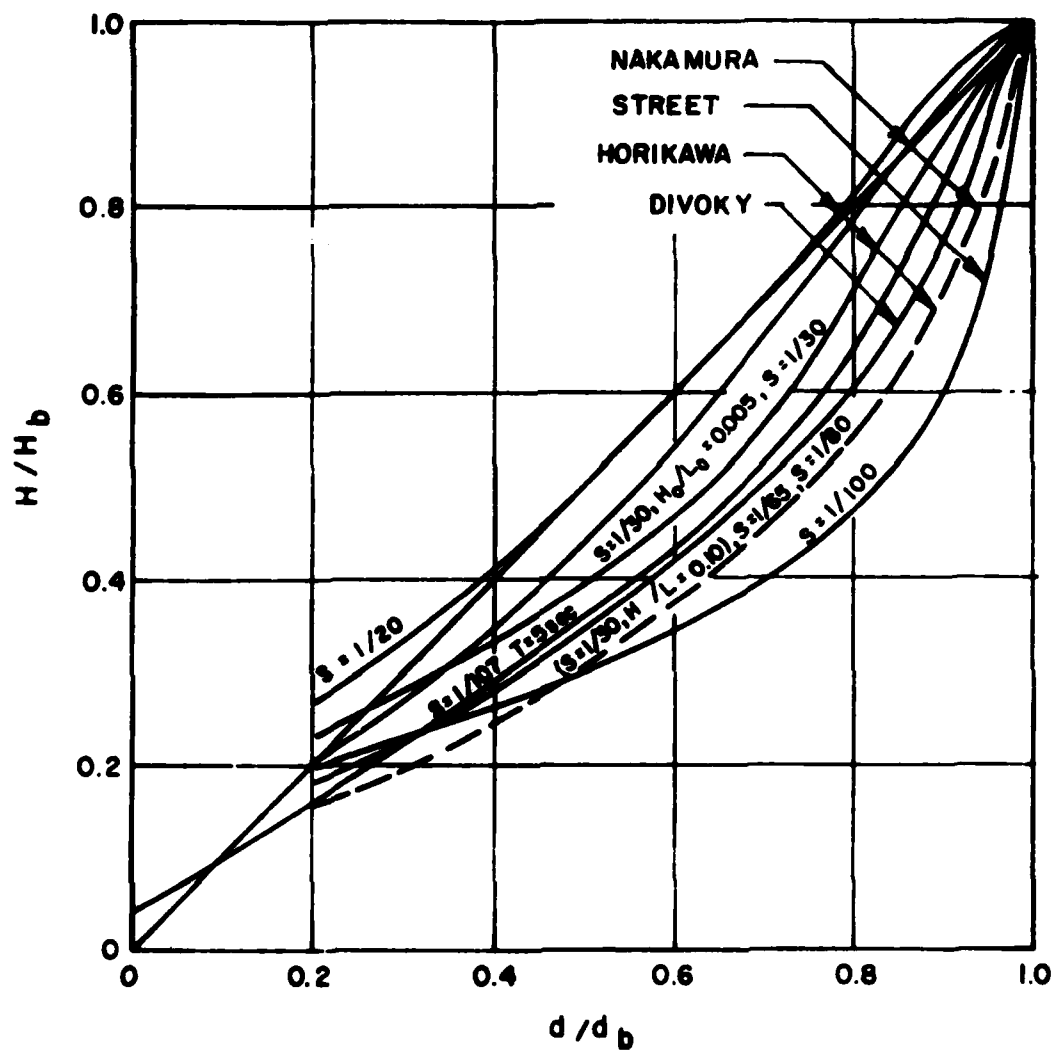
Figure 72. Experimentally determined wave height decay on plane beaches of different slopes (after Collins and Weir, 1969).

measurements of Sawaragi and Iwata (1974) for regular wave dissipation
across a horizontal bed. Their results are repeated here as Figure 73(a).
Recent field measurements by Suhayda and Pettigrew (1977) presented some
confirmation of the fact that the γ ratio varies with distance from the
breakpoint and ranged from 2.0 to 0.6 (Fig. 73,b). The theory of Sawaragi
and Iwata (1974) is also shown in Figure 73(b). It is based on a finite-
difference solution of a set of surf zone equations of motion and contin-
uity that includes excessive amounts of numerical information loss
(numerical viscosity). For this reason it has been omitted from this report.
Finally, the data of van Dorn (1976) are shown in Figure 74. This was
obtained as part of his wave setup results previously discussed. Steep
slopes ($\beta \gtrsim 0.1$) as employed in most laboratory studies of longshore current
profiles produced $\gamma \gtrsim$ constant whereas it is again clearly shown that γ
is not constant for flatter profiles.

Use of constant γ ratio in longshore current profile models introduces
a high sensitivity to bottom profile variations that is unrealistic (Battjes,
1978). As seen in Figures 72, 73 and 74, a constant γ is not applicable
for flat slopes, nor is it physically justifiable for bar-trough profiles.
Consequently, Battjes and Janssen (1978) developed an irregular wave model
for surf zone wave height decay as described in Chapter 3 and shown in
Figure 41 for examples with plane and bar-trough type beaches. It is based
on the conservation of energy equation (44) and not some semiempirical
γ variation. A series of laboratory experiments was then conducted to
check the theory in a basin 45 meters long, 0.8 meters wide using SWL depths
about 0.7 meter. The free-surface fluctuations were measured by parallel-
wire resistance gages and data indicated by x on Figure 40. The theory
was found to give excellent results on a plane beach (tan β = 0.05) with
large wave steepness (Fig. 40,b) than the lower steepness (Fig. 40,a) where
only fair results are indicated. For bar-trough profiles, the theory was
considered quite good. It followed the visual observation of essentially
no wave breaking in the trough region (no energy dissipation) and also
produced a high dissipation rate just inside the bar.

The theory shown in Figure 40 is based on only two closure parameters.
One is K in equation (124) which was expected to be about unity and K = 1
was in fact used in the theoretical calculation. The second is γ_b taken
here as 0.8 for initial wave breaking only. The theory was found to
qualitatively and quantitatively predict wave height decay and MWL changes
on plane and bar-trough beach profiles. Use of the theory in combination
with longshore current calculations has yet to be attempted.

Battjes and Jansen (1978) attribute the disparity between theory and
measurement for low steepness waves ($\lesssim 0.01$) on plane beaches (Fig. 41,a)
to an enhancement effect. In other words, waves with low steepness have
time to shoal up to heights exceeding the deepwater wave height, before
the decay due to wave breaking sets in.

194
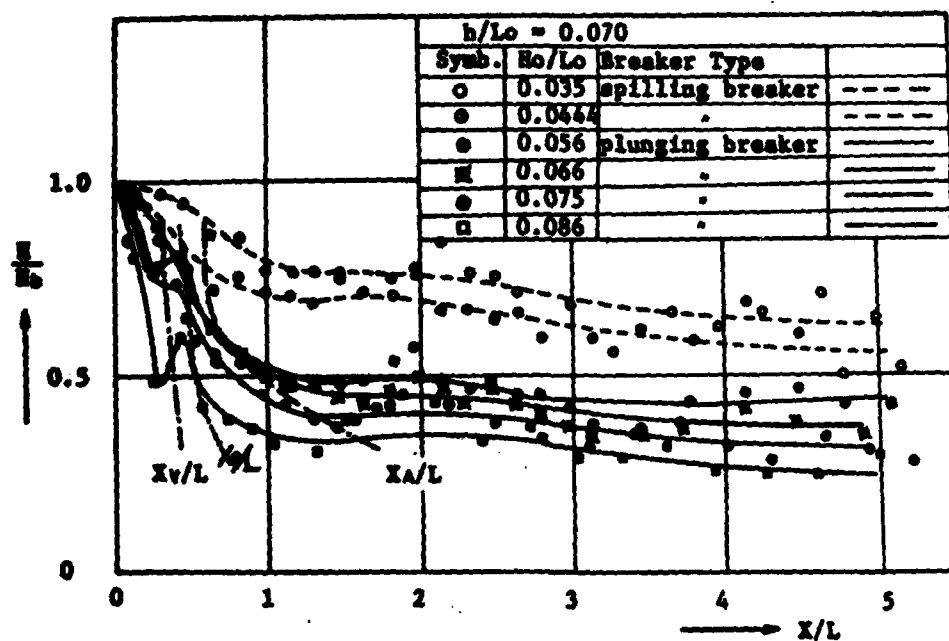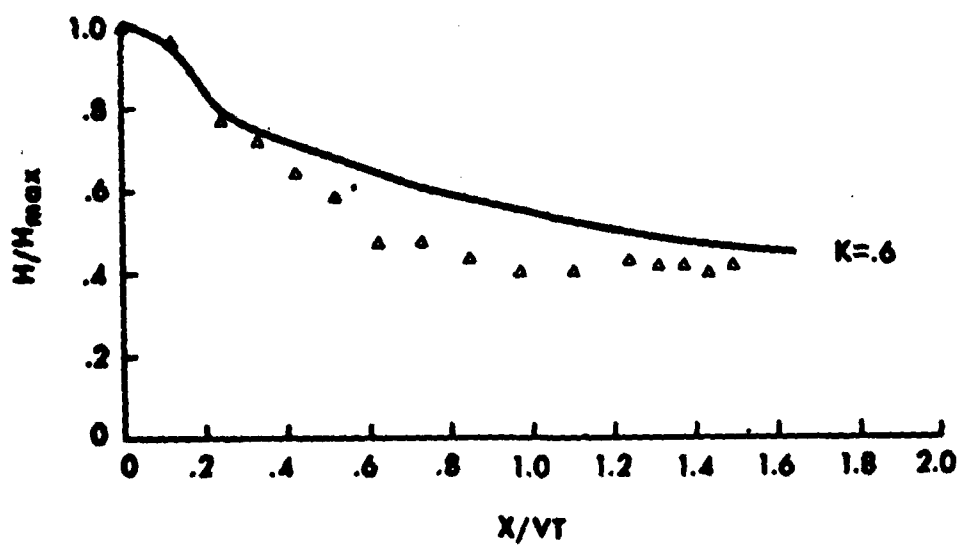
Figure 73. Experimental studies of wave height decay in surf zones as function of distance from breakpoint: (a) laboratory (after Sawaragi and Iwata, 1974); (b) field (after Suhayda and Pettigrew, 1977).

195
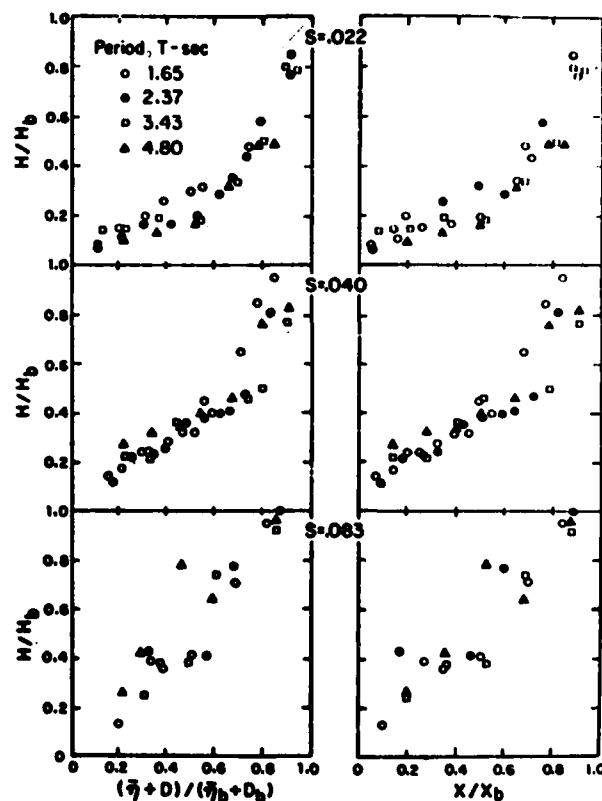
Figure 74. Wave height versus total water depth and surf zone width from
laboratory experiments (after van Dorn, 1976).

The model developed by Goda (1975) is similar to that by Battjes
(1975) and Battjes and Jansen (1978) except that wave breaking is assumed
to occur over a range of wave heights with varying probability. The choice
of the range was arbitrary but found to agree with both laboratory and
field data. This is said to ". . . represent the inherent variability
of breaker heights and partly compensate [for] the inaccuracy of using
a single wave period in the estimation of breaker height" (Goda, 1975).
A semiempirical nonlinear theory of wave shoaling (Shuto, 1974)[69] is also
used in Goda's theory. His theoretical results for various beach slopes
and wave steepnesses versus laboratory data from an irregular wave flume
are presented in Figure 75. Agreement could be classed as better for low
steepness waves which again shoal up considerably on steep beaches before
breaking. In fact, Battjes and Jansen (1978) indicated that their simpler
model was a first effort to be later refined by incorporation of Goda's
smoother cutoff criteria.

The most recent experimental versus theoretical attempt at surf zone
modeling has been reported by Mizuguchi (1980). It also employed the wave

---

[69]SHUTO, N., "Nonlinear Long Waves in a Channel of Variable Section," *Coasta*
Engineering in Japan, Vol. 17, 1974, pp. 1-12 (not in bibliography).
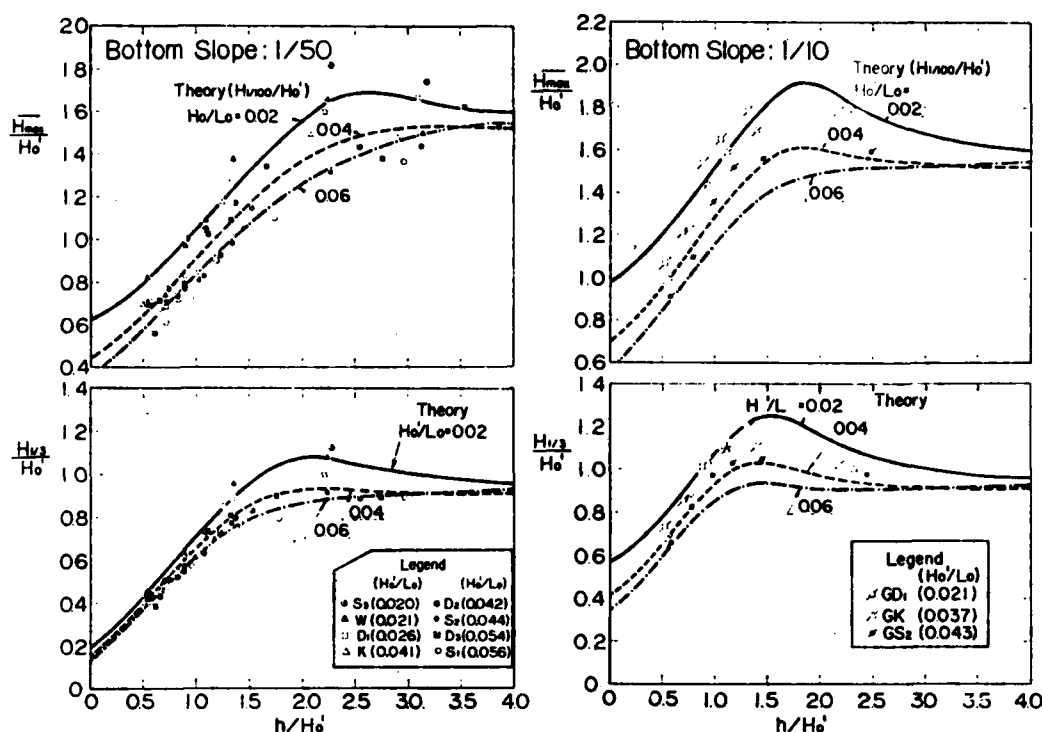
Figure 75. Irregular wave height variation across the surf zone on plane beaches: theory versus laboratory data (after Goda, 1975).

energy conservation equation (44) but then relied on entirely different energy dissipation relations (than Battjes) as briefly described in Chapter 3. Figure 76 shows four separate cases of theory versus experiment. Here, the wave amplitude to amplitude at breaking (a/a_b) is plotted for (a) horizontal, (b) plan 1:10 slope, (c) and (d) stepped beach profiles. Also shown are wave setup results ($\bar{\eta}/d_B$) not of interest here.

The theory (solid line) underestimates the wave height decay in all cases. Better results were obtained (dashline) by using $E = 1/6\rho ga^2$ for the wave energy per unit area rather than the correct value of $E = \frac{1}{2}\rho ga^2$. The factor 1/6 was found empirically to give the correct wave setup for step-type profiles. The necessary empiricism with this theory makes it less attractive than the model of Battjes and Jansen (1978) modified by the smoother, breaking cutoff criteria devised by Goda (1975).

Wave height and set-up in surf zone of __uniform depth__

Uniformly sloping beach

Step-type beach

Field data on step-type beach
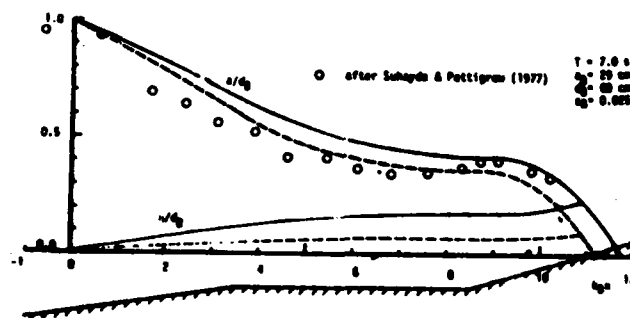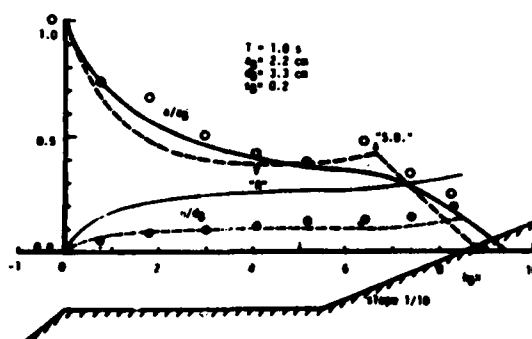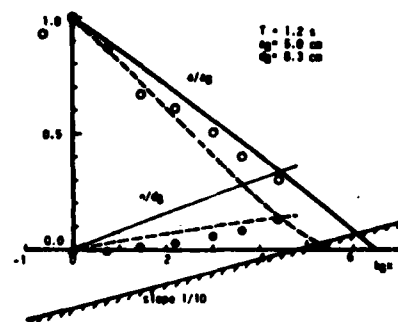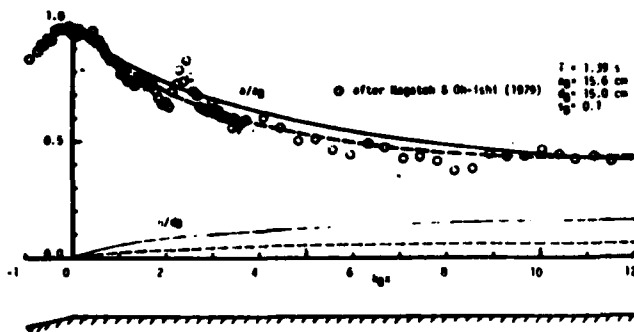
Figure 76. Irregular wave height variation across the surf zone for four different beach profiles: theory versus data (after Mizuguchi, 1980).

III. NEARSHORE CIRCULATIONS

1. Rip Currents.

To date, all theory has concentrated on rip current spacing as discussed in Chapter 3. Mechanisms for rip current generation are categorized in Table 1 and reviewed extensively in Chapter 2. Because of the large number of possible mechanisms that can cause rips to form on beach profiles ranging from the reflective-type (steep) to the dissipative-type (flat, broad), no single theory has emerged for comparison with laboratory and

field spacing measurements. In fact, much of the knowledge in this area must still come from empirical correlations of the available data.

One such effort was made by Sasaki (1977) (see Sasaki and Horikawa, 1975a, 1975b). Field data from the United States, South Africa, and Japan were analyzed in terms of the rip current spacing Y_r (L_r in eq. 111), surf zone width X_b, beach slope tan β, and wave steepness. The latter two variables can be combined into the surf similarity parameter ξ (Battjes, 1974a, 1975, eq. 93) or here defined as the Irribaren Number, I_r. Note that the deepwater wave height H_o is used in contrast to Battjes' similarity parameter ξ which employed H, the height at the "toe" of the slope. Gourlay defined I_{rb} if H_b (at breaker) is involved.

$$I_r = \frac{\tan \beta}{(H_o/L_o)^{\frac{1}{2}}} \tag{166}$$

From the data sources shown in Figure 77 for the correlation between Y_r and X_b, Sasaki plotted the normalized rip current spacing Y_r/X_b against I_r. Considerable scatter was found to exist, as shown in Figure 78, where rip spacing ranged from about one to eight times the surf zone width. From an extensive analysis of the data in which breaker type, beach slope, reflection coefficient, and other factors were considered, Sasaki (1977) hypothesized the three domains for rip current generation mechanisms shown in Figure 78. These were an edge wave, instability, and infragravity domain. A detailed description of each domain for nearshore circulation systems is given in Table 11 (after Sasaki, 1977).

The demarcation between each domain was given as $I_r = 0.23$ and $I_r = 1$ as shown in Table 11. The reasons for this choice were never explicitly stated by Sasaki (1977). The infragravity domain ($I_r < 0.23$) was hypothesized by Sasaki (1977) to explain why flat beaches with wide surf zones (spilling-type breakers) could reflect relatively low waves ($H_b < 0.3$ m) with longer periods of the order 30 to 120 seconds. These waves are known as infragravity waves and are produced by irregular wind waves and also called surf beat. The existence of these low mode edge waves within the surf zone on flat beaches has subsequently been measured by Huntley (1976a) and Sasaki, Horikawa, and Hotta (1976)[70] in the field and Bowen and Guza (1978) in the laboratory.

The data of Figure 78 for each domain give the ratio Y_r/X_b as

(1) infragravity domain ($I_r < 0.23$)

$$Y_r/X_b = 157 \ I_r^2 \tag{167}$$

_____

[70] SASAKI, T., HORIKAWA, K., and HOTTA, S., "Nearshore Current on a Gently Sloping Beach," *Proceedings, 15th Coastal Engineering Conference,* 1976, pp. 626-644 (not in bibliography).
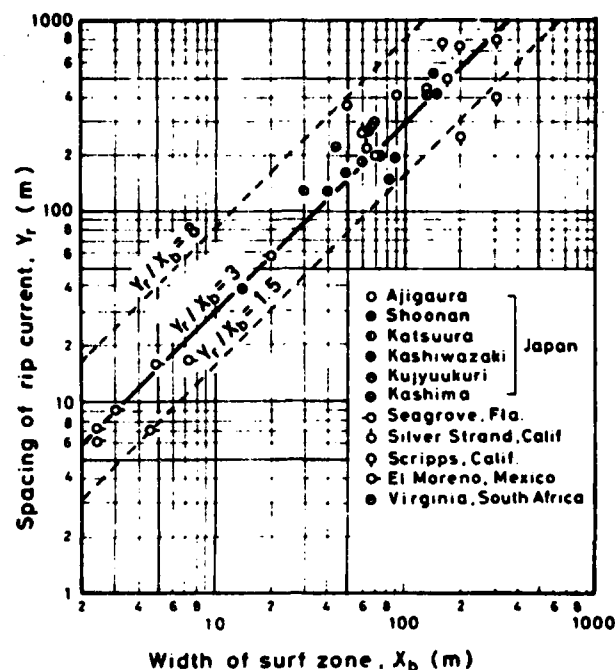
Figure 77. Correlation between rip current spacing Y_r and surf zone width, X_b (after Sasaki, 1977).
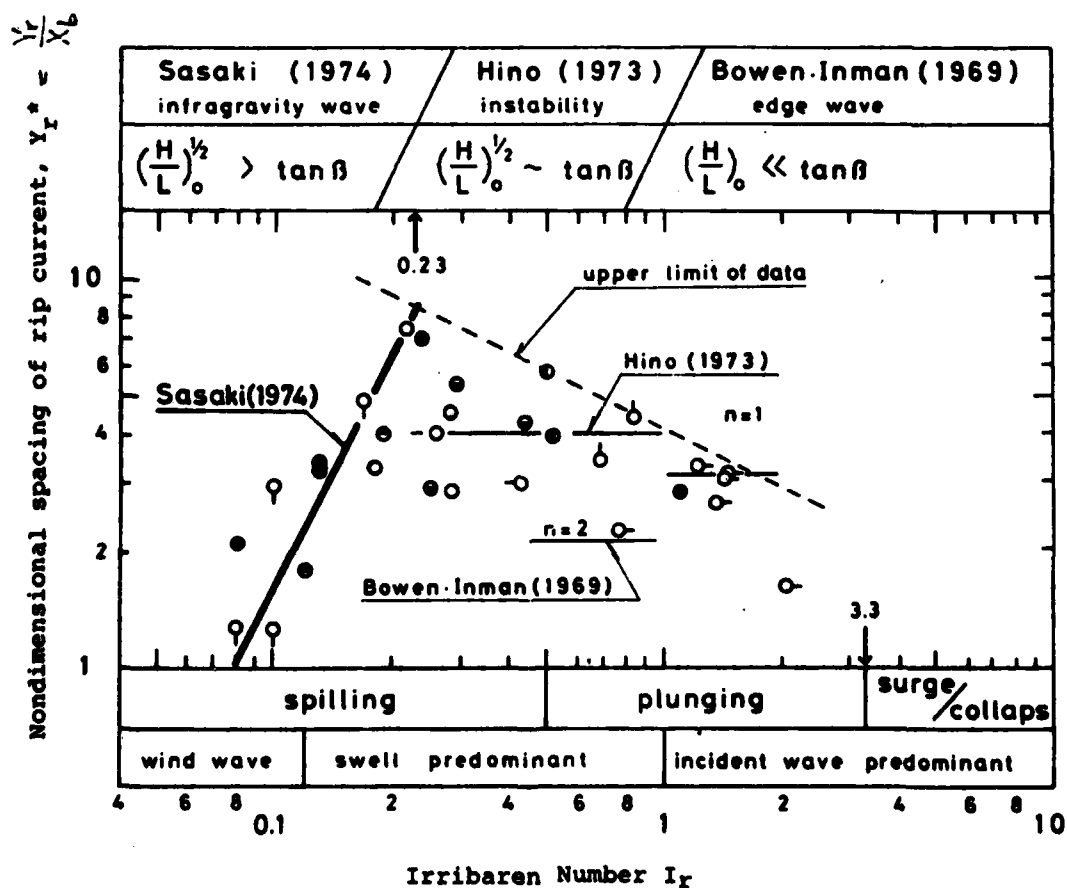
Figure 78. Dimensionless rip current spacing related to Irribaran number and three domains of rip current generation mechanisms (after Sasaki, 1977).

200

Table 11. Three domains of the nearshore current system
(after Sasaki, 1977).

Domain	Infragravity	Instability	Edge wave
Author	Sasaki (1974)	Hino (1973)	Bowen and Inman (1969)
Range of I_r	$0.23 > I_r$	$1 > I_r > 0.23$	$I_r > 1$
Breaker type	Spilling	Spilling∿plunging	Plunging∿surging/collapsing
Surf zone	Always exist	Exists or does not exist	Does not always exist
Number of waves in the surf zone	More than 3 waves	1∿3 waves	Less than 1 wave
Reflection coefficient r	$r < 10^{-2}$	$r \sim 10^{-2}$	$r > 10^{-1}$
Incident wave characteristics	Wind waves & swell	Swell	Arbitrary
Micro-topography	Longshore bar	Crescentic bar	Beach cusp
Classification by Guza and Inman (1975)	Dissipative system		Reflective system
Remarks	Incident wave with large wave steepness Gentle bottom slope $\tan\beta < 1/50$	$\tan\beta = 1/20 \sim 1/40$	Incident waves with small wave steepness Steep bottom slope $\tan\beta > 1/10$

(2)   instability domain $(0.23 < I_r < 1)$

$$Y_r/X_b \approx 4 \qquad\qquad (168)$$

and   (3)   edge wave domain $(I_r > 1)$

$$Y_r/X_b = \begin{cases} \pi & n = 1 \\ \dfrac{2\pi}{3} & n = 2 \end{cases} \qquad\qquad (169)$$

Equation (167) was obtained empirically by Sasaki (1977) from the data shown whereas the other relations are theoretical. The edge wave theory of Bowen and Inman (1969) with modal number n appears to agree well with data from the steep beach (tan $\beta \approx 0.15$) at El Moreno, Mexico (eq. 169).

In the instability regime, the theory of Hino (1974) falls within the variation of data shown. The theory of Dalrymple and Lozano (1978), given by equation (112), and the theory by Miller and Barcilon (1978), given by equation (114), result in $Y_r/X_b \approx 2$ and $Y_r/X_b \approx 10$, respectively, for typical values of tan β, γ, and C_f. Thus, their more sophisticated eigenvalue analyses appear to give results farther outside the range of observed rip current spacings in Figure 78. More data are needed to substantiate the various theories. For example, use of the LEO data gave Bruno and Dalrymple (1978)[71] encouragement for the applicability of equation (112) in the instability regime.

Rip current generation mechanisms can also be categorized as either the free type (instability, eigenvalue theory) or the forced typed (edge wave, structural interaction, etc.). Mizuguchi and Horikawa (1976), based on their experiments, argue that observed rips in the field should all be interpreted as the forced type where irregular bottom bathymetry controls the motion.

Much research remains to be done on rip currents and the development of two-dimensional numerical models such as by Vreugdenhil (1980) to study migrating rip currents will provide needed insight in the future. No theory exists for rip current velocity, width or size, and little field data are available to verify the numerical simulations in this regard. Sasaki (1977) does provide some data and correlation for the offshore extent of rip currents beyond the breaker line (X_r in Fig. 14).

---

[71]BRUNO, R.O., and DALRYMPLE, R.A., "Held Observations of Rip Currents," University of Delaware Report, 1978 (not in bibliography).

2. Nearshore Circulations.

The data base for experimental measurements of mean water surface variation and two-dimensional currents, i.e. nearshore circulations, is extremely limited. Only a few field and laboratory studies have been made, and the results are not readily accessible for use. While significant strides have been made in development of numerical models to simulate near-shore hydrodynamics, data to calibrate, verify, and test these models are practically nonexistent.

The Japanese recognized this problem in the early 1970's and developed their BACS (ballon-borne camera systems) with drogues. It was modified into the STEREO-BACS system by Sasaki, Horikawa, and Hotta (1976)[70] to permit wave height estimates to be included. Two cameras are suspended by ballons that permit stereographic projections. Problems with this method were discussed in Chapter 2. The results are not generally available for use by other researchers.

In the United States, the problem is currently being addressed by General Government agencies such as the National Sea Grant Office of the National Oceanic and Atmospheric Administration (NOAA) in their NSTS project and the CERC in their Atlantic Remote Sensing Land Ocean Experiment project. Data from the NSTS experiments are being made available on magnetic tape. The data could provide the information necessary to substantiate the nearshore circulation models in the near future.

Figure 79 provides an analytic solution, based on Bowen's (1969) linear theory for the same wave characteristics and bathymetry as the field measurements of currents with drogues and current meters by Sonu (1972) shown previously in Figure 2. Comparing the two figures showed general qualitative agreement but the symmetry in the theory was not found, no quantitative comparison of results was attempted. Also, it was observed that the circulations pulsated but the analytic solution was for the steady state. The undulating surf zone bed was postulated as the mechanism triggering rip current formation. It was concluded that the theory substantiated the observations in this regard.

The simplified numerical model NCSS developed by Sasaki (1977) was exercised to simulate two different cases as measured in the field by the BACS system. In one example (CASE-2) drogues were scattered outside the breakers to facilitate comparison and a meandering longshore current-rip current pattern was present. Figure 80(a) is the nearshore current velocity field as deduced from the camera photos, and Figure 80(b) shows the numerically computed velocities under corresponding wave and bottom contour conditions. Sasaki (1977) stated that to the left and near the pier ". . . the direction of the predicted current is different from that of the observations [which] has a predominant offshore component." In fact some of the strongest measured currents (> 30 centimeters per second) appear precisely where the model indicates a large-scale eddy with zero motion. In terms of transport stream-function contours the overall flow

---

[70]SASAKI, HORIKAWA, and HOTTA, *op. cit.*
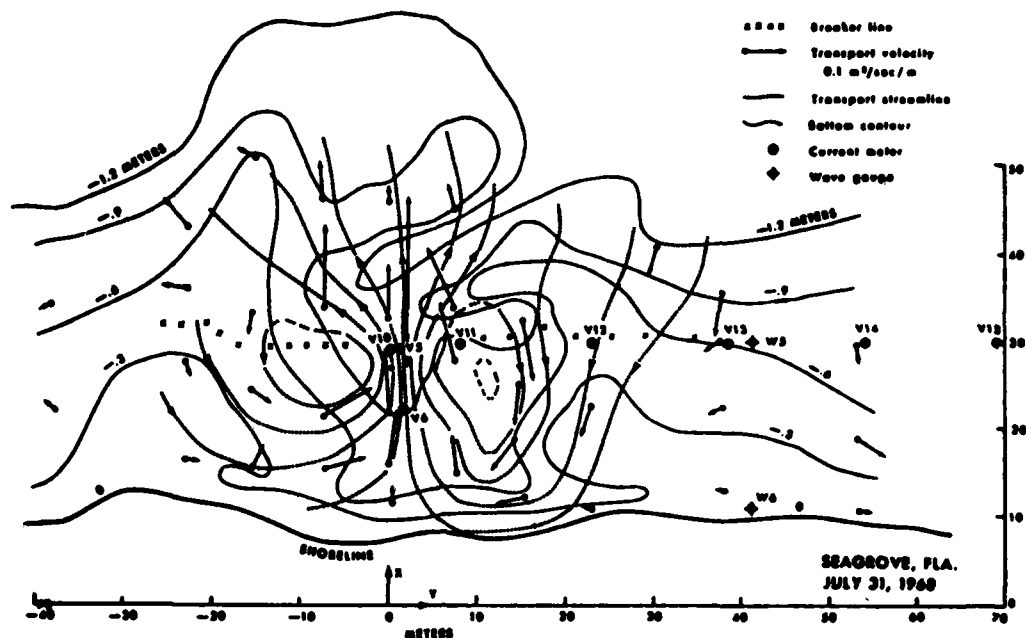
Distribution of transport velocities and streamlines in the circulation cell. Streamline separation is 0.4 m³/sec, $H_b = 0.395$ meter, $T_b = 5.0$ sec, and $\alpha_b = 9$.
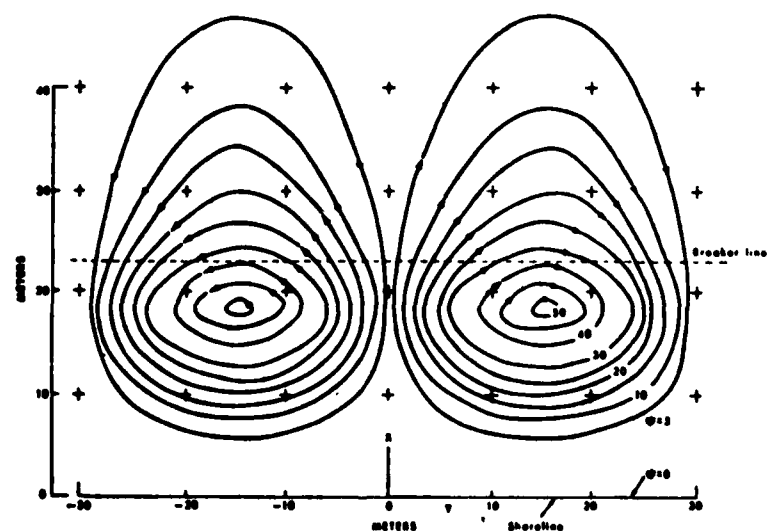
Computed transport streamlines of a circulation system for normal-wave incidence and undulatory surf zone: $H_b = 0.395$ meter, $T_b = 5.0$ sec, $\alpha_b = 0$, $\tan \beta = 0.03$.

Figure 79. Comparisons of field observations of nearshore circulations and analytical theory of Bowen (after Sonu, 1972).

Figure 80. Comparisons of field observations of nearshore circulation
and numerical model of Sasaki (after Horikawa, 1978).

patterns are completely different and no direct quantative comparisons
are presented. Based upon these examples, the numerical model did not
simulate the surf zone for engineering purposes, in contradiction to the
opinion of Horikawa (1978a, p. 229).

Liu and Mei (1975, 1976a) studied examples of currents near offshore and shore-connected breakwaters with their numerical model. Some observational evidences are cited, indicating similar qualitative trends but no quantitative comparisons are attempted.

In 1978, Allender, et al. (1978) measured the nearshore circulations during two storms at a beach near Chicago on Lake Michigan. A towed sea sled similar to that developed by Teleki, Musialowski, and Prins (1975) monitored bidirectional currents measured at six locations across the surf zone (see Fig. 81). Five-minute records were time-averaged to establish the current vectors. Data sets were repeated every 3 hours over a 27-hour storm period. The expressed purpose was to compare the field data with results from the two-dimensional numerical model developed by Berkemeier and Dalrymple (1975, 1976). This original version neglected the convective acceleration and lateral mixing stress terms.
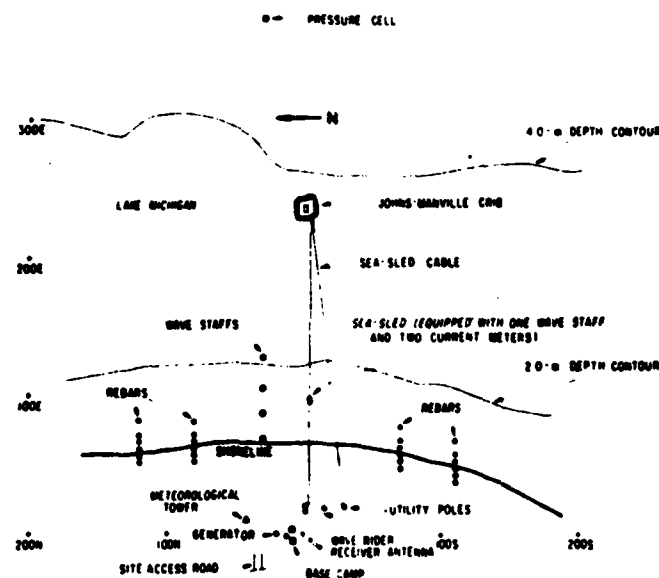
Figure 81. Plan view of experiment site and horizontal coordinate
system (after Allender, et al., 1978).

Model input included local bathymetry, offshore measured wave characteristics, wind histories, and local water level changes. Comparisons between model and observed $\bar{V}$ and $\bar{H}_{rms}$ for six different sled transits (sled position fixed) are shown in Figure 82. In general, for all examples, agreement is far from satisfactory for both currents and rms wave heights. For example, in Figure 82(b), the peak measured currents are less than 30 percent of the peak currents predicted. And, in most cases, the model energy levels in the surf zone are too high (e.g., Fig. 82,d). The peakedness of the model profile could be due to these wave height discrepancies

206
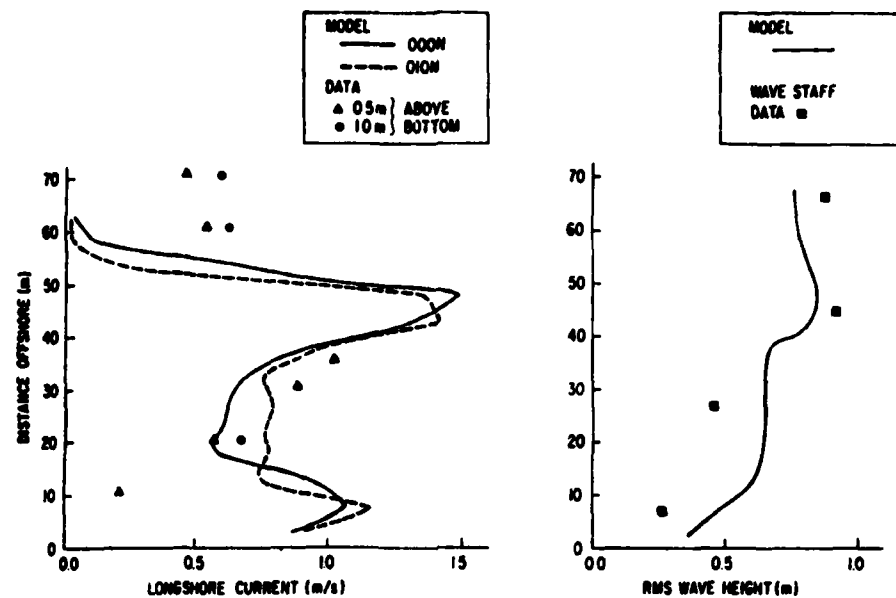
(a) Comparison of model and observed current profiles (a)
and wave heights (b). Model results for adjacent
Computational Rows are shown in (a).
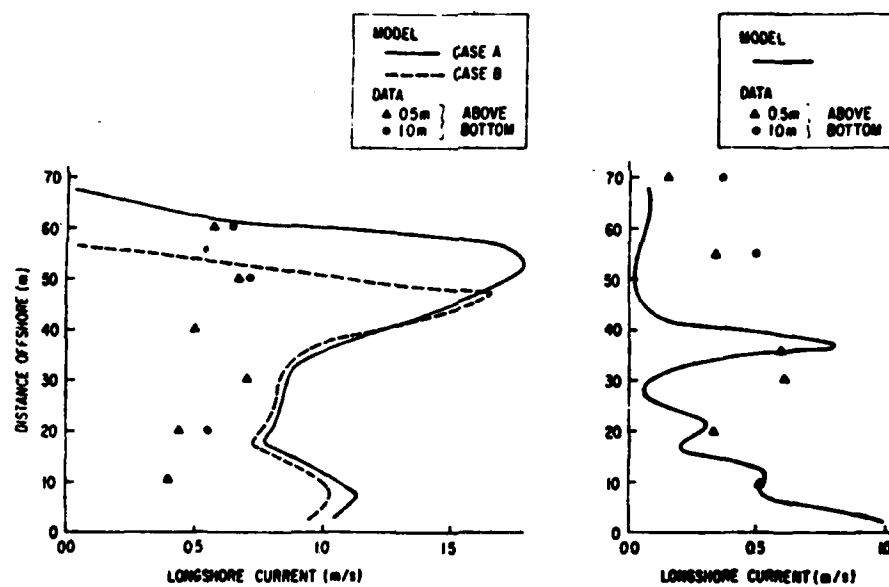
(b) Comparison of model and observed current profiles for
different wave climates at the beginning (Case A) and
end (Case B) of a sled transit (a) and for a less
severe wave climate (b).

Figure 82. Comparisons of field observations of nearshore currents and
numerical model of Birkemeier and Dalrymple (1976) (from
Allender, et al., 1978).

207
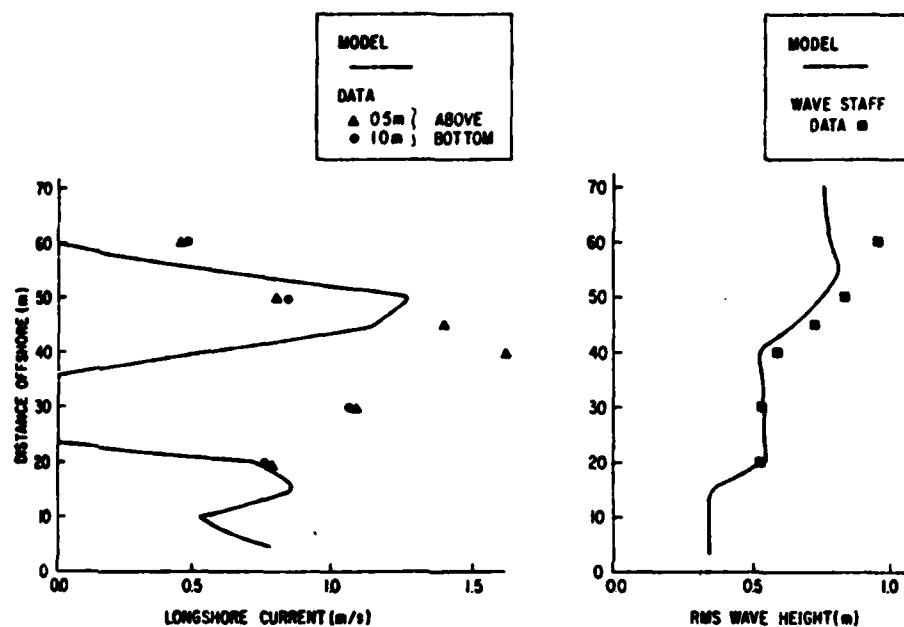
(c) Comparison of model and observed current profiles (a) and wave heights (b). Model underestimates differences between wave heights near breaking and heights inshore of breaker zone (b) resulting in sharply peaked model current profiles (a).
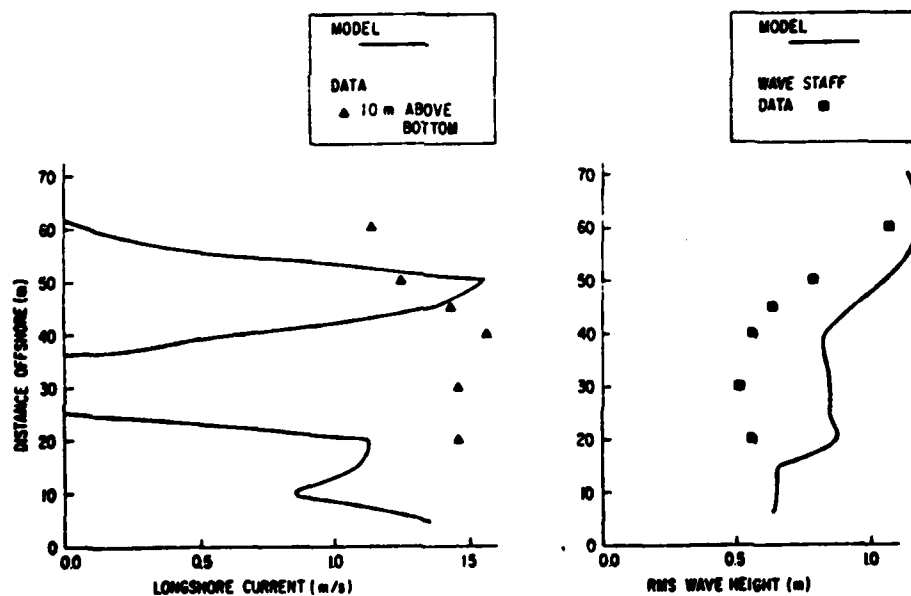
(d) Sharply peaked model current profiles (a) result from underestimation of wave height decay (b) across the surf zone.

Figure 82. Comparisons of field observations of nearshore currents and numerical model of Birkemeier and Dalrymple (1976) (from Allender, et al., 1978).--Continued

208
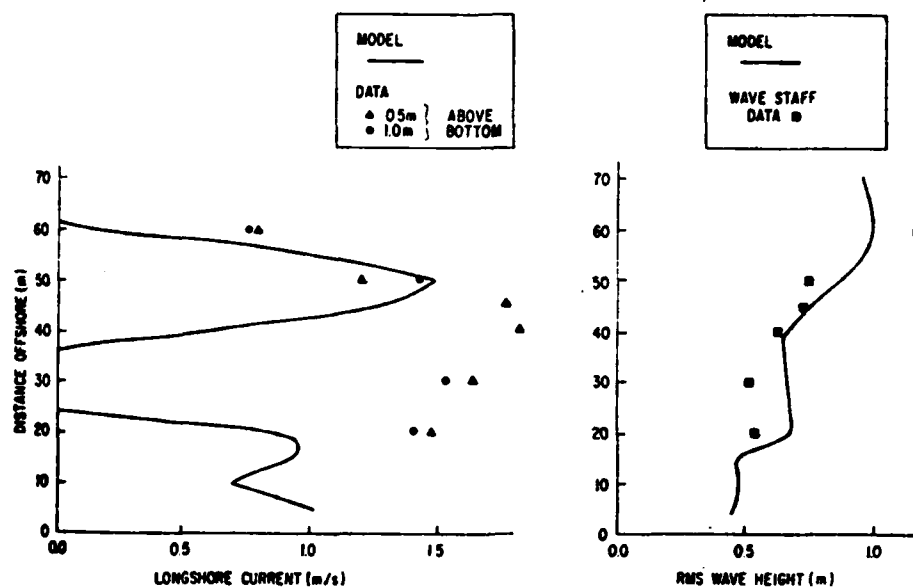
· (e) Additional comparisons of model and observed current
profiles (a) and wave heights (b) suggest that more
energy is extracted from the wave field inshore of
the breaker zone than the model predicts.

Figure 82. Comparisons of field observations of nearshore currents and
numerical model of Birkemeier and Dalrymple (1976) (from
Allender, et al., 1978).--Continued

plus the lack of lateral mixing stress term. Allender, et al. (1978) cited
the surf zone model by Battjes and Janssen (1978) to handle bar and trough
bathymetry and the addition of lateral mixing stress terms as needed improve-
ments.

The latest version (Ebersole and Dalrymple, 1979) includes the convec-
tive acceleration and lateral mixing terms but retains the wave breaking
ratio γ to specify the surf zone energy dissipation. Published comparisons
of numerical versus experimental results are unknown. As previously dis-
cussed (see Fig. 35), the present version contains sufficient numerical
viscosity to negate the quantitative reliability of the results for some
cases. All the above were finite-difference numerical models.

An example of a finite-element solution for the circulation eddy in
the lee of a harbor and some physical model data was previously presented
in Figure 36. No quantitative numbers were given to make a comparison.
This is also true for the finite-element model by Liu and Lennon (1978).

Finally, it should be noted here that the complete experimental results
of Gourlay (1978) from his laboratory experiments with an offshore break-
water (Fig. 8) are included in his Appendix 4. Sufficient current, wave
height, and MWL information is presented to serve as a check on any of the
numerical models cited. Whereas confined laboratory basins posed problems

209

when measuring uniform profiles on infinite beaches, they provide the ideal controlled environment for the much-needed data to check two-dimensional, nearshore circulation models. This is true for both the models based upon radiation stress theory discussed above and the newly emerging Boussinesq theory numerical models.

IV. BOUSSINESQ THEORY

Limitations in the range of application of Boussinesq theory compared with cnoidal and stream-function wave theories were shown in Figure 44. Here, those few examples of numerical solutions of the Boussinesq equations versus experimental results that have been published are presented. Also, the fact that a numerical theory carries with it inherent accuracy limitations based upon the numerical integration methods, grid sizes, and time steps used in the calculation is emphasized. Differences between theory and experiment may also be due to the poor choice of a numerical method with large truncation errors.

1. Wave Shoaling.

One-dimensional wave shoaling studies (solitary and periodic) were conducted first. Early pioneering efforts by Peregrine (1967)[52], Camfield and Street (1969)[59], Madsen and Mei (1969)[49], Madsen, Mei, and Savage (1970)[72], and Chan and Street (1970)[60] concentrated on the physics of solitary and periodic wave propagation (nonpermanent form, soliton development) rather than accuracy of numerical versus experimental data. For example, Figure 83(a) shows the calculated shoaling curves for a solitary wave ($n_o/d = 0.1$) on three different beach slopes by Madsen and Mei (1969)[49] compared with some experiments by Camfield and Street (1969)[59] for

---

[52]PEREGRINE, *op. cit.*

[59]CAMFIELD and STREET, *op. cit.*

[49]MADSEN and MEI, *op. cit.*

[72]MADSEN, O.S., MEI, C.C., and SAVAGE, R.P., "The Evolution of Time-Periodic Long Waves of Finite Amplitude," *Journal of Fluid Mechanics,* Vol. 44, Pt. 1, 1970, pp. 195-205.

[60]CHAN and STREET, *op. cit.*

[49]*Ibid.*

[59]*Ibid.*
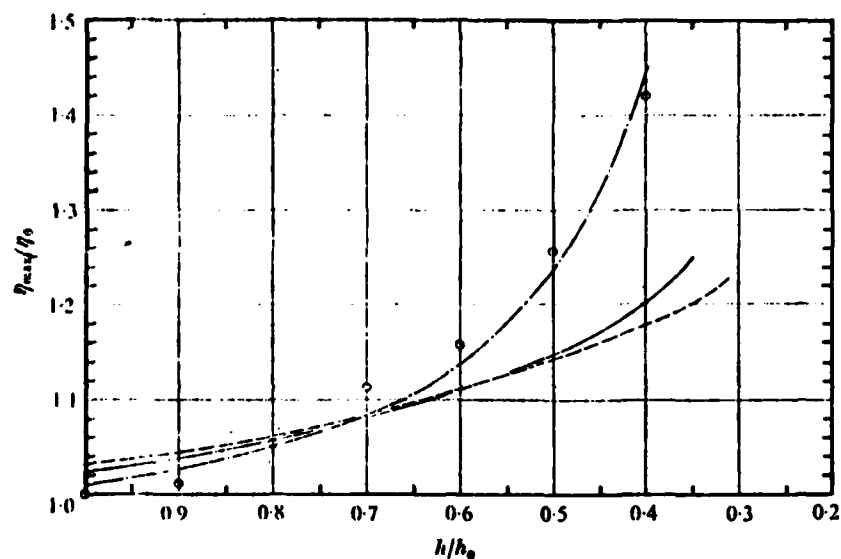
Amplitude variation with depth for initial amplitude to depth ratio, $\eta_0/h_0 = 0.1$. Calculated results for slopes, α: ——, 0.065; ———, 0.05; —·—, 0.023. O, experiments by Camfield & Street for $\alpha = 0.02$.
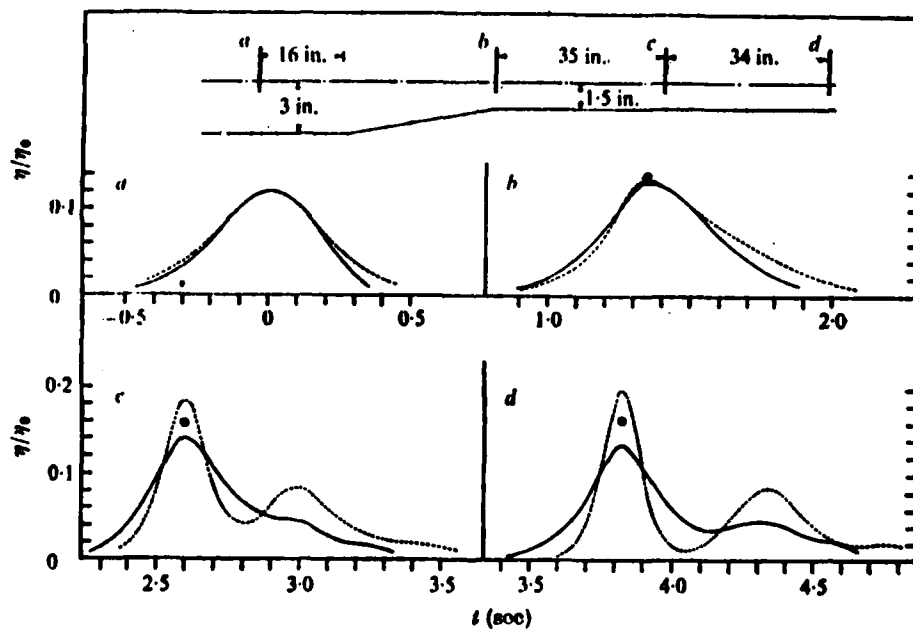
Figure 83. Comparisons of Boussinesq theory and experiments for wave shoaling (after Madsen and Mei, 1969)[49].

tan β = 0.02. The data are seen to agree well with the theory in the present report but they omitted data at large slopes because of too much scatter. Figure 83(b) displays even greater disparity when a second crest appears and this is attributed to the neglect of viscous damping. The Boussinesq

[49] MADSEN and MEI, *op. cit.*

211

theory correctly predicted the disintegration of the solitary wave and
phase of its second peak which was of main interest. Madsen and Mei numer-
ically solved the characteristic form of the equations by the method of
characteristics.

Abbott, Petersen, and Skovgaard (1978) have published the most exten-
sive engineering test results for the Boussinesq theory to date. Figure
84 presents their comparison of the theory (System 21 Mark 8, diamond)
against experiments made by the CERC in their large, outdoor wave tank
(Madsen, Mei, and Savage 1970).[72] The tank is 194 meters long, 6.1 meters
deep and 4.6 meters wide. Four second periodic waves with initial height
of 0.2 meter were observed shoaling on a 1:15 slope. Agreement was said
to be within 5 percent in elevation, over the whole test range.
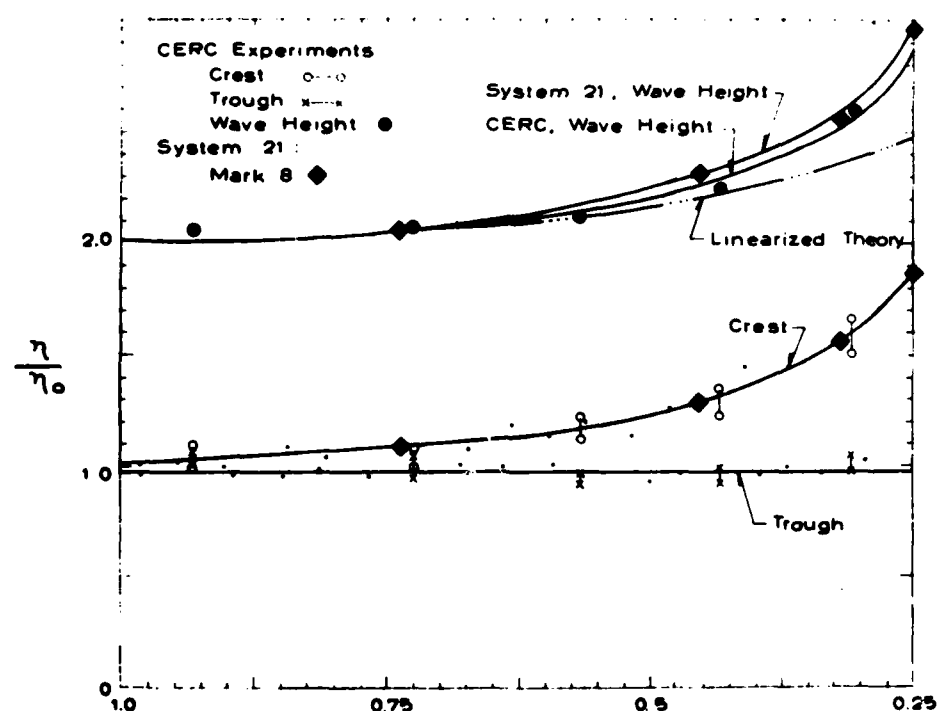
Figure 84. Comparison of numerical computation of shoaling waves obtained
using Boussinesq theory and CERC experimental results (after
Abbott, et al., 1978).

---

[72]MADSEN, MEI, and SAVAGE, *op. cit.*

212

Recently, new laboratory experiments on wave shoaling have been made by Svendsen and Buhr-Hansen (1977)[73] and Flick (1978)[74]. Some experimental results are shown in Figure 85 where it is again apparent that linear wave shoaling theory is far from correct. Most existing radiation stress models use linear shoaling theory to estimate wave height fields. The errors resulting could be excessive. Svendsen and Hansen utilized laboratory equipment with a special flap-type wave generator that eliminated free second harmonies in the wave profile. Test of the Boussinesq theory up to the breaking limit is an active research area and the boundary shear stresses must be included in the theory to affect a fair comparison. In this regard, Svendsen and Buhr-Hansen (1978)[75] have shown that

(1) Both wave height and profile show good agreement near breaking even though the H/h ratio is large;

(2) wave setdown is adequately described; and

(3) the horizontal velocity ". . . shows remarkably good agreement even at the breaking point . . ." with measured values.

The theoretical results were obtained analytically and not by numerical methods.

Field shoaling data for irregular waves are also needed to test the Boussinesq theory. The nonlinear process resulting in transfer of energy from the dominant frequency to harmonics via strong interactions is further discussed by Guza and Thornton (1978) where some field results are presented.

2. Two-Dimensional Tests.

Abbott, Petersen, and Skovgaard (1978) were primarily interested in testing the accuracy of their numerical model in two dimensions. For this purpose they duplicated a series of well-documented physical model experiments of the Danish harbor at Hanstholm. Because of the uncertainties associated with periodic wave tests, irregular waves based upon field-measured, time series of water surface elevations at the harbor entrance were employed. This illustrated the fact that numerical models can be

---

[73]SVENDSEN, I.A., and BUHR-HANSEN, J., "The Wave Height Variation for Regular Waves in Shoaling Water," *Coastal Engineering*, Vol. 1, 1977, pp. 261-284 (not in bibliography).

[74]FLICK, R.E., "Study of Shoaling Waves in the Laboratory," Ph.D. Dissertation, S.I.O., University of California, San Diego, 1978 (not in bibliography).

[75]SVENDSEN, I.A., and BUHR-HANSEN, J., "Prebreaking Behaviour of Waves on a Beach," *Euromech 102*, University of Bristol, July 1978 (not in bibliography).
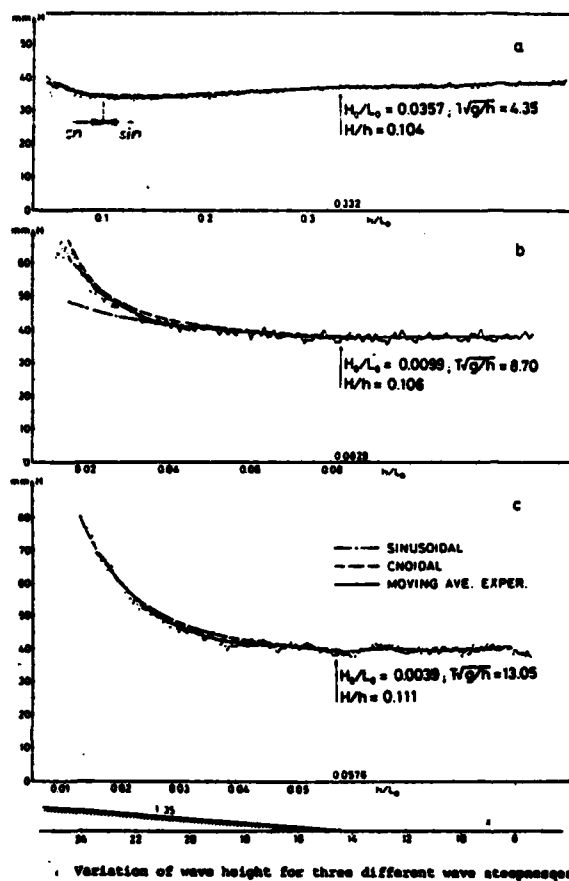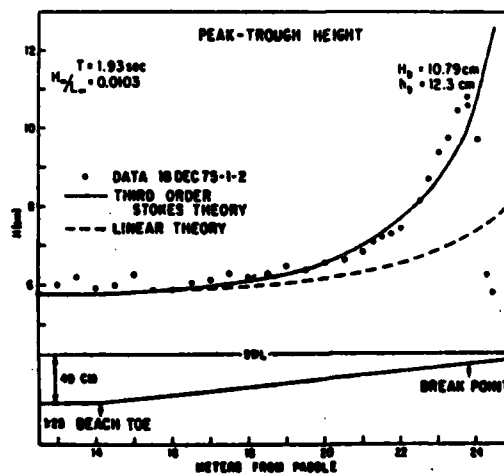
Figure 85. Some results of recent wave shoaling experiments: (a) after Svendsen and Hansen (1977),[75] (b) after Flick (1977).[74]

---

[75]SVENDSEN and BUHR-HANSEN, *op. cit.*

[74]FLICK, *op. cit.*

operated with any type of input boundary data. Their results are presented in Figure 86 (a, b, c). The surface elevation contours (a) result from $H_s = 1.5$ meters ($\bar{T} = 10.5$ seconds) at the harbor entrance and generate the wave amplification factors K shown in (c) for 10 different positions along the quay (b). The difference between rms wave heights in the physical and numerical models was small enough to provide an acceptable level of confidence in the accuracy of the models generated by the Boussinesq theory. Figure 46 is a perspective plot of waves in the outer harbor shown in Figure 86(a). This is the only published comparison of the two-dimensional numerical results with physical experiments found in the literature.

Comparisons of the two-dimensional computations with other analytical methods are also available. Figure 87 demonstrates a comparison for pure diffraction theory with the classical analytical results of Sommerfield for linear, light waves (Abbott, Petersen, and Skovgaard, 1978). The analytical wave orthogonals and fronts shown as dashlines are found to agree with the numerical methods as long as waves with very small amplitude (linearized wave theory) are tested..

Hebenstreit and Reid (1978)[76] tested their numerical model against some experimental results for solitary wave reflection from vertical barriers and linear theory (Snell's Law) refraction over a plane beach. The finite-difference algorithm devised by Street, Chan, and Fromm (1970)[77] was employed. Figure 88 demonstrates the numerical results (solid line) for wave reflection against the ripple tank measurements of Perroud (1957)[78]. The Mach-Stem effect was observed in the numerical work for incident angles between 20° and 45°, as expected. Numerical accuracy was considered quite good since the calculations neglected wall friction, the measured values were quite small, and it was not certain if steady state had been reached in Perroud's values.

The wave refraction studies were very revealing. Significant differences in wave crest bending (refraction) and wave shoaling were observed in the model as compared with that predicted by linear wave theory and Snell's Law for refraction. The Boussinesq theory simulations for solitary

---

[76]HEBENSTREIT, G.T., and REID, R.O., "Reflection and Refraction of Solitary Waves--A Numerical Investigation," Report 78-7-T, Oceanography Department, Texas A&M University, July 1978 (not in bibliography).

[77]STREET, R.L., CHAN, R.K.C., and FROMM, J.E., "Two Methods for the Computation of the Motion of Long Water Waves--A Review and Applications," Stanford University, Department of Civil Engineering, Technical Report No. 136, 1970 (not in bibliography).

[78]PERROUD, P.H., "The Solitary Wave Reflection Along a Straight Vertical Wall at Oblique Incidence," University of California, Berkeley, Technical Department, Series 99, Issue 3, Berkeley, Calif. (not in bibliography).
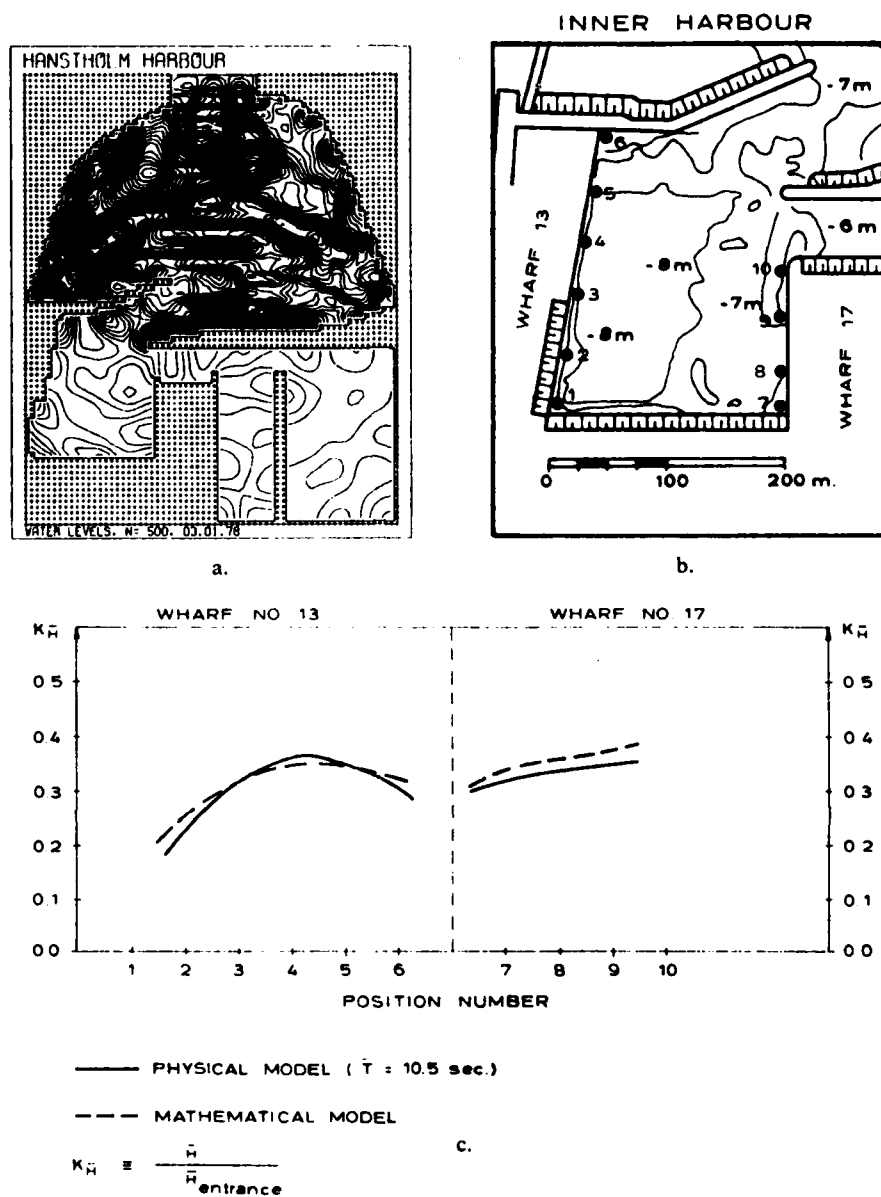
Figure 86. Comparison of wave amplication factors by physical and numerical
models in Hantsholm Harbor, Denmark (after Abbott, et al., 1978).
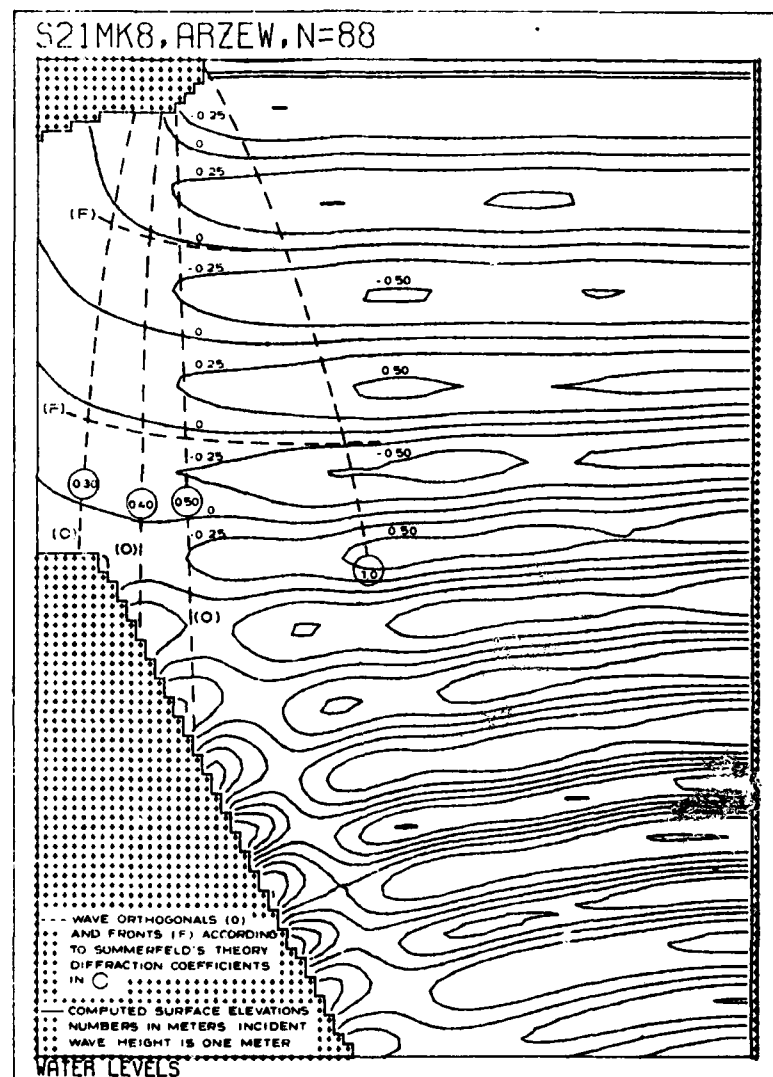
Figure 87. Comparison of pure wave diffraction by numerical model and classical diffraction theory for linear, small amplitude waves (after Abbott, Petersen, and Skovgaard, 1978).
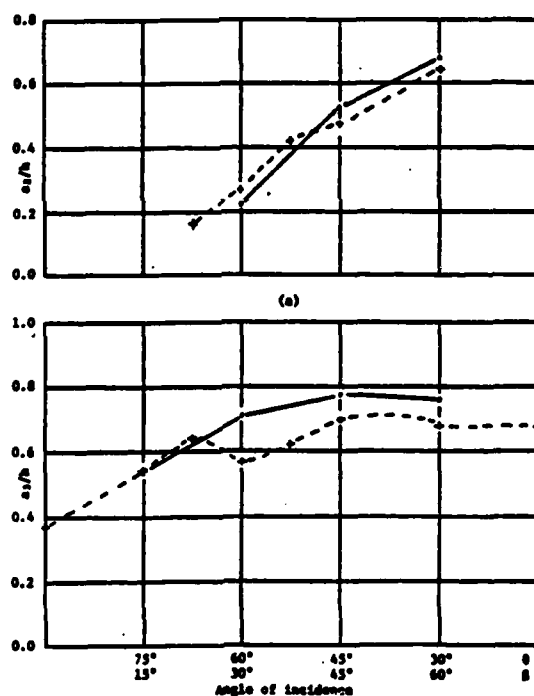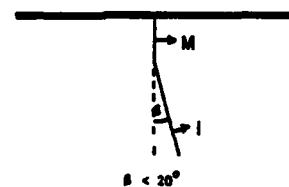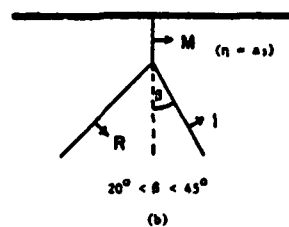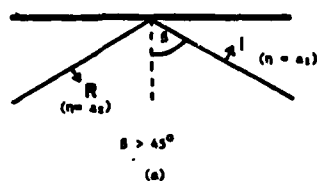
Figure 88. Comparison of pure wave reflection by numerical model and experiments of Perroud (after Hebenstreit and Reid, 1978).[76]

waves consistently produced a smaller degree of wave turning than predicted by Snell's Law. The reason was primarily in the phase speed which was far less in the numerical simulation than $\sqrt{gd}$. Wave heights due to

---

[76]HEBENSTREIT and REID, *op. cit.*

218

shoaling were always greater than given by linear theory which was consistent with the one-dimensional tests above (Fig. 85). Refraction coefficients for the $\alpha = 30°$ and $45°$ tests are shown in Figure 89. Unprimed values are based on angles calculated by Snell's Law. The numerical model showed less departure from linear theory at $30°$ than at $45°$. It was concluded that wave refraction techniques based on linear theory (Snell's Law) do not accurately predict the behavior of nonlinear dispersive waves in shoaling and refraction. Regarding wave refraction, it was also concluded that

> "The lack of similar laboratory and field work inhibits
> the range of conclusions that can be drawn from these
> results (Hebenstreit and Reid, 1978, p. 95).[76]

The limited comparisons between Snell's Law and laboratory measurements shown by Wiegel (1964)[22] exhibit systematic differences and wide scatter in some instances.

It would now appear that these measurements made in the 1950's must be supplemented by more sophisticated experiments to verify the new numerical models of the 1980's.
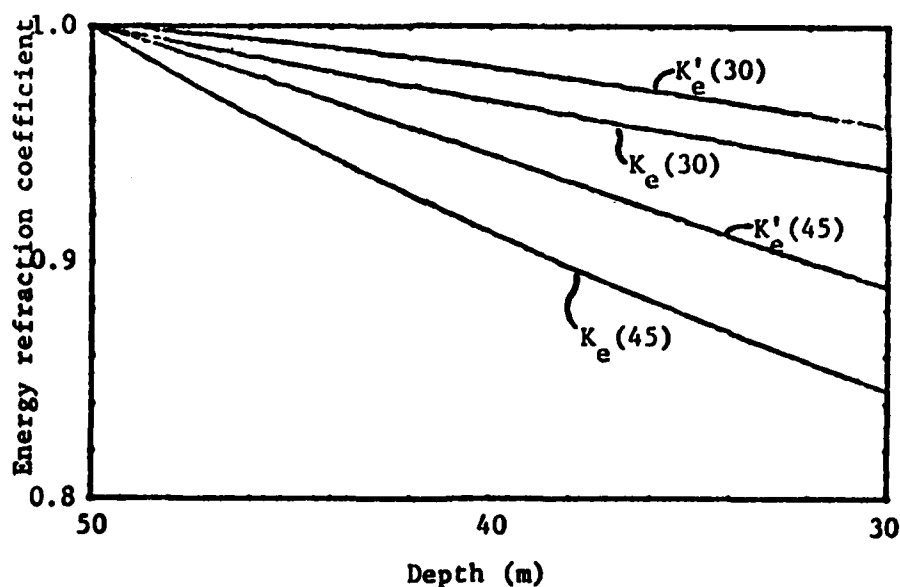
Figure 89. Comparison of pure wave refraction coefficients by numerical
model and linear wave theory (Snell's Law) (after Hebenstreit
and Reid, 1978).

[76]HEBENSTREIT and REID, *op. cit.*

[22]WIEGEL, *op. cit.*

V. SUMMARY OF STATE-OF-THE-ART

1. Physical Description.

A review of more than 60 years of observations and measurements of longshore current, nearshore circulations and rip currents worldwide reveals that longshore currents are primarily caused by oblique wave incidence and breaking at the coast which creates an excess longshore momentum flux to drive the current. In nature, the longshore current varies across the surf zone, along the coast, with depth and in time at any location. Typical values are less than 1 meter per second with maximum 3.5 meters per second or more. The use of continuous recording current meters at fixed points arrayed across the surf zone and down the coast in recent experiments has permitted researchers a look at far more details of the current structure. Literally millions of instantaneous values of these currents are now available from the two NSTS experiments and most have yet to be fully analyzed. The point velocity measurement in the longshore direction continuously varies in time due to the unsteadiness of nature and because many forces are at work together. Wind waves, surface winds, tides, and turbulent eddies from many sources all contribute to the signals recorded. The influence of surface winds has yet to be examined in detail. By definition, the longshore current is a time-averaged current. But, as of today, an appropriate temporal averaging time is not known. This fact plus the ability of these meters to record storm-induced currents has resulted in even larger longshore current values being reported.

Far more is known about horizontal circulations around vertical axes and resulting rip currents than is known about the vertical velocity distributions and circulations about horizontal axes in the surf zone. Many plausible mechanisms have been advanced for triggering rips to form and resulting neashore circulation cells to develop. Whatever the original mechanism, strong bottom currents in rips can create troughs in offshore bars to fix rip positions. The local bathymetry then controls the future flow patterns observed. Beach slope, profile, and sediment characteristics all play important roles in coastal hydrodynamics. A complete understanding of steep (reflective) and flat (dissipative) beaches has yet to be achieved. The existence and role of secondary currents has yet to be firmly established.

New instruments are being studied to measure surf zone currents. Even though problems exist with dynamic calibrations, the EM current meter remains the most proven and rugged type available for multiphase (liquids, sediment, air bubbles) flows in the surf zone, and the new slope array device should prove to be a valuable tool to examine the theory of longshore currents in both the field and the laboratory.

Because of the unsteadiness of nature and all the uncontrollable forces present simultaneously, controlled laboratory experiments have been conducted. Problems with the boundaries are being overcome so that infinite beach theories can be examined at the scale of the laboratory

tests. Additional laboratory experiments are needed to verify new two-dimensional numerical models applied to situations with irregular bathymetry, coastal structures (breakwaters, groins, etc.), and irregular wave fields.

A large number of wave, wind, geometry, fluid, and sediment factors interact to create the currents observed. Considerable simplification and idealization is necessary to formulate the theory and equations needed to obtain a solution.

2. Theory and Experimental Verification.

The time-averaged equations of horizontal motion and continuity, including radiation stress terms, have become the accepted basis for a theory of coastal hydrodynamics in the 1970's. Short-period wind waves when time-averaged create additional momentum flux terms, i.e. the radiation stress gradients, which become the primary driving forces in the theory. Solution of these three equations determines the three dependent variables of interest: the MWL change $\bar{\eta}$, the longshore current $\bar{v}$, and the cross-shore current $\bar{u}$. Wave heights must be specified a priori to affect a solution because the local wave energy appears in the radiation stress terms. This requires use of wave shoaling, refraction, diffraction, reflection etc. theory outside the breakers, a wave breaking criterion, and some model (general, empirical) of surf zone energy dissipation. Additional stress gradient terms appear in the motion equations to account for surface wind and bottom friction shears and lateral, internal, turbulent mixing stresses. All require semiempirical turbulence stress models with appropriate closure coefficients determined experimentally.

The wave breaking and surf zone empirism along with general knowledge of the required closure coefficients remain the weak links in the theory. The original theory makes extensive use of linear (Airy) wave theory. It forms the basis for calculation of the radiation stress components both outside and within the highly nonlinear surf zone and is used in wave shoaling, refraction, diffraction, etc. calculations. Applications to simplified geometrics with appropriate boundary conditions have traditionally been in the following categories:

(1) Mean water level changes (setdown and setup),

(2) uniform longshore current profiles, and

(3) nearshore circulation systems with rip currents.

The findings in these three areas are summarized below. Major modifications to the original theory have taken place in

(1) Bed shear-stress formulations,

(2) extensions to irregular waves,

(3) surf zone energy dissipation models,

(4) different mixing models inside the surf zone and beyond breakers, and

(5) by use of two-dimensional numerical models to compute solutions.

In general, the experimental data from both field and laboratory measurements substantiate the qualitative aspects and trends of the radiation stress theory. However, sufficient data under widely varying conditions are lacking to quantitatively verify all aspects of the theory, to select the best submodels, and to determine the closure coefficients. In some cases (e.g., rip current formulations and spacing) mechanisms are still being studied as part of the theory so that controlled laboratory investigations still play a major part in the research effort. Extensive new field data collection efforts (NSTS, ARSLOE) will significantly enhance efforts to verify the radiation stress theory and establish the needed coefficients in the near future.

This background provides a beginning in understanding the current state-of-the-art, and the radiation stress approach will continue to be researched. Further refinements will be made by use of nonlinear wave theories in both the radiation stress and wave field computations, use of better wave breaking and surf zone simulation models that include breaker type and beach profile features, determination of rational procedures to select closure coefficients, and incorporation of wave-current interactions in all aspects of the computation. Accurate two-dimensional numerical models will be constructed which include all the physically important terms and minimize the numerical inaccuracies. However, significant improvements in knowledge will always be limited by the time-averaged nature of the radiation stress approach.

In effect, a plateau of advancement has been reached in which a somewhat rational framework is now available for time-averaged coastal hydrodynamic theory. This approach will benefit from further research but only moderate improvements in fundamental, physical knowledge are anticipated because the time-averaging omits many local, time-varying details. Waves in the nearshore and surf zones are highly nonlinear. Solitons form and harmonics appear in nature with energy levels on the same order as the dominant period. Unsteady currents appear due to many forces including wave breaking rollers, eddies, and turbulence. The longshore current is by definition a time-averaged current yet a universally accepted averaging time is not known. Efforts to verify the radiation stress theory by new field measurements will be hampered by the need to average the time-series obtained over some time interval yet to be determined.

The Boussinesq theory offers the possibility to eventually raise the fundamental knowledge of coastal hydrodynamics to a higher level. No time-averaging is involved. Nonlinear wave propagation and resulting

222

wave height variations are all automatically produced as part of the calculation procedure. The unsteady asymetrical currents and instantaneous water surface variations as solutions to the governing equations are only obtainable with the aid of large high-speed computers. Solution techniques and applications are in their infancy. Wave breaking and surf zone simulations have yet to be implemented. Nonbreaking solutions have indicated significant differences with linear theories of wave height variation (Snell's Law, diffraction) to require additional experimental data for analysis.

The state-of-the-art summary of all the theories and experiments is presented below.

a. **Mean Water Level Changes.** Generally, the results are for normal wave incidence which in itself greatly limits their practicality. The original theory for wave setdown on plane beaches, based upon linear theory radiation stress, sometimes referred to as first-order theory, cannot be substantiated by the experiments. Consequently, equation (3) and its variations (eqs. 31 and 32) are incorrect. The nonlinear theory (Svendsen and Hansen, 1976) using first-order cnoidal wave theory and given by equation (155), has been verified right up to the breaking limit. It is repeated here

$$\bar{\eta} = -\frac{c^2}{2g}\left[\left(\frac{c}{gh} - 0.35\right)\overline{\frac{\eta^2}{h^2}} - 1.9\overline{\frac{\eta^3}{h^3}}\right]$$

A computer-based solution would facilitate and should be no deterrent to its use. The irregular wave models of Battjes (1974a) or Goda (1975) also derived setdown values close to measured data.

The original theory for wave setup as given by equation (35) can only be verified for relatively steep plane beach slopes (tan $\beta \gtrless 0.1$). It makes use of a constant breaker height-to-depth ratio γ in the surf zone which also has only been verified under steep beach conditions. Wave steepness is also a factor. Consequently, use of equation (35) and variations therefrom (eqs. 68 and 69) should not be generally applied to long-shore current theory as a correction for wave setup effects. This result is contrary to the popular belief that the theory applies to spilling breakers on dissipative-type (relatively flat) beaches. In fact, it has only been verified on steep laboratory beaches with plunging-type breakers.

The nonlinear setup theory of James (1973, 1974a) requires further experimental verification. No cnoidal theory in the surf zone has been attempted.

The irregular wave setup theory of Battjes (1974a) could not be confirmed by laboratory experiments although it gave reasonable agreement with limited field data. However, later efforts of a similar nature by Battjes and Janssen (1976) in which a more sophisticated, hydraulic jump model of surf zone dissipation was employed (eqs. 44 and 124) resulted in good to

223

excellent agreement with new laboratory data. This was for both H_{rms} and $\bar{\eta}$ variations across plane and bar-trough profiles. Improvement in the theory to match the data for low steepness waves is expected by incorporation of a wave breaking criteria over a range of wave heights with varying probability (following Goda, 1975).

Wave height variation across the surf zone and wave-induced setup are obviously related. All experimental evidence indicates that as beach slope decreases, the γ ratio departs further from a constant value across the surf zone. Distance from the breaker line is an important variable. A constant γ ratio in the surf zone is incorrect (eq. 33) for all beach profiles. The surf zone energy dissipation model based upon equation (44) with equation (124), i.e.

$$\frac{dF_x}{dx} + D = 0$$

with

$$D = \frac{1}{4} Q_b \bar{f} \rho g H_m^2$$

as developed by Battjes and Janssen (1976) is the most acceptable for all beach profiles at this time. Local wave heights in the surf zone are found by integrations so they logically depend upon all preceding seaward water depths plus the local depth. It is recommended that Battjes' model of the surf zone be studied further for regular wave setup and wave height decay. Additional comparisons with experimental data plus some minor modifications to the theory are also warranted.

Wave setdown and setup theoretical equations for oblique wave incidence (eqs. 39, 40, and 41) are not recommended. They are based on linear radiation stress theory, constant γ in the surf zone, and neglect the feedback of the longshore current induced on the wave motion. No comparisons with experimental data have been attempted.

b. **Longshore Currents.** If a rough estimate of the average longshore current is needed it is recommended that the expression

$$\bar{v} = K\sqrt{gh_b} \sin (2\alpha_b) \qquad K \approx 0.3\text{-}0.6 \qquad (170)$$

be employed. Komar and Inman (1970) empirically obtained $K \approx 0.6$ for the midsurf velocity $\bar{v}_{\frac{1}{2}}$ from results of sand transport studies. Dette (1974) obtained $K \approx 0.3$ from measurements in the North Sea and an analysis of all formulas including those based upon radiation stresses for the average current. Beach slope and bottom roughness do not appear in the empirically determined equation (169) since it has been found theoretically that the midsurf velocity is relatively insensitive to changes in these independent variables (Kraus and Sasaki, 1979).

The original model theory for uniform longshore current profile on a plane beach includes many assumptions and is based upon the idealized environment in Table 2. It has laid the foundation for all subsequent modified theories by providing both a qualitative and an order-of-magnitude agreement with the data. Consequently, equations (61), (66), and (67) plus those associated with them, must now be replaced by more general and accurate formulations. Longuet-Higgins (1972b) recognized these deficiencies and made some recommendations for improvements that were incorporated in the subsequent modified models. The major limitations of the original model theory were

(a) Bed stress model for weak currents and small angles,

(b) wave setup effects neglected,

(c) excessive lateral mixing stresses outside the surf zone, and

(d) results only applicable to plane beach slopes.

Table 3 identifies the modified theories. All include some wave setup effects based upon a constant γ ratio in the surf zone. For the reasons just discussed, it is concluded that further refinements are possible in the near future. With these limitations, two modified theories have emerged recently that have shown good comparisons with experimental data.

The theory of Skovgaard, Jonsson, and Olsen (1978) is more generally applicable (i.e., monotonically decreasing profiles) but requires numerical solution procedures. Its key strength is a different lateral mixing formulation outside the surf zone that matched some limited laboratory data for currents and also observations of mixing intensities in nature. Its major weakness is the strong current small-angle formulation for bed shear stress. This assumption is inconsistent with the fundamental physical fact that strong longshore currents appear when the angle of wave attack is large. Small incidence angles produce nearshore circulation cells, rip currents, and two-dimensional flow patterns.

The best available analytic theory at this writing is that recently developed by Kraus and Sasaki (1979), but holds only for plane beach slopes. It includes wave refraction effects, wave setup, different lateral mixing formulations within and beyond the breakers, and a weak current large-angle bottom stress formulation. For the latter assumption, the ratio of $\bar{v}_m/u_{Bm}$ is found to be relatively small in the field to justify the weak current large-angle model employed. The results compared favorably with new laboratory data (Fig. 66). The theoretical curves are fitted to the data by requiring the theoretical location of the maximum velocity $\bar{v}_m$ to match the experimental results. The dimensionless longshore current profile given by equation (91) and Appendix D (see also Fig. 30) with key dimensionless parameter P^* (eq. 92) should be employed. It should be tested against other laboratory and field data from which C_f and Γ values can be determined. For bar-trough profiles, a numerical solution procedure is necessary. More exact bottom shear-stress and surf zone dissipation models can then be employed in the numerical procedures.

The nonlinear current profile theory of James (1973, 1974a) requires further experimental verification. No application of cnoidal theory has been attempted. The limited comparisons with James' data were all favorable suggesting that further work needs to be performed. Longuet-Higgins (1972) stated the need to use nonlinear theory in S_{xy}.

Irregular wave theories of Battjes (1974a) and Goda (1975) need experimental verification. Battjes' (1974a) model should be modified to incorporate the Goda (1975) breaking criteria, the new Battjes and Janssen (1976) surf zone model, and include lateral mixing stresses. The available data should be curve fit to the theory at $\bar{v}_m$ to permit extraction of closure coefficients as by Kraus and Sasaki (1979). It was surprising to discover that additional theoretical effort with irregular waves has not been pursued since the mid-1970's. The proven existence of harmonics of the incident wave period in the surf zone and the detailed field test results from the NSTS experiments are two good reasons for further theoretical work with irregular waves.

c. **Closure Coefficients**. Modified bottom shear-stress and lateral mixing stress models were discussed in detail in Chapter 3 (see Tables 3 and 4). The more general expressions for $\bar{\tau}_{By}$ (e.g., eq. 80 by Bijker and v.d. Graaff, 1978)[26] for strong currents and large angles require numerical solution techniques. Solutions for arbitrary variations of bottom profile and roughness require numerical methods. The new surf zone energy dissipation models require numerical integration. Also, different models for lateral mixing stresses across the surf zone further complicate the analysis. In short, all factors indicate that oversimplification to obtain analytic solutions is being abandoned in favor of more general numerical solution techniques. Nonlinear and irregular wave theories require such methods.

The more general bed shear-stress formulations of Jonsson, Skovgaard, and Jacobsen (1974) (eq. 76); Liu and Dalrymple (1978) (eq. 78 and others not included); and Bijker and v.d. Graaff (1978)[26] (eq. 80) should be considered further. In some cases, the closure coefficients for $\bar{\tau}_{By}$ are in themselves calculated from knowledge of the local bed roughness and wave characteristics. This procedure is used in the Jonsson, Skovgaard, and Jacobsen, and Bijker and v.d. Graaff models. It is preferred since it utilizes more fundamental fluid mechanics stress coefficients based upon uniform open channel flow and oscillatory water tunnel experiments. The Bijker model especially warrants further study since it explicitly defines the location above the bed where the velocity components are vectorially combined.

The more general lateral mixing stress models of Skovgaard, Jonsson, and Olsen (1978) and Kraus and Sasaki (1979) (see Table 4) are preferred since they separate the reduced mixing outside the surf zone. Both are variations of earlier efforts and warrant further study.

---

[26]BIJKER and GRAAFF, *op. cit.*

Closure coefficients required in these models can be obtained by
fitting the theory for longshore current profile to available data.
Some results are given in Table 9. They must all be used with caution
since they only apply to the theory and limited range of data involved
in their determination. No state-of-the-art values will be given here
for this reason. The wide range of time-averaged bottom friction
coefficients in the literature is partly due to the many assumptions
in the time-averaged bed shear-stress models employed. Use of the maxi-
mum longshore current and its location to fit the data is better than
use of mean values which are relatively insensitive to bed slope and
bottom roughness. Both friction and mixing coefficients are calculated
from the data by this method. An alternate method would be to specify
the bed roughness, calculate the friction coefficients from fundamental
theory, and use the longshore current profile data to estimate mixing
coefficients. These closure coefficients would be based on the overall
longshore current profile and can be obtained from field or laboratory
experiments. Local closure coefficients in the surf zone can also be
obtained directly from equation (42), local velocity measurements in
the surf zone and independent measurements of S_{xy}. This was done by
Huntley (1976) and Thornton (1980) who both neglected the lateral mixing
stress gradient in the analyses. It may be possible to independently
obtain estimates of $\bar{v}_L$ from the velocity time histories using auto- and
cross-correlation techniques. Then the full equation (42) could be uti-
lized to calculate friction coefficients. Only detailed and extensive
two-component field data are appropriate for this purpose.

The empirical wave breaking ratio, γ_b and surf zone energy dissi-
pation model complete the list of required coefficients to theoretically
estimate current profiles. As stated by Battjes (1978a), use of a con-
stant γ ratio imparts an excessive sensitivity of the currents to bottom
profile variations. Comments above for wave setup and setdown are equally
appropriate for longshore current. It is anticipated that some fundamental
new concepts in wave breaking criteria will result from the present numeri-
cal modeling simulations of the wave breaking process.

d. Nearshore Circulation Systems. All available models are based
on vertically integrated or depth-averaged flows. This implies that
the dominant motions are horizontal and relatively uniform with only
weak secondary currents in the vertical taking place. Little data are
available to substantiate (or refute) this assumption.

The two-dimensional equations of motion written in conservation form
(eqs. 107, 108, and 109) are preferred over the Eulerian form since the
discharges per unit width include wave-induced mass transport. Many
terms were discarded in the early analytic theory. For general application,
all must be included which means numerical solution methods are now neces-
sary. Additional interaction stresses resulting from mean flow, oscilla-
tory motion, and turbulence interactions are present but for lack of suffi-
cient detailed data, they will continue to be lumped with boundary shear
and lateral shear terms.

All the presently available numerical models have serious limitations and none are recommended for engineering purposes. The earlier versions omitted important terms in the momentum balance equations, and the latest models simply lack accuracy due to excessive truncation errors in the algorithm employed. The lateral (eddy viscosity) mixing stress terms physically smooth the current profiles, circulation patterns, and rip current jets. The present models display evidence of excessive numerical viscosity (Fig. 35) that translates into numerical inaccuracy. Calibration of such models requires use of physically unrealistic closure coefficients that could be a disaster for use as predictive models. The evidence to support this conclusion is vividly displayed in the generally poor comparisons between model and experiment shown in Figures 80, 81, and 83.

As outlined by Vreugdenhil (1980), it is clear that the Delft Hydraulic Laboratory has begun a concerted effort to develop a comprehensive numerical model. It is by far the best effort discussed to date because it includes all the physically important terms and proper numerical methods to ensure their accuracy in the simulation. The report by Vreugdenhil (1980) discusses the model requirements, equations, and numerical procedures. Calibrations, tests, and other results will be reported when completed. It is clear that additional comprehensive modeling projects are desirable as both an alternative and in support of physical model tests and expensive field experiments.

Previous efforts were hampered by lack of data to calibrate, verify, and test the two-dimensional models. Some additional controlled laboratory data are now available (Gourlay, 1978; Visser, 1980; Mizuguchi, Oshima, and Horikawa 1978)[67] and can be obtained for this purpose. Also, the extensive NSTS field data tapes can be used.

Some fundamental problems remain with the time-averaged simulation models. The wave height fields must be specified by other means. For this purpose, the model developed by Noda, et al. (1974) for wave shoaling and refraction that includes current interactions remains a popular choice. Wave diffraction, reflection, transmission (breakwaters), etc. transformations must also be prescribed. The numerical programs for wave height transformation may require considerable development effort, by themselves, if not already available. In addition, it was seen earlier in this chapter how direct wave refraction calculations by Boussinesq theory produce significant differences with Snell's Law. This indicates that nonlinear refraction and other wave transformation theories should be employed. Finally, the correct numerical simulation of circulations, eddies, and subgrid-scale turbulence is still an active research area in computational hydraulics.

A verified theory to predict rip current spacing for all possible conditions does not exist. The best engineering estimate available is the semiempirical hypothesis of Sasaki (1977) summarized in Figure 78 and equations (167), (168), and (169). No theory exists for rip current

---

[67]MIZUGUCHI, OSHIMA, and HORIKAWA, *op. cit.*

flow rate, width or size, and surprisingly there are little field data
to compare with numerical simulations.

Finally, for near-normal wave incidence, vertical gradients in the
velocity fields can create vertical radiation stress gradients to drive
circulations about the horizontal axis. No attempts were uncovered to
apply radiation stress theory to this case for estimates of circulation
currents schematized in Figure 22.

e. **Boussinesq Theory**. Research has essentially just begun. Out-
side the surf zone, numerical shoaling results compare very favorably
with experiments. More research and comparisons are necessary near the
breaking limit. Only one comparison of two-dimensional wave transforma-
tions against physical laboratory measurements has been published in
the literature (Fig. 86). Much more evidence is desired.

The correct form of the Boussinesq equations for variable bathy-
metry has yet to be determined. No wave breaking, surf zone, wave setup,
or longshore current simulations have been reported in the literature.

Great care is required in the numerical methods to ensure accuracy
in wave amplitude and phase propagation. Large and high-speed computers
are necssary. For these reasons, future developments will remain for
research purposes rather than engineering applications.

The analogy with time-averaged tidal hydraulics analyses of the
1950's was cited earlier. The digital computer permitted calculations
within each tidal period to enhance knowledge. Guza and Thornton (1978)
in their article on time variability of longshore currents make a similar
comment. In the 1950's, large-scale ocean circulations were thought
to be driven by average winds to produce generally weak and horizontally
smooth currents. The relative importance of drag and eddy diffusivity
terms was discussed, as we have summarized in this report. Nonlinear
terms were then needed to explain the jetlike Gulf Stream; as their
importance in rip current dynamics is now recognized. Still later, instan-
taneous measurements showed large temporal and spatial fluctuations,
in contrast to observations with floats that matched the theory for
yearly means. Large cooperative experiments were then conducted in an
effort to determine the importance of the shorter scale fluctuations
on the longer scale flows. These final questions remain unresolved.
Considering the gross nonlinearity of the surf zone and the strong
analogy cited with oceanic research, Guza and Thornton (1978) concluded
that it is overly optimistic to expect simple solutions to mean nearshore
flows.

The Boussinesq theory does offer some possibilities in this regard
by going beyond the time-averaged mean to look within each wave period
at the physics taking place.

CHAPTER 5

CONCLUSIONS AND RECOMMENDATIONS

The following conclusions and recommendations are based on the entries in the *Surf Zone Currents,* Annotated Bibliography," (Vol. II) and the review and summary of physical processes, theory, and experimental verification described in this report.

I. CONCLUSIONS

1. General.

A general time-averaged coastal hydrodynamic theory now exists based upon sound conservation laws of physics and radiation stress principles. It has been proven to qualitatively describe the mean water surface variations and currents generated by short-period surface gravity waves as shown by laboratory and field data comparisons. However, to improve the quantitative accuracy, further research and development is required. Specific conclusions on various aspects of the time-averaged theory are presented below. Two inherent shortcomings of the method are:

(a) Wave height fields must be specified by independent methods. Are these methods accurate?
(b) Closure coefficients must be determined from field data fitted to the theory. The proper averaging time for the field data is not known.

Spatial and temporal variability of field data cannot be explained nor studied by the method.

The Boussinesq theory offers an alternative approach. It is founded in the same conservation laws of physics but no time-averaging takes place. Instantaneous water surface and current variations are considered. Consequently, the two shortcomings listed are not present in this method. To date, only conditions up to breaking have been simulated by the theory. It is concluded that research efforts to extend the method into the surf zone should be conducted. Specific conclusions on the Boussinesq theory are given below. The theory will primarily serve as a research tool to further understanding of the physical processes taking place in the surf zone within each wave. Consequently, it will also serve to improve the time-averaged method.

Both theories rely on wave breaking and surf zone empirism that requires fundamental research for improvement.

2. Time-Averaged Radiation Stress Theory.

a. General.

230

(1) Nonlinear wave theory (e.g., cnoidal waves) should be studied further. Cnoidal theory fits the data best for wave setdown near breaking. Its use for wave field specification and in radiation stress calculation should be considered in a general higher order current theory.

(2) Irregular wave theory (e.g., Battjes and Goda theory) should be studied further. Surf zone probability models could be devised to include the wave harmonics observed in nature. Lateral mixing terms must also be included.

(3) Analytic theories require too many assumptions and thus limit generality and accuracy. Computer solutions are now necessary for both longshore current (one-dimensional) and nearshore circulation (two-dimensional) computations.

b. Mean Water Level Change.

(1) First-order (linear) theory gives incorrect results for wave setdown. Cnoidal (nonlinear) theory has been verified to near the breaking limit. Use first-order cnoidal wave theory for normal incidence setdown calculations.

(2) First-order (linear) theory is only verified for wave setup on steep plane beaches (tan $\beta \doteq 0.1$) where constant γ ratio is also observed. Use of a constant γ ratio across relatively flat (tan $\beta \doteq 0.01$) and bar-trough profiles in incorrect. New surf zone energy dissipation models (Battjes and Janssen) used to compute wave setup show promise but need further research. Use of wave setup theory based upon constant γ ratio to modify longshore current formulas gives incorrect emphasis on bottom profile. Nonlinear wave theories for wave setup need further research.

(3) Special formulas for setdown and setup under oblique wave incidence should be avoided. Solution must be based on coupled two-dimensional equations where wave-current interaction effects are included.

c. Longshore Currents.

(1) Use $\bar{v} \approx K \sqrt{gH_b} \sin 2\alpha_b$ (K $\doteq$ 0.3-0.6) to roughly estimate the average longshore current.

(2) The original model by Longuet-Higgins (1970), which gives qualitative results, paved the way for all subsequent versions, but is now relatively incorrect.

(3) The analytic model of Kraus and Sasaki (1979) should be used for plane beach computations on relatively steep beaches.

(4) No verified analytical or numerical model exists to compute currents on relatively flat (tan $\beta \cong 0.01$) or bar-trough profiles.

(5) Existing nonlinear and irregular wave current theories require some modification and extensive comparisons with laboratory or field data sets in order to be useful.

(6) The model of Kraus and Sasaki (1979) should be developed further to include flat and bar-trough profiles plus more general bed-stress formulations. Numerical solution methods will then be required.

(7) Complete strong current large-angle bed-stress formulations should be considered in future models where numerical methods are employed. The model devised by Bijker and v.d. Graff is recommended for further study since fundamental closure coefficient and boundary layer principles are applied.

(8) Different lateral mixing stress models should be employed within and outside the breakers. Further research is needed to determine which are most accurate.

(9) No recommendations for state-of-the-art closure coefficients are made. Continued indirect and direct determination from field data is required. Bed friction factors must be correlated with relative boundary roughness. Eddy viscosity closure coefficients should be related to surf zone, Reynolds and Iribarren numbers.

(10) Wind-induced longshore currents can be created in some numerical models but have yet to be studied in detail.

d. Nearshore Circulations.

(1) All theory is based on the assumption (not verified) that the two horizontal motions dominate the flows present nearshore. No three-dimensional theory or models have been attempted.

(2) The two-dimensional, conservation form equations of motion including all acceleration, pressure and stress gradient terms should be employed. Additional interaction terms discussed by Harris and Bodine (1978) are incorporated indirectly by the closure coefficients.

(3) None of the existing two-dimensional models are recommended for engineering use. All exhibit serious limitations due to neglect of important terms or excessive numerical inaccuracies. Additional comprehensive two-dimensional numerical modeling efforts are desirable.

(4) Specification of wave height fields by linear wave theory (shoaling, Snell's Law, diffraction theory) is questionable. Existing numerical schemes for this purpose should be revised to incorporate nonlinear (cnoidal) theory.

(5) Numerical simulation of circulations, gyres, eddies, etc. in free-surface flows is still an active research area in computational hydraulics. The eddy viscosity model is only one of many new turbulence closure models being investigated.

(6) No single theory is valid and verified to predict rip current spacing. Semiempirical engineering estimates are available. While many plausible mechanisms exist to trigger rip currents, bathymetry usually controls their location.

(7) Radiation stress principles can be employed to study vertical circulations about a horizontal axis. No such studies were found in the literature.

3. Boussinesq Theory.

a. General.

(1) The complete and correct form of the equations of motion for variable bathymetry applications have yet to be finalized. Limited applications to date have been for gradually varying bathymetry.

(2) Higher order accuracy numerical methods are required for a solution and are still in the development stage.

(3) Considerable research and development remains for application to surf zone hydrodynamics.

232

b. <u>Specific</u>.

      (1) The theory for plane slopes has been verified near the breaking limit. Further research at the breaking limit is needed, including wave setdown investigations.

      (2) Limited evidence available suggests the theory is applicable to two-dimensional nonbreaking wave transformation studies as presently conducted with physical hydraulic models.

      (3) No wave breaking nor surf zone simulation results have been published in the open literature. Such efforts have been recommended and are currently being pursued by European researchers in coastal hydrodynamics.

      (4) Large high-speed computers are required for accurate simulations.

4. <u>Data Base and Measurement</u>.

a. <u>Data</u>.

      (1) The overall data base to verify the theories is inadequate. However, new laboratory experiments (Visser, 1980; Gourlay, 1978; Mizuguchi, Oshima, and Horikawa, 1978) and field data (NSTS) are becoming available for this purpose.

      (2) Results of the recent extensive NSTS field experiments need further detailed study. The results are readily available for this purpose.

      (3) Additional controlled laboratory tests are needed to study and verify aspects of both theories. A spiral wave maker can be readily designed for this purpose. Tests with relatively flat beach slopes and bar-trough profiles are critically needed to verify new surf zone energy dissipation models.

      (4) New, extensive field investigations should be delayed until analyses of the NSTS results are completed.

      (5) Field investigations of coastal hydrodynamics have yet to be made on Gulf of Mexico beaches. Experiments on this relatively flat low-energy coast are needed.

      (6) No data on the vertical current profiles over the water column exist except for some rip current profiles. Also, long-term current time histories are needed for statistical purposes at selected locations.

      (7) Further extensive use of the slope array device (Seymour, et al.) for direct measurement of S_{xy} and α is recommended.

b. <u>Measurement</u>.

      (1) The use of extensive arrays of fixed current meters in the surf zone is the best way to obtain sufficient and useful field data for verification of theory.

      (2) Current meters with flat gains beyond 2 hertz are needed to obtain additional turbulence information in the surf zone.

      (3) The STEREO-BACS system could be significantly improved to overcome problems with camera drift and surfboarding drogues but will be limited to observations of nonstorm events.

II. RECOMMENDATIONS

It is recommended that fundamental, long-range research be conducted to extend the Boussinesq theory into the surf zone. For practical engineering investigations of coastal hydraulics, knowledge from Boussinesq simulations will be most useful to improve the time-averaged radiation stress approach and its eventual coupling to sediment and pollution transport models. Therefore continued refinement of radiation stress numerical models is also recommended to include nonlinear and irregular wave effects and improved wave breaking and wave energy dissipation models in the surf zone.

FIELD OBSERVATIONS - LONGSHORE CURRENTS

No	Name	Date	Location	No obs.	Wave Data Range			Beach Slope	Mean Longshore Current		Observation Method for Current			Variation Measured		Remarks
					Height H_B (meters)	Period T_B (seconds)	Angle θ_B (degrees)		Maximum m/sec	Mean m/sec	Float	Dye	Meter 1-propmeter 2-EM	Long shore	Surf Zone	
1	Putnam, Munk, Traylor	1949	Oceanside California	18	1.4 - 2.7	7-15	5-17.5°	0.016 - 0.031	1.7	0.9	x	x				Earliest Known Field Data
2	Shepard	1950	Southern California	2012					0.5		x					Direction of chief Concern
3	Shepard, Inman, Quinn	1950 1951	Torrey Pines California	33	0.5 - 2.0	6-16	0 - 7°	0.014 - 0.035	0.4	0.1	x			x		
4	Moore, Scholl	1961	Ogoturuk, Alaska	71	0.1 - 1.8	1 - 7.1	0 - 45°	0.2	0.4	-	x	x				Rough
5	Galvin, Savage	1966	Nagshead North Carolina	5	0.5 - 2.4	5.2-12.3	3.2- 12°	0.026 - 0.030	1.3	0.6	x					
6	Ingle	1966	Southern California Beaches	100	0.9 - 2.1		1 - 16°	0.01- 0.05	1.3	0.3	x	x			x	
7	Harris	1965	Durban South Africa	7	1.4 - 1.7	6 - 9	3 - 12°	Varied- Bar				x				Rips = 1.5 - 2 ft/sec 100-200 wide
8	Harrison, etal	1968	Virginia Beach, Virginia	77				0.0122 - 0.102	1.0			x				
9	Sonu	1967	Outer Banks North Carolina								x	x	x_1		x	unsteadiness detected
10	Thornton	1969	Fernandina Beach Florida	6	0.5 - 1.7	4 - 11	3.5 - 10°	0.019 0.035	1.5	0.6	x	x	x		x	First use of EM meter

FIELD OBSERVATIONS - LONGSHORE CURRENTS

No.	Name	Date	Location	No. Obs.	Wave Data Range Height H_B Meters	Period T_B Seconds	Angle θ_B Degrees	Beach Slope	Mean Longshore Current Maximum m/sec	Mean m/sec	Float	Dye	Meter 1-prop 2-EM	Variation Measured Long shore Zone	Surf Zone	Remarks
11	Komar, Inman	1970	So. Calif. Mexico	22			2.8 – 16°	0.034 0.138	0.6	0.3	x	x		x		
12	Bruno	1971	Florida		0.5-0.6	2 – 12	< 42°		0.3			x				Leo Observ.
13	Fox, Davis	1971	Holland Michigan		< 0.9	2 – 6	± 20°		0.7 South 0.4 North		– Unknown –	x				
14	Horikawa, Sasaki	1972	Shonan Coast, Japan		0.6 - 2.4	4 – 7					x	x	x_1	x	x	Nearshore Circulation Rip Currents
15	SONU	1972	Seagrove Florida		0.2 - 0.5	4 – 10	< 10°		0.5		x	x	x_1	x	x	Nearshore Circulation 5.5ft/sec-rip Depth Variat
16	Eliot	1973	Durras Beach Australia						1.04		x		x_1			rips observed
17	Tsuchiya, Shibano	1973	Ogata Coast, Japan			6 – 10			0.4							
18	Dette, Fuhrboter	1974	Sylt, North Sea	>150	0.9 - 3.4 Max				1.5±0.3	1.0			x_2	x		15 minute duration time Variations
19	Huntley, Bowen	1974 1975 1976	Saunton Beach England	C				0.01		0.1-0.4			x_2		x	
20	Manohar, Mobarek, Morcos	1974	Burullus, Egypt	54					0.8	0.3 ±	x				x	

236

FIELD OBSERVATIONS - LONGSHORE CURRENTS

No	Name	Date	Location	No Obs	Wave Data Range Height H_B (meters)	Period T_B (seconds)	Angle θ_B (degrees)	Beach Slope	Mean Longshore Current Maximum m/sec	Mean m/sec	Observation Method for Current Float	Dye	Meter 1-prop 2-EM	Variation Measured Long Shore	Surf Zone	Remarks
21	Sasaki	1974	Ajigaura Japan	40±	1.2-2.1	8-14	8.5-14.5		0.6	0.3±	X			X	X	Floats "surfboard" 1.6ft/s rips
22	Sharaf	1974	Nile Delta Egypt							0.34	X	X				
23	Balsille	1975	Pt. Mugu California	633							X	X				Leo expts.
24	Lee	1975	Wisconsin Coast Lake Michigan	14	0.07-0.6	2.5-5	5-28°	0.03-0.12	0.4	0.2	X	X				For sediment transport
25	Murty, Veerayya, Varadechari	1975	Calangute Beach, India		1.0-3.5	7-12	5-15°	3-17°				X	X_1			currents not completely 2-D
26	Wood, Meadows	1975 1976 1977	Eastside Lake Michigan	C	0.2-0.6	3.5-4.2	15-21° ±5°		1.0	<0.7		X	X_2	X	X	Depth variations measured
27	Maresca, Seibel	1976	Northern California										X_2		X	CEC Vol. I photogrammetric techniques
28	Brenninkmeyer	1977 1978	Salisbury, Mass.	C			10±			1.0±			X_2		X	Depth variations measured (3-D)
29	Kelly, Bowen	1977	Canada					0.05-0.03	1.2	0.1	X			X		
30	Allender Ditmar Harrison Paddock	1978	Zion, Ill. Lake Michigan		0.5-1.5	3.8-6.5	20-30°	Bar-trough	1.0-1.8				X_1	X	X	Depth Variation Measured

237

FIELD OBSERVATIONS - LONGSHORE CURRENTS

No	Name	Date	Location	No Obs	Wave Data Range Height H_B (meters)	Period T_B (seconds)	Angle θ_B (degrees)	Beach Slope	Mean Longshore Current Maximum m/sec	Mean m/sec	Observation Method for Current Float	Dye	Meter prop. 2-m.	Variation Measured Long Shore	Surf Zone	Remarks
31	Guza, Thornton	1978 1980	Torrey Pines, California										x_2	x	x	
32	Nummedal, Finley	1978	Debidue Beach So. Ca.	250				mild	1.5	0.2-0.4						LEO observations
33	Kraus, Sasaki	1979	Niigata Japan		1.0± RMS	4.1	9°	0.025	0.8	0.7	x				x	
34	Massel Zeidler (eds)	1980 (1974)	Gdansk Poland													
35	Murray	1980	Near Suez Canal, Egypt										x_2	x		Depth variations
36	Sasaki Igarashi Harikai	1980	Haranomach Beach Japan			8-14		0.01	> 2 m/sec		x					Also lab model studies
37	Guza, Thornton	1981	Santa Barbara California										x_2	x	x	
38	Shepard Sayner	1953	LaJolla California							0.3					x	Scripps Pier

238

APPENDIX B

LABORATORY OBSERVATIONS - LONGSHORE CURRENTS

No	Name	Date	Location	No obs.	Wave Data Range			Beach Slope	Mean Longshore Current		Observation Method for Current			Variation Measured		Remarks
					Height H_B (meters)	Period T_B (seconds)	Angle θ_B (degrees)		Maximum m/sec	Mean m/sec	Float	Dye	Meter 1-prop 2-EM	Long shore	Surf Zone	
1	Krumbein	1944	U. Calif. Berkeley		0.02-0.09	0.9-3.5	15°	30°	0.2							Movable Bed
2	Putman, Munk Traylor	1949	F.M. Lab Berkeley California	37	0.04-0.14	0.2-0.7	3.18-17.5	0.066-0.260	0.35			x				
3	Saville	1950	F.M. Lab Berkeley California	9	0.01-0.02	0.7-1.5	4.7-7.7	0.10	0.12			x				Movable Bed (Sand)
4	Brebner, Kamphuis	1963	Queen's University Canada	141	0.03-0.07	0.8-1.13	7-35°	0.05 and 0.01	0.55			x				
5	Galvan, Eagleson	1965	M.I.T Cambridge	38	0.01-0.06	0.9-1.5	1-28°	0.109	0.5		x		x_1		x	
6	Horikawa, Sasaki	1968	Japan													
7	Dalrymple, Dean	1972	University of Florida		0.48-2.70											Spiral wave maker
8	Gourlay	1976 1978	Univ. of Queensland Australia		0.01-0.09	1.0-1.5		0.10	0.4		x			x	x	Non-uniform currents
9	Dalrymple, Eubanks, Birkemeier	1977	Univ. of Delaware Newark							0.06	x					Extremely small Quali-tative only
10	Mizuguchi et al.	1978	Univ. of Tokyo Japan		0.06	0.8	1.4-4.7	0.10	0.22	0.18			x_1		x	See Kraus Sasaki, 1979

LABORATORY OBSERVATIONS - LONGSHORE CURRENTS

No	Name	Date	Location	No obs.	Wave Data Range			Beach	Mean Longshore Current		Observation Method for Current			Variation Measured		Remarks
					Height H$_B$ (meters)	Period T$_B$ (seconds)	Angle θ$_B$ (degrees)	Slope	Maximum m/sec	Mean m/sec	Float	Dye	Meter	Long shore	Surf Zone	
11	Visser	1980	Tech. Univ. Delft Netherlands		0.1	2.0	20.9	0.10	0.7	0.3 ±		x		x		Uniform Longshore profiles
12	Shimano Hom-ma Horikawa	1958	Japan		0.5-0.9			0.10								Nearshore Circulation - Jetty

APPENDIX C
LONGSHORE CURRENT FORMULAS

Authors	Mean Longshore Current, V	Formulation	Eq. No.
Putnam-Munk-Traylor (1949)	$[6.97g \frac{s}{f} \tan\beta \, H_b^2 \frac{\sin 2\alpha_b}{T}]^{1/3}$	Energy Conservation, Solitary waves	1.1
Eagleson (1965)	$[\frac{3}{8} g\kappa H_b \frac{\sin\beta \sin\alpha_b \sin 2\alpha_b}{f}]^{1/2}$	Momentum Conservation, Asymmetric-periodic waves	1.2
Putnam-Munk-Traylor (1949)	$\frac{A}{2}[(1 + \frac{4}{A} \, 2.28gH_b\sin\alpha_b)^{1/2} - 1]$ $A = 20.88 \frac{\tan\beta}{fT}\cos\alpha_b H_b$	Momentum Conservation, Solitary waves	1.3
Galvin-Eagleson (1965)	$gT\tan\beta\sin 2\alpha_b$	Mass Conservation	1.4
Inman-Bagnold (1963)	$2.31 \frac{\kappa\ell\tan\beta}{T} \cos\alpha_b \sin\alpha_b$	Mass Conservation, Rip currents included	1.5
Bruun (1963)	$C_f [\frac{0.95}{\sqrt{g\kappa}} H_b^{3/2} \frac{\tan\beta\sin 2\alpha_b}{T}]^{1/2}$	Mass Conservation	1.6
Bruun (1963)	$2.31 \frac{\kappa\ell\tan\beta\cos\alpha_b}{T}$	Mass Conservation, Rip currents included	1.7
Inman-Quinn (1951)	$[(\frac{1}{4A^2} + 2.28gH_b\sin\alpha_b)^{1/2} - \frac{1}{2A}]^2$ $A = 108.3 \frac{\tan\beta H_b\cos\alpha_b}{T}$	Empirical-based on momentum analysis	1.8
Brebner-Kamphius (1963)	$8.0\sin^{1/3}\beta \frac{H_o^{2/3}}{T^{1/3}} [\sin 1.65\alpha_o + 0.1\sin 3.30\alpha_o]$	Empirical-based on momentum analysis	1.9
Brebner-Kamphius (1963)	$14.0\sin^{1/2}\beta \frac{H_o^{3/4}}{T^{1/2}} [\sin 1.65\alpha_o + 0.1\sin 3.30\alpha_o]$	Empirical-based on energy analysis	1.10
Harrison (1968)	$0.241\, H_b + 0.0318\, T + 0.0374\,\alpha_b + 0.0309\tan\beta - 0.170$	Empirical-least square analysis	1.11

APPENDIX D

LONGSHORE CURRENT PROFILE THEORY EQUATIONS

The equations for the longshore current profile theory of Kraus and Sasaki (1979) are found by expanding $\bar{v}$ in a power series and determining the unknown coefficients by the boundary conditions. Namely, $\bar{v}$ and $d\bar{v}/dx$ must be continuous at the breaker line at $\bar{v}$ finite at the limits $\bar{X} \to 0$ and infinity. Introducing dimensionless variables V and X defined by

$$V = \frac{\bar{v}}{\bar{v}_b} \quad , \quad X = \frac{x}{x_b}$$

where

$$\bar{v}_b = \frac{5}{16} \pi \gamma \frac{\tan \beta}{(1+3/\gamma^2 8)} \sqrt{gh_b} \frac{\sin\alpha_b}{C_f} \tag{D-1}$$

and essentially equivalent to the modified reference velocity with correction for wave setup without the $\cos\alpha_b$ term (eq. 72).

Expressed in dimensionless variables the general solution of equation (42) is

$$V = \begin{cases} \displaystyle\sum_{n=0}^{\infty} (A_n X + B_n X^P) X^n & , \quad 0 < X < 1 \\[2em] \displaystyle\sum_{n=0}^{\infty} C_n X^{q-n} & , \quad 1 < X < \infty \end{cases} \tag{D-2}$$

where

$$A = \begin{cases} \dfrac{1}{1-(5/2)P} & , \quad n = 0 \\[1.5em] \dfrac{a_n - b^2 A_{n-1}}{1-(n+1)(n+5/2)P} & , \quad n = 1,2,\ldots \end{cases} \tag{D-3a}$$

$$a_n = \begin{cases} 1 & , \quad n=0 \\[1.5em] -\dfrac{1}{5}\dfrac{(2n+5)(2n-3)!!}{2^n n!} b^{2n} & , \quad n=1,2,\ldots \end{cases} \tag{D-3b}$$

with, $b = \sin\alpha_b$

and

$$B_n = B_o \begin{cases} 1 & , \quad n=0 \\ \beta_n & , \quad n=1,2,\ldots \end{cases} \qquad \text{(D-3c)}$$

$$\beta_n = \frac{b^2}{(p+n)(p+n+3/2)(P-1)} \beta_{n-1} \quad , \quad \beta_o = 1$$

$$C_n = C_o \begin{cases} 1 & , \quad n=0 \\ \delta_n & , \quad n=1,2,\ldots \end{cases} \qquad \text{(D-3d)}$$

$$\delta_n = \frac{b^2}{(q-n)(q-n+1/4)(Q-1)} \delta_{n-1} \quad , \quad \hat{\delta}_o = 1$$

With the definitions,

$$S = \sum_{n=0}^{\infty} A_n \quad , \quad S_p = \sum_{n=0}^{\infty} \beta_n \quad , \quad S_q = \sum_{n=0}^{\infty} \delta_n$$

$$\text{(D-4)}$$

$$S' = \sum_{n=0}^{\infty} (n+1)A_n \quad , \quad S'_p = \sum_{n=0}^{\infty} (p+n)\beta_n \quad , \quad S'_q = \sum_{n=0}^{\infty} (q-n)\delta_n$$

from continuity at the breaker line,

$$B_o = (SS'_q - S'S_q)/(S'_p S_q - S_p S'_q)$$

$$\text{(D-5)}$$

$$C_o = (SS'_p - S'S_p)/(S'_p S_q - S_p S'_q)$$

where in the above

$$P = \frac{\pi}{2} \frac{\Gamma}{C_f} \frac{\tan\beta}{1+3\gamma^2/8} \qquad Q = \frac{\pi}{2} \frac{\Gamma}{C_f} \tan\beta \qquad \text{(D-6)}$$

and

$$p = -\frac{3}{4} + \sqrt{(9/16)+(1/P)}$$

$$q = -\frac{1}{8} - \sqrt{(1/64)+(1/Q)}$$

Basco, David R.
    Surf zone currents. Volume I. State of knowledge / by David R.
Basco.--Fort Belvoir, Va. : U.S. Army, Corps of Engineers, Coastal
Engineering Research Center, Springfield, Va. : available from NTIS,
1982.
    [243] p. : ill. ; 28 cm.--(Miscellaneous report--U.S. Coastal Engi-
neering Research Center ; no. 82-7, v.I) (Contract DACW72-80-C-0003).
    Prepared by Department of Civil Engineering, Texas A&M University.
    Report provides a state-of-the art summary of research on coastal
hydrodynamics and its three main components: longshore currents,
nearshore circulations, and rip currents. Concentration is on all
theoretical aspects since 1967 but earlier data are included.
    1. Hydrodynamics. 2. Longshore currents. 3. Nearshore circula-
tions. 4. Numerical models. 5. Rip currents. 6. Surf zone currents.
I. Title. II. Coastal Engineering Research Center (U.S.). III. Texas
A&M University. Department of Civil Engineering. IV. Series:
Miscellaneous report (Coastal Engineering Research Center (U.S.));
no. 82-7, v.I.
TC203   .U581mr   no. 82-7, v.I   627

Basco, David R.
    Surf zone currents. Volume I. State of knowledge / by David R.
Basco.--Fort Belvoir, Va. : U.S. Army, Corps of Engineers, Coastal
Engineering Research Center, Springfield, Va. : available from NTIS,
1982.
    [243] p. : ill. ; 28 cm.--(Miscellaneous report--U.S. Coastal Engi-
neering Research Center ; no. 82-7, v.I) (Contract DACW72-80-C-0003).
    Prepared by Department of Civil Engineering, Texas A&M University.
    Report provides a state-of-the art summary of research on coastal
hydrodynamics and its three main components: longshore currents,
nearshore circulations, and rip currents. Concentration is on all
theoretical aspects since 1967 but earlier data are included.
    1. Hydrodynamics. 2. Longshore currents. 3. Nearshore circula-
tions. 4. Numerical models. 5. Rip currents. 6. Surf zone currents.
I. Title. II. Coastal Engineering Research Center (U.S.). III. Texas
A&M University. Department of Civil Engineering. IV. Series:
Miscellaneous report (Coastal Engineering Research Center (U.S.));
no. 82-7, v.I.
TC203   .U581mr   no. 82-7, v.I   627

Basco, David R.
    Surf zone currents. Volume I. State of knowledge / by David R.
Basco.--Fort Belvoir, Va. : U.S. Army, Corps of Engineers, Coastal
Engineering Research Center, Springfield, Va. : available from NTIS,
1982.
    [243] p. : ill. ; 28 cm.--(Miscellaneous report--U.S. Coastal Engi-
neering Research Center ; no. 82-7, v.I) (Contract DACW72-80-C-0003).
    Prepared by Department of Civil Engineering, Texas A&M University.
    Report provides a state-of-the art summary of research on coastal
hydrodynamics and its three main components: longshore currents,
nearshore circulations, and rip currents. Concentration is on all
theoretical aspects since 1967 but earlier data are included.
    1. Hydrodynamics. 2. Longshore currents. 3. Nearshore circula-
tions. 4. Numerical models. 5. Rip currents. 6. Surf zone currents.
I. Title. II. Coastal Engineering Research Center (U.S.). III. Texas
A&M University. Department of Civil Engineering. IV. Series:
Miscellaneous report (Coastal Engineering Research Center (U.S.));
no. 82-7, v.I.
TC203   .U581mr   no. 82-7, v.I   627

B·sco, David R.
    Surf zone currents. Volume I. State of knowledge / by David R.
Basco.--Fort Belvoir, Va. : U.S. Army, Corps of Engineers, Coastal
Engineering Research Center, Springfield, Va. : available from NTIS,
1982.
    [243] p. : ill. ; 28 cm.--(Miscellaneous report--U.S. Coastal Engi-
neering Research Center ; no. 82-7, v.I) (Contract DACW72-80-C-0003).
    Prepared by Department of Civil Engineering, Texas A&M University.
    Report provides a state-of-the art summary of research on coastal
hydrodynamics and its three main components: longshore currents,
nearshore circulations, and rip currents. Concentration is on all
theoretical aspects since 1967 but earlier data are included.
    1. Hydrodynamics. 2. Longshore currents. 3. Nearshore circula-
tions. 4. Numerical models. 5. Rip currents. 6. Surf zone currents.
I. Title. II. Coastal Engineering Research Center (U.S.). III. Texas
A&M University. Department of Civil Engineering. IV. Series:
Miscellaneous report (Coastal Engineering Research Center (U.S.));
no. 82-7, v.I.
TC203   .U581mr   no. 82-7, v.I   627